FORSCHUNGSZENTRUM JÜLICH GMBH
INSTITUTE OF BIO- AND GEOSCIENCES
PLANT SCIENCES (IBG-2)

HIGH-THROUGHPUT PHENOTYPING OF PHOTOSYNTHESIS TRAITS IN DURUM WHEAT UNDER DROUGHT STRESS USING LIGHT-INDUCED FLUORESCENCE TRANSIENTS

Dissertation
zur Erlangung des Grades

Doktor der Agrarwissenschaften (Dr. agr.)

der Landwirtschaftlichen Fakultät
der Rheinischen Friedrich-Wilhelms-Universität Bonn

von
NÍCOLAS ZENDONADI DOS SANTOS
aus
Curitiba, Parana, Brasilien

Bonn 2022

Referent: Prof. Dr. Uwe Rascher
Korreferent: Prof. Dr. Annaliese Mason

Tag der mündlichen Prüfung: 26. November 2021

Angefertigt mit Genehmigung der Landwirtschaftlichen Fakultät der Universität Bonn

To my parents for their endless love, support, and encouragement.

ACKNOWLEDGEMENTS

Firstly, I would like to express my sincere gratitude to my esteemed supervisors, Prof. Dr. Uwe Rascher and Dr. Onno Muller, for providing support and mentorship during the course of my PhD study and related research. My appreciation extends to the Institute of Bio- and Geosciences, Plant Sciences (IBG-2), for the funding opportunity to undertake my project at the Forschungszentrum Jülich. I also thank Dr. Fabio Fiorani, a member of my PhD committee, to promote insightful discussions and provide constructive criticism throughout this research. Moreover, many thanks to Dr. Hendrik Poorter and Dr. Shizue Matsubara for valuable advice, practical suggestions, and thoughtful conversations.

I am deeply grateful to Prof. Dr. Roberto Tuberosa from the Department of Agricultural and Food Sciences, University of Bologna, Italy, who gave me this unique opportunity to collaborate in his research towards plant breeding for drought-tolerance in durum wheat in Maricopa, AZ, USA. From his research team, I would like to thank Dr. Giuseppe Emanuele Condorelli and Dr. Eder Licieri Groli for a cherished time spent together in the field. Additionally, I would like to express my deepest gratitude to Dr. Maria Newcomb and Prof. Dr. Richard Ward from Maricopa Agricultural Center (MAC), University of Arizona, Maricopa, AZ, who granted me access to their research facilities and unparalleled support. Without their precious help, it would not be possible to conduct this research. I must also thank Dr. Pedro Andrade-Sanchez, John T. Heun and Jeffrey Demieville for their valuable hands-on assistance. Apart from MAC, I very much appreciate the support provided by Dr. Alison Thompson, Dr. Matthew Herritt and Matthew M. Conley from the USDA-ARS, U.S. Arid-Land Agricultural Research Center (ALARC), Plant Physiology and Genetics Research Unit, in Maricopa, AZ, particularly for having shared the field phenotyping cart.

Special thanks to Dr. Nicholas W. Galwey for his attention and kindness to guide me through my first and naïve steps into the world of mixed modelling. His book (*Introduction to Mixed Modelling: Beyond Regression and Analysis of Variance*, 2nd ed., Chichester, West Sussex, UK: Wiley, 2014) was rather a watershed in my learning curve. Nonetheless, if I could master somewhat this knowledge, it was undeniably thanks to Prof. Dr. Hans-Peter Piepho from the Biostatistics Unit, Institute of Crop Sciences, University of Hohenheim, Stuttgart, Germany. His remarkable dedication, promptness and patience for thorough teaching and guidance have been invaluable. Thank you for sharing your bright knowledge and being ever so encouraging!

I gratefully acknowledge the help of Dr. Nathalie Wuyts and Thorsten Brehm, who were pivotal to ensure the successful operation of the automatic ScreenHouse shoot

phenotyping platform at the IBG-2. Also, thanks to Beate Uhlig and Katharina Wolter-Heinen for keeping optimal plant growth conditions in the greenhouses. Furthermore, I very much appreciate the almost 24/7 remote technical support provided by Dr. Zbigniew S. Kolber to keep the LIFT instruments up and running. Lastly, a special acknowledgement goes to all Shoot Dynamics team members, an outstanding group at the IBG-2.

I will forever be thankful to my former advisor, Prof. Juarez Gabardo, who has been my life coach and my scientific and career mentor since 2004. Last but not least, hereby, I would like to register my most profound appreciation to Michelle Cia Bartels Zendonadi, who has made countless sacrifices to help me and has been incredibly supportive throughout this endeavour despite my absences, fits of impatience and all the travails. Thank you so much, my beloved wife!

“If I have seen further, it is by standing upon the shoulders of giants.”

Isaac Newton (1675)

ABSTRACT

Agriculture in the twenty-first century faces the double challenge of feeding a growing population in a changing climate. Food security will increasingly rely on the active release of stable high-yielding cultivars with improved resilience to water shortages, particularly for vulnerable drought-prone environments. Therefore, developing new techniques and approaches to improve the efficiency and precision of crop breeding for drought tolerance is essential. Conventional plant phenotyping methods for assessing plant responses to water-limiting conditions, and supporting selective breeding, are usually laborious, time-consuming, and costly. More recently, cost-effective high-throughput phenotyping platforms (HTPPs) have emerged, enabling rapid and accurate phenotypic characterisation of large populations in either controlled or field conditions. HTPPs deploy sensors to non-invasively and non-destructively identify, quantify, and record relevant plant traits. An integrative signal, such as photosynthesis, may serve as a robust selection parameter for crop performance. Chlorophyll fluorescence (ChlF) is an inexpensive, fast, and non-invasive technique for probing photosynthesis and, therefore, for monitoring plant physiological status. Although proposed as a method for drought tolerance screening, ChlF has not yet been fully adopted in physiological breeding, mainly due to limitations in high-throughput phenotyping capabilities. Most of the prior research has relied on the pulse-amplitude modulation (PAM) fluorometry, which typically requires a saturating flash in very close proximity, done mainly by clamping on leaves, limiting its throughput. In this context, the Light-Induced Fluorescence Transient (LIFT) sensor arose as an alternative for acquiring high-throughput ChlF-based traits. The LIFT fluorometer actively monitors ChlF within milliseconds using subsaturating excitation flashlets instead of the saturating pulse. Also, this pump-and-probe method works at a distance, bridging the gap between leaf and canopy levels. LIFT-measured ChlF has proved to provide not only PAM-analogous photosynthetic parameters but also measures the downstream electron transport rates from the primary quinone acceptor (Q_A) to the plastoquinone (PQ) pool, and ultimately, towards the photosystem (PS) I. Nevertheless, little knowledge is available on the overall responses of LIFT-measured ChlF traits in field-grown crops under drought and their native genetic variability, aiding physiological crop breeding towards drought tolerance. To this end, the LIFT instrument was mounted on a manually pushed cart to measure ChlF across time in a large panel of durum wheat genotypes (> 220 elite accessions) subjected to progressive drought in replicated field trials over two growing seasons in Maricopa, Arizona, USA. Secondly, the LIFT sensor was combined with an existing automated HTPP for simultaneous and continuous monitoring of water relations in the soil-plant-atmosphere continuum of wheat plants growing in semi-controlled conditions. The photosynthetic performance was measured at the canopy level by means of the operating efficiency of PSII (F_q'/F_m') and the kinetics of electron transport from Q_A to PQ pool and from PQ pool to PSI measure by reoxidation rates, F_{r1}' and F_{r2}', respectively. Short- and long-term changes in ChlF traits were found in response to soil water availability and interactions with weather fluctuations, namely photosynthetic photon flux density (PPFD) and vapour pressure deficit (VPD). At an unprecedented scale, this high-throughput approach for phenotyping ChlF traits integrated with a high-resolution recording of the environment allowed for estimation of genetic effects over time and shed light on the diurnal dynamics of the photosynthetic apparatus, facilitating the ability to dissect complex physiological traits in fluctuating growing conditions.

***Keywords*:** durum wheat; drought; LIFT; chlorophyll fluorescence; electron transport rate; photosynthesis; high-throughput plant phenotyping; genetic diversity; physiological breeding; fluctuating environment; genotype-by-environment interaction; spatiotemporal modelling.

ZUSAMMENFASSUNG

Die Landwirtschaft steht im 21. Jahrhundert vor der doppelten Herausforderung, dass sie unter sich stets verändernden klimatischen Bedingungen eine wachsende Weltbevölkerung zu ernähren hat. Das Züchten neuer ertragsstabiler Sorten, welche den kontinuierlich verändernden Klimabedingungen standhalten beziehungsweise trockentolerant sind, wird insbesondere in wasserarmen Gebieten entscheidenden zur globalen Ernährungssicherung beitragen. Im Hinblick auf die Trockentoleranz ist daher die Entwicklung neuer Techniken und Ansätze zur Verbesserung der Effizienz und Präzision der Pflanzenzüchtung unerlässlich. Die Untersuchung pflanzlicher Reaktionen auf wasserlimitierende Bedingungen im Zusammenhang mit der selektiven Züchtung gestaltet sich oft schwierig, da herkömmliche Methoden der Pflanzenphänotypisierung in der Regel umständlich, zeitintensiv und kostspielig sind. Neuerdings wurden vermehrt kostengünstige Hochdurchsatz-Phänotypisierungsplattformen (HTPPs) entwickelt, die eine schnelle und akkurate phänotypische Charakterisierung großer Populationen unter kontrollierten und Feldbedingungen ermöglichen. HTPPs greifen auf Sensoren zurück, um relevante Eigenschaften von Pflanzen nicht-invasiv und nicht-destruktiv zu identifizieren, quantifizieren und aufzuzeichnen. Ein integratives Signal, wie die Photosynthese, könnte als robuster Selektionsparameter zur Beurteilung Leistungsfähigkeit der Pflanzen nutzbringend sein. Die Messung der Chlorophyll-Fluoreszenz (ChlF) ist eine kostengünstige, schnelle sowie nicht-invasive Methode zur Untersuchung der Photosyntheseleistung, und somit zur Beobachtung des physiologischen Zustands der Pflanzen. Obschon die ChlF-Methode für das Screening trockentoleranter Sorten mitentwickelt wurde, findet sie bislang, noch keine breite Anwendung in der Pflanzenzüchtung, dies hauptsächlich aufgrund der Einschränkungen bei der Hochdurchsatz-Phänotypisierung. Der Großteil der bisherigen Forschung basiert auf der Puls-Amplituden-Modulation (PAM)-Fluorometrie, die typischerweise einen sättigenden Lichtblitz in unmittelbarer Nähe erfordert. Meistens erfolgt dies durch das Einklemmen von Blättern was aber Probendurchsatz stark begrenzt. Vor diesem Hintergrund wurde der 'Light-Induced Fluorescence Transient' (LIFT)-Sensor entwickelt. Dieser stellt eine Alternative zur Erfassung von ChlF-basierten Eigenschaften mit hohem Durchsatz dar. Unter Verwendung von nicht-sättigenden Anregungs-Lichtblitzen anstatt des Sättigungspulses misst das LIFT-Fluorometer aktiv innerhalb von Millisekunden ChlF. Zudem ermöglicht dieses Pump-Probe-Verfahren eine Messung auf Distanz und überbrückt somit die Lücke zwischen Blattmessungen und Messungen auf Bestandsebene. Die ChlF Messung mit dem LIFT liefert nicht nur PAM-analoge photosynthetische Parameter, sondern misst auch die nachgeschalteten Elektronentransportraten vom primären Chinon-Elektronenakzeptor (Q_A) zum Plastochinon Pool (PQ), und schließlich zum Photosystem (PS) I. Dennoch ist nur wenig über die allgemeinen Reaktionen von LIFT-gemessenen ChlF-Eigenschaften unter trockenen Feldbedienungen und deren genetische Variabilität bekannt. Zur Datenerhebung wurde das LIFT-Gerät auf einem manuell geschobenen Wagen montiert um schließlich ChlF im zeitlichen Verlauf in einem großen Panel von Hartweizen-Genotypen (> 220 Elite-Akzessionen) zu messen. Die Weizenpflanzen wurden über zwei Wachstumsperioden in Maricopa, Arizona, USA, progressiver Trockenheit in Feldbedingungen ausgesetzt. Zur simultanen und kontinuierlichen Aufzeichnung der Wasserverhältnisse im Boden-Pflanze-Atmosphäre-Kontinuum wurden die LIFT Messungen mit einem automatisierten HTPP kombiniert. Die Photosyntheseleistung wurde auf Bestandesebene anhand der Quanteneffizienz des PSII (F_q'/F_m') sowie der Kinetik des Elektronentransport vom Q_A zum PQ Pool und vom PQ Pool zum PSI durch Reoxidationsraten beziehungsweise durch F_{r1}' und F_{r2}' gemessen. Kurz- und langfristige Veränderungen der ChlF-Eigenschaften konnten als Reaktion auf die Wasserverfügbarkeit im Boden und in Wechselwirkung mit Bedingungsschwankungen

(photosynthetischen Photonenflussdichte und dem Sättigungsdampfdruckdefizit) nachgewiesen werden. Dieser Hochdurchsatz-Ansatz zur Phänotypisierung von ChlF-Eigenschaften, verknüpft mit einer hochauflösenden Aufzeichnung der Umweltdaten, ermöglicht in einem erstmaligen Ausmaß die Schätzung von genetischen Effekten im zeitlichen Verlauf. Zudem verdeutlicht er die tageszeitliche Dynamik des photosynthetischen Apparates mit der Fähigkeit komplexe physiologische Eigenschaften unter schwankenden Wachstumsbedingungen getrennt zu betrachten.

Stichworte: Hartweizen; Trockenheit; LIFT; Chlorophyll-Fluoreszenz; Elektronentransportrate; Photosynthese; Hochdurchsatz-Pflanzenphänotypisierung; genetische Vielfalt; physiologische Züchtung; fluktuierende Umwelt; Genotyp-Umwelt-Interaktion; Raum-Zeit Modellierung.

LIST OF ABBREVIATIONS

A_n	Net CO_2 assimilation
ABA	Abscisic acid
AIC	Akaike Information Criterion
BBCH	The universal plant growth scale jointly developed by BASF, Bayer, Ciba-Geigy and Hoechst
BL	Baseline model
BL_{cov}	Baseline model with additional covariates
$BL_{cov+STM}$	Baseline model with additional covariates and spatiotemporal modelling
BLUE	Best Linear Unbiased Estimator
BLUP	Best Linear Unbiased Prediction
C_i	Intercellular CO_2 concentration
CEF	Cyclic electron flow around PSI
CET	Central European Time
ChlF	Chlorophyll fluorescence
CIMMYT	International Maize and Wheat Improvement Center
CKs	Cytokinins
CMS	Leaf cell membrane stability
CRD	Completely randomised design
DAS	Days after sowing
DAWW	Days after withholding water
DLI	Daily light integral
E	Transpiration rate
ETR	Daily evapotranspiration rate
F'	Chlorophyll fluorescence yield of the first flashlet from light-adapted plants
F'_m	Maximum chlorophyll fluorescence yield observed between flashlets 298th and 302nd from light-adapted plants
F'_q	The difference in chlorophyll fluorescence yield between F'_m and F'
F'_{r1}	Reoxidation efficiency of Q_A^- up to ~0.65 ms after F'_m is reached (i.e., the kinetics of electron transfer from Q_A to PQ pool from light-adapted plants)
F'_{r2}	Reoxidation efficiency of Q_A^- up to ~6.64 ms after F'_{r1} (i.e., the kinetics of electron transfer from PQ pool to PSI from light-adapted plants)

F_q'/F_m'	Operating efficiency of PSII
FRR	Fast Repetition Rate
g_s	Stomatal conductance
GS	Plant growth stage
GWAS	Genome-wide association study
G×E	Genotype-by-environment
H^2	Broad-sense heritability on an entry-mean basis
HTPPs	High-throughput phenotyping platforms
ICARDA	International Center for Agricultural Research in the Dry Areas
INRAE	French National Institute for Agriculture, Food and Environment
IRTA	Spanish Institute of Agriculture and Food Research and Technology
LA	Total leaf area per plant
LED	Light-Emitting Diode
LET	Linear electron transport
LIFT	Light-Induced Fluorescence Transient
LMM	Linear mixed model
MAS	Marker-assisted selection
METs	Multi-environment trials
MST	Mountain Standard Time
NDVI	Normalised difference vegetation index
PAW	Plant available water
PLA	Projected leaf area
PPFD	Photosynthetic photon flux density
PQ	Plastoquinone
PSI	Photosystem I
PSII	Photosystem II
PTOX	Plastid terminal oxidase
Q_A	Primary quinone electron acceptor in PSII
Q_A flash	LIFT excitation protocol designed to reduce Q_A and to observe the kinetics of electron transport from Q_A to PQ pool (F_{r1}') and from PQ pool to PSI (F_{r2}')
QTL	Quantitative trait loci
RE	Relative efficiency
REML	Residual maximum likelihood
REMLRT	REML-likelihood ratio test

r_g	Coefficient of genotypic correlation between pairs of traits
r_p	Coefficient of phenotypic correlation between pairs of traits
r_s	Spearman's rank correlation coefficient
ROS	Reactive oxygen species
RQ_A	Relaxation phase of a chlorophyll fluorescence transient induced by a Q_A flash where Q_A is progressively reoxidised
RWC	Leaf relative water content
SDM	Total shoot dry matter per plant
SDMY	Total shoot dry matter yield
SQ_A	Saturation phase of a chlorophyll fluorescence transient induced by a Q_A flash where Q_A is progressively reduced
STM	Spatiotemporal modelling
TPE	Target population of environments
TDR	Time-domain reflectometry
UNIBO	University of Bologna
VPD	Vapour pressure deficit
VOGREI	Vogelmann red edge index
VWC	Soil volumetric water content
WD	Water-limited
WU	Water uptake
WUE	Water-use efficiency
WW	Well-watered
WWC	Water-water cycle
Y1	Growing season 2017/2018 (Year 1)
Y2	Growing season 2018/2019 (Year 2)
ΔRWC	Relative change in RWC
θ_{FC}	Field capacity
θ_{PWP}	Permanent wilting point
%Δ	Relative change (i.e., percentage change)

TABLE OF CONTENTS

1 INTRODUCTION 19

1.1 A Changing World: Setting the Scene 19

1.2 The Drought Phenomenon 20

1.3 Drought Stress in Crop Plants: Effects and Responses 22

1.4 Phenotyping for Assessing Plant-Environment Interactions 25

1.5 Chlorophyll Fluorescence: An Integrative Photosynthetic Signal 29

1.6 Aim and Objectives 32

2 MATERIALS AND METHODS 33

2.1 LIFT Device and Method 33

2.2 Fluorescence Parameters for Field Phenotyping 34

2.3 Field Experiments 36

2.3.1 Plant material 36

2.3.2 Field experimental design 37

2.3.3 Meteorological data and soil moisture monitoring 38

2.3.4 Leaf relative water content 39

2.3.5 Plant height and above-ground biomass 39

2.3.6 LIFT measurements in the field 40

2.3.7 Spectral reflectance data 42

2.3.8 LIFT data cleaning 42

2.3.9 Phenotypic plasticity across genotypes 43

2.3.10 Spatial-temporal statistical analysis 44

2.3.11 Heritability and trait correlation estimation 47

2.4 Greenhouse Experiment 49

2.4.1 Plant material 49

2.4.2 Greenhouse experimental design 50

2.4.3 Growth conditions, meteorological and evapotranspiration data 51

2.4.4 Plant growth development and projected leaf area 52

2.4.5 Leaf gas exchange measurements 53

2.4.6 Measurement of leaf cell membrane stability 53

2.4.7 Final destructive measurements 54

2.4.8 LIFT measurements in the greenhouse 54

2.4.9 LIFT data cleaning 55

2.4.10 Statistical analysis ... 56
3 RESULTS ... 58
3.1 FIELD TRIAL RESULTS ... 58
3.1.1 Weather conditions and drought severity ... 58
3.1.2 Covariates and spatiotemporal modelling of trends ... 60
3.1.3 Effects of drought stress on leaf RWC and above-ground biomass ... 62
3.1.4 Effects of drought stress on the LIFT-measured ChlF traits ... 65
3.1.5 Environmental responses and diurnal courses of ChlF traits ... 69
3.1.6 Changes of heritability over time ... 71
3.1.7 Genetic and phenotypic correlations within ChlF traits over time ... 77
3.1.8 Trait-trait genetic and phenotypic correlations ... 79
3.1.9 Phenotypic plasticity and variability across subpopulations ... 82
3.2 GREENHOUSE TRIAL RESULTS ... 85
3.2.1 Overall effects of drought at the canopy and leaf level ... 85
3.2.2 Effects of drought on plant growth and development ... 86
3.2.3 Effects of drought on leaf gas exchange and cell membrane stability ... 88
3.2.4 Effects of drought stress on the LIFT-measured ChlF traits ... 89
3.2.5 ChlF traits in response to light intensity and VPD ... 95
3.2.6 Trait-trait phenotypic correlations ... 97
4 DISCUSSION ... 99
4.1 FIELD ... 99
4.2 GREENHOUSE ... 103
5 CONCLUSIONS ... 106
REFERENCES ... 108
APPENDIX 1 – LIST OF GENETIC RESOURCES ... 135
APPENDIX 2 – FIELD MAPS ... 140
APPENDIX 3 – STATISTICAL MODELS ... 142
APPENDIX 4 – CONDITIONAL *F*-TEST STATISTIC FOR FIXED EFFECTS ... 154

1 INTRODUCTION

1.1 A CHANGING WORLD: SETTING THE SCENE

The world's population reached 7.7 billion in mid-2019 and will continue to grow to some 9.7 billion by 2050 and 10.9 billion by 2100 (United Nations, 2019), leading to greater demand for food, feed, fibre, water and energy (Godfray et al., 2010). Future global food demand is expected to increase by some 70% by 2050 (Turral, Burke & Faurès, 2011). In terms of agricultural production, Tilman, Balzer, Hill & Befort (2011) estimate that the worldwide demand for crop calories may increase by 100-110% from 2005 to 2050. According to Ray, Mueller, West & Foley (2013), to achieve such a goal of doubling the production, it would require that global yields increase at rates of ~2.4% per year for the top four staple crops – maize, rice, wheat, and soybean – that respond to almost two-thirds of global calories. However, their current yields are increasing at rates ranging from 0.9% to 1.6% per year. Therefore, boosting global food production will require modern technologies and innovative approaches to accelerate crop improvement (Hickey et al., 2019; Tester & Langridge, 2010).

Concurrent with this urge to increase agricultural yields, there is the ongoing climate change, driven by a continual rise in anthropogenic greenhouse gas emissions. Recently, IPCC (2019) reported that the observed mean temperature over the land surface for the period 2006-2015 was 1.53°C warmer than for the pre-industrial period (1850-1900), and 0.66°C higher than the equivalent global (land and ocean) mean temperature. Also, without stringent mitigation of current emissions of greenhouse gases, IPCC (2014) estimates that the globe temperature will likely be between 1.8°C to 3.7°C warmer, on average, by the end of the century. It has been suggested that a global warming between 1.5°C and 2.5°C would have a moderate impact on the planet's biodiversity (Porter et al., 2014), when approximately 20-30% of species could be at increased risk of extinction (UNEP, 2009). Apart from rising temperatures, the hydrological cycle is also expected to change patterns. Precipitation is predicted to rise in the tropics and higher latitudes but to decrease in the subtropics and lower mid-latitudes (Trenberth et al., 2014; Turral et al., 2011). Vulnerable water-scarce areas, such as arid and semi-arid regions, will likely exacerbate the climatic effects, getting drier and hotter (Seager, Naik & Vecchi, 2010). Altogether, both rainfalls and temperatures may become more variable in space and time, with higher frequency and intensity of extreme events, such as heat waves, droughts and floods (United Nations, 2019; UNEP, 2009). As a matter of fact, all potential impacts are not fully understood yet, although the predictions strongly suggest climate

change pose a threat to environmental sustainability and global socioeconomic development (Royal Society, 2012; Stern, 2007), which may cause radical changes in our society.

Undoubtedly, a changing climate can jeopardise the availability of a stable food supply and undermine strategies for doubling agricultural productivity. For instance, Lobell, Schlenker & Costa-Roberts (2011) estimated that global maize and wheat production declined by 3.8% and 5.5%, respectively, from 1980 to 2008 due to changes in temperature and precipitation trends. For every 1°C increase in temperature, yields are expected to decline by 10% in wheat and rice, and decrease by 17% in soybean (Taiz, 2013). Despite the great uncertainties and difficulties in forecasting the agricultural impacts of climate change (FAO, 2016; Lobell & Burke, 2008), Cline (2007) projected potential losses in world agricultural capacity lying in the range of 10-25% by the 2080s. Likewise, Porter et al. (2014) reported that about 10% of their projections for the period 2030-2049 showed yield losses for the major crops (wheat, rice, and maize) higher than 25% compared to the late 20th century, with even greater risks of more severe impacts after 2050. Notably, climate trends may also increase crop vulnerability to pests since various pathogens, insects, and weeds become more active in warmer weather, changing their spatial and temporal population dynamics (Evans, Baierl, Semenov, Gladders & Fitt, 2008; Garrett, Dendy, Frank, Rouse & Travers, 2006; Rosenzweig, Iglesias, Yang, Epstein & Chivian, 2001). Hence, global food security (i.e., availability, stability, utilisation, and access) can be seriously compromised (FAO, 2016; Schmidhuber & Tubiello, 2007). Indeed, feeding a growing population on a limited planet coupled with environmental constraints is certainly one of the greatest challenges of the twenty-first century (Royal Society, 2012).

1.2 The Drought Phenomenon

Drought is a naturally occurring climatic feature; its recurrence is inevitable and can occur in virtually all edaphoclimatic zones (Dai, 2011). Globally, drought (7.5%) is the second-most geographically extensive hazard after floods (11%) of the earth's land area (Nagarajan, 2009). Also, it has been estimated that about 18% and 26% of the world's rural area show respectively moderate and severe constraints to rainfed crop production due to moisture limitations (van Velthuizen et al., 2007). To determine either the onset of drought or its termination, it is a rather tricky task (Wilhite & Glantz, 1985), making the drought event as one of the most complex but least understood of all natural hazards, affecting more people than any other hazard (American Meteorological Society, 1997; Wilhite, 2000). Indeed, Bryant (1991) assessed 31 natural hazard events and ranked drought at first based on its key impacts and

characteristics (e.g., the degree of severity, length of event, total areal extent, total loss of life, total economic loss, social effects, long-term impacts, suddenness, and occurrence of associated hazards). Despite its importance, there is no precise and universally accepted definition of drought, as it reflects multidisciplinary perspectives and consequently incorporates different physical, biological, and socioeconomic variables (Mishra & Singh, 2010; Trenberth, et al., 2014; Wilhite, 2000). As a matter of fact, there are more than 150 definitions of drought published in the literature (Boken, 2005; Wilhite & Glantz, 1985).

Regardless of this variation in definitions, often droughts are broadly grouped into four categories (American Meteorological Society, 1997; Dai, 2011; Heim Jr., 2002; Mishra & Singh, 2010) as follows: i) *Meteorological or climatological drought* is defined as a period of months to years with below-normal precipitation over a region, which is typically caused by persistent anomalies in large-scale atmospheric circulation patterns; ii) *Hydrological drought* occurs when precipitation deficits over a prolonged period affect surface and subsurface water supply, reducing streamflow, groundwater, reservoirs, and lake levels; iii) *Agricultural drought*, usually, refers to moisture deficits within the topmost one metre or so of soil (i.e., around the root zone), as a result of below-average precipitation or above-normal evapotranspiration, at a critical period during the growing season, which impacts crop development and growth, and ultimately leads to yield losses; and iv) *Socioeconomic drought* associates the supply and demand of some economic good with elements of meteorological, agricultural, and hydrological drought. The relationship between these various types of drought and the duration of the event is demonstrated in Figure 1.1.

At the onset of drought, agriculture is frequently the first economic sector to be affected since soil moisture can quickly be depleted, mainly when associated with high temperatures and winds (Wilhite, 2000). As a matter of fact, agricultural drought is acknowledged as the most important and the most complex category of drought, often requiring a good knowledge of soil physics, plant physiology, and economics (Boken, 2005; Palmer, 1965). At the macro-level, agricultural drought has the potential to cause severe food shortage or even famine in some countries, resulting in loss of both the human and livestock population (Boken, 2005). In short, people can be at a higher risk of hunger and poverty (FAO, 2016). This explains why the fight against drought is at high priority in the long-term plan of the World Meteorological Organization (WMO) through its Commission for Agricultural Meteorology, which provides direction and guidance to the Agricultural Meteorology Programme (Sivakumar, 2005, 2011).

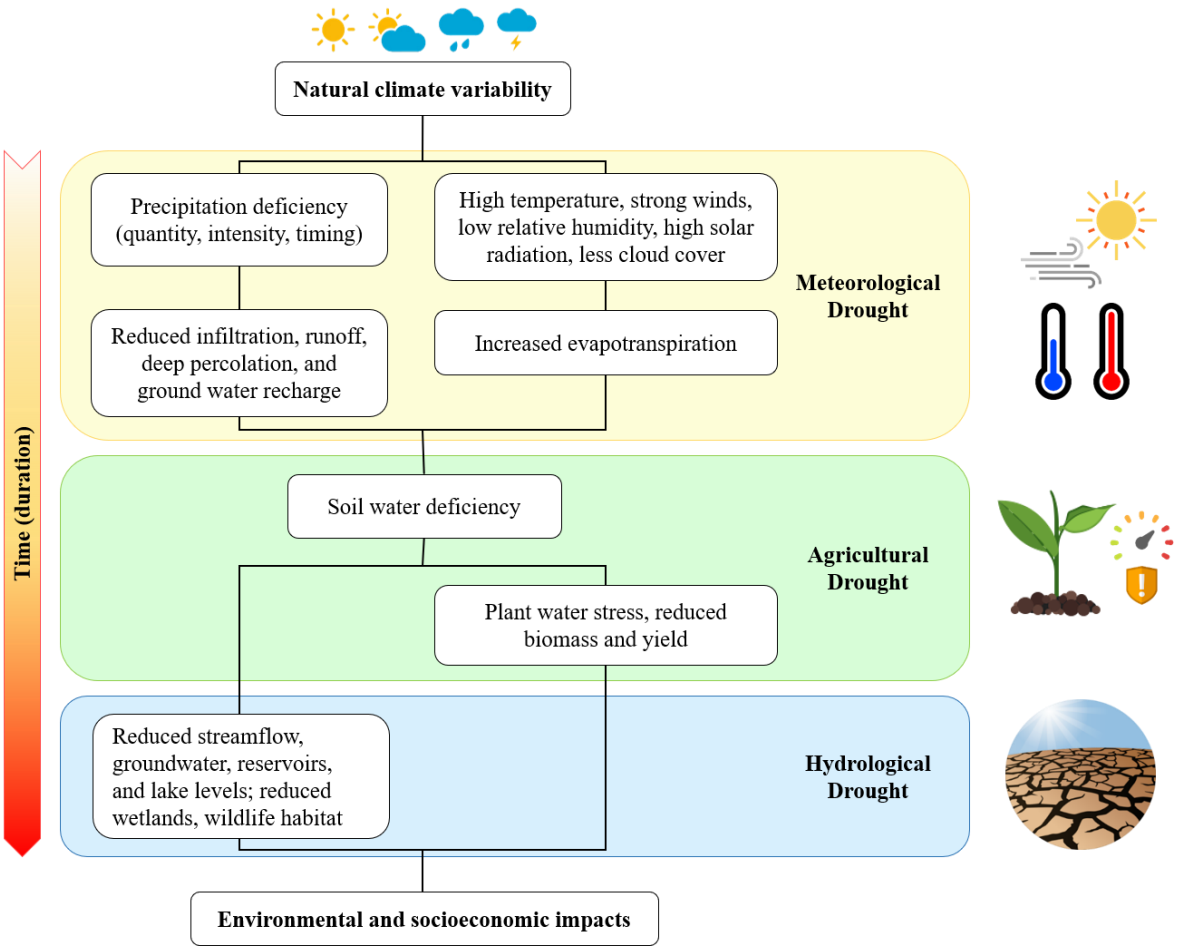

Figure 1.1. The relationship between the various types of drought and the duration of drought events. Adapted from Wilhite (2000).

1.3 Drought Stress in Crop Plants: Effects and Responses

Plants are constantly exposed to environmental fluctuations and not rarely subjected to biotic (e.g., diseases and insect pests) and abiotic stresses (e.g., drought, flood, salinity, excess light, extreme temperatures, nutritional deficiency, and heavy metals). In being sessile organisms, plants have evolved several mechanisms to perceive surrounding environmental stimuli and cope with potential stressors via morphological, anatomical, biochemical, and physiological adjustments (De Micco & Aronne, 2012). These plant responses will vary depending on the type of stress and its time, duration and intensity, as well as on plant species, variety or ecotype (Lefebvre, Kiani & Durand-Tardif, 2009). Indeed, plant responses to stress rely on complex biological regulatory networks (Cramer, Urano, Delrot, Pezzotti & Shinozaki, 2011), which are strongly genetically controlled (Ghatak, Chaturvedi & Weckwerth, 2017; Habash et al., 2014; Hu & Xiong, 2014; Sallam, Alqudah, Dawood, Baenziger & Börner, 2019).

Drought is a severe environmental constraint to crop growth and productivity. Drought-induced yield reduction has been reported to widely vary from 11% to 94% in many crops, such as barley, rice, chickpea, pigeon pea, common beans, soybean, cowpea, sunflower, canola, and potato (Farooq, Wahid, Kobayashi, Fujita & Basra, 2009). In a global meta-analysis, Daryanto, Wang & Jacinthe (2016) estimated average yield losses of 20.6% and 39.3% in wheat and maize, respectively, at approximately 40% water reduction. As a matter of fact, depending upon the growth stage and the severity and duration of the water deficit period, yield losses can broadly range from 9% to 92% in wheat across different geographic locations, as reported by Mohammadi (2018) and Nezhadahmadi, Prodhan & Faruq (2013). If water is the only limitation, the upper limit of water productivity (i.e., the water-use efficiency) of rainfed wheat in dry environments is typically 20-22 kg ha^{-1} mm^{-1} (grain yield per water transpired), as shown by Passioura (2006) and Sadras & Angus (2006). Water is indeed an essential element of life.

In general, plants have evolved three major strategies to cope with water-limiting conditions (Blum, 2011a; Fang & Xiong, 2015; Hu & Xiong, 2014; Kooyers, 2015; Lefebvre et al., 2009; Levitt, 1980; Verslues, Agarwal, Katiyar-Agarwal, Zhu & Zhu, 2006; Verslues & Juenger, 2011) as follows: i) *Drought escape*: allows plants to adjust their life cycle to avoid stress; in other words, shortening life cycle to complete maturation before the environment becomes drier by altering the flowering time; ii) *Drought avoidance* (or *dehydration avoidance*): occurs when plants increase water-use efficiency (WUE) by reducing transpiration, limiting vegetative growth, or increasing root growth; so it is mostly characterised by the maintenance of high plant water potentials, which involves growth adjustments to minimise water loss and/or to optimise water uptake and so tolerating low internal potentials without excessive tissue dehydration; and iii) *Drought tolerance* (or *dehydration tolerance*): is defined as the plant's ability to function at low water availability; allows plants to survive and sustain a certain level of physiological activity through accumulation of osmoprotectants, antioxidants, and reactive oxygen species (ROS) scavengers. Nevertheless, this division in strategies is somewhat theoretical, and there is no clear cut since soil drying is a stochastic process. Plants might experience a variety of stress conditions leading to complex and mixed responses.

Crop root and shoot growth are intimately linked (Bingham, 2001; Vercruyssen, Gonzalez, Werner, Schmülling & Inzé, 2011), in a way that roots can sense soil moisture depletion and signal its status to the shoot, mediating adjustments in leaf growth and stomatal aperture, and finally aiming to conserve internal water content (Neumann, 2008). Both chemical and hydraulic signals are involved in this signalling mechanism, where the chemical ones (e.g.,

abscisic acid (ABA), cytokinins (CKs), a precursor of ethylene, malate and other unidentified factors) tend to predominate during early water deficit sensing stages, leading to reduced transpiration and decreased leaf growth (Schachtman & Goodger, 2008). These plant growth adjustments to environmental changes are driven by numerous cell wall modifying proteins, such as expansins, xyloglucan endotransglucosylase/hydrolases (XTHs), endo-β-1,4-glucanases (EGases), and pectin methylesterases (PMEs), which alter cell wall structure and properties, facilitating plant acclimation (Sasidharan, Voesenek & Pierik, 2011). Notably, drought-responsive phytohormones (e.g., ABA, CKs and ethylene; Wilkinson & Davies, 2010) are known to regulate expansins and XTHs (Cho & Cosgrove, 2010; Yokoyama & Nishitani, 2001). While shoot growth is inhibited, roots tend to keep elongating in water-limiting environments, probably as an adaptive strategy to exploit better the water stored in the soil matrix (Sasidharan et al., 2011; Vile et al., 2012). This improvement in root biomass is crucial but limited to some extent. As Bengough, McKenzie, Hallett & Valentine (2011) reviewed, the root elongation rate decreases in soil drying, by decreasing the soil matric potential (i.e., increasing water stress) there is a rapid increase in soil strength and, consequently, roots will encounter natural physical limitations to keep growing.

Apart from vegetative growth attenuation and transpiration reduction, many other biochemical and physiological processes are also drought-induced. Osmolyte accumulation (i.e., osmotic adjustment) under environmental stress, for instance, plays an essential role in protecting subcellular structures, as well as various proteins, lipids, and enzymes critical for the photosynthetic apparatus (Blum, 1996; Chaves & Oliveira, 2004; Gururani, Mohanta & Bae, 2015; Kapoor et al., 2020). In plants, the common osmoprotectants are proline, glycine betaine, mannitol, sucrose, trehalose, sorbitol, antioxidants (e.g., ascorbate, glutathione, tocopherols), late embryogenesis abundant (LEA) proteins, and others (Bartels & Sunkar, 2005; Seki, Umezawa, Urano & Shinozaki, 2007; Yang, Vanderbeld, Wan & Huang, 2010; Yordanov, Velikova & Tsonev, 2003). These metabolites accumulate and act as protectors and/or scavengers, helping plants acclimate, avoid and/or tolerate the unfavourable conditions. For example, sugars are essential signals in plant metabolism regulation and can induce leaf senescence under stress (Wingler & Roitsch, 2008). Moreover, as discussed by Munné-Bosch & Alegre (2004), drought-induced leaf senescence contributes to nutrient remobilisation and prevents excessive water loss via transpiration, mainly when leaf abscission follows, thereby improving the whole-plant water balance. As a matter of fact, as recently reviewed by Zhang, Zhao & Zhu (2020), plant regulatory networks for stress response and plant growth-control

pathways are in constant crosstalk at multiple levels, which is essential to ensure a balance between stress tolerance and crop productivity.

1.4 Phenotyping for Assessing Plant-Environment Interactions

Protecting, or even improving, crop yield under drought-prone environments is a core challenge for modern agriculture. Yield alone is a complex trait controlled by numerous genes, each with minor effects, functioning within networks strongly dependent on epistasis (gene-by-gene interaction), pleiotropy (one gene influencing multiple traits) and genotype-by-environment (G×E) interaction effects (Bernardo, 2008; Cooper, Podlich & Smith, 2005; Podlich, Winkler & Cooper, 2004;). From the genomics perspective, drought tolerance adds another layer of complexity for plant breeders (Blum, 2011b; Messina, Podlich, Dong, Samples & Cooper, 2011). Similar to yield trait, drought tolerance also displays quantitative inheritance (i.e., polygenic inheritance) affected by the environment, whose genetic complexity and architecture can be assessed through quantitative trait loci (QTL) analysis, for example (Araus, Slafer, Royo & Serret, 2008; Mohammadi, 2018; Reynolds & Langridge, 2016; Yadav et al., 2019; Yang et al., 2010). Linkage-based mapping and association mapping (e.g., genome-wide association study, GWAS) are methods commonly used for identifying QTLs, and so facilitating gene cloning, marker-assisted selection (MAS), and genomic selection or prediction (Sehgal, Singh & Rajpal, 2016; Verdeprado et al., 2018). In short, these are advanced statistical methods that link phenotypic data (trait measurements) and genotypic data (molecular markers). Therefore, meaningful genetic variation and accurate phenotypic data based on robust and reliable phenotyping methods are of great importance to identify genes and QTLs associated with agronomically important traits (e.g., grain yield and drought tolerance).

However, the challenge is to define one feature (plant trait) able to feasibly and realistically characterise the whole-plant modulation induced by drought. Spurious or weak associations between genotype and phenotype due to low-quality phenotyping methods might result in diminished genetic gains (Campos et al., 2011). Indeed, inappropriate plant phenotyping for drought tolerance has been regarded as one of the main causes of past difficulties towards plant breeding progress for water-limited environments (Blum, 2011). In fact, trait-based breeding and genetic dissection of drought tolerance have been fostered since the advent of the Passioura (1977) equation [grain yield = water used × water-use efficiency × harvest index]. Generally, the morphophysiological traits are categorised as constitutive (or non-adaptive; i.e., also expressed in non-limiting conditions) or drought-responsive (or

adaptive; i.e., expressed only in pronounced stress) (Blum, 1996, 1997; Tuberosa, 2012). Plant phenology, canopy architecture, root size and depth, photosynthetic capacity, carbon storage and utilisation, and yield potential are examples of constitutive traits, whereas osmotic adjustment, relocation of water-soluble carbohydrates, and ABA accumulation are examples of drought-adaptive traits. Regardless of such categories, drought is commonly measured by phenotyping specific and relevant attributes related to dehydration avoidance and dehydration tolerance (Blum, 2011). Symptoms of wilting (e.g. leaf rolling), stomatal conductance, leaf water potential, leaf relative water content (RWC), water-use efficiency (WUE), water uptake (WU), sap flow, osmoprotectant content, cell membrane stability (CMS), chlorophyll content, carbon isotope discrimination, root-shoot ratio, and leaf canopy temperature are only a few examples of traits from an extensive list of phenotyping protocols for quantifying and qualifying drought effects in crops (Araus, Slafer, Reynolds & Royo, 2002; Araus et al., 2008; Blum, 2011; Monneveux, Jing & Misra, 2012; Pask, Pietragalla, Mullan & Reynolds, 2012; Salekdeh, Reynolds, Bennett & Boyer, 2009; Tuberosa, 2012; Verslues et al., 2006). Even though incorporating these traditional phenotyping methods in conventional breeding pipelines has facilitated the release of drought-tolerant cultivars, most of these phenotyping approaches rely on destructive measures, often seen as time-consuming, laborious and costly (Ashraf, 2010; Furbank & Tester, 2011). Physiological phenotyping is mostly limited by detailed, sophisticated and usually complex and expensive methodologies (Ghanem, Marrou & Sinclair, 2015).

Attempts to exploit new molecular tools to their full potential, particularly to dissect the genetics of quantitative traits, such as yield and stress tolerance, are limited by our ability to quantify relevant traits with the necessary throughput (Araus & Cairns, 2014; Tuberosa, 2012). Indeed, novel low-cost high-throughput molecular '*omics*' (e.g., genomics, epigenomics, transcriptomics, proteomics, and metabolomics) approaches and knowledge have evolved exponentially faster than high-throughput 'plant phenomics', i.e., the measurement of structural and/or functional plant traits at scales from molecules to ecosystems (Campos, Cooper, Habben, Edmeades & Schussler, 2004; Furbank & Tester, 2011; Tardieu, Cabrera-Bosquet, Pridmore & Bennett, 2017). This mismatch between technologies may have hindered our biological understanding of the G×E interaction, especially for complex traits, ultimately leading to a 'genotype-phenotype gap' (Blum, 2011). As argued by Cabrera-Bosquet, Crossa, von Zitzewitz, Serret & Araus (2012) and Edmeades, McMaster, White & Campos (2004), the integration of high-throughput phenotyping with genotyping may shed light on the fundamentals of complex adaptive physiological traits. Actually, over the past decade,

significant investments and progress were made to improve the precision and throughput of plant phenotyping methods, aiming to bridge this gap between gene or genotype to phenotype. High-throughput plant phenotyping approaches mostly rely on remote sensing technologies, such as sensors and imaging systems, allowing the rapid, repeatable, reproducible, non-destructive and non-invasive acquisition of relevant qualitative and quantitative crop traits (Cendrero-Mateo et al., 2017; Granier & Vile, 2014; Normanly, 2012). Outstanding reviews have extensively covered the recent efforts, achievements and challenges regarding crop phenomics and high-throughput phenotyping in open fields and controlled environments (Fiorani & Schurr, 2013; Reynolds et al., 2020; Tardieu et al., 2017; Watt et al., 2020; Yang et al., 2020).

The most suitable set of sensors and techniques for monitoring a trait of interest will depend on the scientific objectives. According to Cendrero-Mateo et al. (2017) and Reynolds et al. (2020), the applicability and value of root and/or shoot phenotyping tools vary based on the target traits, whether morphoanatomical (e.g., phenology, architecture, structure) or physiological (e.g., WUE, transpiration, photosynthesis), and the scales (i.e., leaf, whole plant, canopy, large-scale fields, mega-environments, or ecosystems). Also, there are always trade-offs between precision, resolution, time, costs, and the number of genotypes or plots to be characterised (Reynolds et al., 2020).

High-throughput techniques allow breeders to investigate multiple traits in a large panel of genotypes under naturally fluctuating ambients and/or drought-induced stress (Berger, Parent & Tester, 2010; Cendrero-Mateo et al., 2017; Granier & Vile, 2014; Winterhalter, Mistele, Jampatong & Schmidhalter, 2011). Optimal phenotyping of photosynthetic traits in breeding for drought tolerance may require measurements at multiple scales (leaf to canopy) and phenological stages (Sanchez-Bragado et al., 2020). Undoubtedly, the simultaneous and continuous monitoring of water relations in the soil-plant-atmosphere continuum through high-throughput functional physiological phenotyping, as proposed by Halperin, Gebremedhin, Wallach & Moshelion (2017), is extremely valuable to the screening of drought-tolerant genotypes, aiding the physiological breeding (Gosa, Lupo & Moshelion, 2019; Negin & Moshelion, 2017; Reynolds & Langridge, 2016). Also, multi-trait plant phenotyping implies that a primary trait, such as grain yield, may be combined with secondary traits (i.e., any trait consistently exhibiting enough genetic variability, genetic correlation with yield, and greater heritability than yield itself), boosting crop breeding for higher yield and stability under drought conditions (Araus et al., 2002, 2008). Indeed, there are still substantial opportunities to explore selectable secondary traits for improving crop photosynthesis and yield through conventional

breeding (Richards, 2000). In line with this statement, using high-throughput phenotyping, Sun et al. (2017) reported an average improvement of 70% in genomic prediction for wheat grain yield when including secondary traits (canopy temperature and normalised difference vegetation index, NDVI). Similar improvements were also reported by Rutkoski et al. (2016). Additionally, combining high-throughput hyperspectral reflectance data (i.e., vegetation indices) with other agronomic traits benefited the prediction of biomass yield in winter rye hybrids (Galán et al., 2020). Under field terminal drought stress and using both aerial- and ground-based high-throughput phenotyping, Condorelli et al. (2018) identified QTLs for NDVI in durum wheat, which showed concomitant QTL effects on leaf chlorophyll content, leaf rolling and biomass. Altogether, high-throughput plant phenotyping is a powerful tool for unlocking complex traits' genetic basis under naturally varying environments.

Last but not least, data mining, analysis and interpretation arise as the critical next challenges following the latest technological advances in plant phenomics. As argued by Granier & Vile (2014), due to novel technologies, robust high-throughput acquisition of phenotypic and environmental data are no longer limiting factors to disentangle plant traits but rather statistical and mathematical modelling. In agreement with this view, Kissoudis, van de Wiel, Visser & van der Linden (2016) stated that integrating phenotypic and genotypic data fine-tuned with environmental variables by modelling approaches is critical to successful crop breeding for stress resilience. Breeding for yield and drought tolerance typically involves multi-environment trials (METs) to evaluate the relative performance of genotypes for a target population of environments (TPE; i.e. the set of conditions to which future-release genotypes might be subjected) and to unlock the G×E interaction (Chenu, 2015; Chenu et al., 2011). Hence, accurate environmental data collection is vital to a comprehensive assessment of 'confounding factors' in field trials, and so to clarify differences among genotypes (Reynolds et al., 2020). Therefore, closing the genotype-phenotype gap with phenomics will demand dynamic and advanced statistical strategies, including spatial and temporal modelling of environmental data, for improving the effectiveness of new phenotyping techniques (van Eeuwijk et al., 2019). In this context, Resende et al. (2021) recently introduced the concept of '*enviromics*', large-scale envirotyping data, applied to envirotypic-assisted selection in plant breeding (i.e., the study and integration of the environmental markers or attributes for genetic selection, allowing to exploit the G×E interaction patterns among locations). Hence, a broad and better comprehension of high-throughput phenotyping and genotyping involves integration with high-resolution environmental data, whose interpretation will rely on modern statistics.

1.5 Chlorophyll Fluorescence: An Integrative Photosynthetic Signal

Light energy absorbed by chlorophylls can (i) drive photosynthesis (photochemistry), (ii) be thermally dissipated, or (iii) be re-emitted as light (fluorescence), and these three processes coexist in competition (Figure 1.2; see details in Baker, 2008; Maxwell & Johnson, 2000; Stirbet, Lazár, Guo & Govindjee, 2020). Chlorophyll *a* fluorescence emanates from both Photosystem (PS) II and PSI, and at room temperature, it is mainly emitted by PSII at wavelengths between 650-780 nm, peaking at around 685-740 nm (Drusch et al., 2017). There has been a long-standing acknowledgement that ChlF-based parameters are powerful, inexpensive, fast, and non-invasive tools for probing photosynthesis and, therefore, for monitoring the physiological status of plants, even remotely (Baker, 2008; De Sousa, Hilker, Waring, De Moura & Lyapustin, 2017; Drusch et al., 2017; Fu, Meacham-Hensold, Siebers & Bernacchi, 2020; Govindjee, 2004; Kalaji et al., 2017; Krause & Weis, 1984, 1991; Mohammed et al., 2019; Murchie & Lawson, 2013; Pérez-Bueno, Pineda & Barón, 2019). The operating light use efficiency of PSII (F_q'/F_m'), for instance, has been demonstrated to be a reliable ChlF-derived parameter to monitor the linear electron transport (LET) from water through PSII and PSI, and consequently, provides a good relative measure of the quantum yield of CO_2 assimilation (ϕ_{CO_2}) in both C_3 and C_4 plants, when photorespiration is at a minimum (Genty, Briantais & Baker, 1989; Habash, Paul, Parry, Keys & Lawlor, 1995; Krall & Edwards, 1990). Biotic and abiotic stresses disturb this linear relationship due to concurrent electron-driven biological processes apart from CO_2 assimilation (Baker, 2008). However, even in harsh conditions, ChlF has proven to be a robust integrative technique for assessing plant photosynthetic performance (Baker & Rosenqvist, 2004; Kalaji et al., 2017; Pérez-Bueno et al., 2019; Wang et al., 2018).

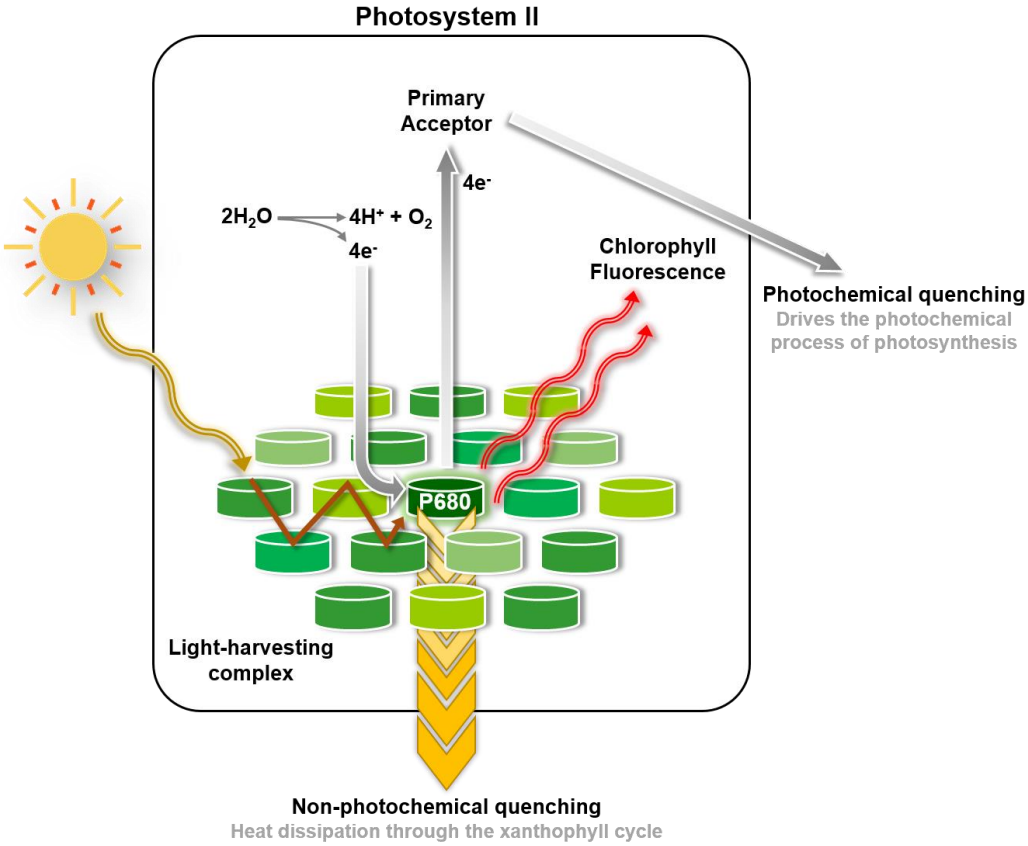

Figure 1.2. Photosynthesis is a core biological process by which plants utilise sunlight, water (H_2O), nutrients, and atmospheric carbon dioxide (CO_2) to produce energy-rich biomolecules and oxygen (O_2). Light-harvesting complex (LHC), a pigment-protein structure embedded in chloroplast thylakoid membranes, acts as an antenna, gathering sunlight. The photon's excitation energy is transferred to the reaction centre (P680) in the photosystem II (PSII). Then, through an intricate and highly regulated cascade of biophysical and biochemical interactions, the solar energy is stepwise converted into energy-storing molecules, such as adenosine triphosphate (ATP) and nicotinamide adenine dinucleotide phosphate (NADPH). If the absorbed light exceeds the photochemical quenching capacity, the surplus of energy in the RC may lead to photo-oxidative damage. Thus, the excess energy must dissipate through heat (i.e., a non-photochemical quenching, NPQ, via the xanthophyll cycle) and/or red-light re-emission (i.e., chlorophyll fluorescence). Adapted from De Sousa et al. (2017).

Due to technological advances, chlorophyll fluorometry techniques have rapidly evolved, and commercial instruments for measuring ChlF in plants have become available. Indeed, chlorophyll fluorometry developed into various types with different timescales of signal capturing where *in vivo* ChlF might be passively or actively acquired at both leaf and canopy scales (Aasen et al., 2019; Cendrero-Mateo et al., 2016). While passive techniques rely solely on solar irradiance to retrieve the fluorescence emission, active techniques stimulate fluorescence emission using dedicated light sources. In the last decades, several studies have taken advantage of the ChlF approach to assess the impact of water deficit on an extensive list

of plant species, ranging from native Mediterranean plants (e.g., rosemary and lavender) to various agricultural crops, including barley, wheat, rice, maize, beans, soybean, cotton, potato, and grapevine (Kao & Tsai, 1998; Longenberger, Smith, Duke & McMichael, 2009; Mathobo, Marais & Steyn, 2017; Nogués & Alegre, 2002; O'Neill, Shanahan & Schepers, 2006; Oukarroum, Madidi, Schansker & Strasser, 2007; Ranalli, di Candilo & Bagatta, 1997; Wada, Takagi, Miyake, Makino & Suzuki, 2019; Wang et al., 2012; Yan et al., 2017; Zivcak, Kalaji, Shao, Olsovska & Brestic, 2014). By far, the vast majority of the prior research relies on the pulse-amplitude modulation (PAM) fluorometry (Schreiber, 1986). This commonly used technique typically requires a dark-adaptation and/or a saturating flash in very close proximity, mostly done by clamping on leaves. However, such requirements can be time-consuming, have limited application at a distance, and are prohibitive in less accessible field locations (Cendrero-Mateo et al., 2017; Osmond et al., 2017). Hence, despite the advantages of using ChlF for monitoring plant physiological status, applying this method to a large number of experimental units growing in open fields, as is required for plant breeding programmes, is still challenging.

High-throughput phenotyping platforms (HTPPs) have been deployed to quantify ChlF and other traits to circumvent existing bottlenecks in phenotypic and genomic selection (e.g., Barbagallo, Oxborough, Pallett & Baker, 2003; Chen et al., 2014; Flood et al., 2016; Humplík et al., 2015; Jansen et al., 2009; McAusland, Atkinson, Lawson & Murchie, 2019; Tschiersch, Junker, Meyer & Altmann, 2017; Wang et al., 2018). Even though these approaches may successfully help to elucidate and dissect genetic variability in ChlF-based traits (e.g., Chen et al., 2014; Flood et al., 2016), these HTPPs are generally confined to operate under controlled or semi-controlled environments and restricted to detached leaves or small and medium-sized plants, and only a few are suitable for large plants (> 1.50 m). The 'Field Scanalyzer' is one of the very few examples of an automated fixed-site phenotyping platform that quantifies multiple plant traits, including ChlF through imaging, for high-throughput monitoring of field-grown crops (Virlet, Sabermanesh, Sadeghi-Tehran & Hawkesford, 2017). Indeed, HTPPs for measuring ChlF under natural fluctuating field conditions are hitherto scarce, although its importance for supporting crop improvement and plant breeding has been highlighted (Araus, Amaro, Voltas, Nakkoul & Nachit, 1998; Fu et al., 2020; Hamdani et al., 2019; Marcial & Sarrafi, 1996).

More recently, the LIFT fluorometer (Kolber et al., 2005) has emerged as an alternative high-throughput approach for continuous remote measurement of the photosynthetic status of terrestrial vegetation (Ananyev et al., 2005). The LIFT method monitors ChlF induction and relaxation within milliseconds using subsaturating excitation flashlets in a fast

repetition rate (FRR) instead of the saturating pulse (Kolber, Prášil & Falkowski, 1998). This pump-and-probe technique works at a distance, bridging the gap between leaf and canopy levels, and has demonstrated a great potential for monitoring agricultural systems (Pieruschka, Klimov, Kolber & Berry, 2010; Raesch, Muller, Pieruschka & Rascher, 2014; Rascher & Pieruschka, 2008). LIFT-measured ChlF empirically provides not only PAM-analogous photosynthetic parameters but also measures the downstream electron transport rates from the primary quinone acceptor (Q_A) to the plastoquinone (PQ) pool, and ultimately, towards PSI (Osmond, Chow, Pogson & Robinson, 2019; Osmond et al., 2017; Pieruschka et al., 2010). By monitoring the kinetics of LIFT-based electron transport rates over different timeframes beyond Q_A, Keller et al. (2019b) developed the Q_A^- reoxidation efficiency parameters ($F'_{r1;r2}$) for photosynthesis phenotyping. Using the LIFT method for automated plant phenotyping under semi-field conditions, Keller et al. (2019a) demonstrated that the ChlF-based parameters not only facilitated the understanding of photosynthetic interactions with varying environmental factors but also identified differences between and within crop species. Nevertheless, to the best of our knowledge, the LIFT approach has not yet been applied to large-scale field phenotyping of ChlF traits under natural fluctuating growing conditions.

1.6 Aim and Objectives

This research primarily aimed to assess the inherent genetic variation in photosynthetic traits at the canopy level in a large durum wheat panel (> 220 elite accessions) under progressive drought in the field over two growing seasons. The photosynthetic performance was measured using the LIFT method, by means of ChlF-based traits: F'_q/F'_m and the newly developed reoxidation efficiency parameters, F'_{r1} and F'_{r2}, which were slightly modified from Keller et al. (2019b). In particular, this study aimed (1) to estimate relevant population parameters (genotypic variation and heritability) for the LIFT-measured ChlF traits; (2) to evaluate the phenotypic plasticity of ChlF-related traits in response to drought; (3) to assess correlations between ChlF traits and other relevant plant traits (e.g., above-ground biomass and leaf relative water content); and (4) to assess the spatiotemporal effects of a fluctuating environment, in terms of light intensity, vapour pressure deficit (VPD), and their interactions with varying soil moisture, on ChlF traits.

In a second study, the LIFT sensor was combined with an existing automated high-throughput shoot phenotyping platform in a semi-controlled glasshouse for simultaneous and

continuous monitoring of water relations in the soil-plant-atmosphere continuum of potted plants growing under fluctuating ambient. The selected contrasting wheat genotypes, based on their maturity group and responses to drought stress, were employed to investigate drought-induced changes in the LIFT-measured ChlF traits over time, from early vegetative to reproductive stages. Besides monitoring whole-plant physiological status, the phenotypic correlations between ChlF-based traits and other plant traits (e.g., plant phenology, daily evapotranspiration rate, projected leaf area, total above-ground biomass, leaf area, and cell membrane stability) were also estimated. Moreover, the underlying roles of light intensity (i.e., photosynthetic photon flux density, PPFD) and VPD over the ChlF traits were investigated by statistical modelling.

2 MATERIALS AND METHODS

2.1 LIFT Device and Method

Active ChlF was measured by means of a portable LIFT instrument (model LIFT-REM 1.0, Soliense Inc., Shoreham, NY, USA; https://soliense.com/LIFT_Terrestrial.php), which is able to induce and record the resulting changes in the ChlF yield of a target leaf/plant canopy at a distance of up to 5 m. The LIFT apparatus relies on the fast repetition rate (FRR) fluorescence technique (Kolber et al., 1998), using high-frequency subsaturating excitation pulses, or 'flashlets', of a blue (λ 445 nm) light-emitting diode (LED) to manipulate the level of photosynthetic activity of PSII. A 685 nm ± 10 nm optical interference filter separates the red ChlF emission from the reflected excitation light. The system operates with a FRR fluorescence saturation/relaxation protocol with variable duty cycles. Firstly, during the saturation phase (SQ_A), at high duty cycle the primary quinone electron acceptor (Q_A) in PSII reduces progressively, leading to a transient increase in ChlF yield. Subsequently, during the relaxation phase (RQ_A), at exponentially decreasing duty cycle Q_A reoxidises, as electrons flow towards PSI, and the ChlF yield decreases. The number of flashlets, their energy and frequency are software-controlled to selectively activate different components of the photosynthetic machinery for real-time quantifying a range of biophysical features that govern the photosynthesis (Kolber et al., 2005; Osmond et al., 2017, 2019).

Throughout the different experiments performed in either field or greenhouse conditions, the Q_A flash reproduced the $FRRF_{0.75ms}$ protocol introduced by Keller et al. (2019b). According to this protocol, the SQ_A phase (lasting ~0.75 ms) consists of a sequence of 300

subsaturating flashlets (1.6 µs pulse length) applied at 2.5 µs discrete intervals. And the RQ_A phase (lasting ~209 ms) consists of 127 flashlets (1.6 µs pulse length) with an initial interval between flashlets of 20 µs followed by exponential increments. The exponent factor increases from 1.025 to 1.05, linearly over the length of the RQ_A sequence to best cover the temporal dynamics of the fluorescence relaxation signal. The excitation power of the Q_A flash was measured at 1% duty cycle using a 5-second calibration flash (a sequence of 50,000 flashlets with 1 µs pulse length at 100 µs intervals) measured by a quantum sensor (LI-190R, LI-COR, Inc., Lincoln, NE, USA).

Apart from the ChlF sensor, the LIFT device is also equipped with a Vis microspectrometer (STS-VIS, Ocean Optics, Inc., Winter Park, FL, USA) with an optical resolution of 1.5 nm (FWHM) for acquiring spectral bands within the 400 nm and 800 nm range from the target area. In both field experiments, the acquisition of a single spectral data was synchronized to be performed immediately after completion of a single LIFT Q_A flash with an integration time of 790 ms.

2.2 Fluorescence Parameters for Field Phenotyping

From the LIFT-measured ChlF transients, photosynthetic parameters are derived, such as functional and optical absorption cross-sections of PSII, time constants of electron transport, and non-photochemical quenching (Osmond et al., 2017, 2019; Wyber, Osmond, Ashcroft, Malenovský & Robinson, 2018). Some of these measures, though, may require a dark-adaptation period, or stable and controlled conditions to be reliably interpretable and comparable across samples. However, such requirements are rarely met when the target is to assess large populations in the field. To overcome this challenge, Keller et al. (2019a, 2019b) developed LIFT traits which are suitable for field phenotyping conditions. Hence, based on a slight modification of the procedure reported by Keller et al. (2019b), the LIFT-measured ChlF transients acquired by the Q_A flash protocol were here used to derive the photosynthetic traits. The PSII operating efficiency (F_q'/F_m') from light-adapted plants was estimated as $\left[\frac{F_m'-F'}{F_m'}\right]$, where F' is the ChlF yield of the first flashlet and F_m' is the maximum ChlF yield observed between flashlets 298th and 302nd inclusive (Figure 2.1).

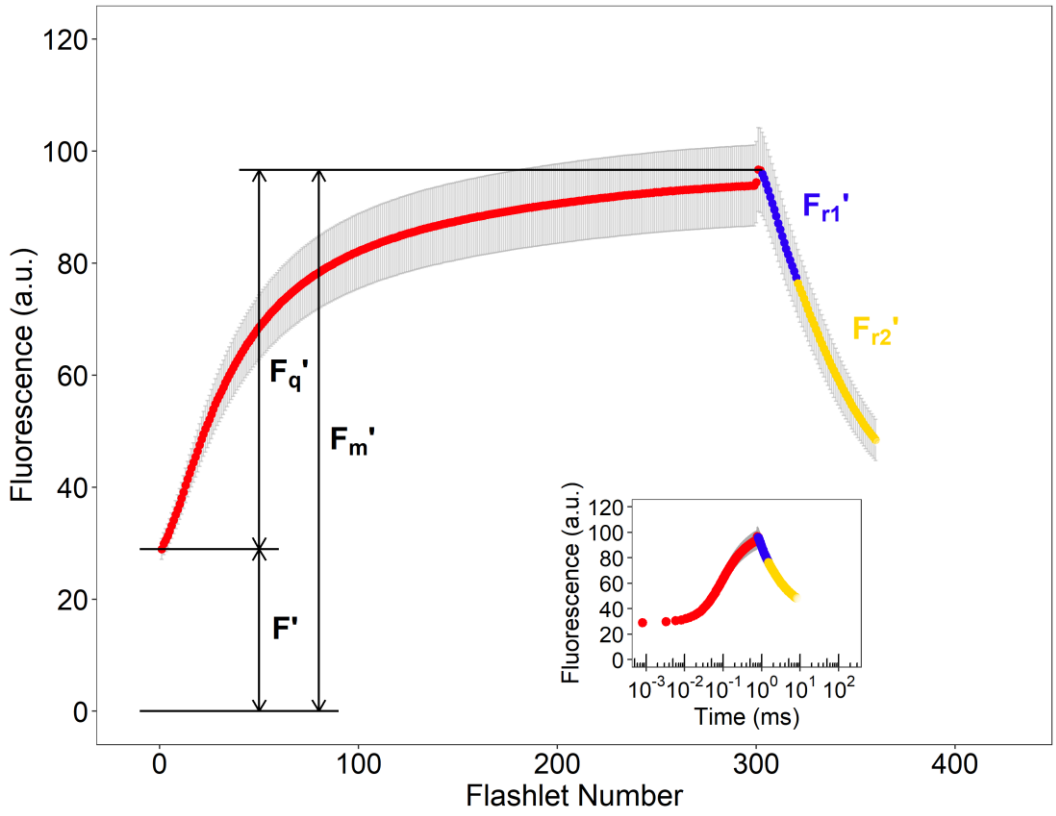

Figure 2.1. Schematic summary of a typical LIFT-measured chlorophyll fluorescence (ChlF) transient acquired by the Q_A flash protocol at the canopy level from a light-adapted plant, where F' is the ChlF yield of the first flashlet, F'_m is the maximum ChlF yield observed between flashlets 298th and 302nd inclusive, and F'_q is the difference between F'_m and F'. The saturation phase (SQ_A) is red highlighted and the relaxation phase (RQ_A) is blue (F'_{r1}) and yellow (F'_{r2}) highlighted. The kinetics of the ChlF relaxation was directly assessed by fitting log-log regression models for the time intervals of interest, namely F'_{r1} from 303rd to 320th flashlets (or from 0.82 ms to 1.44 ms), and F'_{r2} from 321st to 360th flashlets (or from 1.56 ms to 8.08 ms). The inset shows the same ChlF transient on a logarithmic time scale.

The Q_A^- reoxidation efficiency trait (F_r) is typically estimated by integrating the ChlF yield curve at a specific time interval and using the normalised integral area as a proxy for the slope of the ChlF transient to assess the kinetics of the relaxation phase (Keller et al., 2019a, 2019b). Herein, however, the kinetics was directly assessed by fitting log-log regression models for the time intervals of interest, namely t_1 from 0.82 ms to 1.44 ms (i.e., from 303rd to 320th flashlets) and t_2 from 1.56 ms to 8.08 ms (i.e., from 321st to 360th flashlets), where both variables, independent (time) and dependent (ChlF yield), were natural log-transformed. According to the power-law relationship in the form of $f(x) = \alpha x^{\beta}$, the slope and the constant of a straight line from a log-log model equal β and $\ln \alpha$, respectively (Marquet et al., 2005). Therefore, the efficiency of electron transport up to ~0.65 ms after reducing Q_A in light-adapted

plants (F'_{r1}) was estimated as the slope β of the log-log regression fitted within the t_1 interval, while the efficiency of electron transport up to ~6.64 ms after F'_{r1} (i.e., F'_{r2}) was equal to the slope β of the log-log model fitted within the t_2 interval (Figure 2.1). The time intervals t_1 and t_2 approximate the time frame in which electron transfer from Q_A to the plastoquinone (*PQ*) pool, and to some extent from the *PQ* pool to PSI, respectively (de Wijn & van Gorkom, 2001; Govindjee, 2004; Keller et al., 2019b; Kolber et al., 1998; Osmond et al., 2017, 2019; Stirbet & Govindjee, 2011). These time intervals are also supported by various *in silico* models (Lazár, 2003; Lazár & Jablonský, 2009; Stirbet & Strasser, 1995; Xin, Yang & Zhu, 2013; Zhu et al., 2005).

2.3 Field Experiments

2.3.1 Plant material

We evaluated in two growing seasons a set of elite durum wheat (*Triticum turgidum* L. ssp. d*urum* Desf.) accessions, mainly cultivars and advanced lines, from the association mapping population 'UNIBO-Durum Panel' assembled at the University of Bologna (UNIBO), Italy (see list of materials in Appendix 1). This panel contains a representative selection of the genetic diversity existing in the major improved durum wheat gene pools adapted to Mediterranean environments (Maccaferri et al., 2006, 2011). The collection includes 'founder genotypes' used extensively worldwide as parents in breeding programmes, as well as accessions bred and released by CIMMYT (the International Maize and Wheat Improvement Center), ICARDA (the International Center for Agricultural Research in the Dry Areas), INRAE (the French National Institute for Agriculture, Food and Environment), IRTA (the Spanish Institute of Agriculture and Food Research and Technology), and by public breeding programmes in Italy, in the Northern Great Plains of the USA and Canada (North Dakota, Montana, Saskatchewan and Alberta), and materials from the Southwestern USA, namely "Desert Durum®", a registered certification mark owned jointly by the Arizona Grain Research and Promotion Council and the California Wheat Commission. Recently, Condorelli et al. (2018) reported the occurrence of a strong population genetic structure in the UNIBO-Durum Panel, identifying eight distinct subpopulations, despite a considerable admixture mostly among germplasm from ICARDA, CIMMYT and Italy. These subgroups were also considered for further assessment in our study.

2.3.2 Field experimental design

Field experiments were conducted at the Maricopa Agricultural Center of the University of Arizona (33.07454°N, 111.97494°W, elevation 360 m) in Maricopa, AZ, USA, on a Casa Grande sandy loam soil (fine-loamy, mixed, superactive, hyperthermic Typic Natrargids) under a semi-arid low desert climate. In the first growing season 2017/2018 (Year 1 = Y1), a total of 252 accessions were planted on 28 November 2017, while in the subsequent season, 2018/2019 (Year 2 = Y2), 224 accessions were planted on 18 December 2018. In both trials, genotypes were sown in 2-row plots, 3.5 m long with 0.76 m between rows, with an average seeding rate of 16.8 seeds per meter, which were laid out in a resolvable row-column incomplete block design (α-design) (Patterson & Williams, 1976; Piepho, Williams & Michel, 2015) with two replicates (14 rows × 18 columns per rep) in Y1, and with three replicates (14 rows × 16 columns per rep) in Y2. Pre-plant granular nitrogen fertiliser at 112 kg ha^{-1} and phosphorus (P_2O_5) at 56 kg ha^{-1} were incorporated into the soil. Fields were managed following the standard agricultural practices for the region and were regularly monitored to prevent damage from above-ground insect pests and pathogens.

Sprinkler irrigation was used to germinate the seeds and establish the crop, followed by subsurface drip irrigation as needed for optimal plant growth, once or twice a week. The pressurised subsurface drip irrigation system was installed before planting when one dripline with emitters spaced every 0.30 m was buried at ~0.10 m depth along each seed row. In Y1, the final irrigation event was on 11 March 2018 (i.e., 103 days after sowing, DAS) when ca. 50% of the genotypes had their flag leaf sheath opened (i.e., at growth stage (GS) 47; Zadoks, Chang & Konzak, 1974). From this time point, the whole experiment was subjected to a progressive water deficit until 2-3 April 2018 when plants at the anthesis halfway stage (GS65, on average) were harvested to measure total above-ground biomass. By contrast, in Y2, on 5 March 2019 (77 DAS), when ca. 50% of the genotypes were at late tillering phase (GS26), well-watered (WW) and water-limited (WD) treatments were implemented and assigned to entire single seed rows in an alternating pattern across the whole field, such that the initial 2-row plots where split into two side by side subplots of one-row each (i.e., a strip-plot type design with water treatment as one main-plot factor). Due to operational limitations, the water treatment could not be randomised, and this alternating pattern of WW and WD strips was assigned to keep a homogeneous field. Control subrows remained well watered by regular subsurface drip irrigation, whereas water-stressed subrows experienced a progressive water deficit. Both water

treatments were imposed until 9 April 2019 (112 DAS) at early anthesis (GS61, on average) when the experiment was terminated and plots were harvested to determine total above-ground biomass.

2.3.3 Meteorological data and soil moisture monitoring

Daily and hourly meteorological reports for both growing seasons were obtained from the Arizona Meteorological Network (AZMET; https://cals.arizona.edu/azmet/06.htm). Also, high temporal resolution meteorological data, particularly air temperature, relative humidity and photosynthetic photon flux density (PPFD), for the experimental site were recorded at 5-second interval with an automated weather station (Clima Sensor US, Adolf Thies GmbH & Co. KG, Göttingen, Germany) and a quantum sensor (SQ-214, Apogee Instruments, Inc., Logan, UT, USA). These data were made available by the TERRA Phenotyping Reference Platform (TERRA-REF; https://terraref.org/). VPD was calculated as the difference between the saturation (e_s) and actual vapour pressure (e_a) (Allen et al., 1998). The saturation vapour pressure [kPa] was estimated as $\left\{e_s = 0.6108\, exp\left[\frac{17.27 \cdot T}{T+237.3}\right]\right\}$, where exp is 2.7183 (base of natural logarithm) and T is air temperature [°C]. The actual vapour pressure [kPa] was estimated as $\left[e_a = e_s \times \frac{RH}{100}\right]$, where e_s is the saturation vapour pressure [kPa] and RH is relative humidity [%].

In Y1, the volumetric water content (VWC) was monitored in and between seed rows with time-domain reflectometry (TDR) sensors (True TDR-315, Acclima, Inc., Meridian, ID, USA) installed at three locations within the experiment, and at 1 cm, 10 cm and 50 cm depths at each location. In Y2, the TDR sensors (True TDR-310S, Acclima, Inc., Meridian, ID, USA) were installed in both WW and WD seed rows at three locations within the experimental field at 2 cm, 10 cm, 25 cm and 50 cm depths, and at 15 cm and 35 cm depths, between seed rows. Additional soil sensors were installed between rows at 15 cm depth for measuring the soil matric potential (Tensiomark, ecoTech GmbH, Bonn, Germany). All soil sensors recorded data at 15-min intervals throughout the entire growing seasons. Based on characterisations of the soil hydraulic and physical properties of the experimental site by Prof. Dr. Markus Tuller at the University of Arizona (Tucson, AZ, USA) under the TERRA-REF project, the permanent wilting point (θ_{PWP}) and the field capacity (θ_{FC}) at 10-15 cm depth, based on the van Genuchten (1980) model, corresponded to approximately 0.110 $m^3\ m^{-3}$ and 0.282 $m^3\ m^{-3}$, respectively.

2.3.4 Leaf relative water content

The plant water status was monitored by leaf relative water content (RWC) as described by Mullan & Pietragalla (2012). In Y1, flag leaf samples from all plots (252 genotypes × 2 reps) were collected on 12 March 2018 (104 DAS), as the initial RWC ($iRWC$), and on 27 March 2018 (119 DAS), as the final RWC ($fRWC$). The relative change in RWC [%Δ] was calculated at the plot level as $\left[\Delta RWC = \frac{fRWC - iRWC}{iRWC} \times 100\right]$. In Y2, young fully expanded leaves from all plots of a single replicate (224 genotypes × 2 water treatments) were sampled on 26 March 2019 (98 DAS, and 21 days after imposing the irrigation treatments). Excised leaf samples were inserted into plastic tubes, sealed, placed in a cooled and insulated container, and immediately transferred to the laboratory. Fresh samples were weighted (FW) and then submerged in distilled water for 12 h at 4 °C in the dark. After rehydration, samples were quickly blotted dry with a paper towel, and the turgid weight (TW) was recorded. After oven-drying for three days at 60 °C, total dry weight (DW) was recorded. Leaf RWC [%] was then determined as the ratio $\left[RWC = \frac{FW - DW}{TW - DW} \times 100\right]$ (Barrs & Weatherley, 1962).

2.3.5 Plant height and above-ground biomass

Plant height was manually measured with a ruler as the distance from the soil surface to the base of the spike, or to the uppermost level of leaves in the absence of the spike. To reduce the influence of plot edge effects, median height was measured in the central portion of the plots. In Y1, plant height was recorded only once at 122 DAS, whilst multiple measurements over time (82, 93, 101 and 107 DAS) were taken in Y2.

Plants were harvested prior to the ripening stage to allow for planting the next phenotyping experiment, and therefore biomass data indicate the status at a point in time rather than direct estimates of final yields. In Y1, at the end of the experiment (125-126 DAS), plants within the 2-row plots were cut with a mechanical forage harvester (Carter Manufacturing Company, Inc.) for above-ground whole plot weights, while subsamples for moisture content [%] were hand-cut prior to mechanical harvesting for measurements of fresh weight and dry weight after oven-drying for 2-3 days. Total shoot dry matter yield (SDMY) was adjusted to 0% moisture and is reported as [kg ha^{-1}]. In Y2, the experiment was ended at 112 DAS, and SDMY was obtained for two replicates by hand-cutting lengths of 0.914 m of plants from each

single-row plot (WW and WD), which were bundled and placed into large driers until a constant mass was achieved.

2.3.6 LIFT measurements in the field

The LIFT instrument was installed to the front end of a cart (model based on White & Conley, 2013) in the vertical direction pointing downward (nadir) and above the plant canopy, perpendicular to the crop row (Figure 2.2). The distance from the LIFT lens to the median uppermost-canopy (i.e., the target area) was ~0.60 m, being regularly adjusted as plants grew. The blue LED light beam was ~30 mm in diameter at the focal point over the target area. Aiming to operate with an optimal signal-to-noise ratio, the gain of the fluorescence channel was adjusted at the beginning of each day of measurement in order to maintain the raw fluorescence within 2000-20000 signal range. At a distance of 0.60 m, the average excitation power for the SQ_A phase was ~72000 µmol photons m^{-2} s^{-1} in Y1 and ~55000 µmol photons m^{-2} s^{-1} in Y2.

The cart was manually pushed across the plots at an average speed of 8 cm s^{-1} while a total of 20 independent measurements, each one carried out in a time frame of ~1 s (ChlF transient in ~210 ms followed by reflectance data in 790 ms), were acquired from every experimental unit per day of measurement. In Y1, the entire field trial (252 genotypes × 2 reps) was measured at 0, 1, 2, 3, 4, 5, 6, 8, 10, 12 and 16 days after withholding water (DAWW). On average, measurements were performed between 09:20-16:40 hours local Mountain Standard Time (MST). In Y2, aiming to achieve three different levels of drought severity between WW and WD (D1, D2 and D3), field data were collected at three time points after imposing water treatment. However, due to the size of the trial (224 genotypes × 2 treatments × 3 replicates), only one replicate per day was operationally possible between 08:45-15:55 hours MST, on average. Thus, three consecutive days were required to phenotype the entire experiment with three replicates: D1 was taken between 12 and 14 days after imposing water treatment, D2 between 17 and 19 days, and D3 between 23 and 25 days.

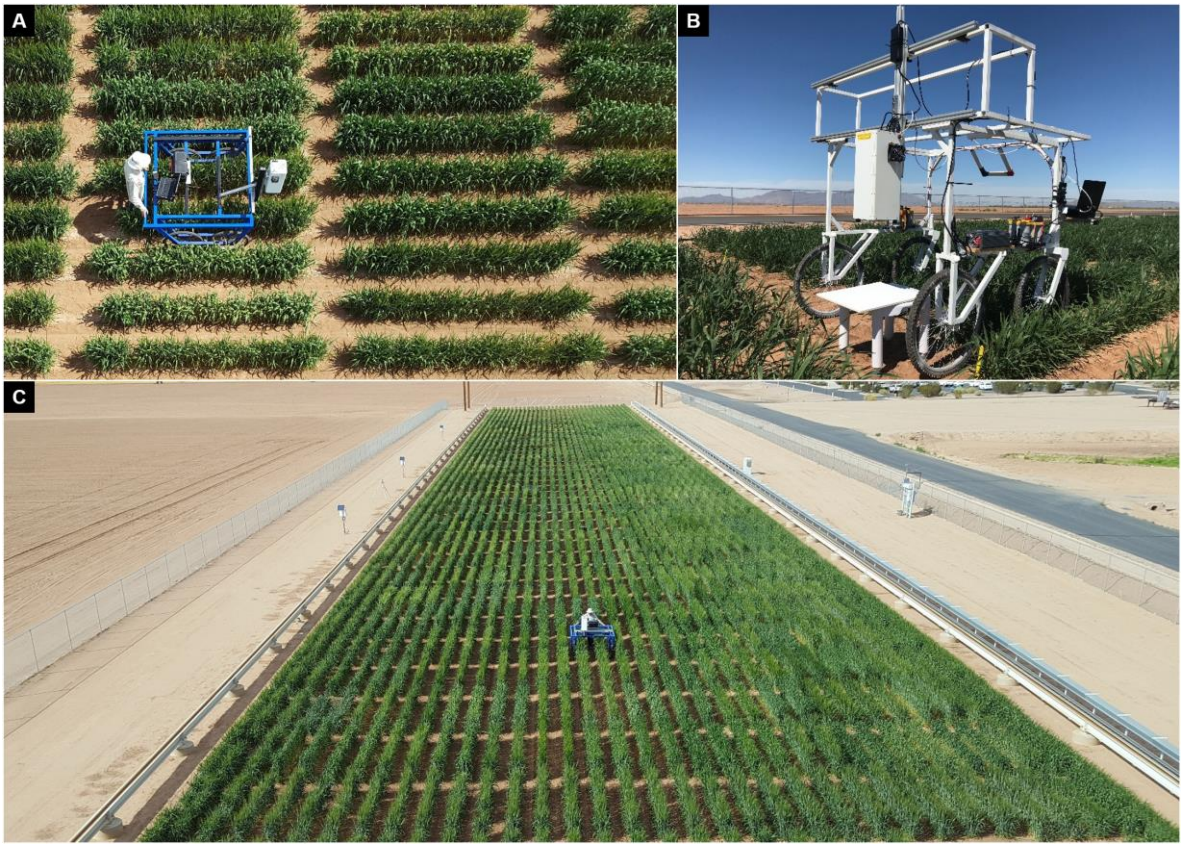

Figure 2.2. The LIFT apparatus was installed to the front end of a cart in the vertical direction pointing downward and above the plant canopy (~0.60 m distant from the median uppermost-canopy). **(A)** Top view of the default setting of the LIFT sensor mounted on a cart in the growing season 2017/2018 (Y1). **(B)** Left side view of the default setting in the growing season 2018/2019 (Y2). The spectral data were calibrated by a white reference panel (95% reflectance) horizontally placed at 0.60 m in front of the LIFT lens. **(C)** The cart was manually pushed across the field while a total of 20 independent measurements were acquired from every plot per day of measurement. Overall view of the field experiment carried out in Y1 in Maricopa, AZ, USA, under a semi-arid low desert climate.

Regardless of the growing season, the day of measurement and the time of day, the front end of the cart was always facing south, in order to avoid self-shadowing over the target area. In Y1, all LIFT data were only taken in the western subplot row within the 2-row plots. The cart was manually pushed from north to south along the rows, one at a time, and from west to east within each replicate separately. Replicate two was collected from early mornings up to midday and replicate one from midday up to late afternoons with a ~30-min break between replicates (see Appendix 2 – Figure A.2.1). In Y2, LIFT data were taken in all the 1-row plots by following a zigzag path within each replicate. Pushing the cart forwards from north to south a WD subrow was measured and, immediately after, when pulling it backwards from south to north, the neighbouring WW subrow was collected. This pattern moved from west (early

mornings) to east (late afternoons) with a ~40-min break at around midday when half of a replicate was done (see Appendix 2 – Figure A.2.2).

The spectral data were calibrated by a 0.50 m × 0.50 m white reference panel with 95% reflectance (Zenith Lite™ diffuse target, SphereOptics GmbH, Herrsching, Germany) horizontally placed at 0.60 m in front of the LIFT apparatus (Figure 2.2B). Over the course of a field phenotyping day, white reference measurements were regularly taken every 36 plots (~30 min interval) in Y1 and every 32 plots (~25 min interval) in Y2. Dark reference measurements were acquired in a dark room with the LIFT lens covered with a dark cloth.

2.3.7 Spectral reflectance data

The calibrated reflectance was estimated by normalising the target spectrum against the dark and white references. Thus, plant canopy reflectance (%) at 1 nm interval from 400 nm to 800 nm was calculated as $\left[\frac{DN_{raw}-DN_{dark}}{DN_{white}-DN_{dark}}\right]$, where DN_{raw} is the raw digital value of the target, DN_{dark} is the dark reference measurement, and DN_{white} is the white reflectance measurement (Bruning, Berger, Lewis, Liu & Garnett, 2020).

Red edge-based vegetation indices have been shown as useful indicators of leaf area index (LAI), leaf and canopy chlorophyll content, and plant water content (Bruning et al., 2020; Filella & Peñuelas, 1994; le Maire, François & Dufrêne, 2004; Liu, Miller, Haboudane & Pattey, 2004a; Liu et al., 2004b; Mutanga & Skidmore, 2007). Also, they are less sensitive to background conditions, leaf angle and stacking, and saturation due to dense vegetation (Dong et al., 2019; Katsoulas et al., 2016; Vogelmann, Rock & Moss, 1993). Therefore, the Vogelmann red edge index (VOGREI) was derived from the calibrated spectrum reflectance as the ratio $\left(\frac{\lambda\ 740\ nm}{\lambda\ 720\ nm}\right)$ (Vogelmann et al., 1993).

2.3.8 LIFT data cleaning

The LIFT sensor relies on its artificial excitation light source to induce ChlF emission from the target canopy, and a ChlF transient, such as in Figure 2.1, is only possible in the presence of living photosynthetic tissues. However, due to the highly fluctuating environment, particularly solar irradiation and winds, shifting of the leaves, off-target measurements (e.g., soil), and/or technical constraints, low-quality data can occur. Hence, a data cleaning pipeline was defined and implemented in the R environment (R Core Team, 2020).

In Y1, a total of 110,880 ChlF transients and spectral data were collected over time. Data were assessed and discarded in accordance with the following: i) data points acquired with signal-to-noise ratio < 40; ii) F'_q/F'_m values outside the 0-1 range; iii) the adjusted coefficient of determination (R^2_{adj}) from the log-log model at t_1 (for F'_{r1}) was < .95 for data collected between 0 and 6 DAWW, < .9025 for data collected at 8 and 10 DAWW, or < .81 for data at 12 and 16 DAWW; and iv) R^2_{adj} from the log-log model at t_2 (for F'_{r2}) was < .90 for data collected between 0 and 6 DAWW, < .85 for data collected at 8 and 10 DAWW, or < .80 for data at 12 and 16 DAWW. A high R^2_{adj} ensures that only reasonably formed ChlF transients (i.e., showing typical relaxation stages as close as possible to the schematic shown in Figure 2.1) are kept in the datasets. After performing the previous steps, outliers at plot level per day of measurement for each trait (ChlF and VOGREI) were detected and removed based on the Tukey's boxplot method by using 1.5 times the interquartile range (IQR) (Sim, Gan & Chang, 2005), as implemented in the base package *grDevices* (R Core Team, 2020). As F'_q/F'_m, F'_{r1} and F'_{r2} are derived from the same transient, in the case of an outlier, none of the ChlF traits for that particular transient was considered for further analysis. Finally, after data cleaning, the remaining data points, 100,947 (91%) ChlF transients, were averaged, resulting in one value per trait per plot per time of measurement (N = 5544 data points per trait).

In Y2, a total of 80,640 ChlF transients and spectral data were collected over time. Data were assessed and discarded as follows: i) data points acquired with signal-to-noise ratio ≤ 100; ii) F'_q/F'_m values outside the 0-1 range; and iii) R^2_{adj} from the log-log models at t_1 (for F'_{r1}) and t_2 (for F'_{r2}) were < .95 and < .90, respectively, regardless of timing. Then, outliers for each trait (ChlF and VOGREI) were detected and removed at plot level per day of measurement in the same way as done in Y1. Lastly, after data cleaning, the remaining data points, 77,946 (97%) ChlF transients, were averaged, resulting in one value per trait per plot per time of measurement (N = 4032 data points per trait).

The processed and cleaned datasets, as well as the raw data for both growing seasons, are publicly accessible (DOI: 10.5281/zenodo.4305673).

2.3.9 Phenotypic plasticity across genotypes

The phenotypic plasticity of a given genotype for a ChlF trait in Y1 was based on the overall drought-induced relative change (%Δ), being estimated as $\left[\frac{ChlF_{final}-ChlF_{initial}}{ChlF_{initial}} \times 100\right]$,

where $ChlF_{initial}$ is the mean value of genotype i for a ChlF trait (F_q'/F_m', F_{r1}' or F_{r2}') at 0 DAWW (non-stress), and $ChlF_{final}$ is the mean value of genotype i for a ChlF trait at 16 DAWW (severe stress).

2.3.10 Spatial-temporal statistical analysis

A linear mixed model (LMM) approach was used to analyse the resolvable row-column incomplete block design experiments with repeated measures for both Y1 and Y2 growing seasons. Single-stage analysis models were applied to partition variance components and to estimate genotypic effects for all traits based on 'Best Linear Unbiased Prediction' (BLUP) (Robinson, 1991). A standard LMM is defined as $\boldsymbol{y} = \mathbf{X}\boldsymbol{\beta} + \mathbf{Z}\boldsymbol{u} + \boldsymbol{\varepsilon}$, where $\boldsymbol{y}$ is an n-vector of observations, $\boldsymbol{\beta}$ is the p-vector of parameters for fixed effects, $\mathbf{X}$ is an $n \times p$ indicator-variable matrix for fixed effects, $\boldsymbol{u}$ is the q-vector of random effects assumed to be distributed as $\boldsymbol{u} \sim N(\mathbf{0}, \boldsymbol{G})$, that is, normally distributed with mean zero and variance-covariance matrix $\boldsymbol{G}$, $\mathbf{Z}$ is an $n \times q$ indicator-variable matrix for random effects, and $\boldsymbol{\varepsilon}$ is a random residual vector assuming $\boldsymbol{\varepsilon} \sim N(\mathbf{0}, \boldsymbol{R})$. The distribution of observed data is assumed to be $\boldsymbol{y} \sim N(\mathbf{X}\boldsymbol{\beta}, \boldsymbol{V})$, where $\boldsymbol{V} = \mathbf{Z}\boldsymbol{G}\mathbf{Z}^{\boldsymbol{T}} + \boldsymbol{R}$.

Positive-constrained variance components for each phenotypic variable (trait) were estimated in the LMM by residual maximum likelihood (REML) using the Average Information (AI) algorithm with sparse matrix methods (Gilmour, Thompson & Cullis, 1995), as implemented in GENSTAT (VSN International, 2019).

In Y1, a LMM for each phenotype trait measured in a single day was defined as

$$\gamma = R : G + ROW + R \cdot ROW + R \cdot COL + \underline{R \cdot ROW \cdot COL}, \qquad [1]$$

where γ is the vector of observed phenotype, G stands for the genotypes, R the replicates, ROW the rows, COL the columns, and the underscored term ($R \cdot ROW \cdot COL$ in this case) is the residual error effect (ε) associated with the observation γ. All models were herein outlined according to the syntax described in Piepho, Büchse & Emrich (2003), where the dot operator ($\cdot$) specifies crossed effects ($A \cdot B$), the crossing operator ($\times$) defines a full factorial model ($A \times B = A + B + A \cdot B$), and the nesting operator ($/$) describes that a factor B is nested within another factor A ($A/B = A + A \cdot B$). Fixed and random terms are separated by a colon ($:$), listing fixed effects first. Model [1] takes all factors except R as random, and was used to

fit SDMY and ΔRWC; both traits were log-transformed. Also, one- and two-dimensional spatial analyses were performed at the residuals by fitting covariance structures (Payne, Welham & Harding, 2019; Wolfinger, 1993), such as autoregressive (AR), moving average (MA), autoregressive moving average (ARMA) or linear variance (LV), for modelling correlations among the neighbouring experimental units along rows and columns. For BLUEs ('Best Linear Unbiased Estimator') estimation, G factor was fitted as fixed in the model [1].

Repeated measures were incorporated into the model [1] as proposed by Piepho, Büchse & Richter (2004). Hence, the single-stage baseline model (BL) which considers the entire observed data in Y1 in one stage at the level of individual plots was defined as

$$\gamma = R \times T : G/T + ROW/T + (R \cdot ROW)/T + (R \cdot COL)/T + R \cdot ROW \cdot COL + \underline{R \cdot ROW \cdot COL \cdot T}, \quad [2]$$

where T is time points (i.e., days after withholding water), the repeated factor. On top of the model [2], covariates were also included and the full baseline model (BL_{Cov}) for Y1 was defined as

$$\gamma = R \times T + RelF + iZDS + VOGREI + PPFD \times VPD : VOGREI \cdot T + G/T + ROW/T + (R \cdot ROW)/T + (R \cdot COL)/T + R \cdot ROW \cdot COL + \underline{R \cdot ROW \cdot COL \cdot T}, \quad [3]$$

where $iZDS$ is the initial growth stage in the Zadoks scale measured two days before withholding water, $VOGREI$ the Vogelmann red edge index, $PPFD$ the photosynthetic photon flux density, VPD the vapour pressure deficit, and $RelF$ is the relative deviation of the target area from the focal point of the LIFT light beam set at 0.60 m, calculated as $\left[\frac{LIFT_{height} - PH}{60}\right]$, where $LIFT_{height}$ is the distance from the soil surface to the LIFT lens [cm] and PH is the plant height [cm]. $RelF$ and $iZDS$ were time-constant covariates, whilst $VOGREI$, $PPFD$ and VPD were time-varying covariates. Model [3] was used to fit F_q'/F_m', F_{r1}' and F_{r2}'. Besides the spatial modelling of trends along rows and columns, temporal correlation structures (Littell, Pendergast & Natarajan, 2000; Payne et al., 2019), such as compound symmetry (CS), banded Toeplitz (BAND), power (POW), ante-dependence (ANTE), unstructured (UN) or general correlation (COR), with equal or unequal variances were also fitted to the residuals to accommodate trends over time due to multiple observations on the same experimental unit. Modelling of serial correlation was also extended to $G \cdot T$ in order to assess genetic correlations

for the same trait across time, allowing for heterogeneity of genetic variances. For estimating BLUEs for each time point, G/T were fitted as fixed in the model [3].

In Y2, a LMM for each phenotype trait measured in each time point after imposing water treatment was defined as

$$\gamma = TRT + R : G/TRT + ROW/SUB + R \cdot ROW + R \cdot COL + R \cdot ROW \cdot COL + R \cdot ROW \cdot SUB + \underline{R \cdot COL \cdot ROW \cdot SUB}, \quad [4]$$

where TRT is the water treatment and SUB the subrows. Model [4] was used to fit SDMY, which was log-transformed. For estimating BLUEs within each water treatment, G/TRT were fitted as fixed in the model [4].

For assessing the differences among levels of drought severity, repeated measures were incorporated into the model [4]. Therefore, the BL model, which considers the entire observed data in Y2 in one stage at the level of individual plots, was defined as

$$\gamma = (TRT + R) \times T : G/T + (G \cdot TRT)/T + ROW/T + (ROW \cdot SUB)/T + (R \cdot ROW)/T + (R \cdot COL)/T + (R \cdot ROW \cdot COL)/T + (R \cdot ROW \cdot SUB)/T + R \cdot COL \cdot ROW \cdot SUB + \underline{R \cdot COL \cdot ROW \cdot SUB \cdot T}, \quad [5]$$

where T is time points after imposing water treatment (i.e., the levels of drought severity), the repeated factor. Taking into account the fluctuating environment during the measurements, covariates were also added as fixed in the model [5] and so the BL_{Cov} model for Y2 was defined as

$$\gamma = (TRT + R + RelF + ZDS + VOGREI) \times T + (RelF + ZDS + VOGREI + PPFD \times VPD) \times TRT : G/T + (G \cdot TRT)/T + ROW/T + (ROW \cdot SUB)/T + (R \cdot ROW)/T + (R \cdot COL)/T + (R \cdot ROW \cdot COL)/T + (R \cdot ROW \cdot SUB)/T + R \cdot COL \cdot ROW \cdot SUB + \underline{R \cdot COL \cdot ROW \cdot SUB \cdot T}, \quad [6]$$

where ZDS is the growth stage in the Zadoks scale. $RelF$, ZDS, $VOGREI$, $PPFD$ and VPD were time-varying covariates. Model [6] was used to fit F_q'/F_m', F_{r1}' and F_{r2}' in Y2. Modelling of spatiotemporal (STM) correlations was also performed at the residuals, only. For

estimating BLUEs within each water treatment and across time points, G/T and $(G \cdot TRT)/T$ were fitted as fixed in the model [6].

In all models, covariates were mean centred, except $RelF$ which was centred to 1 (i.e., target area at a distance of 0.60 m). $PPFD$ and VPD were also log-transformed and fitted to BL_{Cov} models to evaluate whether a nonlinear relationship with the ChlF traits would improve model fit.

Comparison between candidate models was assessed by the REML-likelihood ratio test (REMLRT), provided that the two models being compared were nested and had the same fixed effects model (Galwey, 2014). Otherwise, when models were non-nested, yet with the same fixed effects, the Akaike Information Criterion (AIC) was used to assess their goodness-of-fit, judged by the 'smaller the better' form of the criterion (Cheng, Edwards, Maldonado-Molina, Komro & Muller, 2010). The adjusted R^2-like statistic for the final 'best' LMM was estimated based on the average semivariance approach (Ω_{β}^{ASV}), as proposed by Piepho (2019). Conditional *F*-test statistic was used to test fixed effects. The Fisher-Hayter procedure, a modified LSD (MLSD) test using the Studentized Range statistic (Hayter, 1986), was used to perform pairwise comparisons between adjusted means.

The impact of adding covariates (BL_{Cov}) and modelling the spatiotemporal correlations ($BL_{Cov+STM}$) was evaluated by means of relative efficiency (RE) in terms of the size of the error. Thus, RE was used to assess the improvement in precision of the alternative models over the BL models [2] and [5] (i.e., models without covariates and/or spatiotemporal covariance structures) for seasons Y1 and Y2, respectively. The RE (%) was calculated as suggested by Qiao, Basford, DeLacy & Cooper (2000) and can be defined as $\left(\frac{SED_{BL}}{SED_{AT}} \times 100\right)$, where SED is the REML-based average standard error of the difference between genotype means for the baseline model (SED_{BL}) and for the alternative models (SED_{AT}). The higher the RE estimate, the better the precision of the field evaluation of genotypes.

2.3.11 Heritability and trait correlation estimation

Broad-sense heritability on an entry-mean basis (H^2), or repeatability, of a trait for a single time point was estimated according to Cullis, Smith & Coombes (2006) as

$$H^2 = 1 - \frac{\bar{v}_{\Delta\cdot\cdot}^{BLUP}}{2\sigma_g^2},$$

where $\bar{v}_{\Delta..}^{BLUP}$ is the mean variance of a difference of two BLUPs for the genotypic effect and σ_g^2 is the genotypic variance.

Bivariate LMM (see details in Piepho, 2018; Piepho & Möhring, 2011) were used to estimate genetic correlations between each pair of traits (e.g., between ChlF traits and SDMY or ΔRWC) in each time point. Assuming $\gamma = \begin{bmatrix}\gamma_1 \\ \gamma_2\end{bmatrix}$ as the response vector of observed phenotype for the trait k ($k = 1, 2$), the bivariate model for a single time point was defined as

$$\gamma = TRAIT + R \cdot TRAIT : G \cdot TRAIT + ROW \cdot TRAIT + R \cdot ROW \cdot TRAIT + R \cdot COL \cdot TRAIT + \underline{R \cdot ROW \cdot COL \cdot TRAIT}, \quad [7]$$

where $TRAIT$ stands for the traits of interest. Model [7] was used to assess the correlation between SDMY and ΔRWC traits in Y1. Covariates were also accommodated to the bivariate models for assessing the genetic correlations between each ChlF trait and SDMY or ΔRWC in Y1 as

$$\gamma = Z \cdot RelF + Z \cdot iZDS + Z \cdot VOGREI + Z \cdot (PPFD \times VPD) + TRAIT + R \cdot TRAIT : G \cdot TRAIT + ROW \cdot TRAIT + R \cdot ROW \cdot TRAIT + R \cdot COL \cdot TRAIT + \underline{R \cdot ROW \cdot COL \cdot TRAIT}, \quad [8]$$

where Z is a quantitative variable, being set to $Z = 0$ when $TRAIT =$ SDMY or ΔRWC, and to $Z = 1$ when $TRAIT = F_q'/F_m'$, F_{r1}' or F_{r2}'.

Coefficients of genotypic correlation between pairs of traits were estimated as

$$\rho_g = \frac{\sigma_{g_1 g_2}}{\sqrt{\sigma_{g_1}^2 \times \sigma_{g_2}^2}},$$

where $\sigma_{g_1 g_2}$ is the genetic covariance between two traits, $\sigma_{g_1}^2$ and $\sigma_{g_2}^2$ are the genotypic variances of both traits under analysis; such variance-covariance components were estimated through the random $G \cdot TRAIT$ effect in the model [7] or [8]. The REML estimate of ρ_g is denoted as r_g. The REMLRT was used to estimate the significance of the genetic correlations by comparing the model with varying genetic covariance between the two traits and the model with the genetic covariance fixed to zero.

Coefficients of phenotypic correlation r_p between traits across time points and within traits over time were calculated from the BLUE of genotypes by Pearson's coefficients of correlation.

2.4 GREENHOUSE EXPERIMENT

2.4.1 Plant material

This greenhouse study was performed using ten wheat genotypes: eight durum wheat (*Triticum turgidum* L. ssp. *durum* Desf.) accessions, a subset of the association mapping population 'UNIBO-Durum Panel' assembled at the University of Bologna (UNIBO), Italy; and two common wheat (*Triticum aestivum* L.) accessions, namely MGS Brilhante and PF020037, which are commercial cultivars adapted to rainfed environments (Soares et al., 2021) and were released by public breeding programmes in Brazil.

Table 2.1. The subset of durum wheat accessions from the UNIBO-Durum Panel included in the greenhouse experiment. The mean growth stage, according to Zadoks et al. (1974), at 121 days after planting (18 days after withholding water), and the respective mean drought-induced relative change in leaf relative water content (ΔRWC) from a previous field experiment performed during the growing season 2017/2018 (Y1) in Maricopa, AZ, USA.

UNIBO Panel Code	**Accession Name**	**Origin**[†]	**Growth Stage**	**ΔRWC (%)**
DP_140	Gezira 17	ICARDA	50	-16.3
DP_242	Colorado	Desert Durum®	53	-15.1
DP_079	Arcangelo	Italy	65	-32.1
DP_119	Ainzen 1	ICARDA	68	-30.2
DP_213	Semperdur	Australia	72	-27.3
DP_116	Westbred 881	Desert Durum®	74	-17.9
DP_033	Bolenga	IRTA	75	-36.5
DP_041	Gallareta	IRTA	77	-41.1

[†]International Center for Agricultural Research in the Dry Areas (ICARDA); Spanish Institute of Agriculture and Food Research and Technology (IRTA); materials from the Southwestern USA, namely "Desert Durum®", a registered certification mark co-owned by the Arizona Grain Research and Promotion Council and the California Wheat Commission.

In order to have a representative sample of the biological diversity observed within the UNIBO-Durum Panel, the durum wheat genotypes were selected according to their maturity group and contrasting responses to drought stress by means of relative change in leaf relative water content (ΔRWC), see Table 2.1. These phenotypic data were based on the field experiment previously carried out during the growing season 2017/2018 (Y1) in Maricopa, AZ, USA.

2.4.2 Greenhouse experimental design

The genotypes were evaluated in a pot experiment under the automatic ScreenHouse shoot phenotyping platform (Nakhforoosh, Bodewein, Fiorani & Bodner, 2016) at the Institute of Bio- and Geosciences, Plant Sciences (IBG-2), Forschungszentrum Jülich GmbH (50.90976°N, 6.41313°E, elevation 100 m), in Jülich, Germany. The experiment was set up in a factorial completely randomised design (CRD) with 6 replicates for each genotype and water treatment (i.e., well-watered, WW, and water-limited, WD). In total, there were 120 pots (10 genotypes × 2 water regimes × 6 reps). After each measurement, the pots were automatically re-randomised via a laser positioning system and a robotic crane to avoid systematic spatial bias within the greenhouse.

Single seeds were sowed in plastic germination trays on 04 September 2018. Uniformly emerged seedlings at the one-leaf stage (BBCH scale = 11; Lancashire et al., 1991) were then individually transplanted to 5 L plastic pots (23 cm × 17 cm) containing a peat-sand-pumice substrate (Dachstaudensubstrat SoMi 513; Hawita Gruppe GmbH, Vechta, Germany). According to the physical analysis performed by LUFA NRW, Landwirtschaftskammer Nordrhein-Westfalen (Münster, Germany), on 29 June 2018, the dry bulk density (ρ_d) of the substrate was 644 kg m^{-3}. Moreover, based on the characterisation of the substrate water retention curve performed at the Institute of Plant Nutrition and Soil Science, Kiel University (Kiel, Germany) in 2013, the permanent wilting point (θ_{PWP}; at matric potential, ψ_m = -15000 hPa) and the field capacity (θ_{FC}; ψ_m = -100 hPa), derived from the van Genuchten (1980) model, corresponded to approximately 0.129 m^3 m^{-3} and 0.313 m^3 m^{-3}, respectively. The plant available water (PAW), therefore, estimated as the substrate volumetric water content (θ_v) difference between θ_{FC} and θ_{PWP}, was ~0.185 m^3 m^{-3}, which equals a gravimetric water content (θ_m) of ~0.286 kg kg^{-1}.

During the first week after transplanting, the substrate moisture level of all potted plants was maintained at the field capacity to ensure the optimum establishment of seedlings.

Afterwards, starting on 25 September 2018 at 21 days after sowing (DAS), when plants were, on average, with two detectable tillers (BBCH = 22), all pots were gradually dried down to the predefined water regimes, namely well-watered (WW; 75% of PAW) and water-limited (WD; 25% of PAW). From 21 to 40 DAS, when most plants had their flag leaf visible (on average, BBCH = 38), WD pots were maintained at 25% of PAW, but from 41 to 62 DAS the water stress was further intensified, and thus WD plants were re-watered to keep only 15% of PAW. However, WW pots were maintained at 75% of PAW throughout the experiment (i.e., from 21 to 62 DAS). Also, at 24 DAS on 28 September 2018, a layer of white plastic beads (Masterbatches, MACOMASS Verkaufs AG, Aschaffenburg, Germany) was placed on the substrate surface of every pot to limit evaporation, thus ensuring that water loss from the potted plants was mostly from transpiration. Each pot's water content level was kept constant by automated irrigation after weighing twice a week in the first two weeks, and then three times a week.

2.4.3 Growth conditions, meteorological and evapotranspiration data

The greenhouse environmental conditions were recorded at 1-min interval through five weather stations with sensors to measure the air temperature (DS18B20, Maxim Integrated Products, Inc., San Jose, CA, USA), air relative humidity (HMP110, Vaisala Corporation, Vantaa, Finland), and photosynthetic photon flux density (PPFD; LI-190R, LI-COR, Inc., Lincoln, NE, USA). Vapour pressure deficit (VPD) was calculated as the difference between the saturation (e_s) and actual vapour pressure (e_a) (Allen et al., 1998).

Plants were grown in a semi-controlled glass greenhouse under a photoperiod of 16 h/8 h (light/dark) with additional supplemental lighting from high-pressure sodium lamps (MASTER SON-T PIA Plus 400W, Philips) whenever natural light intensity was < 400 μmol m^{-2} s^{-1} between 06:00-22:00 hours local Central European Time (CET). The average ambient temperature and relative humidity were 23.0 °C (standard deviation, *SD* = 3.25) and 54.0% (*SD* = 9.87), respectively, in the daytime. Moreover, at night, the average ambient temperature and relative humidity were respectively 17.7 °C (*SD* = 1.35) and 64.7% (*SD* = 6.03). Also, the mean daily light integral (DLI) at the canopy level was 8.52 mol m^{-2} d^{-1} (*SD* = 1.97).

Water lost through evapotranspiration was quantified by automatically weighing the individual pots at regular intervals throughout the experiment (i.e., twice a week in the first two weeks, and then three times a week). In total, there were 18 days (time points) of measurements.

Daily evapotranspiration rate (ETR) was then expressed as the amount of water loss per day [ml d^{-1}].

2.4.4 Plant growth development and projected leaf area

Plant development, and thus plant phenology, was visually monitored twice a week, and each potted plant was scored according to the BBCH scale (Lancashire et al., 1991). The automated ScreenHouse shoot phenotyping platform provided non-invasive data of plant growth based on projected leaf area (PLA) by imaging of individual plant shoots at a regular basis (i.e., twice a week in the first two weeks, and then three times a week). In total, there were 18 days (time points) of shoot phenotyping. The platform is equipped with three RGB (red, green, blue colour space) cameras fixed at 0° (nadir), 45° and 90° angle to acquire four images per camera from different side views of the above-ground plant biomass (further technical details in Nakhforoosh et al., 2016).

Four images taken at 45° angle in each of the 18 time points were processed to estimate the average PLA per potted plant per day of measurement. The greenness thresholding approach, therefore, was employed on the grayscale representation of the RGB colour space in order to perform image segmentation (Müller-Linow et al., 2019). The intensity values of each image pixel were compared to a threshold α resulting in a binary mask B with values of 1 indicating intensity values above α and 0 otherwise. These values were attributed to plant and non-plant pixels, by which the PLA could be estimated. The greenness was computed based on the Excess Green Excess Red index (ExGR; Camargo Neto, 2004; Meyer & Camargo Neto, 2008). According to this greenness index a pixel intensity value, $I(x,y)$, at position (x,y) was classified to B as

$$B(x,y) = \begin{cases} 1, & \text{if } 3 \cdot I'_G(x,y) - 2.4 \cdot I'_R(x,y) - I'_B(x,y) > \alpha \\ 0, & \text{otherwise} \end{cases},$$

where the threshold α was set at 1.3 and the normalised RGB channel intensities (I'_R, I'_G, and I'_B) were defined as

$$I'_R(x,y) = \frac{I_R(x,y)}{I_R(x,y)+I_G(x,y)+I_B(x,y)},$$

$$I'_G(x,y) = \frac{I_G(x,y)}{I_R(x,y)+I_G(x,y)+I_B(x,y)}, \text{ and}$$

$$I'_B(x,y) = \frac{I_B(x,y)}{I_R(x,y)+I_G(x,y)+I_B(x,y)}.$$

2.4.5 Leaf gas exchange measurements

Instantaneous point measurements of leaf gas exchange from intact and mature leaves were conducted between 10:00-15:30 hours CET, using the LI-6400XT portable photosynthesis system equipped with the standard 6 cm^2 leaf cuvette fitted with the 6400-02B Red/Blue (665 nm/470 nm) LED light source (LI-COR, Inc., Lincoln, NE, USA). Light intensity was set to 700 μmol m^{-2} s^{-1}, block temperature controlled at 25 °C, airflow rate at 500 μmol s^{-1}, CO_2 concentration in the airstream maintained at 400 μmol mol^{-1}, and vapour pressure deficit at the leaf level (VpdL) was held approximately 1.31 kPa (SD = 0.143). Leaves were equilibrated inside the cuvette until net CO_2 assimilation (A_n) and stomatal conductance (g_s) were constant when then intercellular CO_2 concentration (C_i) and transpiration rate (E) were also recorded. Measurements were performed at the central portion of the youngest fully-expanded leaf of the main stem from three plants per treatment at 37 and 58 DAS (i.e., at 16 and 37 days after imposing water treatment, respectively), when plants were, on average, at 37 (flag leaf just visible) and 61 (beginning of flowering) BBCH-scale, respectively. This gas exchange procedure followed the best practice protocols proposed by Evans & Santiago (2014) and Molero & Lopes (2012).

2.4.6 Measurement of leaf cell membrane stability

At 56 DAS (35 days after imposing water treatment), when plants were, on average, at the end of the heading stage (BBCH = 59), leaf cell membrane stability (CMS) was measured by means of electrolyte leakage from the leaf cells based on Blum & Ebercon (1981) and Bajji, Kinet & Lutts (2002). Three 1.5-cm leaf segments were randomly collected from the lower, middle and upper canopy of each potted plant, and placed in a 50 ml sterile polypropylene tube (Corning®, Merck KGaA, Darmstadt, Germany). Samples were quickly washed for three times with distilled deionised water and then were immersed in 20 ml of distilled deionised water. An initial electrical conductivity measure (iEC) was taken at the beginning of this hydration period using a portable digital conductivity meter (AK83, Akso Electronic Products Ltd., São Leopoldo, RS, Brazil). Then, all capped tubes were incubated in the dark for 24 h at 10 °C. After incubation, samples were warmed up to room temperature for about one hour, were vigorously shaken, and then another round of electrical conductivity measure (fEC) was taken. Following this, samples were autoclaved at 120 °C for 20 min. Tubes were cooled down to

room temperature and the total electrical conductivity (EC_T) was measured. Electrolyte leakage [%] was expressed as $\left[\frac{fEC-iEC}{EC_T-iEC} \times 100\right]$.

2.4.7 Final destructive measurements

The experiment was terminated on 05 November 2018 at 62 DAS (41 days after imposing water treatment), when ca. 40% of plants were at the end of the flowering stage (BBCH = 69). Plants were hand-cut near the substrate surface, placed in individual plastic bags and immediately weighed to determine the total above-ground fresh biomass. Leaves were detached from stems and, subsequently, the total leaf area (LA) per plant was quantified using a leaf area meter (LI-3100C, LI-COR, Inc., Lincoln, NE, USA). Finally, samples were placed in paper bags, oven-dried at 75 °C for 72 h, and weighted to obtain the final total shoot dry matter (SDM) per plant.

2.4.8 LIFT measurements in the greenhouse

The LIFT instrument was mounted on a commercial tripod (Advanced VX, Celestron, Torrance, CA, USA) and remained stationary in an adjacent area to the ScreenHouse's weighing station throughout the experiment. The sensor acquired ChlF data from an oblique side view of the plant canopy, being regularly adjusted as plants grew (Figure 2.3A). The off-nadir angle, therefore, shifted from 65° to 70° between the first and the last day of measurements. The distance from the LIFT lens to the middle-lower canopy (i.e., the target area) remained at ~0.90 m throughout the experiment. The blue LED light beam was ~35 mm in diameter at the focal point over the target area (Figure 2.3B). Aiming to operate with an optimal signal-to-noise ratio, the gain of the fluorescence channel was adjusted at the beginning of each day of measurement in order to maintain the raw fluorescence within 2000-20000 signal range. At a distance of 0.90 m, the average excitation power for the SQ_A phase was ~27000 µmol photons m^{-2} s^{-1}.

The ChlF measurements were performed in parallel with the routine operations of the automated ScreenHouse shoot phenotyping platform. For each day of measurement, a minimum of 20 Q_A flashes was acquired from every experimental unit whilst a potted plant stood alone on the weighing table for automated gravimetric measures and subsequent irrigation. The LIFT sensor operated in the continuous scanning mode throughout a day of measurement, where

single Q_A flashes were executed at ~1-second interval. In total, there were 16 time points (at 16, 21, 23, 28, 30, 34, 36, 38, 41, 43, 50, 52, 55, 57, 59, and 62 DAS), which were carried out, on average, between 09:50-13:50 hours CET.

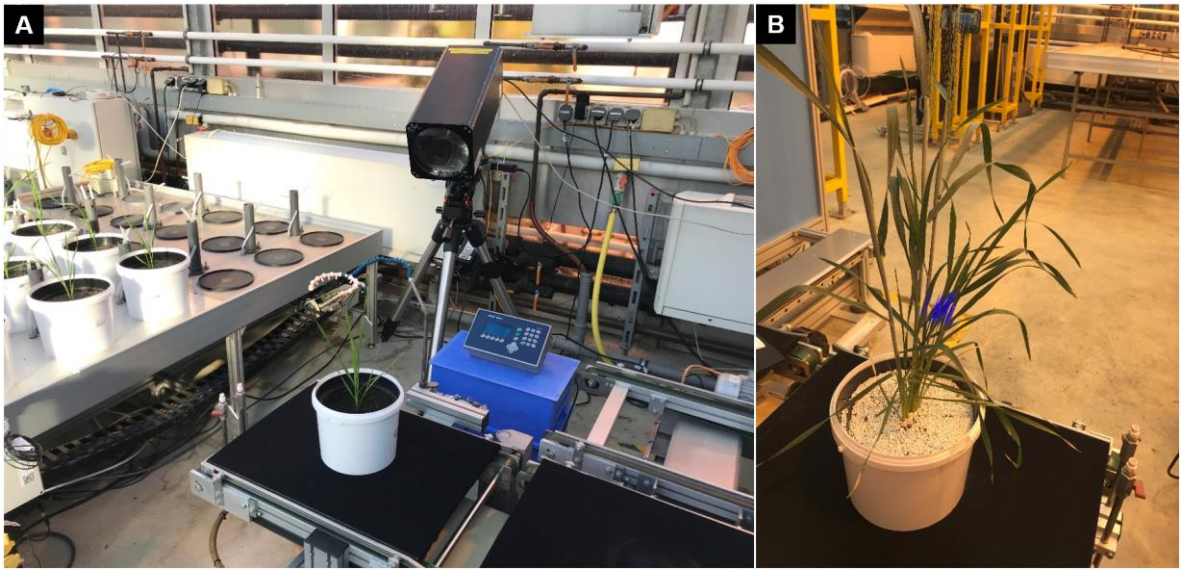

Figure 2.3. In the semi-controlled greenhouse experiment, **(A)** the LIFT instrument was mounted on a tripod, remained stationary in an adjacent area to the automated weighing and irrigation station, and acquired chlorophyll fluorescence data from an oblique side view of the plant canopy. **(B)** At a distance of ~0.90 m from the LIFT lens, the blue LED light beam was ~35 mm in diameter over the middle-lower canopy.

2.4.9 LIFT data cleaning

Due to off-target measurements (i.e., non-photosynthetic tissues), fluctuating lighting (either natural sunlight or supplemental lighting) and/or technical constraints, low-quality data can occur. Hence, a data cleaning pipeline was defined and implemented in the R environment (R Core Team, 2020).

A total of 40,306 ChlF transients were collected over time. Data were assessed and discarded in accordance with the following: i) data points acquired with signal-to-noise ratio ≤ 55; ii) F'_q/F'_m values outside the 0-1 range; iii) the adjusted coefficient of determination (R^2_{adj}) from the log-log model at t_1 (for F'_{r1}) was < .90; and iv) R^2_{adj} from the log-log model at t_2 (for F'_{r2}) was < .85. After performing the previous steps, outliers were detected and removed for each ChlF trait per day of measurement according to a four-step approach sequentially executed as follows: 1) at plot level based on adjusted boxplot for skewed distributions as proposed by Hubert & Vandervieren (2008) and implemented in the R package *robustbase* (Maechler et al.,

2020); 2) at genotype level also based on adjusted boxplot; 3) again at plot level but this time based on the standard Tukey's boxplot method by using 1.5 times the interquartile range (IQR) (Sim et al., 2005) and implemented in the base package *grDevices* (R Core Team, 2020); and lastly, 4) at genotype level also based on a standard boxplot. As F_q'/F_m', F_{r1}' and F_{r2}' are derived from the same transient, in the case of an outlier, none of the ChlF traits for that particular transient was considered for further analysis. Finally, after data cleaning, the remaining data points were averaged, resulting in one value per trait per plot per time of measurement (N = 1920 data points per trait).

2.4.10 Statistical analysis

A linear mixed model (LMM) approach was used to analyse the factorial completely randomised design experiment with repeated measures. Positive-constrained variance components for each phenotypic variable (trait) were estimated in the LMM by residual maximum likelihood (REML) using the Average Information (AI) algorithm with sparse matrix methods (Gilmour et al., 1995), as implemented in GENSTAT (VSN International, 2019). Patterson's model syntax, including its related operators, herein used were previously described in item 2.3.10.

A simple LMM for a trait measured in a single day was defined as

$$\gamma = G \times TRT : \underline{PLOT}, \qquad [9]$$

where γ is the vector of observed phenotype, G stands for the genotypes, TRT the water treatment, and $PLOT$ indexes the plots (i.e., the pots). The underscored term ($PLOT$ in this case) is the residual error effect (ε) associated with the observation γ. Model [9] was used to fit cell membrane stability (CMS), final total shoot dry matter (SDM), and final total leaf area (LA) traits, which were log-transformed.

Repeated measures were then incorporated into the model [9] as proposed by Piepho et al. (2004). The single-stage baseline model (BL) which considers the entire observed data in one stage at the level of individual plots was defined as

$$\gamma = G \times TRT + T/TRT : G \cdot T + G \cdot TRT \cdot T + PLOT + \underline{PLOT \cdot T}, \qquad [10]$$

where T is time points, the repeated factor. On top of the model [10], covariates were also included and the full baseline model (BL_{Cov}) was defined as

$$\gamma = G \times TRT + T/TRT + (\log PPFD \times \log VPD)/TRT : G \cdot T + G \cdot TRT \cdot T + PLOT + \underline{PLOT \cdot T} \quad [11]$$

where $\log PPFD$ is the log-transformed PPFD, and $\log VPD$ the log-transformed VPD, both were time-varying covariates. Model [11] was used to fit F_q'/F_m', F_{r1}' and F_{r2}' traits. Temporal correlation structures (Littell et al., 2000; Payne et al., 2019), such as banded Toeplitz (BAND), power (POW), ante-dependence (ANTE), linear variance (LV), autoregressive moving average (ARMA), unstructured (UN) or general correlation (COR), with equal or unequal variances, were also fitted to the residuals in models [10] and [11] to accommodate trends over time due to multiple observations on the same experimental unit. In all models, covariates were mean centred.

Projected leaf area (PLA), evapotranspiration rate (ETR) and growth stage (BBCH) traits were analysed by Model [10] but with $TRT \cdot T$ effect fitted as random. PLA and ETR traits were log-transformed. Due to a limited number of days of measurement (only two time points), the leaf gas exchange traits (A_n, g_s, C_i, and E) were analysed by Model [10] but with $G \cdot T$ effect fitted as fixed. Both C_i and g_s traits were log-transformed.

Comparison between candidate models was assessed by the REML-likelihood ratio test (REMLRT), provided that the two models being compared were nested and had the same fixed effects model (Galwey, 2014). Otherwise, when models were non-nested, yet with the same fixed effects, the Akaike Information Criterion (AIC) was used to assess their goodness-of-fit, judged by the 'smaller the better' form of the criterion (Cheng et al., 2010). Conditional *F*-test statistic was used to test fixed effects. The Fisher-Hayter procedure, a modified LSD (MLSD) test using the Studentized Range statistic (Hayter, 1986), was used to perform pairwise comparisons between adjusted means.

The strength of phenotypic association between two traits was calculated from the overall BLUEs ('Best Linear Unbiased Estimator') of genotypes by Spearman's rank correlation coefficients (r_s), regardless of time. Moreover, the drought-induced percentage change (%Δ) in a trait (e.g., PLA or ChlF traits), either for a particular genotype or point in time, was estimated as $\left[\frac{WD-WW}{WW} \times 100\right]$, where WD is the mean value of genotype or time point

i for a trait under water-limited conditions, and WW is the mean value of genotype or time point *i* for a trait under well-watered conditions.

3 RESULTS

3.1 FIELD TRIAL RESULTS

3.1.1 Weather conditions and drought severity

Overall, south-central Arizona's climate conditions were quite distinct between the two growing seasons. According to the National Centers for Environmental Information (NOAA, 2020), the 6-month period (November-April) in the 2017/2018 season (Y1) was characterised as the warmest and the driest on record for a 126-year period (1895-2020), whereas the 2018/2019 season (Y2) was the 53rd warmest and the 75th driest for the same period. The average temperature, precipitation and Palmer Z Index, as a measure of short-term drought severity, for the 6-month period (Nov-Apr) in Y1 were 16.6 °C (+3.0 °C anomaly compared to the 1901-2000 mean), 41.7 mm (-99.1 mm anomaly) and -2.28 (severe drought; -2.39 anomaly), against 13.9 °C, 147.3 mm and 0.19 in Y2, overall a near-normal season (NOAA, 2020).

Mean meteorological data for the time period when LIFT data were recorded in both growing seasons are in Figure 3.1. The higher atmospheric water demand in Y1 led to a faster and more acute reduction in soil moisture compared to Y2 (Figure 3.2). After withholding water, θ_{PWP} at 10 cm depth was reached in roughly 3 days and 17 days in Y1 and Y2, respectively. From this time point until the last day of field measurements with the LIFT sensor, the soil VWC dropped ~27.1% up to 16 DAWW in Y1, and only ~11.2% up to 25 DAWW in Y2. The WD rows in Y2 were, on average, 31.1% drier at 10 cm depth compared to the WW counterpart rows in D1, even though soil VWC was still slightly above (~8.5%) the θ_{PWP} (Figure 3.2). In D2 and D3 time points, WD rows were, on average, 43.1% and 45.5% drier than WW rows, respectively. The soil VWC for WD rows was just around and slightly below (~10.0%) the θ_{PWP} in D2 and D3, respectively (Figure 3.2). Overall, soil moisture in WW rows at 10 cm depth remained at 68.5% (*SD* = 7.2) of the θ_{FC} over time in Y2.

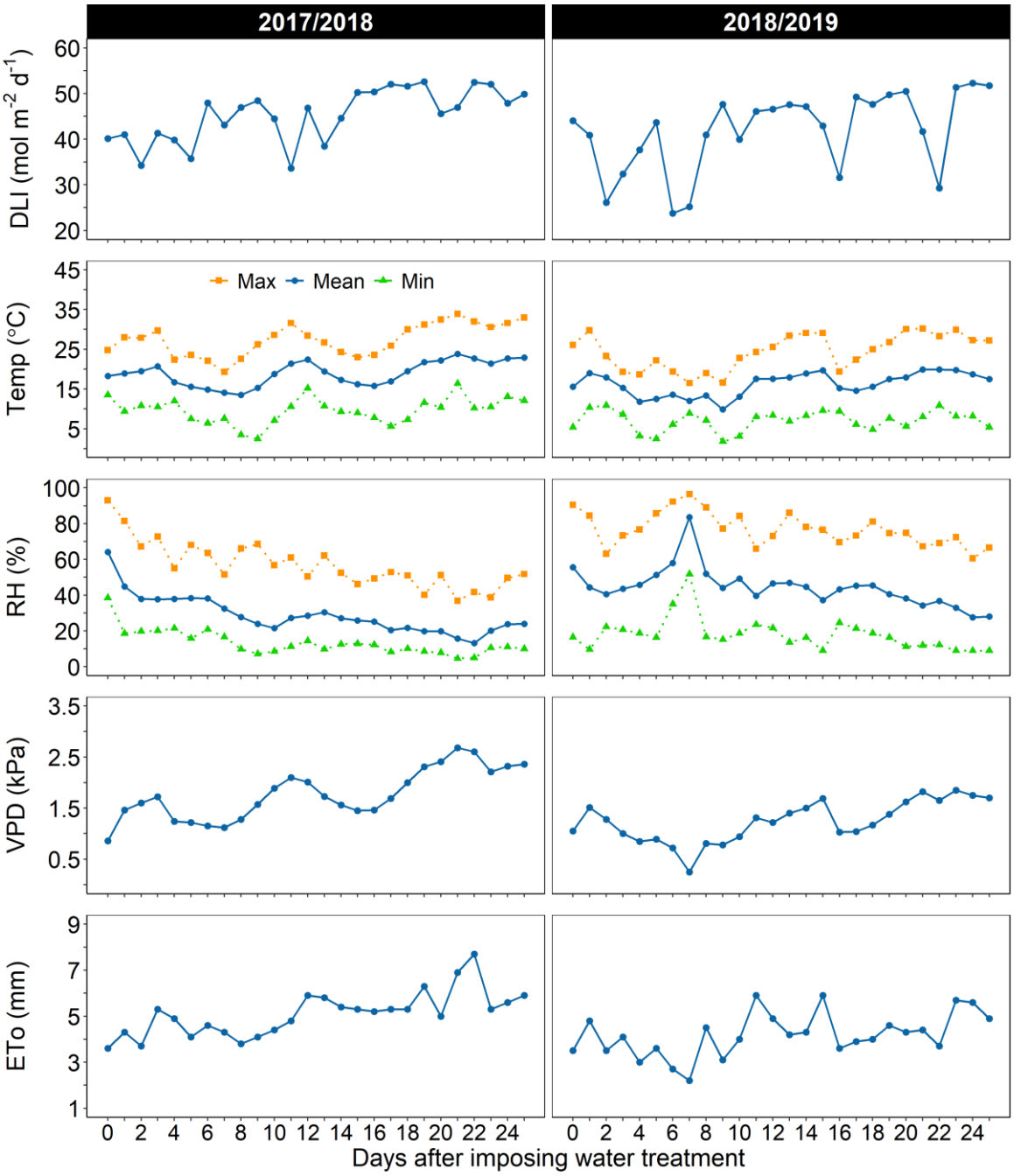

Figure 3.1. Daily light integral (DLI; mol m^{-2} d^{-1}), daily mean, maximum and minimum air temperature (Temp; °C), daily mean, maximum and minimum relative humidity (RH; %), daily mean air vapour pressure deficit (VPD; kPa), and daily reference evapotranspiration (ETo; mm) for the time period (in days after imposing water treatment) when LIFT data were recorded in both growing seasons, 2017/2018 (Y1) and 2018/2019 (Y2), at the Maricopa Agricultural Center of the University of Arizona (33.07454°N, 111.97494°W, elevation 360 m) in Maricopa, AZ, USA.

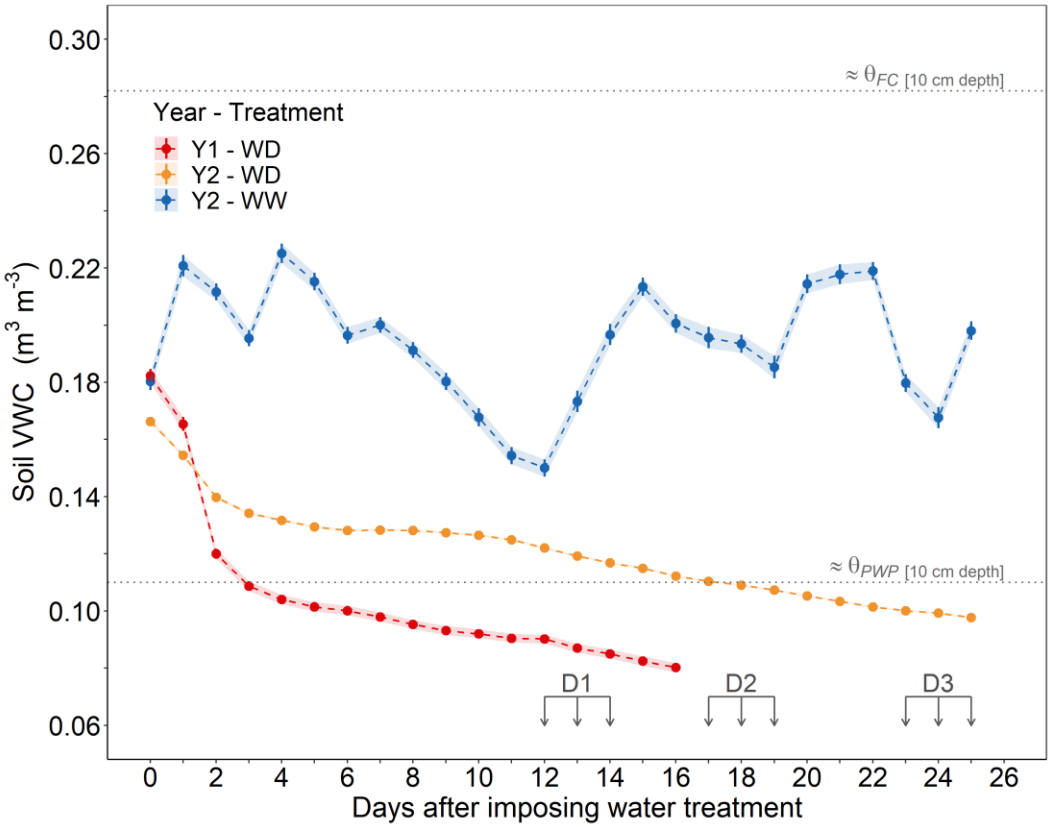

Figure 3.2. Daily mean soil volumetric water content (VWC) ± *SE*, n = 288, at 10 cm depth for seed rows in growing season 2017/2018 (Y1), and for well-watered (WW) and water-limited (WD) seed rows in growing season 2018/2019 (Y2). Dotted lines approximate to the soil permanent wilting point (θ_{PWP}) and the soil field capacity (θ_{FC}) at 10 cm depth. In Y2, three consecutive days (see arrows) were required to phenotype the entire durum wheat field with three replicates: D1 was taken between 12 and 14 days after imposing water treatment, D2 between 17 and 19 days, and D3 between 23 and 25 days.

3.1.2 Covariates and spatiotemporal modelling of trends

The model fit for the ChlF traits considerably improved after accounting for the biological and experimental sources of variation, as well as for the spatiotemporal correlations among neighbouring plots (Table 3.1). All models fitted to ChlF traits for Y1 and Y2 are found in Appendix 3 from Tables A.3.1 to A.3.6. The addition of fixed regression coefficients on top of the baseline models (i.e., BL_{Cov}) to accommodate differences in plant height (i.e., $RelF$), in plant growth and development ($iZDS$ or ZDS), in canopy structure and leaf pigments (i.e., $VOGREI$), along with fluctuating environmental factors which were recorded at a 5-s interval (e.g., $PPFD$ and VPD), promoted a net gain in precision, in terms of relative efficiency (RE) estimates, by 25.5%, 28.9% and 23.4%, on average, for F_q'/F_m', F_{r1}' and F_{r2}', respectively. Models with the further addition of spatiotemporal trends ($BL_{Cov+STM}$) resulted in smaller but

meaningful gains in precision relative to BL_{Cov}, yielding total final improvements of 29.6%, 36.5% and 27.3%, on average, for F'_q/F'_m, F'_{r1} and F'_{r2}, respectively. These final 'best' fit models ($BL_{Cov+STM}$, as indicated in Appendix 3 from Tables A.3.1 to A.3.6), whose coefficients of determination (Ω_β^{ASV}) ranged from .49 to .73 (Table 3.1), served as the basis for all results hereafter reported. The conditional *F*-test statistics for fixed effects are reported in Appendix 4.

Table 3.1. Relative efficiency (RE) in percentage in terms of the average standard error of difference between genotype means (SED) for baseline models after adding covariates (BL_{Cov}), and after adding covariates and modelling spatiotemporal correlations ($BL_{Cov+STM}$) for each chlorophyll fluorescence trait (F'_q/F'_m, F'_{r1} and F'_{r2}) in both growing seasons, 2017/2018 (Y1) and 2018/2019 (Y2). The baseline model without covariates and spatiotemporal modelling (BL) is the reference (RE = 100%). Ω_β^{ASV} is the coefficient of determination, an R^2_{adj}-like statistic, for the 'best' fit models ($BL_{Cov+STM}$).

Model	**Measure**	F'_q/F'_m		F'_{r1}		F'_{r2}	
		Y1	**Y2**	**Y1**	**Y2**	**Y1**	**Y2**
Baseline (BL)	SED	0.0159	0.0113	0.0116	0.0102	0.0084	0.0076
	RE	100.0	100.0	100.0	100.0	100.0	100.0
BL_{Cov}	RE	122.3	128.7	134.2	123.6	116.5	130.2
$BL_{Cov+STM}$	RE	127.6	131.6	145.1	127.8	121.9	132.6
	Ω_β^{ASV}	.71	.49	.73	.60	.72	.54

The display of sample variograms can be informally used as a major diagnostic tool for checking for the presence of natural and extraneous variation in the analysis of field experiments (Gilmour, Cullis & Verbyla, 1997). Terms added to a model are then formally tested with *F*-statistics (fixed terms) or REML-likelihood ratio tests (random terms). To exemplify this approach of graphically checking models, Figures 3.3 and 3.4 show residual variograms for the growing seasons Y1 and Y2, respectively, for both the intercept only (without covariates and spatiotemporal covariance structures) and the final best-fitting ($BL_{Cov+STM}$) models. Overall, the sample variograms of the residuals for the intercept only model in Y1 (Figures 3.3A, 3.3C, and 3.3E) indicate that the semi-variance within both directions (columns and rows) has an increasing trend component. Likewise, the sample variograms of the residuals for the intercept only model in Y2 (Figures 3.4A, 3.4C, and 3.4E) indicate that the semi-variance within the same subrow appears fairly constant across all columns, while within each column has an increasing trend component. Solely for the F'_{r1} trait in Y2 (Figure 3.4C), an additional steps component was also observed within each column.

Such trends in both seasons, Y1 and Y2, seem to follow the walking path patterns imposed for the field data acquisition (see details in item 2.3.6), which also match the diurnal courses of sunlight and vapour pressure deficit (which will be discussed later). A first-order autoregressive moving average, ARMA(1, 1), model fitted to both directions (columns and rows), or a second-order autoregressive, AR(2), model fitted to columns only, smoothly accommodated the majority of the spatial trends observed in Y1 and Y2, respectively (Appendix 3 from Tables A.3.1 to A.3.6). Indeed, the addition of these polynomial functions combined with temporal modelling and covariates, as previously presented, were key to account for trends (Figures 3.3B – 3.4B, 3.3D – 3.4D, and 3.3F – 3.4F), and to improve the precision of estimates of genotype effects and contrasts (Table 3.1).

3.1.3 Effects of drought stress on leaf RWC and above-ground biomass

In Y1, when the drought was severe, the mean relative change in leaf RWC (ΔRWC) from 0 to 15 DAWW was -25.3%Δ, 95% confidence interval (CI) [-23.1, -27.7], see Figure 3.5A. Among the 252 genotypes, the least and the most dehydrated genotypes dropped their leaf RWC by -14.9%Δ (standard error, *SE* = 1.98) and -44.1%Δ (*SE* = 2.98), respectively. In Y2, when the drought was milder, even after imposing 21 days of water-limiting conditions, leaf RWC of WD plants decreased, on average, only by -1.83%Δ (*SE* = 0.13) compared to WW plants (Figure 3.5B). Despite this mild stress and a minor drop in RWC in Y2, the water treatment had a major effect on the total shoot dry matter yield (SDMY), $F(1, 27.2) = 176$, $p < .001$, where WD plants produced, on average, 4815 kg ha^{-1} (*SE* = 52.4), and WW plants produced 6020 kg ha^{-1} (*SE* = 65.6). However, the genotype-by-water treatment interaction was not significant ($p = .258$), and so the relative reduction in SDMY was similar across genotypes, ranging from -19.3% to -25.2% (Figure 3.5B). In Y1, the mean SDMY at the end of the severe stress was 5161 kg ha^{-1}, 95% CI [4959, 5371], varying from 4343 kg ha^{-1} (*SE* = 267) to 5801 kg ha^{-1} (*SE* = 146) among genotypes (Figure 3.5A). However, because the progressive drought was imposed throughout the entire experiment, a comparison with a WW condition within the same growing season was not possible.

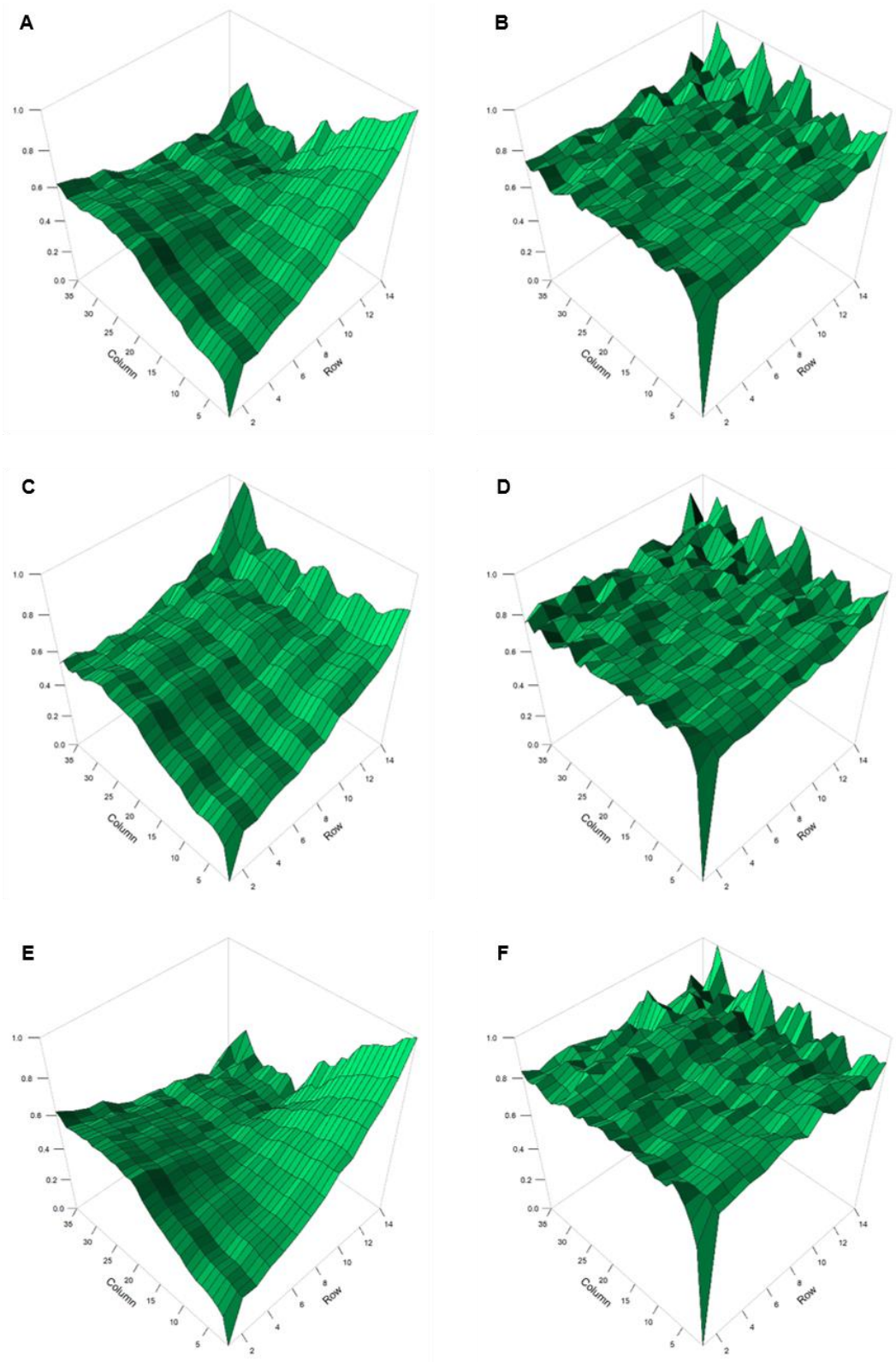

Figure 3.3. Three-dimensional plot of sample variograms of the residuals for the intercept only models, on the left-hand side, and for the final best-fitting models ($BL_{Cov+STM}$), on the right-hand side, for **(A – B)** operating efficiency of PSII (F_q'/F_m'), and both reoxidation processes, **(C – D)** F_{r1}' and **(E – F)** F_{r2}'. The variograms were scaled onto a 0-1 (i.e., unit) scale for plotting. All models are related to the first growing season in 2017/2018 (Y1).

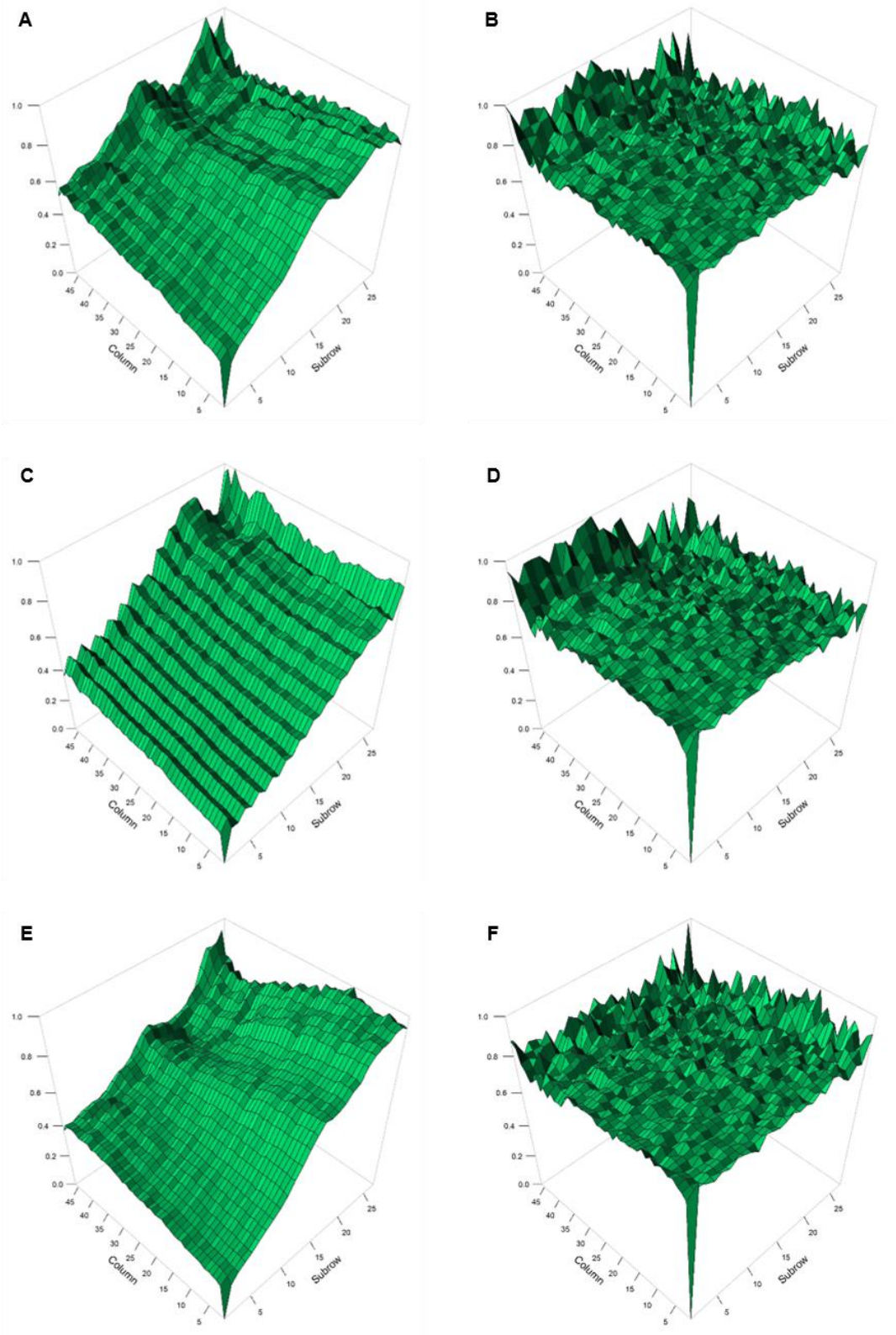

Figure 3.4. Three-dimensional plot of sample variograms of the residuals for the intercept only models, on the left-hand side, and for the final best-fitting models ($BL_{Cov+STM}$), on the right-hand side, for **(A** – **B)** operating efficiency of PSII (F_q'/F_m'), and both reoxidation processes, **(C** – **D)** F_{r1}' and **(E** – **F)** F_{r2}'. The variograms were scaled onto a 0-1 (i.e., unit) scale for plotting. All models are related to the second growing season in 2018/2019 (Y2).

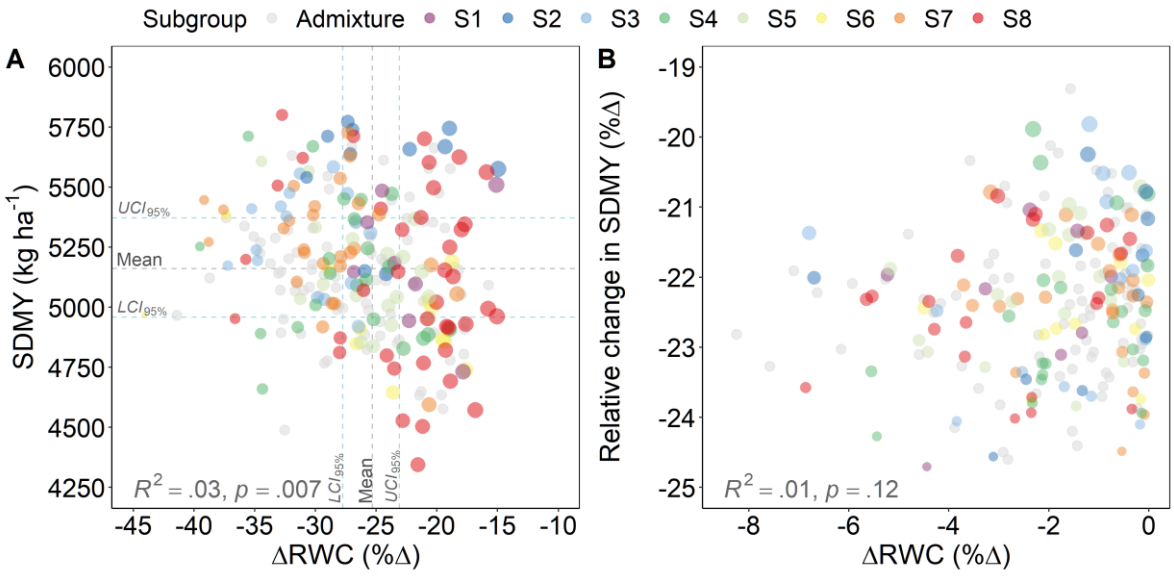

Figure 3.5. Relationships across durum wheat genotypes between **(A)** the relative changes in leaf relative water content (ΔRWC in %) and the total shoot dry matter yield (SDMY in kg ha^{-1}) at the end of the severe drought period in Y1. Dashed lines indicate mean, lower (LCI) and upper (UCI) 95% confidence intervals; or **(B)** the relative changes in leaf relative water content (ΔRWC in %) and the relative changes in total shoot dry matter yield (ΔSDMY in %) induced by mild drought in Y2, in comparison to non-stressed plants (WW). Genotypes were assembled into subgroups (S) according to the population genetic structure reported by Condorelli et al. (2018).

3.1.4 Effects of drought stress on the LIFT-measured ChlF traits

The increasing severity of drought stress condition in Y1 resulted in a slow but steady reduction in F_q'/F_m' and in both reoxidation efficiency traits, F_{r1}' and F_{r2}' (Figures 3.6A and 3.6B). At 16 DAWW, F_q'/F_m', F_{r1}' and F_{r2}' significantly decreased by -14.4%, -17.8% and -20.3%, 95% CIs [-6.24, -22.5], [-9.28, -26.4], and [-8.18, -32.4], respectively, relative to 0 DAWW (Figure 3.6C). This downregulation of ChlF traits was well aligned with the combined effect of progressive soil moisture dry-down at 10 cm and 50 cm depths (Figure 3.7). Indeed, the soil VWC at 50 cm depth strongly correlated with overall daily means for ChlF traits (Figure 3.8). Although linearly slowing down over time, F_{r1}' tended to accelerate immediately after the onset of drought (up to 3 DAWW) before decelerating in the long term (Figures 3.6C and 3.8B). Simultaneously, θ_{PWP} at 10 cm depth was reached around 3 DAWW.

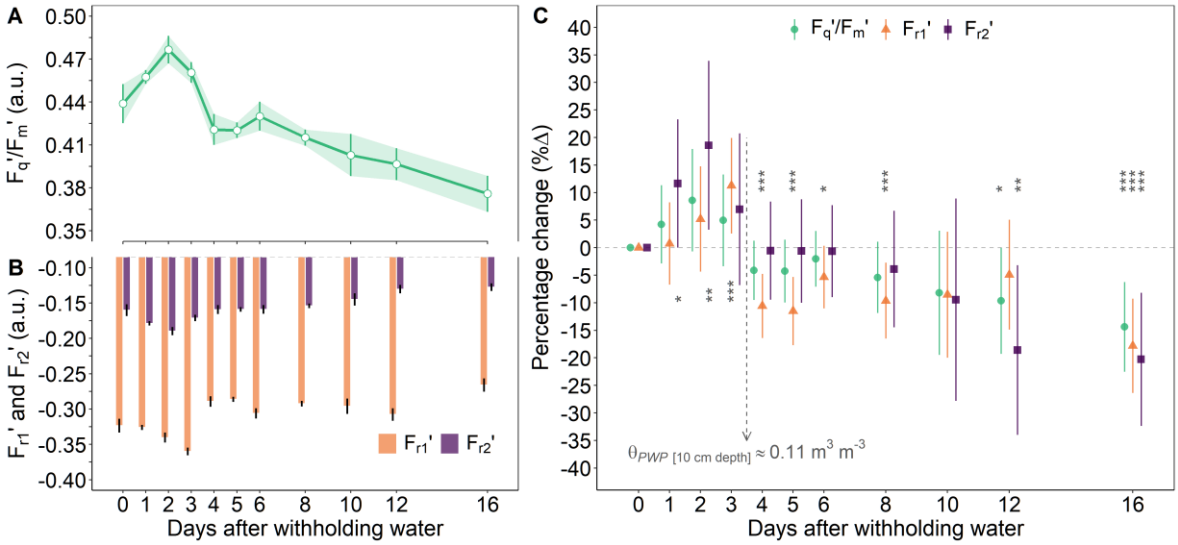

Figure 3.6. LIFT-measured chlorophyll fluorescence (ChlF) traits from light-adapted durum wheat plants in response to progressive drought stress, from 0 to 16 days after withholding water (DAWW), in Y1. **(A)** Operating efficiency of PSII (F_q'/F_m'); and **(B)** efficiency of electron transport up to ~0.65 ms after reducing Q_A (i.e., F_{r1}'; the kinetics of electron transfer from Q_A to *PQ* pool), and up to ~6.64 ms after F_{r1}' (i.e., F_{r2}'; the kinetics of electron transfer from *PQ* pool to PSI). Values are means, averaged across genotypes, with ± 95% confidence intervals (CIs), n = 252. **(C)** Percentage changes (%Δ) in ChlF traits over time. Mean relative changes with ± 95% CIs are shown with respect to the baseline value at 0 DAWW. Pairwise comparisons between time points and baseline within each ChlF trait were performed by the Fisher-Hayter procedure. The levels of significance are indicated by * ($p \leq .05$), ** ($p \leq .01$), and *** ($p \leq .001$), otherwise blank if $p > .05$. Dashed arrow indicates when the soil permanent wilting point (θ_{PWP} = 0.11 m^3 m^{-3}) at 10 cm depth was reached.

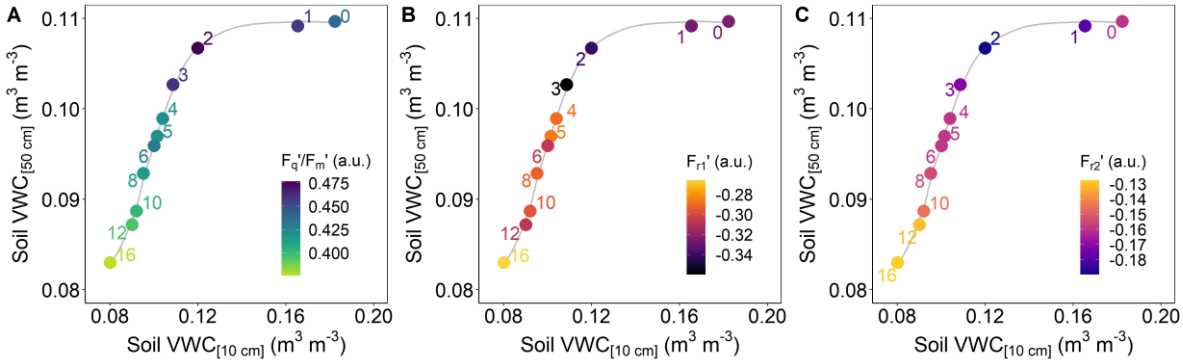

Figure 3.7. LIFT-measured chlorophyll fluorescence traits from light-adapted durum wheat plants as a function of the soil volumetric water content (VWC) at 10 cm and 50 cm depths in Y1. **(A)** Operating efficiency of PSII (F_q'/F_m'); **(B)** efficiency of electron transport up to ~0.65 ms after reducing Q_A (i.e., F_{r1}'); and **(C)** efficiency of electron transport up to ~6.64 ms after F_{r1}' (i.e., F_{r2}'). Values are means, averaged across genotypes, n = 252. Nearby points, the numerical label indicates the timing (in days) after withholding water (DAWW).

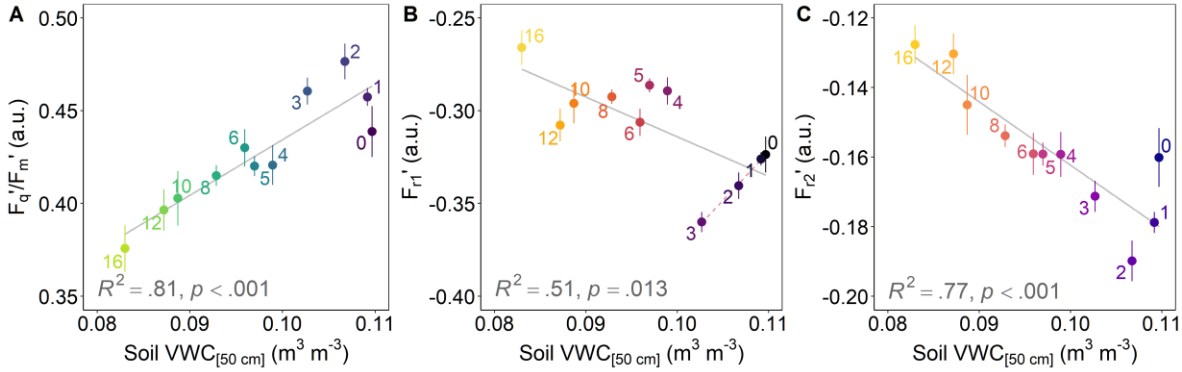

Figure 3.8. Relationships between LIFT-measured chlorophyll fluorescence traits from light-adapted durum wheat plants and the soil volumetric water content (VWC) at 50 cm depth in Y1. **(A)** Operating efficiency of PSII (F_q'/F_m'); **(B)** efficiency of electron transport up to ~0.65 ms after reducing Q_A (i.e., F_{r1}'); and **(C)** efficiency of electron transport up to ~6.64 ms after F_{r1}' (i.e., F_{r2}'). Values are means, averaged across genotypes, with ± 95% confidence intervals, n = 252. Nearby points, the numerical label indicates the timing (in days) after withholding water (DAWW). The colour schemes indicate drought progression over time, from non-stress (darker colours) to severe stress (lighter colours).

The overall main effect of water treatment in Y2, averaged across time, was minor but significant for F_q'/F_m', $F(1, 13.3) = 54.7$, $p = < .001$, where WD plants (mean, $M = 0.507$, $SE = 0.0008$) had slightly higher values than WW plants ($M = 0.497$, $SE = 0.0008$). Also, F_{r1}' for WD plants ($M = -0.368$, $SE = 0.001$) was faster than for WW plants ($M = -0.347$, $SE = 0.001$), $F(1, 13.0) = 205$, $p < .001$. However, F_{r2}' for both treatments, WD ($M = -0.212$, $SE = 0.0006$) and WW ($M = -0.210$, $SE = 0.0006$), performed alike, $F(1, 13.4) = 1.73$, $p = .211$. The water treatment-by-time interaction was significant for F_q'/F_m', $F(2, 111) = 5.99$, $p = .003$, and for F_{r1}', $F(2, 111) = 29.1$, $p < .001$, but of minor effect for F_{r2}', $F(2, 110) = 2.01$, $p = .139$. At time point D1, when the soil in the WD rows was only marginally dry, F_q'/F_m' for WD plants was +1.08% relative to control plants (Figure 3.9). At D2 and D3, with further depletion of soil VWC, stressed plants showed higher F_q'/F_m' compared to non-stressed plants, +2.72% and +2.58%, respectively (Figure 3.9). Likewise, F_{r1}' for WD plants was faster than for WW plants throughout the season in the order of +3.10%, +7.50%, and +7.86% for D1, D2, and D3, respectively (Figure 3.9). These drought-induced trends for F_{r1}' in Y2 (milder drought) were similar to those observed at the onset of the water-limiting conditions in Y1, particularly around 3 DAWW (Figure 3.6C).

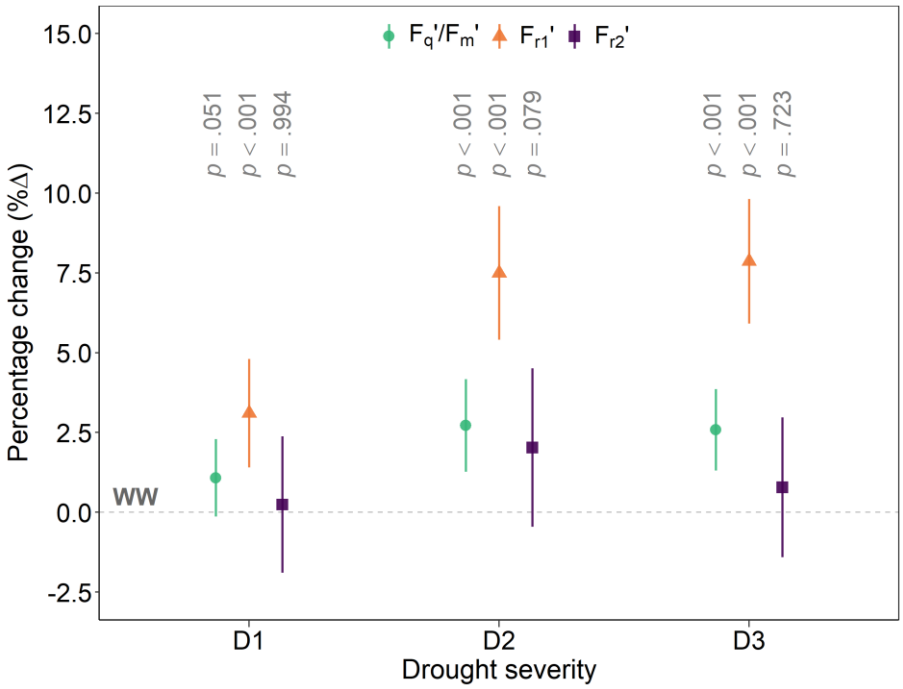

Figure 3.9. Percentage changes (%Δ) in chlorophyll fluorescence (ChlF) traits according to the drought severity D1, D2, and D3 imposed in Y2. Mean relative changes with ± 95% confidence intervals are shown with respect to non-stressed plants (i.e., WW as the reference, 0%) within each ChlF trait per time point (drought severity). Exact *p*-values are displayed.

Independent of the environment, the three ChlF traits operated in a highly coordinated manner, which was clearly observed in Y1 (Figure 3.10) across multiple time points with varying ambient conditions, either above or below ground. Daily means for F'_{r1} and F'_q/F'_m (Figure 3.10A) were strongly correlated, indicating that the faster or slower the electron flow from Q_A towards *PQ* pool, the higher or lower the PSII operating efficiency. Moreover, F'_{r2} and F'_q/F'_m (Figure 3.10B) were even better correlated, suggesting that the faster or slower the electron flow from *PQ* pool towards PSI, the higher or lower the PSII operating efficiency. Interestingly, this correlation was even stronger than the relationship between both reoxidation processes, F'_{r1} and F'_{r2} (Figure 3.10C).

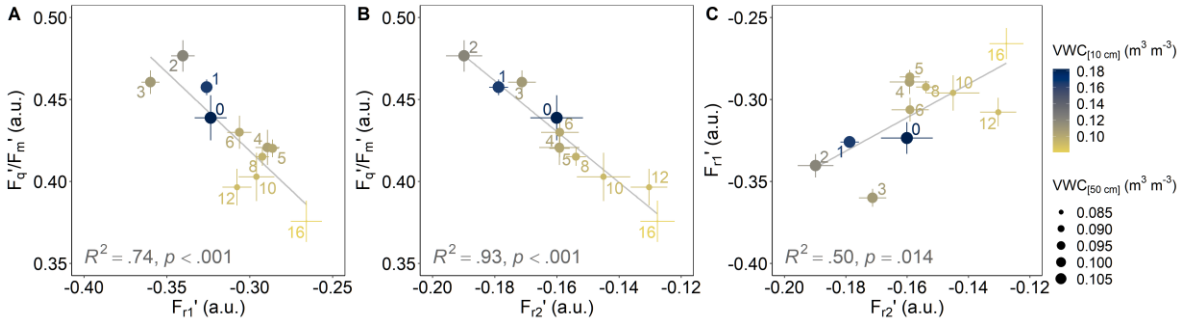

Figure 3.10. Relationships among LIFT-measured chlorophyll fluorescence traits from light-adapted durum wheat plants under progressive drought stress in Y1. Relationships between **(A)** F'_{r1} (the kinetics of electron transport from Q_A to PQ pool) and operating efficiency of PSII (F'_q/F'_m); **(B)** F'_{r2} (the kinetics of electron transport from PQ pool to PSI) and F'_q/F'_m; **C)** both reoxidation processes, F'_{r1} and F'_{r2}. Values are means, averaged across genotypes, with ± 95% confidence intervals, n = 252. Nearby points, the numerical label indicates the timing (in days) after withholding water (DAWW). The colour scale for points is based on the soil volumetric water content (VWC) at 10 cm depth, and the point sizes are based on the soil VWC at 50 cm depth.

3.1.5 Environmental responses and diurnal courses of ChlF traits

Both $PPFD$ and air VPD were major fluctuating environmental factors driving nonlinear changes in the ChlF traits from light-adapted plants within a measurement day. In fact, their interaction effect ($\log PPFD \cdot \log VPD$; i.e., both variables were log-transformed) was very important for accounting for the variations observed in the ChlF traits under severe drought, as in Y1 (Appendix 4). Increasing light intensity from 150 to 2500 µmol m^{-2} s^{-1} induced a continuous but nonlinear reduction in F'_q/F'_m (Figure 3.11A) and a deceleration in F'_{r2} (Figure 3.11C). Furthermore, such effects were even more pronounced when VPD increased from 1.5 to 2.5 kPa. F'_{r1} (Figure 3.11B) accelerated under higher VPD, especially at low light intensity (< ~450 µmol m^{-2} s^{-1}), whereas this effect was negligible when $PPFD$ was > ~900 µmol m^{-2} s^{-1}. Neither the $PPFD$ by VPD interaction nor its interaction with water treatments were significant (p > .10) for explaining the variations in the ChlF traits in Y2. Accordingly, these effects were dropped from the final fitted models. Nevertheless, the single main effects of $\log PPFD$ and $\log VPD$ were still important in Y2 and did show similar trends as in Y1 (Appendix 4). Notably, solely for F'_{r1} trait (Appendix 4), the $\log VPD$ by water treatment interaction effect was significant, indicating that the faster rate of F'_{r1} induced by increasing VPD occurred even more rapidly in WD than in WW plants (Figure 3.11D).

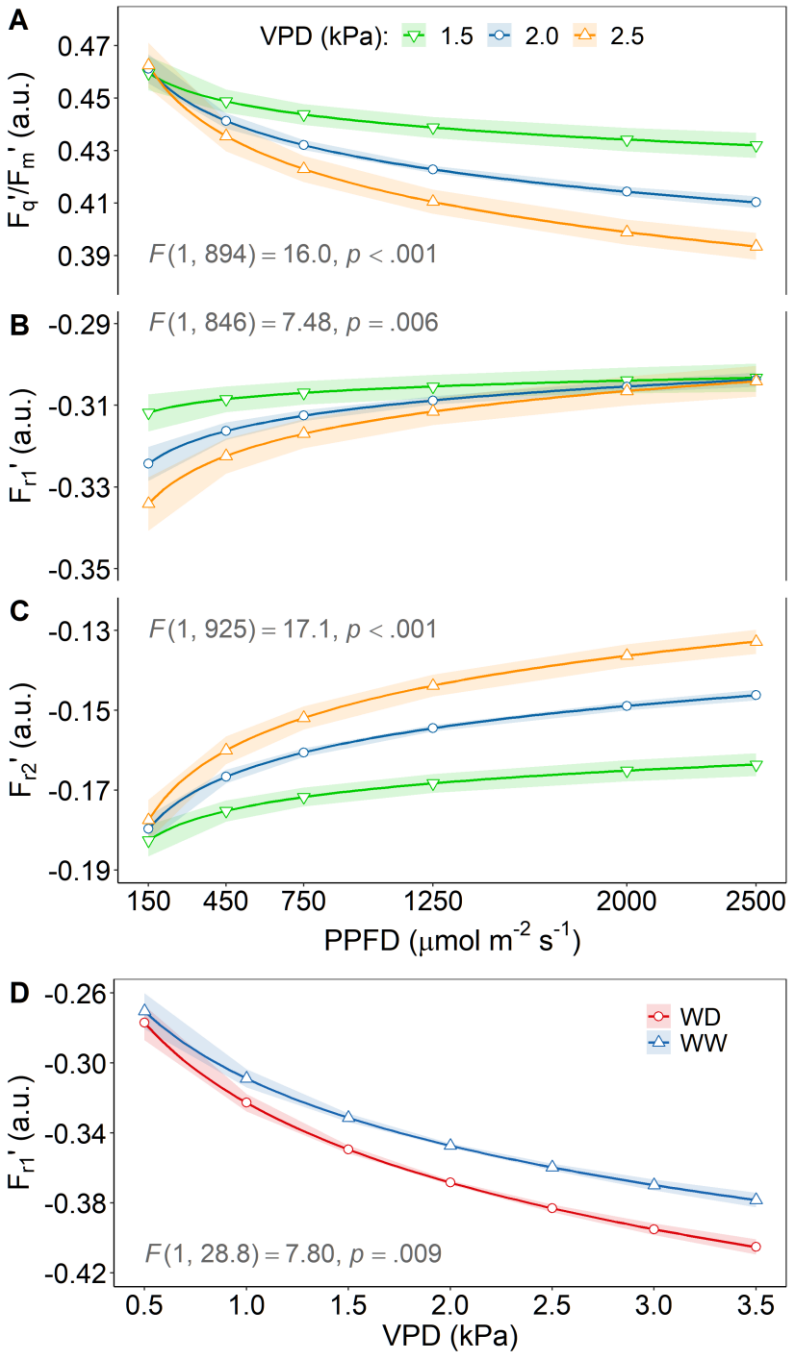

Figure 3.11. Predicted values ± *SE*, *n* = 5044, for **(A)** operating efficiency of PSII (F_q'/F_m'), and both reoxidation processes, **(B)** F_{r1}' and **(C)** F_{r2}', from light-adapted durum wheat plants under progressive drought stress as a function of photosynthetic photon flux density (PPFD) and vapour pressure deficit (VPD). **(D)** Predicted F_{r1}' values ± *SE*, *n* = 4032, for well-watered (WW) and water-limited (WD) durum wheat plants in light-adapted conditions as a function of VPD. Predicted values are based on the best-fitting for models [3] and [6] in Y1 and Y2, respectively (see item 2.3.10).

Over the course of the day, ChlF traits exhibited clear patterns which were consistent across multiple days and growing seasons, and generally followed diurnal courses of $PPFD$ and VPD (Figures 3.12 and 3.13). The diurnal course of F_q'/F_m' (Figures 3.12B and 3.13B) showed a local minimum around midday at the peak of incoming sunlight. Relative to WW conditions (Figure 3.12B), WD plants tended to have slightly higher F_q'/F_m' values towards the afternoon, when $PPFD$ was decreasing but VPD was at the highest. The diurnal course of F_{r2}' (Figure 3.12D and 3.13D) mirrored that displayed by F_q'/F_m', showing a local maximum (i.e., slowest rate) around midday. However, there were no evident changes between diurnal patterns of WD and WW plants (Figure 3.12D). By contrast, F_{r1}' (Figures 3.12C and 3.13C) was fairly stable early morning to midday and then decreased linearly (i.e., gradually accelerating the rates of Q_A^- reoxidation) towards the afternoon. Although stressed plants always had faster rates of F_{r1}' throughout the day (Figure 3.12C), especially in the afternoon under increasing VPD and decreasing $PPFD$, the shape of the diurnal patterns of WW and WD plants were comparable.

Since the LIFT field data were regularly acquired by following systematically two-dimensional paths (columns and rows), see details in item 2.3.6, the diurnal courses of the ChlF traits can also be assessed from a spatial perspective. Therefore, contour plots for each ChlF trait were produced for Y1 and Y2, and are found in Figures 3.14 and 3.15, respectively. From these figures, it is possible to observe the spatial responses of ChlF traits over the course of the field phenotyping day, regardless of genotype. As previously presented, these overall responses were mainly driven by diurnal changes in $PPFD$ and VPD.

3.1.6 Changes of heritability over time

Varying temporal dynamics of genotypic effects were observed for all ChlF traits during progressively increasing drought severity in Y1. The broad-sense heritability (H^2; Figure 3.16) for F_q'/F_m' increased from 0.55 to 0.64 between 0 to 5 DAWW (i.e., from non-stress to moderate drought) and then gradually decreased to 0.46 in severe drought at 16 DAWW. H^2 for F_{r1}' marginally increased to 0.59 within the first 2 DAWW, remained stable up to 5 DAWW, and then continuously decreased to 0.40 up till 16 DAWW (Figure 3.16). H^2 for F_{r2}', likewise, had starting values of 0.61, peaked at 0.68 in 3 DAWW, and decreased to a minimum of 0.40 (Figure 3.16). The unknown (residual) environmental effects increased from moderate to severe stress conditions, which could explain the decline in heritabilities (i.e., the decreasing relative contribution of genetic effects to phenotypic variance).

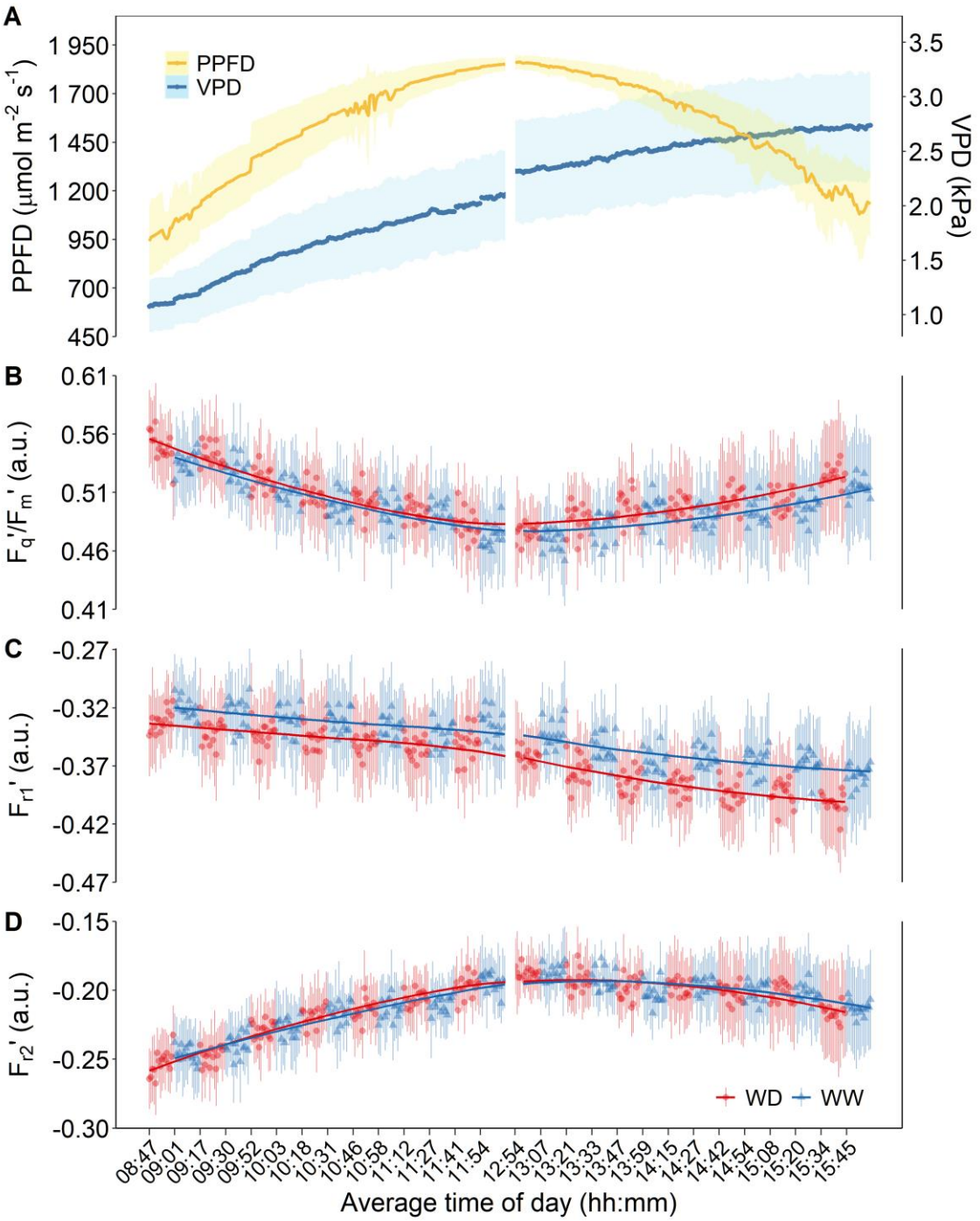

Figure 3.12. Diurnal course of **(A)** photosynthetic photon flux density (PPFD) and air vapour pressure deficit (VPD), **(B)** operating efficiency of PSII (F_q'/F_m'), and both reoxidation processes, **(C)** F_{r1}' and **(D)** F_{r2}', for well-watered (WW) and water-limited (WD) durum wheat plants in light-adapted conditions in Y2. Values are means ± *SD*, averaged across days of field phenptyping, *n* = 9. The local time zone is Mountain Standard Time (MST). The discontinuity around midday relates to a daily operational break during the LIFT data collection (see details in Appendix 2 – Figure A.2.2).

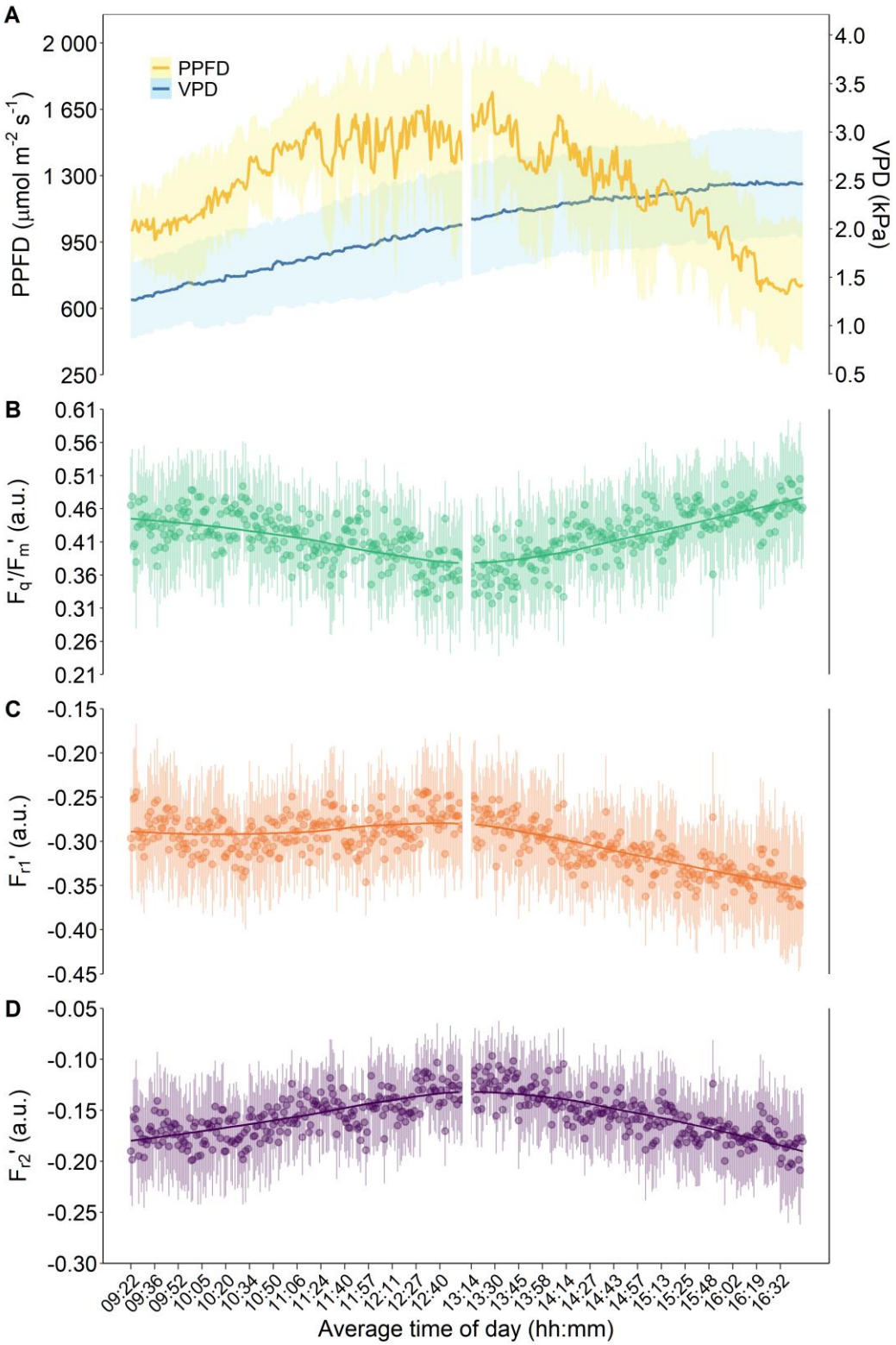

Figure 3.13. Diurnal course of **(A)** photosynthetic photon flux density (PPFD), and air vapour pressure deficit (VPD), **(B)** operating efficiency of PSII (F_q'/F_m'), and both reoxidation processes, **(C)** F_{r1}' and **(D)** F_{r2}', from light-adapted durum wheat plants under progressive drought stress in Y1. Values are means ± *SD*, averaged across days of field phenotyping, n = 11. The local time zone is Mountain Standard Time (MST). The discontinuity around midday relates to a daily operational break during the LIFT data collection (see details in Appendix 2 – Figure A.2.1).

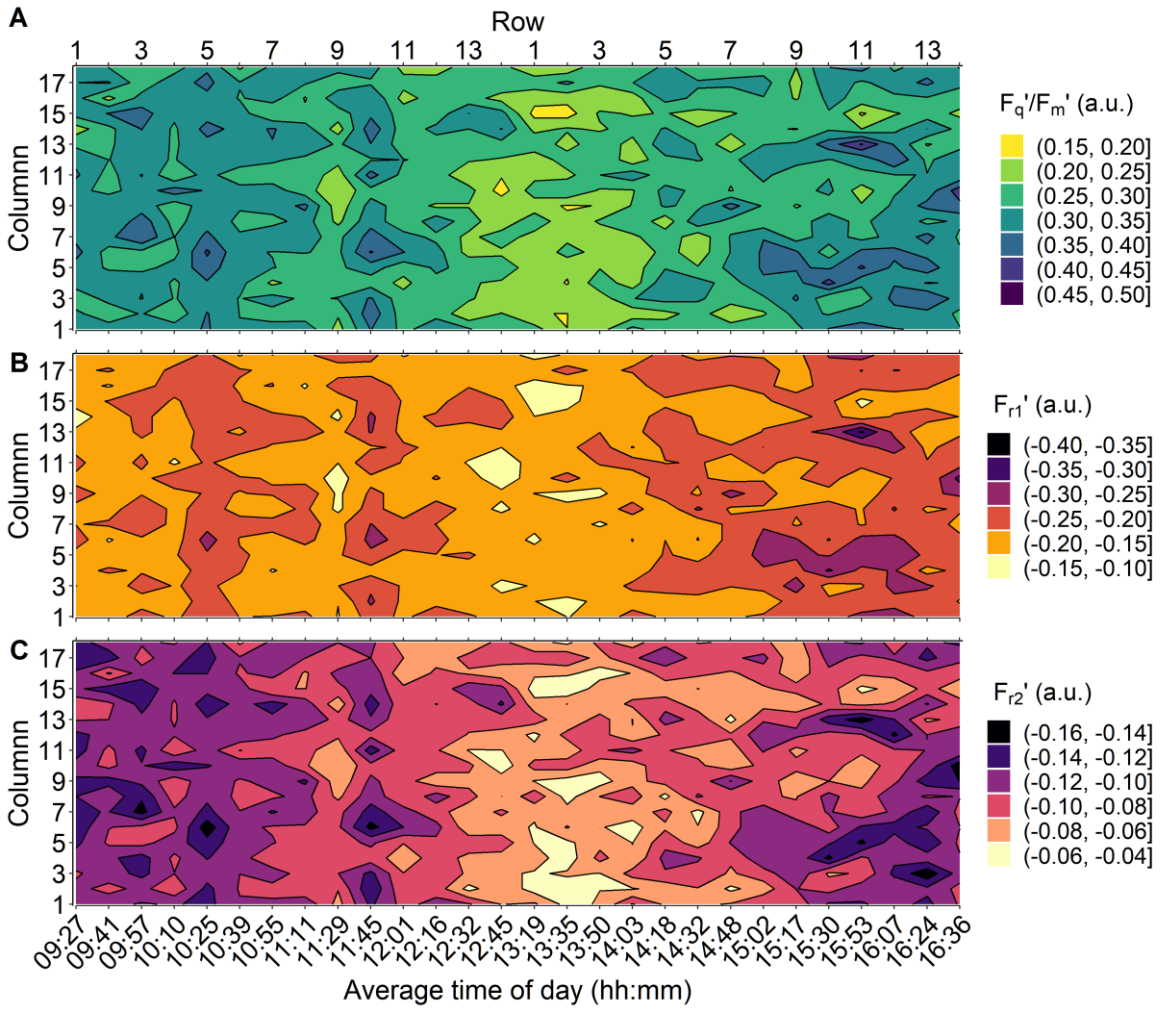

Figure 3.14. Average spatial and temporal variation for the chlorophyll fluorescence traits from light-adapted durum wheat plants under progressive drought stress in Y1. **(A)** Operating efficiency of PSII (F'_q/F'_m), and both reoxidation processes, **(B)** F'_{r1} and **(C)** F'_{r2}. The contour plots were built based on the mean values of 11 days of field phenotyping, from 0 to 16 days after withholding water. The local time zone is Mountain Standard Time (MST).

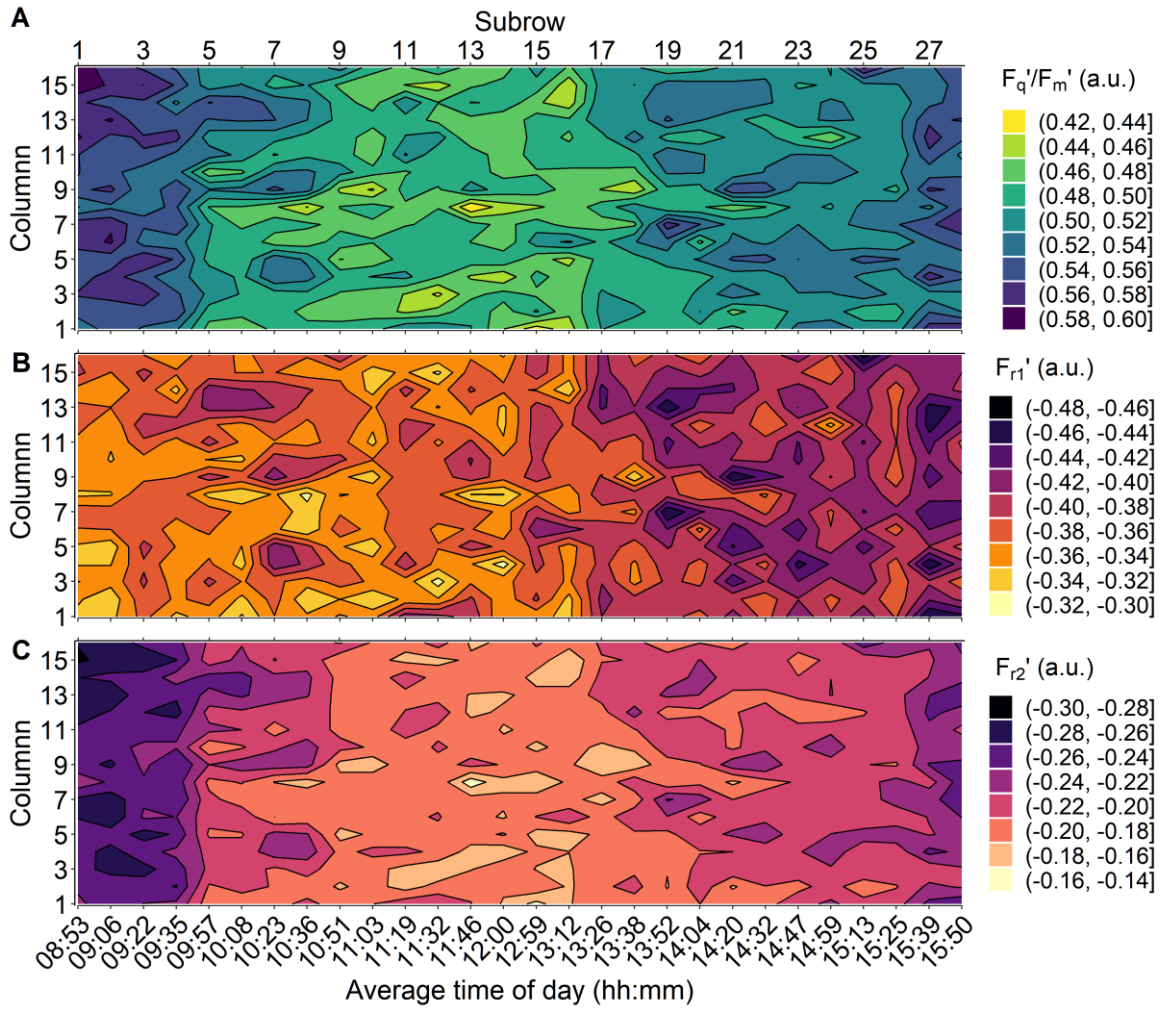

Figure 3.15. Average spatial and temporal variation for the chlorophyll fluorescence traits from light-adapted durum wheat plants grown under both well-watered (i.e., the even subrows) and water-limited conditions (i.e., the odd subrows) in Y2. **(A)** Operating efficiency of PSII (F_q'/F_m'), and both reoxidation processes, **(B)** F_{r1}' and **(C)** F_{r2}'. The contour plots were built based on the mean values of 9 days of field phenotyping, which were carried out at D1, D2, and D3 time points. The local time zone is Mountain Standard Time (MST).

For Y2, on average, H^2 for F'_q/F'_m, F'_{r1} and F'_{r2} were 0.65, 0.74 and 0.64, respectively, regardless of time (drought severity) and water treatment (WD and WW). Neither the genotype by treatment interaction effect nor the three-way interaction of genotype, treatment and time for ChlF traits were significant ($p > .10$) under the mild drought conditions in Y2.

Values of H^2 for SDMY and ΔRWC were 0.63 and 0.80, respectively, under the severe drought conditions in Y1. And H^2 for SDMY was 0.45 for both WD and WW plants in Y2 since the genotype by water treatment interaction effect was not significant ($p = 0.26$).

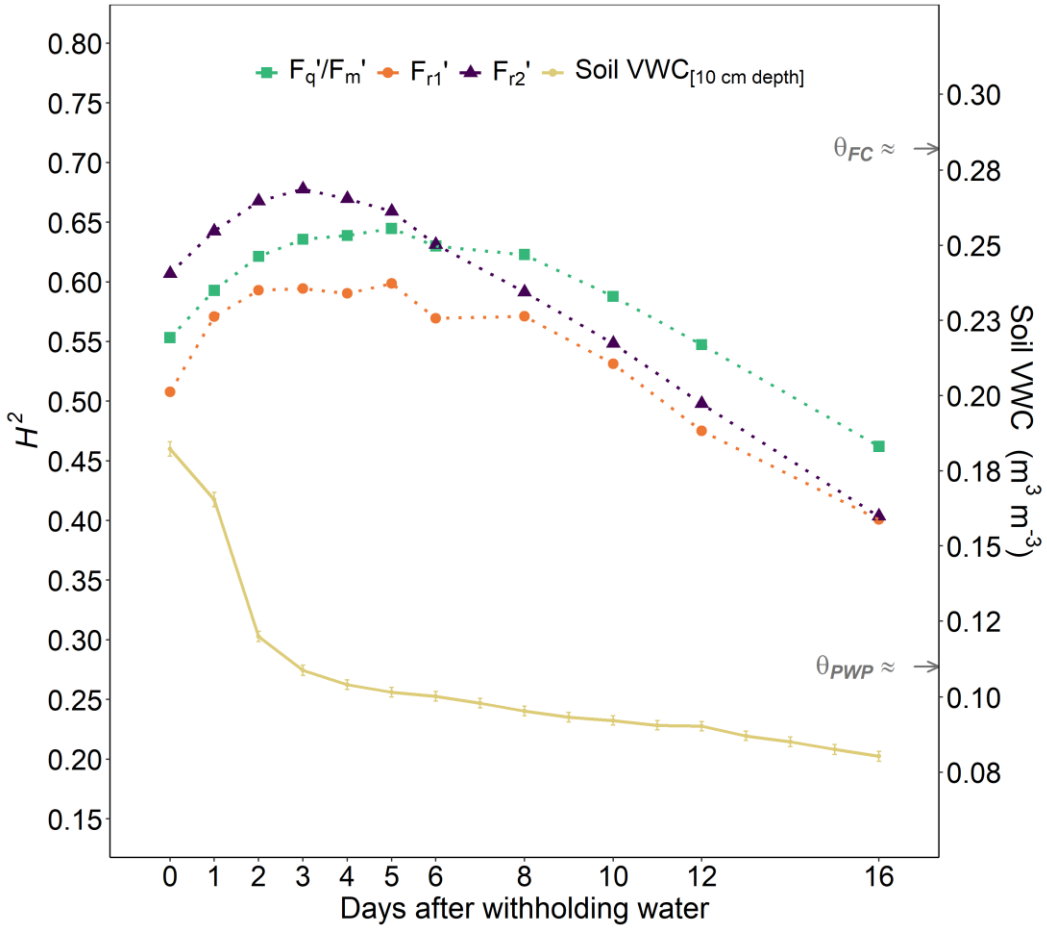

Figure 3.16. Dynamics of broad-sense heritability on an entry-mean basis (H^2) for operating efficiency of PSII (F'_q/F'_m) and both reoxidation processes, F'_{r1} and F'_{r2}, from light-adapted durum wheat plants under progressive drought stress, between 0 and 16 days after withholding water (DAWW), in Y1. The progression of soil volumetric water content (VWC) at 10 cm depth over time is also displayed. Small arrows on the right-hand side approximate to the soil permanent wilting point (θ_{PWP}) and the soil field capacity (θ_{FC}) at 10 cm depth.

3.1.7 Genetic and phenotypic correlations within ChlF traits over time

Pearson's correlation coefficients were used to assess the phenotypic correlations (r_p) within each ChlF trait while progressively increasing drought over time in Y1 (see Figure 3.17). The phenotypic correlations were variable and rarely found above 0.50, even between neighbouring time points, indicating that the fluctuating environment played a crucial role in driving the ChlF responses. Phenotypic correlations were almost null between non-stress (0 DAWW) and severe drought (16 DAWW) scenarios; r_p were 0.06 (p = .318), 0.11 (p = .074) and 0.08 (p = .181) for F_q'/F_m', F_{r1}' and F_{r2}', respectively.

To assess the genetic correlations (r_g) within each ChlF trait over time, in an evolving drought environment, serial correlation structures were fitted to the genotype by time interaction effect (i.e., the $G \cdot T$ term) in the LMM for Y1. The heterogeneous linear variance (LVH) was the best-fitting model for all ChlF traits, indicating unequal genetic variances among field phenotyping days, whose covariances also varied. In general, genetic correlations within each ChlF trait (Figure 3.17) were strong and positive among the nearest neighbouring time points (> 0.80 for a time-lag up to 3 days) and smoothly decayed according to the increasing temporal distance. Hence, r_g between contrasting environments, such as non-stressed at 0 DAWW and severe drought at 16 DAWW in Y1, for F_q'/F_m', F_{r1}' and F_{r2}' were as low as 0.28 (*SE* = 0.12), -0.10 (*SE* = 0.14) and 0.24 (*SE* = 0.12), respectively. The smooth decrease in r_g within ChlF traits over time strongly suggests that drought gradually induced a significant shifting in the estimated genotypic values over time. However, a relative increase in noise could not be ruled out as well.

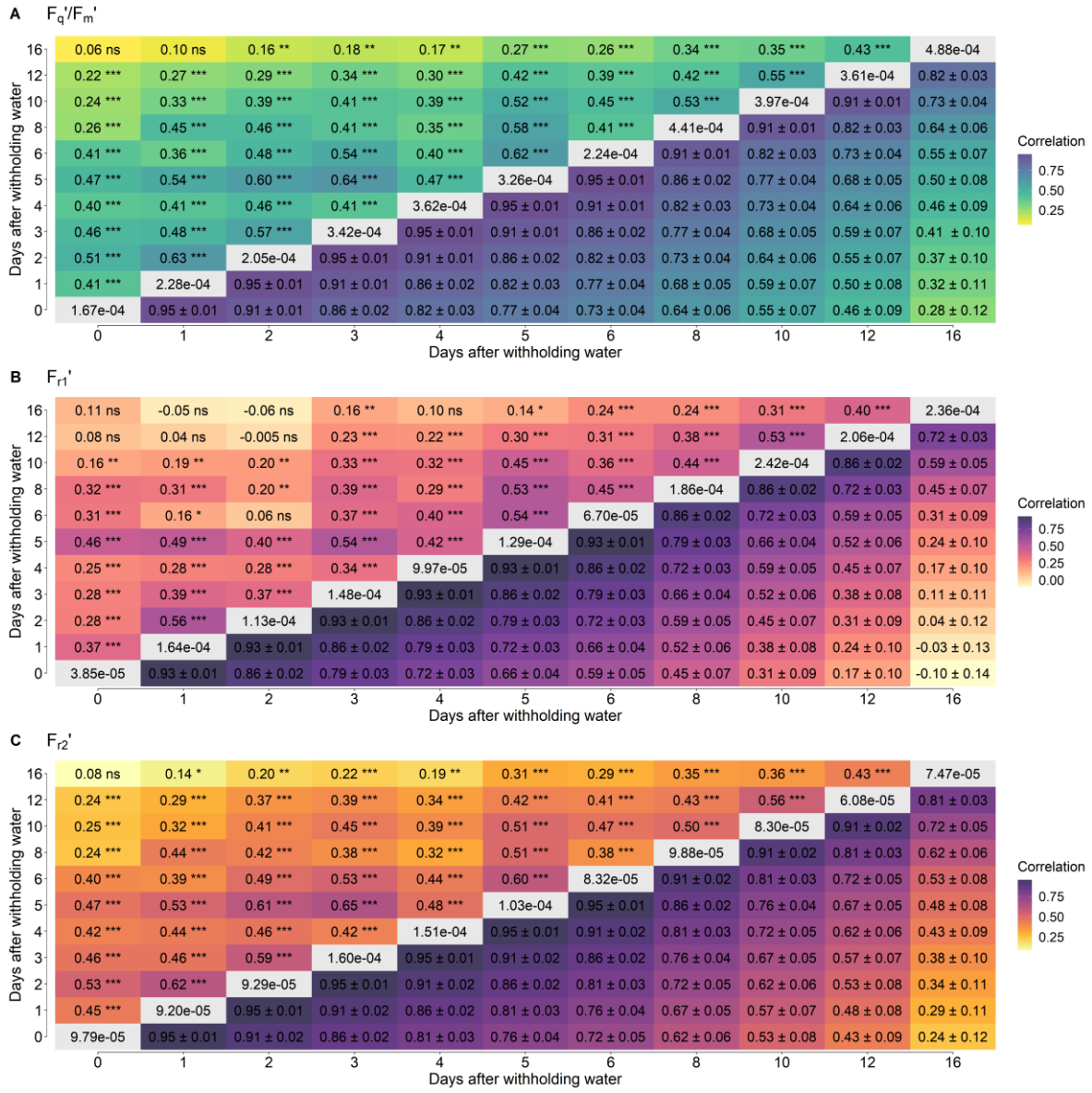

Figure 3.17. Phenotypic (r_p; above the diagonal) and genotypic (r_g; below the diagonal) correlation coefficients across different time points (i.e., days after withholding water) from 252 durum wheat genotypes under progressive drought assessed within each chlorophyll fluorescence trait: **(A)** operating efficiency of PSII (F_q'/F_m'), and both reoxidation processes, **(B)** F_{r1}' and **(C)** F_{r2}'. Values in the diagonal are the estimated genotypic variance (σ_g^2) component over time. Genotypic correlation coefficients are means ± *SE*. The levels of significance for the phenotypic correlation coefficients are indicated by *ns* (nonsignificant; $p > .05$), * ($p \leq .05$), ** ($p \leq .01$), and *** ($p \leq .001$).

3.1.8 Trait-trait genetic and phenotypic correlations

Bivariate LMMs for testing the genetic overlap between traits (see Methods) were fitted to investigate the trait-trait genetic correlations (r_g) over time between ChlF traits and SDMY or ΔRWC. The correlation patterns changed according to the drought severity (Figure 3.18). The r_g between F_q'/F_m' and SDMY (Figure 3.18A) decreased during the steady progression of drought, with the highest positive correlation at 1 DAWW (0.65, *SE* = 0.14, $p <$ .001), and a weak negative correlation at 16 DAWW (-0.21, *SE* = 0.34, p = .274). Both F_{r1}' and F_{r2}' (Figure 3.18A) showed similar r_g patterns with final SDMY over time, and they mirrored that displayed by F_q'/F_m'. During the mild drought in Y2, the r_g between ChlF traits and final SDMY (Figure 3.19) were, on average, 0.70, -0.45 and -0.65 for F_q'/F_m', F_{r1}' and F_{r2}', respectively, which were similar to those correlations observed at the onset of water-limiting conditions in Y1, particularly between 1 and 5 DAWW.

Time-varying genetic correlations were also evident between ChlF traits and the relative change in leaf RWC (Figure 3.18B). Within the first week after withholding water, r_g between F_q'/F_m' and ΔRWC was, on average, -0.36, and increased to 0.35 (*SE* = 0.28, p = .128) under severe stress at 16 DAWW. On the other hand, an opposite trend was seen for both reoxidation traits, F_{r1}' and F_{r2}', whose r_g with ΔRWC were, on average, 0.36 and 0.31, respectively, throughout the first week after imposing drought, and then shifted to -0.33 (*SE* = 0.22, p = .109) and -0.34 (*SE* = 0.33, p = .162), respectively, at 16 DAWW. For these same plants experiencing severe stress in Y1, r_g between SDMY and ΔRWC was -0.43 (*SE* = 0.10, $p <$ .001).

Trait-trait phenotypic correlations (r_p) over time between ChlF traits and SDMY (Figure 3.20A) or ΔRWC (Figure 3.20B) were estimated by Pearson's correlation coefficients. Similar to the genetic correlations (Figure 3.18), the phenotypic correlation patterns dynamically changed according to the drought severity. Indeed, all results for r_p exhibited analogous trends to those described for the trait-trait r_g, but the magnitude of the phenotypic associations were lower, especially between ChlF traits and SDMY. In Y1, r_p between SDMY and ΔRWC was -0.17 (p = .008).

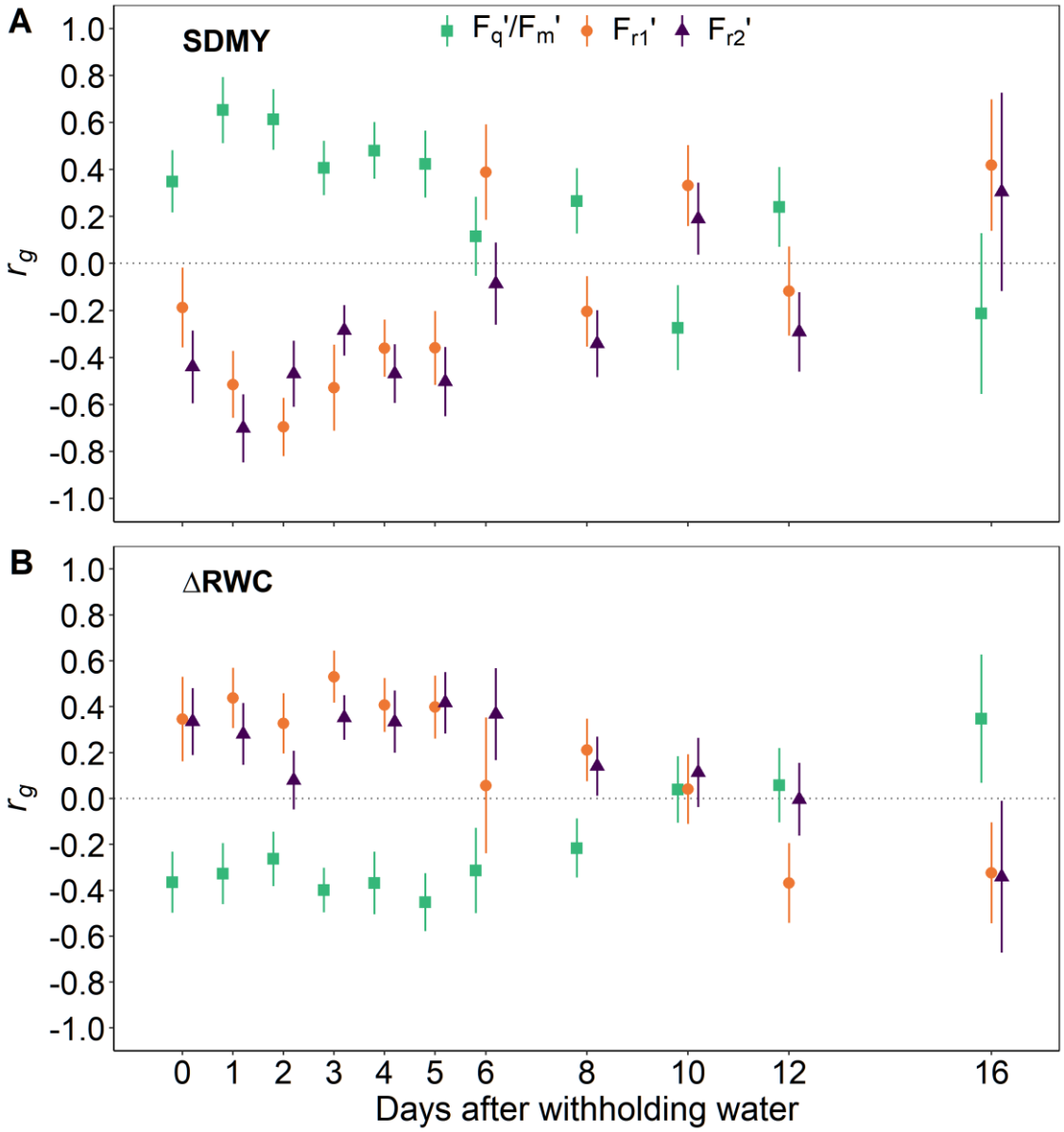

Figure 3.18. Mean trait-trait genetic correlations (r_g) ± *SE*, n = 252, from 0 to 16 days after withholding water (DAWW), between each chlorophyll fluorescence trait (F_q'/F_m', F_{r1}' and F_{r2}') and **(A)** the total shoot dry matter yield (SDMY) at the end of the stress period, and **(B)** the relative change in leaf relative water content (ΔRWC) as a consequence of the severe drought stress imposed in Y1.

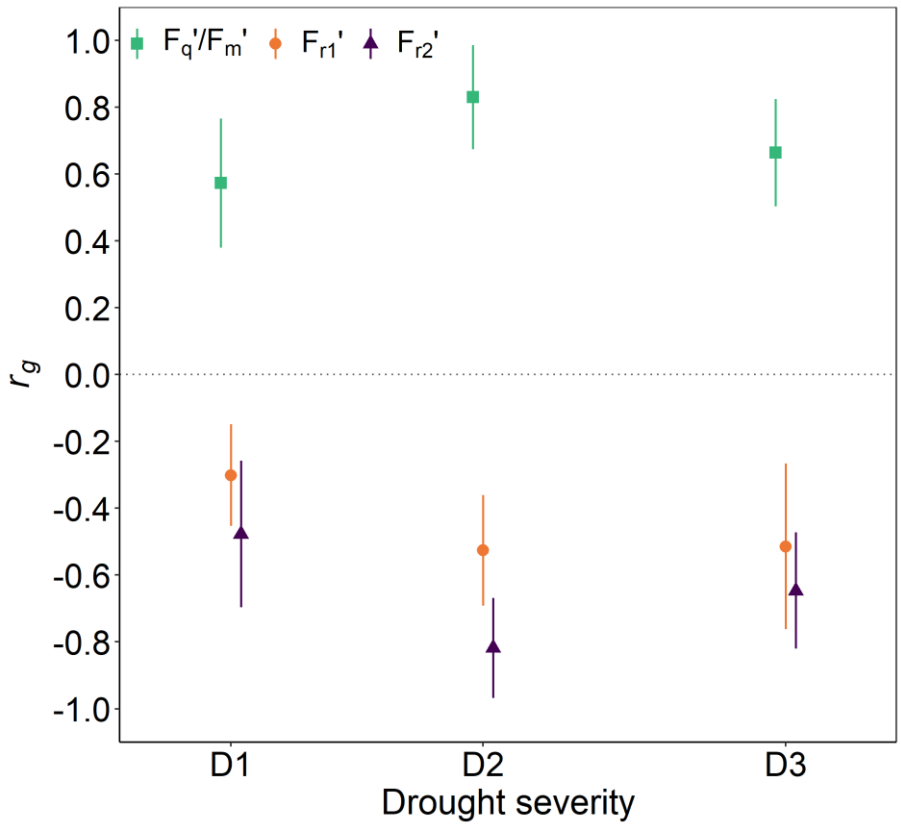

Figure 3.19. Mean trait-trait genetic correlations (r_g) ± *SE*, *n* = 224, over time (i.e., levels of drought severity D1, D2 and D3) between each chlorophyll fluorescence trait (F_q'/F_m', F_{r1}' and F_{r2}') and the total shoot dry matter yield (SDMY) at the end of the mild drought in Y2.

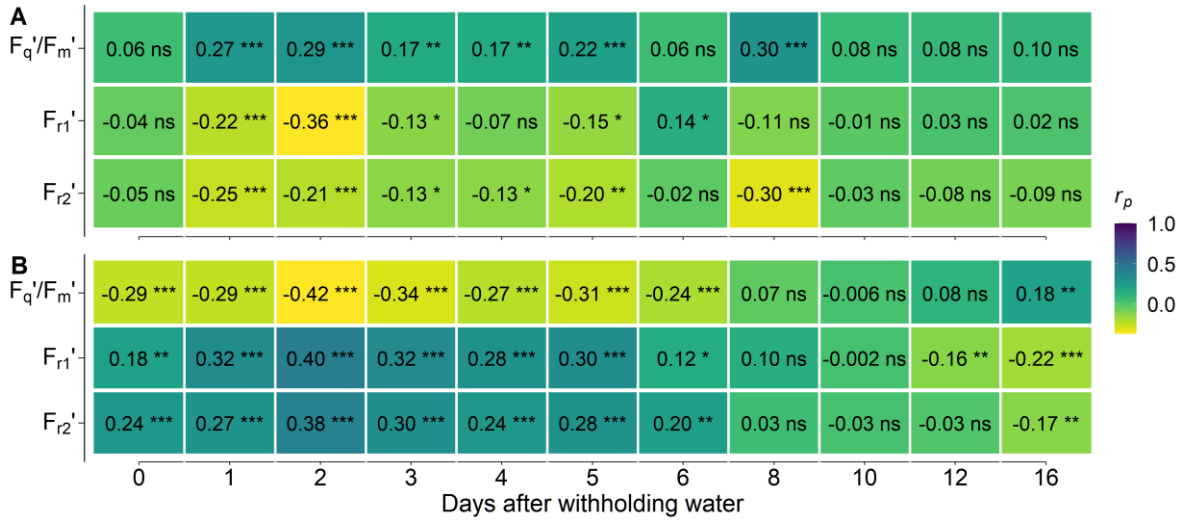

Figure 3.20. Pearson's coefficients of correlation (r_p), *n* = 252 genotypes, over time (days after withholding water) between each chlorophyll fluorescence trait (F_q'/F_m', F_{r1}' and F_{r2}') and **(A)** the total shoot dry matter yield (SDMY) at the end of the stress period, and **(B)** the relative change in leaf relative water content (ΔRWC) induced by the severe drought stress imposed in Y1. The levels of significance are indicated by *ns* (nonsignificant; $p > .05$), * ($p \leq .05$), ** ($p \leq .01$), and *** ($p \leq .001$).

3.1.9 Phenotypic plasticity and variability across subpopulations

The relationships between overall drought-induced percentage changes (%Δ), as a measure of phenotypic plasticity, and initial (non-stress) or final (severe stress) values for ChlF traits were evaluated for the subgroups of genotypes (Figure 3.21). For this assessment, we grouped genotypes into subpopulations (*S*) based on the genetic structure in the UNIBO-Durum Panel reported by Condorelli et al. (2018), as follows: *S*1 includes Mediterranean and North African germplasm; *S*2 includes cultivars bred for dryland areas at ICARDA (Syria) in the early 1970s; *S*3 includes mainly IRTA (Spain) and INRAE (Morocco) accessions bred in early 1970s, and CIMMYT and ICARDA accessions selected for temperate areas; *S*4 contains predominantly high-yielding materials for temperate zones from ICARDA, and some Italian accessions from the 1970s; *S*5 comprises materials derived from broadly adapted (photoperiod-insensitive) CIMMYT germplasm released between the late 1970s and the early 1980s; *S*6 includes Italian accessions from the mid-1970s; *S*7 includes mostly high-yielding CIMMYT genotypes released from the late 1980s and the early 1990s; *S*8 contains American (North Dakota), Canadian, French and Australian genotypes; and finally, due to a significant exchange of genetic resources among international breeding programmes, there is an admixture subgroup composed mainly by ICARDA, CIMMYT and Italian materials.

A weak negative correlation was found between the initial F_q'/F_m' values for genotypes under well-watered conditions at 0 DAWW and their respective %Δ after experiencing severe drought up to 16 DAWW (Figure 3.21A). On the other hand, moderate positive correlations were found for F_{r1}' (Figure 3.21B) and F_{r2}' (Figure 3.21C), whose initial values explained (by means of R^2) nearly 20% and 45%, respectively, of variability in %Δ throughout genotypes. Nevertheless, there was a strong positive correlation between the final F_q'/F_m' values for genotypes at 16 DAWW and their corresponding overall drought-induced percentage changes (Figure 3.21D), which explained around 70% of the variability. Similarly, there was a very strong correlation (negative) for final F_{r1}' values (Figure 3.21E), which explained almost 90% of %Δ variability. Final F_{r2}' values (Figure 3.21F) were moderately and negatively correlated with their respective %Δ, explaining roughly 30% of the variability. In short, based on Figures 3.21A and 3.21B, it is possible to state that F_q'/F_m' and F_{r1}' from non-stressed plants inform little about the a posteriori effect of drought across genotypes. On the other hand, F_q'/F_m' and F_{r1}' from severely stressed plants can better indicate those genotypes most and least affected by

drought (i.e., with the highest and the lowest %Δ), Figures 3.21D and 3.21E. Notably, F'_{r2} from both non-stressed and severely stressed plants may serve as indicators of the potential magnitude of drought effect across genotypes, but interpretations require caution since opposite relationships occurred (Figures 3.21C and 3.21F). It is noteworthy that genotypes grouped at the tail end of %Δ within each ChlF trait (i.e., the two extreme groups of 15 genotypes ranked at the top and bottom according to drought-induced relative changes in F'_q/F'_m, F'_{r1} or F'_{r2}) also had contrasting means for leaf ΔRWC, but equal means for SDMY (Table 3.2).

The variation among subpopulations alone accounted for approximately 7.5% (p < .001), 8.0% (p < .001) and 16.7% (p < .001) of the overall observed variation in the drought-induced %Δ for F'_q/F'_m, F'_{r1} and F'_{r2}, respectively. The subgroup *S*8 had the lowest overall %Δ in ChlF traits (Table 3.3), suggesting that genotypes from *S*8 were less prone to reduce photosynthetic activities even after severe drought stress.

Table 3.2. The average, median and median difference with ± 95% confidence interval (CI) between the two extreme groups of 15 durum wheat genotypes, ranked according to the drought-induced relative changes (%Δ) within each chlorophyll fluorescence (ChlF) trait (F'_q/F'_m, F'_{r1} and F'_{r2}), for the relative change in leaf relative water content (ΔRWC) and the total shoot dry matter yield (SDMY) traits in 2017/2018 (Y1). L and H stand for the groups with the lowest and the highest %Δ, respectively, within each ChlF trait. The Mann-Whitney *U*-test was used to compare differences between the two groups.

Measure	**%Δ in F'_q/F'_m** †		**%Δ in F'_{r1}** ‡		**%Δ in F'_{r2}** §	
	L	**H**	**L**	**H**	**L**	**H**
			ΔRWC (%Δ)			
Average	-20.2	-30.2	-21.4	-31.0	-20.6	-28.8
Median	-20.2	-32.1	-21.3	-31.6	-20.8	-30.2
Median difference [95% CI]	11.2 [5.94, 14.4]		10.1 [6.44, 12.9]		9.07 [5.13, 12.2]	
U-statistic (*p*-value)	19.0 (< .001)		15.0 (< .001)		26.0 (< .001)	
			SDMY (kg ha^{-1})			
Average	5241	5160	5121	5260	5115	5117
Median	5251	5198	4994	5228	5100	5081
Median difference [95% CI]	99.6 [-155, 336]		-152 [-366, 116]		-4.94 [-264, 274]	
U-statistic (*p*-value)	92.0 (.412)		81.0 (.202)		112.0 (1.00)	

†Average drought-induced relative changes in F'_q/F'_m for L and H groups were -7.81 and -23.2 %Δ, respectively; ‡Average drought-induced relative changes in F'_{r1} for L and H groups were -11.8 and -28.6 %Δ, respectively; §Average drought-induced relative changes in F'_{r2} for L and H groups were -10.7 and -32.3 %Δ, respectively.

Table 3.3. The average overall drought-induced relative changes (%Δ) within each chlorophyll fluorescence trait (F'_q/F'_m, F'_{r1} and F'_{r2}) among the durum wheat subpopulations in 2017/2018 (Y1). Genotypes were assembled into subgroups (*S*) according to the population genetic structure reported by Condorelli et al. (2018). Values are means ± *SE*. Different lowercase letters within the same trait are statistically different, according to the Fisher-Hayter procedure at p = .05.

Subgroup	%Δ in F'_q/F'_m		%Δ in F'_{r1}		%Δ in F'_{r2}	
Admixture	-15.7 ± 0.39	b	-19.6 ± 0.43	ab	-23.1 ± 0.42	b
*S*1	-17.8 ± 1.31	b	-23.2 ± 1.43	b	-24.0 ± 1.43	b
*S*2	-15.4 ± 1.11	ab	-22.8 ± 1.22	b	-23.4 ± 1.21	b
*S*3	-17.4 ± 0.92	b	-21.4 ± 1.01	b	-25.7 ± 1.00	b
*S*4	-16.4 ± 0.79	b	-19.1 ± 0.86	ab	-24.9 ± 0.85	b
*S*5	-16.5 ± 0.87	b	-20.0 ± 0.95	ab	-26.0 ± 0.95	b
*S*6	-16.4 ± 1.07	b	-19.5 ± 1.17	ab	-22.6 ± 1.16	ab
*S*7	-16.4 ± 0.71	b	-21.0 ± 0.78	b	-23.2 ± 0.77	b
*S*8	-13.2 ± 0.59	a	-17.6 ± 0.65	a	-17.9 ± 0.64	a

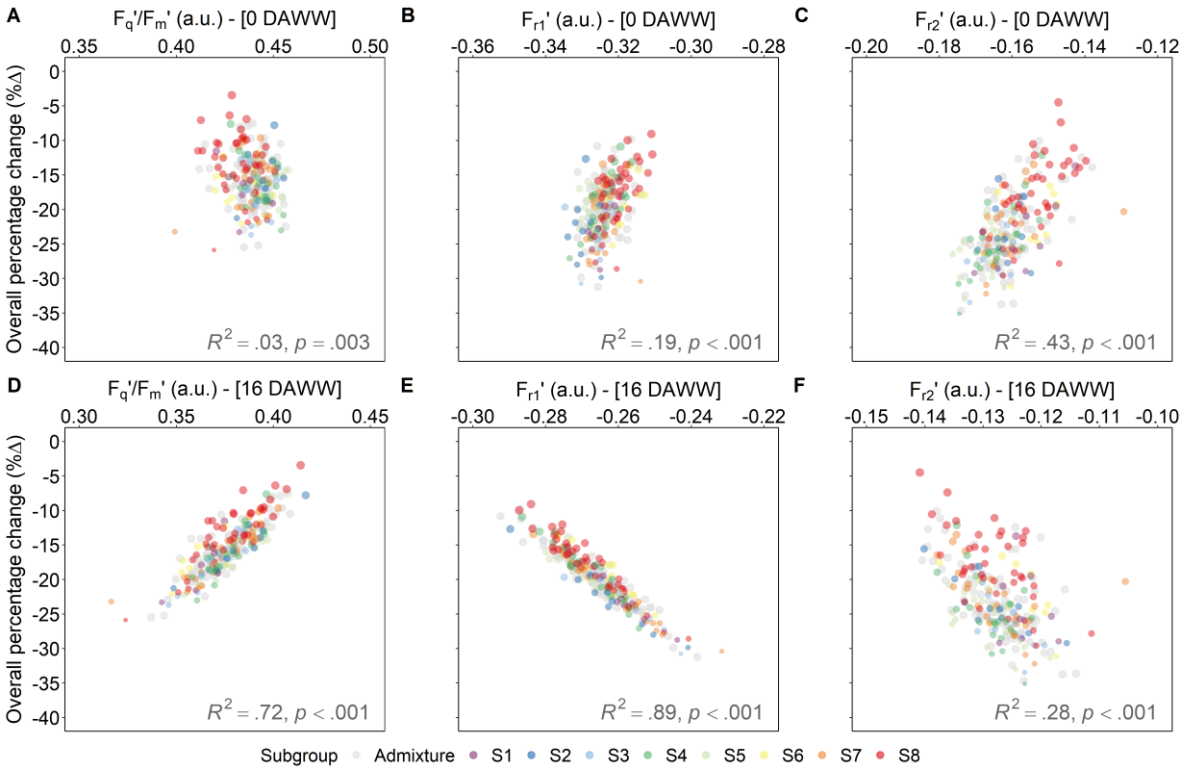

Figure 3.21. Relationships across durum wheat genotypes between the overall percentage changes (%Δ; i.e., the size of the absolute change between 0 to 16 DAWW in comparison to the reference value at 0 DAWW) in chlorophyll fluorescence (ChlF) traits induced by severe drought and their initial **(A)** F'_q/F'_m, **(B)** F'_{r1}, and **(C)** F'_{r2} values measured in non-stressed plants at 0 days after withholding water (DAWW), or their final **(D)** F'_q/F'_m, **(E)** F'_{r1}, and **(F)** F'_{r2} values measured in severely stressed plants at 16 DAWW. Genotypes were assembled into subgroups (S) according to the population genetic structure reported by Condorelli et al. (2018).

3.2 GREENHOUSE TRIAL RESULTS

3.2.1 Overall effects of drought at the canopy and leaf level

The imposed drought stress was able to drive changes on all of the plant traits measured either at the canopy or leaf level (Table 3.4). Nonetheless, some of the traits quantified at the leaf level and low-throughput, such as leaf gas exchange (i.e., net CO_2 assimilation, A_n; stomatal conductance, g_s; intercellular CO_2 concentration, C_i; and transpiration rate, E), were unable to statistically distinct the genotypes or to uncover either the genotype-by-water treatment or the genotype-by-water treatment-by-time interaction effect.

Table 3.4. Probability values (exact *p*-values) for the estimates of variance components (genotypic, σ_g^2; water treatment, σ_w^2; time, σ_t^2; genotype-by-water treatment interaction, σ_{gw}^2; genotype-by-time interaction, σ_{gt}^2; water treatment-by-time interaction, σ_{gt}^2; and genotype-by-water treatment-by-time interaction, σ_{gwt}^2) for each trait measured in semi-controlled greenhouse conditions.

Trait†	σ_g^2	σ_w^2	σ_t^2	σ_{gw}^2	σ_{gt}^2	σ_{wt}^2	σ_{gwt}^2
F'_q/F'_m	< .001	.011	< .001	.050	< .001	.017	.116
F'_{r1}	< .001	< .001	< .001	.053	< .001	.009	.336
F'_{r2}	< .001	.057	< .001	.011	< .001	.015	.312
PLA	< .001	< .001	< .001	< .001	< .001	< .001	.340
ETR	< .001	< .001	.019	.302	< .001	< .001	.001
BBCH	< .001	.032	< .001	.859	< .001	< .001	< .001
A_n	.101	< .001	< .001	.487	.151	< .001	.500
g_s	.329	< .001	.548	.640	.245	.002	.225
C_i	.633	< .001	.053	.977	.153	.005	.054
E	.245	< .001	.028	.296	.387	.004	.216
SDM	< .001	< .001	-	< .001	-	-	-
LA	< .001	< .001	-	.009	-	-	-
CMS	< .001	< .001	-	.016	-	-	-

†Traits are operating efficiency of PSII (F'_q/F'_m), electron transfer rate from Q_A to PQ pool (F'_{r1}), electron transfer rate from PQ pool to PSI (F'_{r2}), projected leaf area (PLA), daily whole-plant evapotranspiration rate (ETR), plant phenological growth stage (BBCH), leaf net CO_2 assimilation (A_n), leaf stomatal conductance (g_s), leaf intercellular CO_2 concentration (C_i), leaf transpiration rate (E), final total shoot dry matter per plant (SDM), final total leaf area per plant (LA), and cell membrane stability (CMS).

At the leaf level, only the cell membrane stability (CMS) trait, in terms of the electrolyte leakage, was able to differentiate genotypes and their interactions with the imposed water treatment (Table 3.4). On the other hand, at the canopy level, the traits measured at both low (e.g., SDM, LA and BBCH) and high-throughput (e.g., ChlF traits, PLA and ETR) facilitated the assessment of drought effects among genotypes (i.e., σ^2_{gw}), across time (i.e., σ^2_{wt}), and/or their triple interaction (i.e., σ^2_{gwt}), see Table 3.4. In short, these traits were able to identify differences among genotypes and/or water treatment over time.

3.2.2 Effects of drought on plant growth and development

The imposed drought stress of 25% of the plant available water (PAW) up to 38 days after sowing (DAS) had no evident impact on plant phenological development (Figure 3.22A), at least not at early vegetative stages. Significant differences in phenological growth stages, due to water treatment, were only observed at 41 DAS ($p < .001$) and 43 DAS ($p = .030$), when plants were at either late vegetative stages or the beginning of the inflorescence emergence (i.e., beyond the late booting or beginning of heading), whilst the drought was further increased up to 15% of PAW. Overall, during these time points, WD plants had a slight anticipated development compared to WW plants. This difference, though, became less noticeable after 51 DAS. However, as the phenology was visually monitored by scoring plants based on the BBCH scale (i.e., non-destructively), the assessment of late reproductive stages (i.e., anthesis and grain filling) can be subjective and error-prone.

Despite the minor effects on plant development, drought stress caused a significant reduction in plant growth by means of projected leaf area (PLA; Figure 3.22B). After the first week of drought, it was already observed an overall reduction of 25.2% in the PLA of WD plants compared to WW plants. This difference further increased till 50 DAS (i.e., 30 days after imposing drought), where the PLA of non-stressed plants was about 2.3-fold higher than of drought-stressed plants. Relationship across genotypes between PLA and the final total shoot dry matter per plant (SDM) was assessed at 62 DAS (i.e., 41 days after imposing drought; Figure 3.22D). Regardless of water treatment, PLA positively correlated with SDM ($R^2 = .93$, $p < .001$), indicating that PLA may serve as a sound proxy for quantifying total above-ground biomass non-invasively.

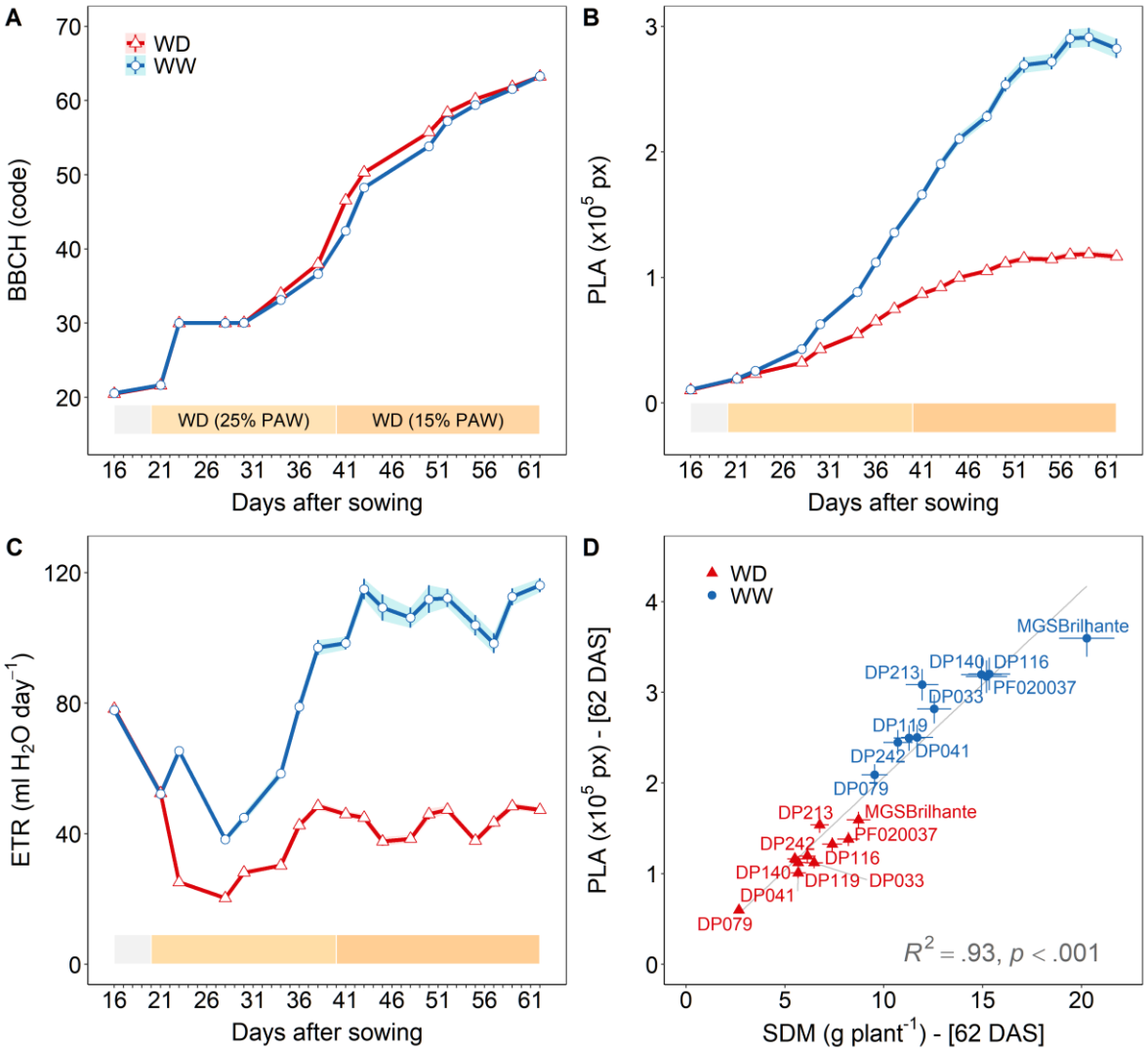

Figure 3.22. The effects of drought stress on **(A)** plant phenological development by means of BBCH scale, **(B)** projected leaf area (PLA), and **(C)** daily evapotranspiration rate (ETR) of wheat plants growing in semi-controlled greenhouse conditions. Values are means ± *SE*, averaged across genotypes, n = 10. Drought severity was 25% of plant available water (PAW), between 21 and 40 days after sowing (DAS), and 15% of PAW, between 41 and 62 DAS. **(D)** Relationship across genotypes between the final total shoot dry matter (SDM) and the PLA at 62 DAS for both well-watered (WW) and water-limited (WD) plants. Values are means ± *SE*, n = 6.

The changes over time in projected above-ground biomass reflected in the estimated daily evapotranspiration rates (ETR; Figure 3.22C). During the first two weeks after transplanting, between 16 and 30 DAS, while plants were still acclimating to the newly offered growth conditions with minor increases in PLA, both WW and WD plants reduced the ETR. However, this reduction was more exacerbated in WD plants. Subsequently, from 36 to 62 DAS, ETR for WD plants remained stable at ~44.2 ml day^{-1}, without being meaningfully affected by increasing drought intensity from 25% to 15% of PAW (Figure 3.22C). On the other hand, ETR for WW plants sharply rose from 30 to 43 DAS, during the exponential plant growth

phase, and then remained stable at ~109 ml day^{-1} until 62 DAS (Figure 3.22C), when plants reached their maximum projected above-ground biomass and were at reproductive stages, Figures 3.22B and 3.22A, respectively.

3.2.3 Effects of drought on leaf gas exchange and cell membrane stability

The drought stress adversely affected net CO_2 assimilation (A_n), stomatal conductance (g_s), intercellular CO_2 concentration (C_i), and transpiration rate (E) at the leaf level (Figure 3.23). Significant drought-induced reductions of 11.7%, 13.5%, 46.3%, and 32.1% in A_n, C_i, g_s, and E, respectively, were evident at 37 DAS (i.e., when flag leaves were just visible) but not at 58 DAS (i.e., when plants were at the beginning of flowering). Solely WW plants had their A_n, g_s, and E reduced, on average, by 15.3%, 21.1%, and 19.3%, respectively, at 58 DAS relatively to 37 DAS (Figures 3.23A, 3.23C and 3.23D). These decreases in the photosynthetic activities of WW plants over time, but not for WD plants, may explain the lack of a significant drought effect at 58 DAS.

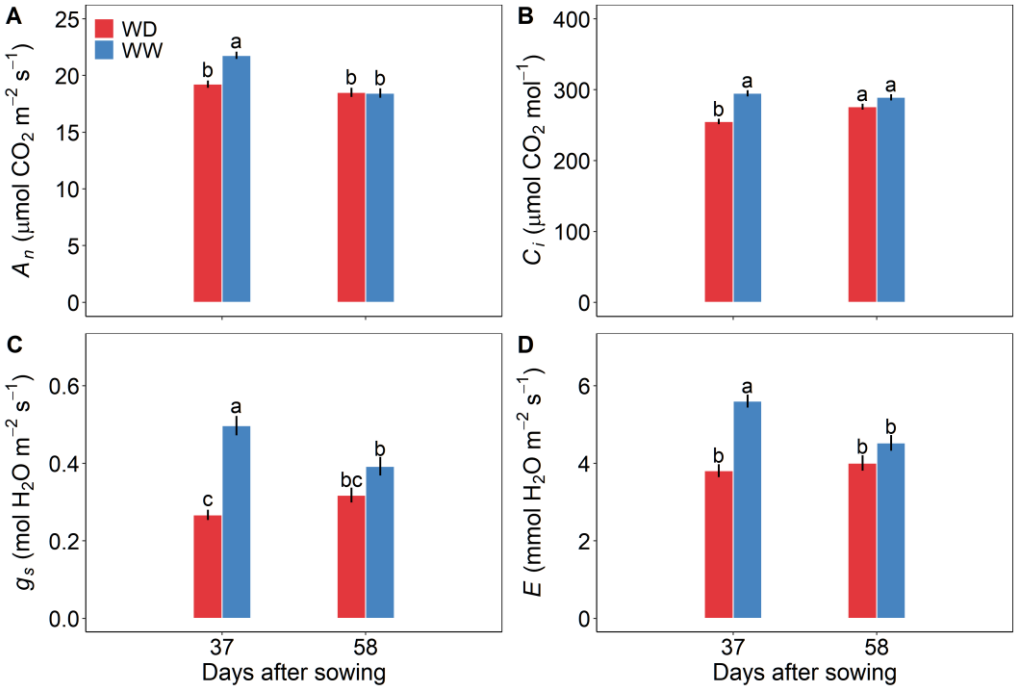

Figure 3.23. (A) Net CO_2 assimilation (A_n), **(B)** intercellular CO_2 concentration (C_i), **(C)** stomatal conductance (g_s), and **(D)** transpiration rate (E) at the leaf level of well-watered (WW) and water-limited (WD) wheat plants growing in semi-controlled greenhouse conditions at 37 and 58 days after sowing. Values are means ± *SE*, averaged across genotypes, n = 10. Different lowercase letters within the same trait are statistically different, according to Fisher-Hayter's test at p = .05.

Leaf cell membrane stability (CMS), in terms of percentage of electrolyte leakage, varied among genotypes ($p < .001$), and between water treatments ($p < .001$), Table 3.4. Overall, WD plants (M = 4.69%, SE = 0.15) had more leaf electrolyte leakage (i.e., lower CMS) than WW plants (M = 3.42%, SE = 0.11). However, the magnitude of this drought-induced leaf injury significantly varied among genotypes (p = .016), as reported in Figure 3.24. In general, genotypes with lower CMS (i.e., leaked the most) in well-watered conditions also tended to leak to a greater extent under drought stress; in other words, a greater leaf cell injury was observed.

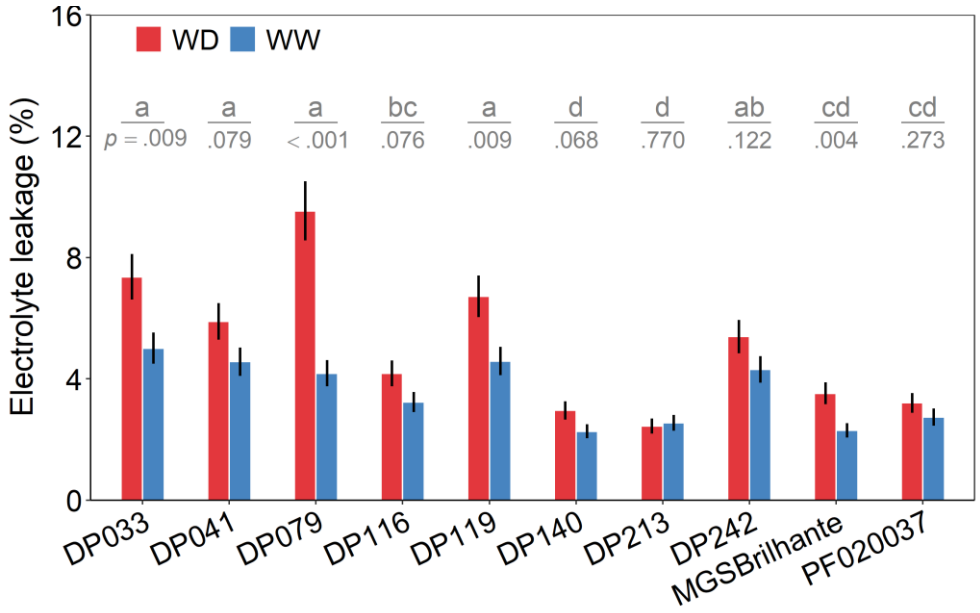

Figure 3.24. Leaf cell membrane stability, by means of percentage of electrolyte leakage, per wheat genotype under well-watered (WW) and water-limited (WD) conditions at 56 days after sowing (i.e., 35 days after imposing water treatment). Potted plants were grown in a semi-controlled greenhouse. Values are means ± *SE*, n = 6. Different lowercase letters above the line segments (i.e., at the genotypic level) are statistically different, according to Fisher-Hayter's test at p = .05. The probability values (exact p-values) for comparing WW and WD treatments within a genotype are displayed below the line segments.

3.2.4 Effects of drought stress on the LIFT-measured ChlF traits

Apart from the main effect of genotype being significant ($p < .001$) for all of the ChlF traits, the water treatment also did impact F'_q/F'_m (p = .011) and F'_{r1} ($p < .001$) but only marginally F'_{r2} (p = .057), Table 3.4. In fact, the LIFT-measured ChlF traits dynamically changed over time (Figure 3.25). The sources of variations were essentially due to the genotype-

by-time and the water treatment-by-time interactions, whereas the triple interaction between genotype, water treatment and time revealed not significant ($p > .10$) for any of the ChlF traits (Table 3.4). The overall daily changes during the vegetative stages, between 16 and 40 DAS, particularly in F_q'/F_m' (Figure 3.25A) and F_{r2}' (Figure 3.25E), may also be partially explained by variations in daily light intensity (i.e., PPFD) and VPD, the latter largely being driven by temperature (Figure 3.26). For instance, the combination of low PPFD and VPD observed at 28 DAS (Figure 3.26) may have resulted in a higher F_q'/F_m' and a faster F_{r2}', which were even more exacerbated in WD plants (Figures 3.25A and 3.25E). Conversely, at 38 DAS, when there was a sudden peak of high PPFD and VPD (Figure 3.26), F_q'/F_m' reduced and F_{r2}' slowed down (Figures 3.25A and 3.25E). Furthermore, plant development may also help clarify some of the overall daily changes in the ChlF traits. F_{r1}' (Figure 3.25C), for example, linearly accelerated from the early vegetative stages towards the beginning of the heading phase at 43 DAS, when there was the fastest kinetics of electron transfer from Q_A to *PQ* pool. After this peak, however, F_{r1}' linearly decelerated with advancing plant maturity up to 62 DAS. Likewise, F_{r2}' also slowed down, and F_q'/F_m' decreased upon mature plants (Figure 3.25).

The drought-induced relative changes in ChlF traits over time is reported in Figures 3.25B, 3.25D and 3.25F. F_q'/F_m' and F_{r2}' displayed similar trends over time, where mostly no significant differences between WW and WD plants were observed from 21 to 43 DAS (i.e., between 0 and 22 days after imposing water treatment). The exception was at 28 DAS, where F_q'/F_m' and F_{r2}' for WD plants were increased by +1.50% (SE = 0.58, p = .011) and +3.71% (SE = 1.09, $p < .001$), respectively, compared to WW plants (Figures 3.25B and 3.25F). However, upon reproductive stages (from 50 to 62 DAS), F_q'/F_m' and F_{r2}' for WD plants were reduced, on average, in -2.07% and -2.35%, respectively, compared to WW plants. By contrast, F_{r1}' (Figure 3.25D) for WD plants remained consistently higher (i.e., accelerated) compared to WW plants, +3.65% on average, from 23 to 50 DAS (i.e., between 2 and 29 days after imposing water treatment). However, no differences between WW and WD plants for F_{r1}' were observed beyond 50 DAS (Figure 3.25D).

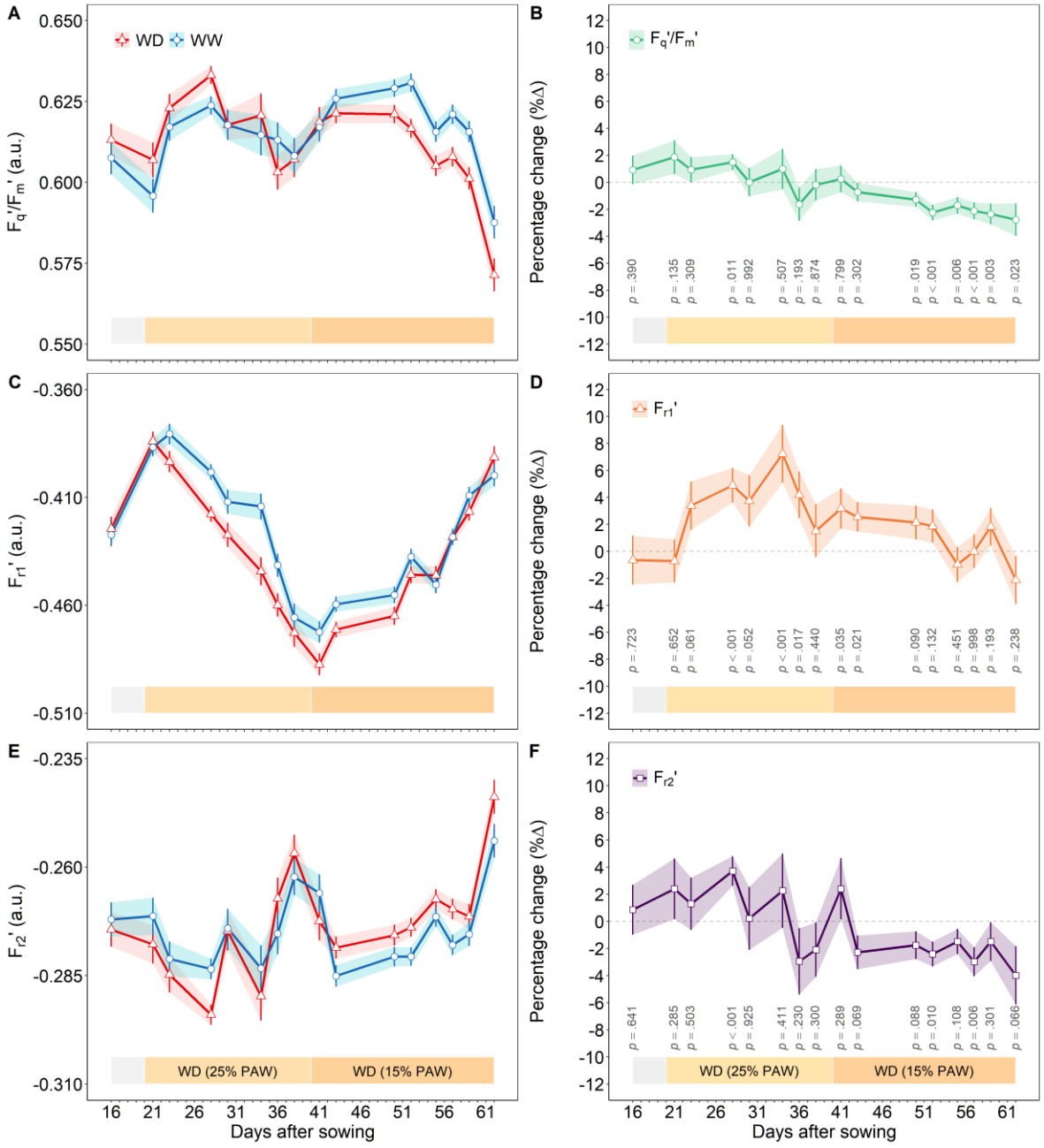

Figure 3.25. LIFT-measured chlorophyll fluorescence traits over time from light-adapted wheat plants growing in semi-controlled greenhouse conditions. On the left-hand side, mean values ± *SE*, averaged across genotypes, n = 10, for well-watered (WW) and water-limited (WD) plants. On the right-hand side, mean relative changes ± *SE* are shown with respect to non-stressed plants (i.e., WW as the reference, 0%); exact *p*-values are displayed. **(A – B)** Operating efficiency of PSII (F_q'/F_m'), and both reoxidation processes, **(C – D)** F_{r1}' and **(E – F)** F_{r2}'. Drought severity was 25% of plant available water (PAW), between 21 and 40 days after sowing (DAS), and 15% of PAW, between 41 and 62 DAS.

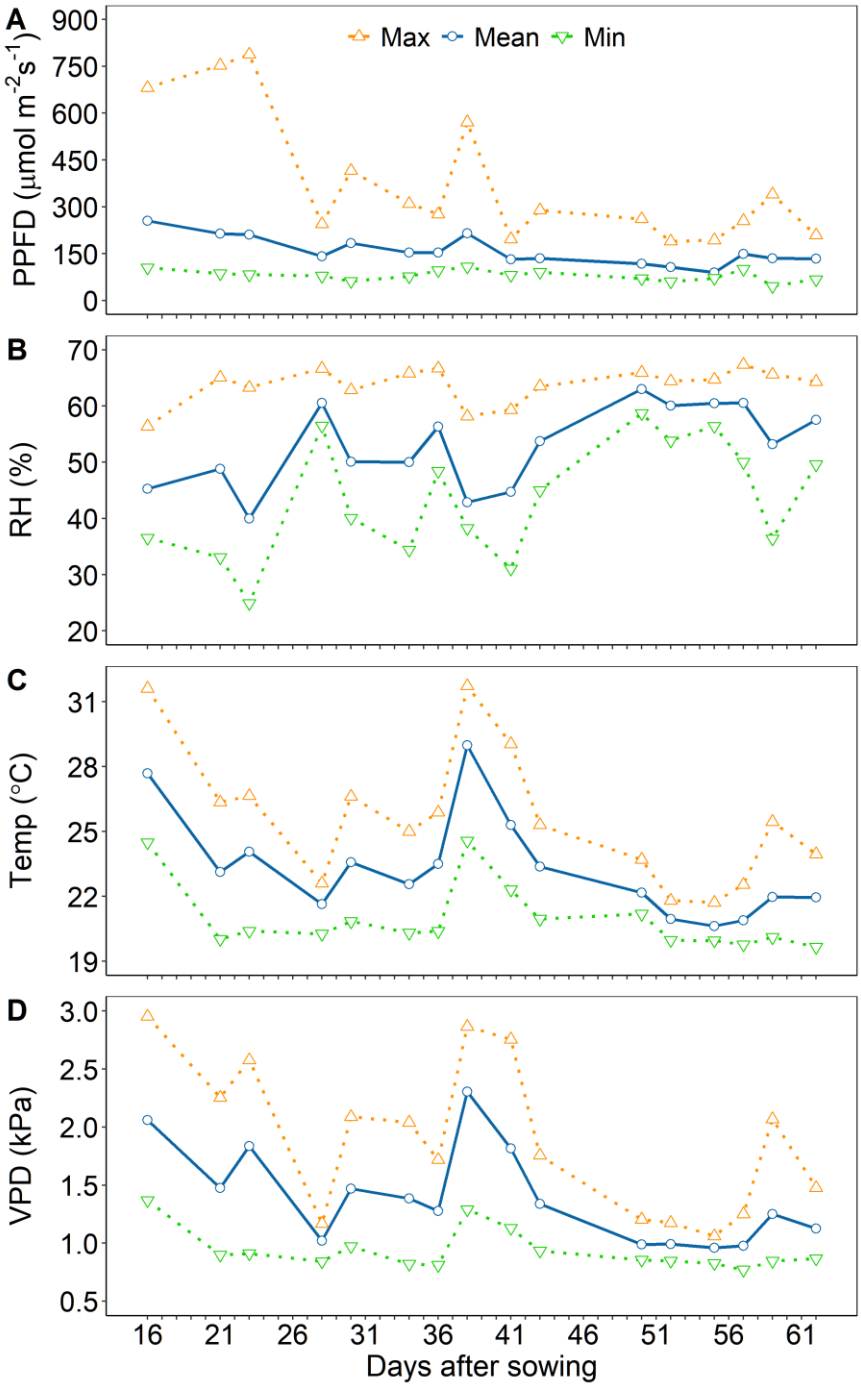

Figure 3.26. Daily mean, maximum and minimum values for **(A)** photosynthetic photon flux density (PPFD; µmol m^{-2} s^{-1}), **(B)** air relative humidity (RH; %), **(C)** air temperature (Temp; °C), and **(D)** air vapour pressure deficit (VPD; kPa) for the time period when LIFT data were acquired between 20 September and 05 November 2018 (i.e., between 16 and 62 days after sowing). Environmental data were recorded at 1-min interval in a semi-controlled glass greenhouse at the Institute of Bio- and Geosciences, Plant Sciences (IBG-2), Forschungszentrum Jülich GmbH (50.90976°N, 6.41313°E, elevation 100 m), in Jülich, Germany.

Strong relationships among the relative changes in ChlF traits across genotypes were observed in response to drought (Figure 3.27). The relative changes in F_q'/F_m' positively correlated with the relative changes in F_{r1}' (R^2 = .77, p < .001) and F_{r2}' (R^2 = .88, p < .001), as shown in Figures 3.27A and 3.27B, respectively. There was also a positive correlation between the relative changes in both reoxidation processes (R^2 = .81, p < .001), Figure 3.27C. These results indicate that ChlF traits were highly coordinated, and their drought-induced changes were plastically modulated at the genotypic level. In other words, those genotypes that accelerated or slowed down their reoxidation processes, both F_{r1}' and F_{r2}', also did better or worse at alleviating the decrease in the operating efficiency of PSII due to drought stress (Figure 3.27). Even though the magnitude of these modulation processes did not differ between vegetative and reproductive stages, small or no reductions in F_q'/F_m' and F_{r2}', relative to WW conditions, were noticed predominantly at vegetative stages (Figure 3.27).

Strong relationships were also observed between the relative changes in ChlF traits and the relative changes in PLA across genotypes in response to drought (Figure 3.28). The relative changes in PLA positively correlated with the relative changes in F_q'/F_m' (R^2 = .59, p < .001) and both reoxidation processes, F_{r1}' (R^2 = .51, p < .001) and F_{r2}' (R^2 = .61, p < .001), as reported in Figures 3.28A, 3.28B and 3.28C, respectively. Altogether, those genotypes that had the smallest or the largest reductions in their photosynthetic activities in terms of ChlF traits, relatively to WW treatment, also tended to have the smallest or the largest reductions in their PLA due to drought stress (Figure 3.28). Even though the magnitude of these effects did not differ between vegetative and reproductive stages, the cumulative drought did affect PLA more adversely at reproductive stages (i.e., when there were the largest reductions in PLA), see Figure 3.28.

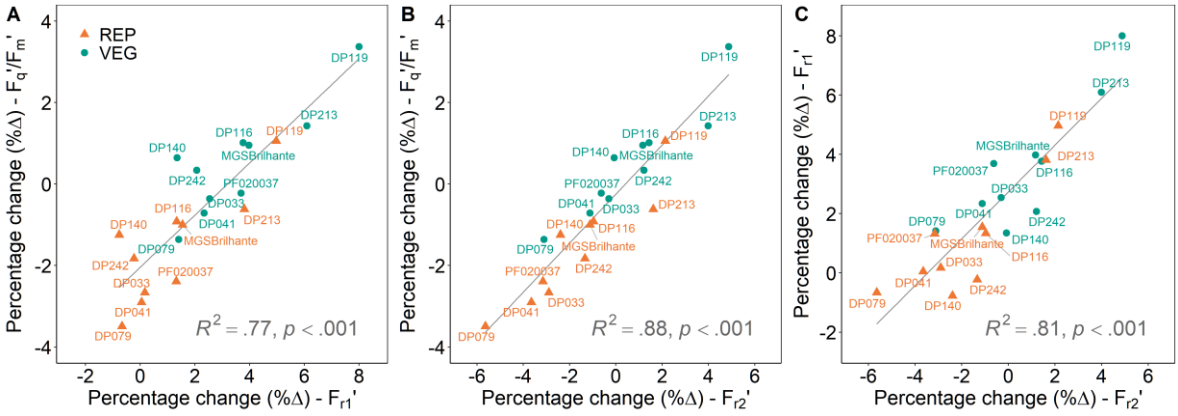

Figure 3.27. Relationships across genotypes among the drought-induced percentage changes (%Δ) in chlorophyll fluorescence (ChlF) traits from light-adapted wheat plants growing in semi-controlled greenhouse conditions. Relationships between **(A)** F'_q/F'_m and F'_{r1}; **(B)** F'_q/F'_m and F'_{r2}; and **(C)** both reoxidation processes, F'_{r1} and F'_{r2}. Values are overall means at the genotypic level for the relative changes in ChlF traits during the vegetative period (VEG; i.e., the average relative changes between 21 and 40 days after sowing, DAS, n = 6), and the reproductive period (REP; i.e., the average relative changes between 41 and 62 DAS, n = 8). The well-watered treatment set as the reference at 0%.

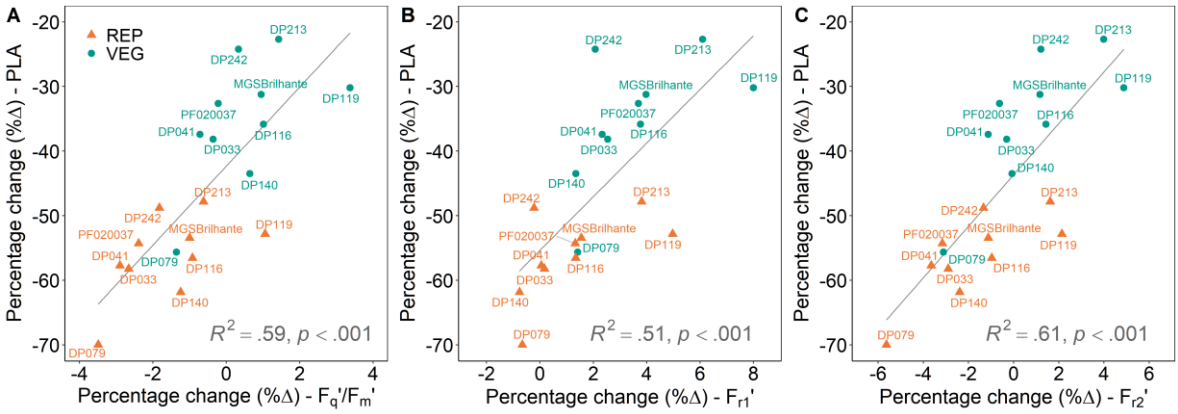

Figure 3.28. Relationships across genotypes between the drought-induced percentage changes (%Δ) in projected leaf area (PLA) and in chlorophyll fluorescence (ChlF) traits from light-adapted wheat plants growing in semi-controlled greenhouse conditions. Relationships between PLA and **(A)** F'_q/F'_m; **(B)** F'_{r1}; **(C)** F'_{r2}. Values are overall means at the genotypic level for the relative changes during the vegetative period (VEG; i.e., the average relative changes between 21 and 40 days after sowing, DAS, n = 6), and the reproductive period (REP; i.e., the average relative changes between 41 and 62 DAS, n = 8). The well-watered treatment set as the reference at 0%.

3.2.5 ChlF traits in response to light intensity and VPD

Variable ambient light ($PPFD$) and air VPD, both log-transformed, as well as their interaction effect ($\log PPFD \cdot \log VPD$), were major fluctuating environmental factors driving nonlinear changes in the ChlF traits from light-adapted plants (Table 3.5). Increasing light intensity from 50 to 750 µmol m^{-2} s^{-1} induced a continuous but nonlinear reduction in F_q'/F_m' (Figure 3.29A) and a deceleration in F_{r2}' (Figure 3.29B). These effects were even more pronounced when VPD increased from 1.0 to 2.0 kPa, especially for F_{r2}', while VPD had a minor effect on F_q'/F_m' when light intensity was > 500 µmol m^{-2} s^{-1}. On the one hand, F_{r1}' (Figures 3.29C and 3.29D) also slowed down under increasing $PPFD$, but on the other hand, it accelerated under higher VPD, especially at light intensity > 250 µmol m^{-2} s^{-1}. Notably, solely for F_{r1}' trait (Table 3.5) the triple interaction between $PPFD$, VPD and water treatment was significant (p = .027). F_{r1}' for WD plants, for instance, remained almost unchanged (M = -0.44) in VPD at 2.0 kPa and increasing $PPFD$ from 50 to 750 µmol m^{-2} s^{-1} (Figure 3.29C), whereas F_{r1}' for WW plants decelerated roughly 14.2% over the same environmental conditions (Figure 3.29D). Moreover, under low light intensity (i.e., < 150 µmol m^{-2} s^{-1}) and low VPD (i.e., at 1.0 kPa), F_{r1}' was faster in WD than in WW plants (Figures 3.29C and 3.29D).

Table 3.5. Effect size, standard error (*SE*), conditional *F*-test statistic, and probability values of environmental covariates for each chlorophyll fluorescence trait (F'_q/F'_m, F'_{r1} and F'_{r2}) from light-adapted wheat plants under drought stress in semi-controlled greenhouse conditions. $PPFD$ is photosynthetic photon flux density, VPD is vapour pressure deficit, and TRT is water treatment.

Trait	Covariate[†]	Effect	*SE*	*F*-statistic (*ndf*, *ddf*)	*p*-value
$\boldsymbol{F'_q/F'_m}$					
	$\log PPFD$	-0.017	0.002	152 (1, 1183)	< .001
	$\log VPD$	-0.044	0.004	110 (1, 973)	< .001
	$\log PPFD \cdot \log VPD$	0.021	0.006	13.2 (1, 784)	< .001
	$\log PPFD \cdot TRT$			0.17 (1, 1196)	.681
	$\log VPD \cdot TRT$			0.06 (1, 975)	.810
	$\log PPFD \cdot \log VPD \cdot TRT$			0.001 (1, 802)	.949
$\boldsymbol{F'_{r1}}$					
	$\log PPFD$	0.032	0.004	137 (1, 1283)	< .001
	$\log VPD$	-0.009	0.007	19.7 (1, 1093)	< .001
	$\log PPFD \cdot \log VPD$	-0.059	0.010	41.9 (1, 904)	< .001
	$\log PPFD \cdot TRT$			0.48 (1, 1289)	.487
	$\log VPD \cdot TRT$			1.62 (1, 1098)	.203
	$\log PPFD \cdot \log VPD \cdot TRT$			4.93 (1, 921)	.027
$\boldsymbol{F'_{r2}}$					
	$\log PPFD$	0.017	0.002	217 (1, 1239)	< .001
	$\log VPD$	0.049	0.004	183 (1, 1054)	< .001
	$\log PPFD \cdot \log VPD$	-0.013	0.005	7.14 (1, 748)	.008
	$\log PPFD \cdot TRT$			0.001 (1, 1252)	.998
	$\log VPD \cdot TRT$			0.60 (1, 1054)	.437
	$\log PPFD \cdot \log VPD \cdot TRT$			0.02 (1, 757)	.891

[†]Covariates: $\log PPFD$ is the log-transformed photosynthetic photon flux density; $\log VPD$ is the log-transformed vapour pressure deficit; TRT is the water treatment.

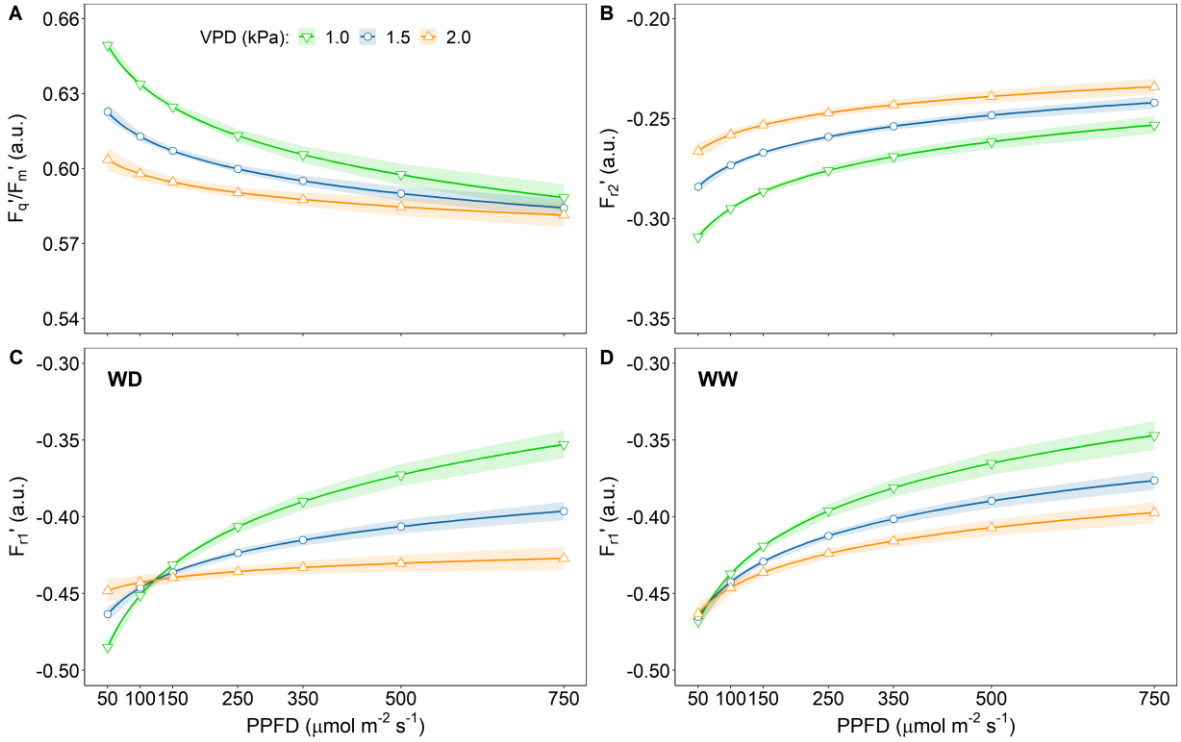

Figure 3.29. Predicted values ± *SE*, *n* = 1920, for **(A)** operating efficiency of PSII (F_q'/F_m'), and **(B)** the reoxidation process F_{r2}' from light-adapted wheat plants, regardless of water treatment, as a function of photosynthetic photon flux density (PPFD) and vapour pressure deficit (VPD). Predicted F_{r1}' values ± *SE*, *n* = 1920, for **(C)** water-limited (WD) and **(D)** well-watered light-adapted wheat plants growing in semi-controlled greenhouse conditions as a function of PPFD and VPD.

3.2.6 Trait-trait phenotypic correlations

Spearman's rank correlation coefficients (r_s) across the genotype BLUEs estimated the strength of phenotypic association between traits within each water treatment, regardless of time (Figure 3.30). As neither genotype nor genotype-by-water treatment effects for leaf gas exchange traits (i.e., A_n, g_s, C_i, and E) were statistically significant (Table 3.4), their phenotypic correlations with the other traits were not investigated.

The correlations among plant traits under WD conditions (Figure 3.30A) had similar trends to those estimated under WW conditions (Figure 3.30B), even though r_s tended to be stronger in drought stress. Overall, plant phenology (i.e., BBCH) negatively correlated with F_q'/F_m', F_{r2}', PLA, CMS, and final total leaf area (LA). Notably, F_q'/F_m' and F_{r2}' positively correlated with PLA, LA and CMS, whereas F_{r1}' negatively correlated with ETR, SDM, and PLA. By contrast, F_{r1}' weakly correlated with BBCH and CMS.

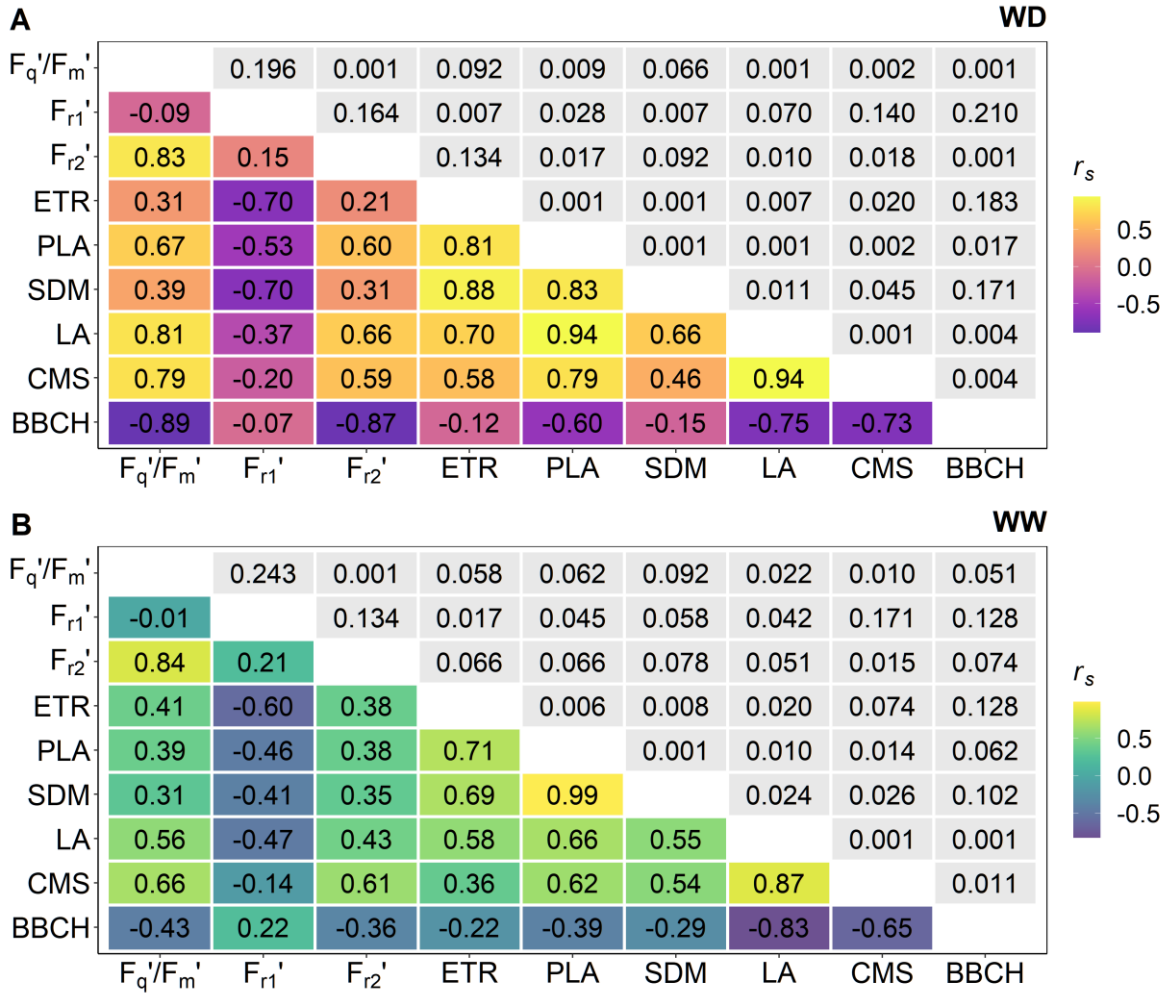

Figure 3.30. Spearman's rank correlation coefficients (r_s; below the diagonal) and their respective probability values (*p*-values; above the diagonal) between traits averaged across time points from 10 wheat genotypes under **(A)** drought stress (WD) and **(B)** well-watered (WW) conditions, and growing in a semi-controlled greenhouse. The plant traits are operating efficiency of PSII (F_q'/F_m'), electron transfer rate from Q_A to *PQ* pool (F_{r1}'), electron transfer rate from *PQ* pool to PSI (F_{r2}'), daily whole-plant evapotranspiration rate (ETR), projected leaf area (PLA), final total shoot dry matter per plant (SDM), final total leaf area per plant (LA), leaf cell membrane stability (CMS), and plant phenological growth stage (BBCH).

4 DISCUSSION

4.1 FIELD

Changes in LIFT-measured ChlF traits of light-adapted durum wheat plants subjected to progressive soil drying were induced in both the short and long term. In fact, a reduced photosynthetic activity, estimated by the LIFT parameters (F_q'/F_m', F_{r1}' and F_{r2}'), was only observed under a persistent moderate to severe drought (Figure 3.6C). Though, it is worthy of note that the absence of a contiguous control treatment (WW) in Y1 may have limited our ability to isolate small changes caused solely by drought, particularly when it was not severe. Indeed, the photosynthetic machinery, especially PSII photochemistry, is known to be relatively resilient to water stress (Flexas et al., 2009; Flexas, Escalona & Medrano, 1998; Havaux, 1992; Kaiser, 1987). Such a resilience, however, has been shown more pronounced for ChlF traits measured in dark-adapted plants as the maximum quantum efficiency of PSII photochemistry (F_v/F_m), rather than in light-adapted plants as F_q'/F_m' (Athar & Ashraf, 2005; Lu & Zhang, 1999; Zivcak et al., 2014). Therefore, these findings indicate that light-adapted ChlF traits might be physiologically preferable for assessing the effects of environmental stressors.

Concurrent electron acceptor sinks (i.e., photosynthetic carbon reduction and carbon oxidation) may explain the high resilience of ChlF traits, particularly F_q'/F_m' and F_{r2}', even after ten days of water-limiting conditions in Y1 (Figure 3.6C) and also the fact that no declines relative to WW plants were found under mild drought in Y2. Stomatal (g_s) and mesophyll (g_m) conductance are key CO_2 diffusion components that regulate leaf transpiration efficiency, playing pivotal roles in plant acclimation to drought (Flexas et al., 2009; Ouyang, Struik, Yin & Yang, 2017). In the short term, at the onset of water-limiting conditions, stomatal closure is induced to reduce water loss, and thereby CO_2 availability, leading to increased photorespiration (Cornic, 2000; Lawlor, 2002). In C_3 plants under mild drought, the O_2 uptake via photorespiratory activity can almost entirely replace the lower CO_2 availability as an electron acceptor pathway (Cornic & Fresneau, 2002). Drought-stressed tomato plants, for instance, doubled electron dissipation through photorespiration relative to non-stressed plants (Haupt-Herting & Fock, 2002). This repartitioning of light energy, or energy balancing network (Walker, Kramer, Fisher & Fu, 2020), may result in minor changes in ChlF-based traits in mild stress. Nevertheless, if drought progresses, LET might be electron sink-limited, as both photorespiration and the Calvin-Benson cycle can be repressed, causing impairment of ribulose

bisphosphate (RuBP) regeneration and adenosine triphosphate (ATP) synthesis (Flexas & Medrano, 2002; Tezara, Mitchell, Driscoll & Lawlor, 1999). Ultimately, whole photosynthetic electron transport activity will be down-regulated (Cornic & Fresneau, 2002; Haupt-Herting & Fock, 2002; Medrano, Escalona, Bota, Gulías & Flexas, 2002; Schöttler & Tóth, 2014). Hence, these considerations can explain the decrease in F_q'/F_m' co-occurring with reduced F_{r1}' and F_{r2}' in response to long-term severe drought stress observed in Y1.

The very strong linear relationship between F_q'/F_m' and F_{r2}' (i.e., the kinetics of electron transport from *PQ* pool towards PSI; Figure 3.10B) supports the mechanism of photosynthetic control of electron transfer when metabolism is repressed under environmental stresses to prevent photodamage in both PSII and PSI. According to Kanazawa et al. (2017), ATP synthase activity decreases in limiting CO_2, slowing proton efflux from the thylakoid lumen and, consequently, increasing proton motive force (*pmf*) across the thylakoid membrane. As a consequence, a more acidic lumen can concomitantly (i) trigger the energy-dependent (q_E) non-photochemical quenching (*NPQ*), which thermally dissipates the surplus of absorbed light energy from the light-harvesting complexes (LHCs) to prevent over-excitation of PSII, as well as (ii) slow down the electron transfer through the cytochrome b_6f complex (Cytb_6f), which prevents over-reduction of PSI electron acceptors (Kanazawa et al., 2017; Tikhonov, 2013). These mechanisms of photoprotection governed by ATP synthase activity are known to be at the core of plant acclimation to long-term drought stress (Kohzuma et al., 2009). Therefore, a slower F_{r2}' might suggest a deceleration of electrons through Cytb_6f with simultaneous decreasing in F_q'/F_m' due to a higher *NPQ*.

Regardless of drought, LIFT-measured ChlF traits displayed similar diurnal temporal patterns (Figures 3.12 and 3.13), demonstrating the high level of inherent regulation of the photosynthetic apparatus under fluctuating growing conditions, particularly through, but not limited to, *NPQ*. Similar patterns have also been observed in various other plant species growing in open fields (Pieruschka et al., 2010, 2014; Raesch et al., 2014). Instantaneous light intensity and temperature have been reported by Keller et al. (2019a) as the key drivers of such dynamics, in agreement with our findings. Actually, because air VPD is strongly correlated with air temperature (Gates, Zolnier & Buxton, 1998; Yuan et al., 2019) and includes air relative humidity, the impacts of VPD was investigated instead. It is well known that adjustments in the PSII/PSI stoichiometry are crucial to optimise the quantum efficiency of photosynthesis under fluctuating environment (Chow, Melis & Anderson, 1990; Külheim, Ågren & Jansson, 2002). Indeed, the efficiency of electron transport under changing ambient conditions is highly

dependent on the tight co-ordination among the several electron carriers between PSII and PSI, whose intricate regulatory processes occur at different time scales and multiple sites (see details in Dietz, 2015; Horton, 2012; Kono & Terashima, 2014; Rochaix, 2011; Schöttler & Tóth, 2014; Tikkanen et al., 2012; Walters, 2005).

The sustained faster F'_{r1} (i.e., the kinetics of electron transport from Q_A towards *PQ* pool) in Y2 relative to control (Figure 3.12C) was the most remarkable effect of mild drought. This suggests that plants were able to sense a subtle shortage of soil moisture and quickly modulate their photosynthetic electron transport, and potentially trigger responses to either acclimate or cope with reduced water availability. Interestingly, increasing atmospheric VPD intensified this response (Figure 3.11D). A plausible hypothesis is that stomata responses combined with alternative electron flows apart from the LET, such as water-water cycle (WWC), cyclic electron flow around PSI (CEF) and/or chlororespiration mediated by the plastid terminal oxidase (PTOX) (Cruz et al., 2005; Kono & Terashima, 2014), might explain a faster F'_{r1} at the onset of drought. Takahashi, Milward, Fan, Chow & Badger (2009) demonstrated that CEF enhances the *pmf* and helps to alleviate photoinhibition by either suppressing photodamage to PSII via a q_E-independent mechanism or preventing the inhibition of the repair of photodamaged PSII via a q_E-dependent mechanism. It has long been recognised that CEF is enhanced under drought (Golding, Finazzi & Johnson, 2004; Golding & Johnson, 2003; Zivcak et al., 2014). Also, PTOX mediates the electron transfer from plastoquinol (PQH_2) to reduce O_2 to H_2O via a non-electrogenic process (Shirao et al., 2013), potentially acting as a safety valve by protecting the *PQ* pool and mediating physiological responses (Krieger-Liszkay & Feilke, 2016; McDonald et al., 2011; Nawrocki, Tourasse, Taly, Rappaport & Wollman, 2015). Indeed, both CEF and PTOX are dependent on the redox state of the *PQ* pool, a vital component of photosynthesis with multiple functions, including photoprotection and stress tolerance (Havaux, 2020). Remarkably, Wang et al. (2016) recently demonstrated the role of the *PQ* pool over-reduction as a mechanism of chloroplast-mediated stomatal closure. Moreover, it is known that rising VPD increases atmospheric demand for water, leading to stomatal closure (Franks, Cowan & Farquhar, 1997; Massmann, Gentine & Lin, 2019). Besides VPD, diurnal and seasonal stomata kinetics are also driven by combined effects of temperature, irradiance, and soil moisture (Matthews, Vialet-Chabrand & Lawson, 2018; McAusland et al., 2016; Neukam, Böttcher & Kage, 2016; Sack & Holbrook, 2006). Altogether, early changes in F'_{r1} may appear as acclimation responses to the onset of water-limiting conditions, which might promote photoprotection, even when drought stress effects are not obvious at the whole-plant level.

Under fluctuating light conditions, Sakoda, Yamori, Groszmann & Evans (2021) reported that the carbon gain in plants, in terms of CO_2 assimilation rate, was primarily limited by g_s and electron transport rate rather than g_m. Additionally, when assessing wheat growing in progressive drought and fluctuating light, Grieco et al. (2020) remarkably identified short- and long-term regulatory mechanisms by which plants acclimated their photosynthetic machinery through changes in the *NPQ* kinetics and in the enzymatic stoichiometry, particularly by modifying the PSII and light-harvesting complex II (PSII-LHCII) phosphorylation pattern. The authors shed light on the complexity of the photosynthetic apparatus' re-configuration, impacting both cyclic and linear electron flows, where plant acclimation did respond according to drought severity and light dynamics simultaneously.

Due to changes in the relative contribution of genetic variance over time, it was observed dynamic fluctuations in broad-sense heritability for ChlF traits (Figure 3.16). Even after correcting the ChlF traits for biological (e.g., plant height, phenology, and canopy reflectance) and environmental (e.g., PPFD and VPD) variations, strong significant differences between genotypes were still found, demonstrating that there was substantial genetic variability that could not be explained by those covariates alone. Araus et al. (1998) have similarly reported such a genetic variability for ChlF traits in durum wheat under field conditions, where phenology was also considered. In our data, the highest H^2 for F_q'/F_m', F_{r1}' and F_{r2}' were observed in mild drought but with gradual reductions when the soil became drier. It is noteworthy that H^2 values estimated in Y2 (milder drought) were of similar orders of magnitude as in Y1 at the onset of drought stress (i.e., when the soil VWC of both seasons were comparable). Using a high-throughput image phenotyping approach, Chen et al. (2014) also observed dynamic changes in heritability over time for fluorescence-based traits in barley under drought, where H^2 similarly decreased during progressive stress. Time-varying H^2 for F_q'/F_m' in *Arabidopsis* growing in fluctuating light has also been reported by Flood et al. (2016). It has been argued that the dynamic change of heritability over time is due to changes in the magnitude of genotype and environment effects, as well as their interaction (Visscher, Hill & Wray, 2008). Fluctuations in H^2 for a trait can be challenging for plant breeding programmes, particularly in drought-prone environments, where a lower heritability under severe stress could negatively impact the effectiveness of selection.

The changing genetic and phenotypic correlations between ChlF traits and above-ground biomass yield (Figures 3.18A and 3.20A) or ΔRWC (Figures 3.18B and 3.20B) during soil drying might suggest that multiple water use strategies are in place to cope with water

deficit. In mild drought, genotypes with high photosynthetic activity tended to have both high biomass yield and high dehydration, altogether indicating a high transpiration rate. As the opposite behaviour was also true (i.e., low photosynthetic activity with low biomass yield and low dehydration), the identification of water savers and spenders (Nakhforoosh et al., 2016) may be somewhat facilitated by ChlF values, at least under mild stress. Nonetheless, such correlations were weaker, or even shifted directions, in severe drought. These circumstances were probably due to other traits related to drought tolerance which may also affect ChlF responses, including stay-green (delayed senescence), osmotic adjustment and antioxidant defence (Chen et al., 2017; Christopher, Christopher, Borrell, Fletcher & Chenu, 2016; Farooq, Hussain & Siddique, 2014). For instance, Shangguan, Shao & Dyckmans (1999) noted that higher degree of osmotic adjustment induced by a gradual soil drying, compared to a fast-drying process, allowed wheat plants to maintain a greater photosynthetic capacity. Besides, it is also known that plants under drought stress can adapt by altering biomass partitioning among roots and grain development (Davies & Zhang, 1991; Fang et al., 2017). However, it was beyond the scope of this study to evaluate root dynamics and possible changes due to drought.

Apart from the high level of phenotypic plasticity for ChlF traits among genotypes, a crossover interaction was noticed (Figure 3.21), especially for F'_{r1} and F'_{r2}, which reinforces the roles of genotype-by-time (i.e., drought severity) effect and the genetic complexity of plant responses to drought. In other words, genotypes with high photosynthetic activity (high F'_q/F'_m and fast F'_{r1} and F'_{r2}) in non-limiting environments will likely perform worse when grown under very poor conditions compared to those with low photosynthetic activity, and vice versa. A crossover effect has also been reported for grain yield (Araus et al., 2002, 2008; Cooper, Stucker, DeLacy & Harch, 1997) and is a 'source of frustration' (Blum, 2005) to plant breeding for drought stress adaptation. Properly setting the target environment, therefore, seems to be essential for accurate comprehension of and good use of the genetic variation in ChlF traits.

4.2 GREENHOUSE

In general, the trends for the LIFT-measured ChlF traits from light-adapted and drought-stressed wheat plants growing in semi-controlled greenhouse conditions were in good agreement with those trends observed in open field conditions. For instance, a sustained reduction in plant photosynthetic activity, estimated by the parameters F'_q/F'_m, F'_{r1} and F'_{r2}, also occurred only after a prolonged period of moderate to severe drought (Figure 3.25).

Furthermore, as it also occurred in the field, F'_{r1} (i.e., the kinetics of electron transport from Q_A towards *PQ* pool; Figures 3.25C and 3.25D) remained remarkably accelerated in stressed plants in the greenhouse, particularly under mild and moderate drought. Moreover, increasing atmospheric VPD notably intensified this response (Figure 3.29C). Altogether, this endorses, once more, the hypothesis that plants were capable of early sensing a subtle shortage of water supply and rapidly modulated their photosynthetic machinery to potentially trigger responses to either acclimate or cope with reduced water availability.

As previously discussed, stomatal closure is one of the earliest plant responses to drought, minimising water loss by transpiration. The results here also support a consistent reduction in leaf g_s and, therefore, in whole-plant evapotranspiration rate (ETR) under drought (Figures 3.22C and 3.23C). Interestingly, a strong negative correlation between F'_{r1} and ETR at the genotypic level was observed under water-limiting conditions (Figure 3.30A), suggesting a putative link between the photosynthetic electron transport efficiency and the whole-plant water use efficiency (WUE). In line with this suggestion, Wang et al. (2016) showed that the over-reduction of the *PQ* pool in mesophyll chloroplasts promotes the synthesis of hydrogen peroxide (H_2O_2), a reactive oxygen species (ROS), which may diffuse to the guard cells, mediating stomatal closing. Additionally, Karpinska, Wingsle & Karpinski (2000) demonstrated that, before stress, a transient higher concentration of H_2O_2 in the chloroplast regulated by the redox status of the quinone B (Q_B) and *PQ* pools might protect the photosynthetic apparatus and the plant cell from photoinhibition and photooxidative damage. Altogether, a faster F'_{r1} (i.e., Q_A^- reoxidation efficiency up to 0.65 ms) at the onset of drought may either trigger plant acclimation responses or promote the production of signalling molecules. Nonetheless, whether mechanistic links between these complex biological processes exist, this still requires further investigation.

Indeed, plants activate an intricate root-to-shoot signalling network in drying soil conditions to modulate WUE (Dodd et al., 2015; Schachtman & Goodger, 2008). The hormone abscisic acid (ABA), for example, is known to play a pivotal role in this signalling network by regulating stomatal aperture and gene expression to cope with water deficit (Cutler, Rodriguez, Finkelstein & Abrams, 2010; Liang, Zhang & Wong, 1997; Martin-Vertedor & Dodd, 2011; Saradadevi, Palta & Siddique, 2017; Takahashi, Kuromori, Urano, Yamaguchi-Shinozaki & Shinozaki, 2020; Tardieu, Parent & Simonneau, 2010; Zhou et al., 2019). Pei et al. (2000) demonstrated that ABA also induces the production of H_2O_2 in guard cells, which activates plasma membrane calcium (Ca^{2+}) channels and, ultimately, leading to stomatal closing. As a matter of fact, plants modulate photosynthesis and photoprotection under environmental stress

not by ABA alone but through various other phytohormones (including, but not limited to, ethylene, jasmonates, brassinosteroids, and salicylates) and their complex crosstalk (Gururani, et al., 2015; Müller & Munné-Bosch, 2021), which are beyond the scope of this study, however.

Electrolyte leakage has been shown as a robust approach for assessing the cell membrane stability (CMS) under stress (Bajji et al., 2001; Blum & Ebercon, 1981), and facilitating the prediction of genetic variation for dehydration tolerance in crops (Qaseem, Qureshi & Shaheen, 2019; Rehman et al., 2016; Tripathy, Zhang, Robin, Nguyen & Nguyen, 2000). Given the positive correlations between CMS ranks and the ranks for F_q'/F_m', F_{r2}', PLA, SDM, and LA herein reported (Figure 3.30), there was compelling evidence that wheat genotypes with higher CMS under drought stress managed to sustain a higher photosynthetic performance, producing more above-ground biomass. Unfortunately, grain yield traits were not available for this study, so no direct links or inferences regarding yield components and CMS could be made. However, Abid et al. (2018) showed that a drought-tolerant wheat genotype had less-pronounced yield loss under severe stress than a sensitive genotype, primarily due to its greater ability to scavenge ROS and to osmotically adjust, resulting in improved membrane stability and higher photosynthetic rates during drought. There is a longstanding acknowledgement that leaf dehydration results in chloroplast membrane rupture (Hincha, Höfner, Schwab, Heber & Schmitt, 1987). In fact, biological membranes are the first target of many abiotic stresses (Tenhaken, 2015). Prolonged, severe drought compromises cell membrane integrity and stability leading to irreversible damage since water is essential for maintaining the membrane fluidity and functional structure (Blum, 2011a; Bodner, Nakhforoosh & Kaul, 2015; Farooq et al., 2009).

5 CONCLUSIONS

Short- and long-term changes in ChlF traits induced by progressive drought were rapidly and non-invasively monitored at canopy level in field-grown durum wheat. Integrating LIFT-measured ChlF traits with high temporal resolution environmental data facilitated the assessment of genotype-by-environment interaction effects under drought stress. Simultaneous statistical modelling of spatial patterns and temporal trends combined with time-varying covariates (e.g., plant height and phenology, canopy structure and leaf pigments, PPFD, and VPD) helped to improve the precision and interpretation of experiments under changing ambient conditions. Indeed, modelling experimentally and naturally arising confounding effects improved precision by an average of 31%. Soil drying conditions at both 10 cm and 50 cm depths progressively induced changes in ChlF traits. In severe drought stress, field-grown plants down-regulated their photosynthetic activities, resulting in a reduction of 14%, 18% and 20% in F_q'/F_m', F_{r1}' and F_{r2}', respectively. To a lesser extent, prolonged drought under controlled conditions also induced reductions in the ChlF traits of the order of 3%, 2% and 4% in F_q'/F_m', F_{r1}' and F_{r2}', respectively. In mild stress, F_q'/F_m' and F_{r2}' were little affected, while F_{r1}' remarkably accelerated up to 8% relative to well-watered plants, and increasing VPD exacerbated such behaviour. Apart from soil water content, light intensity (PPFD) and VPD were key environmental factors to drive nonlinear changes in the ChlF traits, including their diurnal course patterns. The three ChlF traits worked in a highly coordinated manner, indicating a high level of inherent regulation of the photosynthetic apparatus under fluctuating growing conditions.

Strong significant differences in ChlF traits were found among genotypes, demonstrating substantial genetic variability for breeding programmes to select for drought-adaptive traits. Indeed, broad-sense heritability for the LIFT-measured ChlF traits was, on average, 0.60 under non-limiting conditions up to moderate drought. It slightly dropped to 0.49 in severe drought stress, indicating genotype-by-environment interaction effects and/or increasing environmental noise. Moderate genetic correlations between final above-ground biomass yield or drought-induced relative change in leaf RWC and the ChlF traits were observed, but they changed over time, and so, care should be taken when interpreting these correlations. Positive moderate to strong correlations between the ranking of wheat genotypes by F_q'/F_m' or F_{r2}' and the leaf CMS or PLA were revealed under drought in controlled conditions. As well, a strong negative correlation between the rank of genotypes for F_{r1}' and for daily

evapotranspiration rate was displayed. These correlations emphasise the complexity of plant physiological responses to coping with drought stress. The observed genetic variation suggests that the LIFT method can enable genome-wide association studies (GWAS) for dissecting the QTLome of photosynthetic traits, and assess the effects on yield associated with the relevant quantitative trait loci (QTLs). At an unprecedented scale, this high-throughput approach for field phenotyping ChlF traits (which may also be integrated into existing HTPPs in controlled environments) allowed for estimation of genetic effects over time in a large durum wheat panel and shed light on the diurnal dynamics of the photosynthetic apparatus leveraging the ability to dissect complex physiological traits. Therefore, plant ecophysiology studies and physiological plant breeding may benefit from this flexible and versatile LIFT method, enabling knowledge of the mechanisms of drought-adaptive traits under natural plant stand and agricultural field conditions alike.

REFERENCES

Aasen, H., van Wittenberghe, S., Medina, N. S., Damm, A., Goulas, Y., Wieneke, S., . . . Mac Arthur, A. (2019). Sun-induced chlorophyll fluorescence II: review of passive measurement setups, protocols, and their application at the leaf to canopy level. *Remote Sensing, 11*(8), 927.

Abid, M., Ali, S., Qi, L. K., Zahoor, R., Tian, Z., Jiang, D., . . . Dai, T. (2018). Physiological and biochemical changes during drought and recovery periods at tillering and jointing stages in wheat (Triticum aestivum L.). *Scientific Reports, 8*, 4615.

Allen, R. G., Pereira, L. S., Raes, D., & Smith, M. (1998). *Crop Evapotranspiration: guidelines for computing crop water requirements. FAO Irrigation and Drainage Paper No. 56.* Rome: FAO.

American Meteorological Society. (1997). Meteorological drought - policy statement. *Bulletin of the American Meteorological Society, 78*(5), 847-849.

Ananyev, G., Kolber, Z. S., Klimov, D., Falkowski, P. G., Berry, J. A., Rascher, U., . . . Osmond, B. (2005). Remote sensing of heterogeneity in photosynthetic efficiency, electron transport and dissipation of excess light in Populus deltoides stands under ambient and elevated CO2 concentrations, and in a tropical forest canopy, using a new LIFT device. *Global Change Biology, 11*(8), 1195-1206.

Araus, J. L., & Cairns, J. E. (2014). Field high-throughput phenotyping: the new crop breeding frontier. *Trends in Plant Science, 19*(1), 52-61.

Araus, J. L., Amaro, T., Voltas, J., Nakkoul, H., & Nachit, M. M. (1998). Chlorophyll fluorescence as a selection criterion for grain yield in durum wheat under Mediterranean conditions. *Field Crops Research, 55*(3), 209-223.

Araus, J. L., Slafer, G. A., Reynolds, M. P., & Royo, C. (2002). Plant breeding and drought in C3 cereals: what should we breed for? *Annals of Botany, 89*(7), 925-940.

Araus, J. L., Slafer, G. A., Royo, C., & Serret, M. D. (2008). Breeding for yield potential and stress adaptation in cereals. *Critical Reviews in Plant Science, 27*(6), 377-412.

Ashraf, M. (2010). Inducing drought tolerance in plants: recent advances. *Biotechnology Advances, 28*(1), 169-183.

Athar, H.-u.-R., & Ashraf, M. (2005). Photosynthesis under drought stress. In M. Pessaraki (Ed.), *Handbook of Photosynthesis* (2nd ed., pp. 793-809). Boca Raton, FL, USA: CRC Press.

Bajji, M., Kinet, J.-M., & Lutts, S. (2002). The use of the electrolyte leakage method for assessing cell membrane stability as a water stress tolerance test in durum wheat. *Plant Growth Regulation, 36,* 61-70.

Baker, N. R. (2008). Chlorophyll fluorescence: a probe of photosynthesis in vivo. *Annual Review of Plant Biology, 59*(1), 89-113.

Baker, N. R., & Rosenqvist, E. (2004). Applications of chlorophyll fluorescence can improve crop production strategies: an examination of future possibilities. *Journal of Experimental Botany, 55*(403), 1607-1621.

Barbagallo, R. P., Oxborough, K., Pallett, K. E., & Baker, N. R. (2003). Rapid, noninvasive screening for perturbations of metabolism and plant growth using chlorophyll fluorescence imaging. *Plant Physiology, 132*(2), 485-493.

Barrs, H. D., & Weatherley, P. E. (1962). A re-examination of the relative turgidity technique for estimating water deficits in leaves. *Australian Journal of Biological Sciences, 15*(3), 413-428.

Bartels, D., & Sunkar, R. (2005). Drought and salt tolerance in plants. *Critical Reviews in Plant Sciences, 24*(1), 23-58.

Bengough, A. G., McKenzie, B. M., Hallett, P. D., & Valentine, T. A. (2011). Root elongation, water stress, and mechanical impedance: a review of limiting stresses and beneficial root tip traits. *Journal of Experimental Botany, 62*(1), 59-68.

Berger, B., Parent, B., & Tester, M. (2010). High-throughput shoot imaging to study drought responses. *Journal of Experimental Botany, 61*(13), 3519-3528.

Bernardo, R. (2008). Molecular markers and selection for complex traits in plants: learning from the last 20 years. *Crop Science, 48*(5), 1649-1664.

Bingham, I. J. (2001). Soil-root-canopy interactions. *Annals of Applied Biology, 138,* 243-251.

Blum, A. (1996). Crop responses to drought and the interpretation of adaptation. *Plant Growth Regulation, 20,* 135-148.

Blum, A. (1997). Constitutive traits affecting plant performance under stress. In G. O. Edmeades, M. Bänziger, H. R. Mickelson, & C. B. Peña-Valdivia (Ed.), *Developing Drought- and Low N-Tolerant Maize. Proceedings of a Symposium, March 25-29, 1996, CIMMYT, El Batán, Mexico* (pp. 131-135). Mexico, D.F.: CIMMYT.

Blum, A. (2005). Drought resistance, water-use efficiency, and yield potential - are they compatible, dissonant, or mutually exclusive? *Australian Journal of Agricultural Research, 56*(11), 1159-1168.

Blum, A. (2011a). *Plant Breeding for Water-Limited Environments.* New York, NY, United States of America: Springer.

Blum, A. (2011b). Drought resistance - is it really a complex trait? *Functional Plant Biology, 38*(10), 753-757.

Blum, A., & Ebercon, A. (1981). Cell membrane stability as a measure of drought and heat tolerance in wheat. *Crop Science, 21*(1), 43-47.

Bodner, G., Nakhforoosh, A., & Kaul, H.-P. (2015). Management of crop water under drought: a review. *Agronomy for Sustainable Development, 35*, 401-442.

Boken, V. K. (2005). Agricultural drought and its monitoring and prediction: some concepts. In V. K. Boken, A. P. Cracknell, & R. L. Heathcote (Eds.), *Monitoring and Predicting Agricultural Drought: A Global Study* (pp. 3-10). New York, NY, United States of America: Oxford University Press.

Bruning, B., Berger, B., Lewis, M., Liu, H., & Garnett, T. (2020). Approaches, applications, and future directions for hyperspectral vegetation studies: an emphasis on yield-limiting factors in wheat. *The Plant Phenome Journal, 3*(1), e20007.

Bryant, E. A. (1991). *Natural Hazards.* Cambridge, United Kingdom: Cambridge University Press.

Cabrera-Bosquet, L., Crossa, J., von Zitzewitz, J., Serret, M. D., & Araus, J. L. (2012). High-throughput phenotyping and genomic selection: the frontiers of crop breeding converge. *Journal of Integrative Plant Biology, 54*(5), 312-320.

Camargo Neto, J. (2004). *A combined statistical-soft computing approach for classification and mapping weed species in minimum-tillage systems.* University of Nebraska, Department of Biological Systems Engineering. Lincoln, NE: University of Nebraska.

Campos, H., Cooper, M., Habben, J. E., Edmeades, G. O., & Schussler, J. R. (2004). Improving drought tolerance in maize: a view from industry. *Field Crops Research, 90*(1), 19-34.

Campos, H., Heard, J. E., Ibañez, M., Luethy, M. H., Peters, T. J., & Warner, D. C. (2011). Effective and efficient platforms for crop phenotype characterisation under drought. In P. Monneveux, & J.-M. Ribaut (Eds.), *Drought phenotyping in crops: from theory to practice* (pp. 37-47). Texcoco, Mexico: CGIAR Generation Challenge Programme.

Cendrero-Mateo, M. P., Moran, M. S., Papuga, S. A., Thorp, K. R., Alonso, L., Moreno, J., . . . Wang, G. (2016). Plant chlorophyll fluorescence: active and passive measurements at canopy and leaf scales with different nitrogen treatments. *Journal of Experimental Botany, 67*(1), 275-286.

Cendrero-Mateo, M. P., Muller, O., Albrecht, H., Burkart, A., Gatzke, S., Janssen, B., . . . Rascher, U. (2017). Field phenotyping: concepts and examples to quantify dynamic plant traits across scales in the field. In A. Chabbi, & H. W. Loescher (Eds.), *Terrestrial Ecosystem Research Infrastructures: Challenges and Opportunities* (pp. 53-80). Boca Raton, FL, United States of America: CRC Press.

Chaves, M. M., & Oliveira, M. M. (2004). Mechanisms underlying plant resilience to water deficits: prospects for water-saving agriculture. *Journal of Experimental Botany, 55*(407), 2365-2384.

Chen, D., Neumann, K., Friedel, S., Kilian, B., Chen, M., Altmann, T., & Klukas, C. (2014). Dissecting the phenotypic components of crop plant growth and drought responses based on high-throughput image analysis. *The Plant Cell, 26*(12), 4636-4655.

Chen, Y.-E., Cui, J.-M., Su, Y.-Q., Zhang, C.-M., Ma, J., Zhang, Z.-W., . . . Yuan, S. (2017). Comparison of phosphorylation and assembly of photosystem complexes and redox homeostasis in two wheat cultivars with different drought resistance. *Scientific Reports, 7*, 12718.

Cheng, J., Edwards, L. J., Maldonado-Molina, M. M., Komro, K. A., & Muller, K. E. (2010). Real longitudinal data analysis for real people: building a good enough mixed model. *Statistics in Medicine, 29*(4), 504-520.

Chenu, K. (2015). Characterizing the crop environment - nature, significance and applications. In V. O. Sadras, & D. F. Calderini (Eds.), *Crop Physiology: Applications for Genetic Improvement and Agronomy* (2nd ed., pp. 321-348). London, United Kingdom: Academic Press.

Chenu, K., Cooper, M., Hammer, G. L., Mathews, K. L., Dreccer, M. F., & Chapman, S. C. (2011). Environment characterization as an aid to wheat improvement: interpreting genotype-environment interactions by modelling water-deficit patterns in North-Eastern Australia. *Journal of Experimental Botany, 62*(6), 1743-1755.

Cho, H.-T., & Cosgrove, D. J. (2010). Expansins as agents in hormone action. In P. J. Davies (Ed.), *Plant Hormones: Biosynthesis, Signal Transduction, Action!* (Revised 3rd ed., pp. 262-281). Dordrecht, The Netherlands: Springer.

Chow, W. S., Melis, A., & Anderson, J. M. (1990). Adjustments of photosystem stoichiometry in chloroplasts improve the quantum efficiency of photosynthesis. *Proceedings of the National Academy of Sciences of the United States of America, 87*(19), 7502-7506.

Christopher, J. T., Christopher, M. J., Borrell, A. K., Fletcher, S., & Chenu, K. (2016). Stay-green traits to improve wheat adaptation in well-watered and water-limited environments. *Journal of Experimental Botany, 67*(17), 5159-5172.

Cline, W. R. (2007). *Global Warming and Agriculture: Impact Estimates by Country.* Washington, DC, United States of America: Center for Global Development and Peterson Institute for International Economics.

Condorelli, G. E., Maccaferri, M., Newcomb, M., Andrade-Sanchez, P., White, J. W., French, A. N., . . . Tuberosa, R. (2018). Comparative aerial and ground based high throughput phenotyping for the genetic dissection of NDVI as a proxy for drought adaptive traits in durum wheat. *Frontiers in Plant Science, 9*, 893.

Cooper, M., Podlich, D. W., & Smith, O. S. (2005). Gene-to-phenotype models and complex trait genetics. *Australian Journal of Agricultural Research, 56*(9), 895-918.

Cooper, M., Stucker, R. E., DeLacy, I. H., & Harch, B. D. (1997). Wheat breeding nurseries, target environments, and indirect selection for grain yield. *Crop Science, 37*(4), 1168-1176.

Cornic, G. (2000). Drought stress inhibits photosynthesis by decreasing stomatal aperture - not by affecting ATP synthesis. *Trends in Plant Science, 5*(5), 187-188.

Cornic, G., & Fresneau, C. (2002). Photosynthetic carbon reduction and carbon oxidation cycles are the main electron sinks for photosystem II activity during a mild drought. *Annals of Botany, 89*(7), 887-894.

Cramer, G. R., Urano, K., Delrot, S., Pezzotti, M., & Shinozaki, K. (2011). Effects of abiotic stress on plants: a systems biology perspective. *BMC Plant Biology, 11*, 163.

Cruz, J. A., Avenson, T. J., Kanazawa, A., Takizawa, K., Edwards, G. E., & Kramer, D. M. (2005). Plasticity in light reactions of photosynthesis for energy production and photoprotection. *Journal of Experimental Botany, 56*(411), 395-406.

Cullis, B. R., Smith, A. B., & Coombes, N. E. (2006). On the design of early generation variety trials with correlated data. *Journal of Agricultural, Biological, and Environmental Statistics, 11*(4), 381-393.

Cutler, S. R., Rodriguez, P. L., Finkelstein, R. R., & Abrams, S. R. (2010). Abscisic acid: emergence of a core signaling network. *Annual Review of Plant Biology, 61*(1), 651-679.

Dai, A. (2011). Drought under global warming: a review. *WIREs Climate Change, 2*(1), 45-65.

Daryanto, S., Wang, L., & Jacinthe, P.-A. (2016). Global synthesis of drought effects on maize and wheat production. *PLOS ONE, 11*(5), e0156362.

Davies, W. J., & Zhang, J. (1991). Root signals and the regulation of growth and development of plants in drying soil. *Annual Review of Plant Physiology and Plant Molecular Biology, 42*(1), 55-76.

De Micco, V., & Aronne, G. (2012). Morpho-anatomical traits for plant adaptation to drought. In R. Aroca (Ed.), *Plant Responses to Drought Stress: From Morphological to Molecular Features* (pp. 37-61). Heidelberg: Springer.

De Sousa, C. R., Hilker, T., Waring, R., De Moura, Y. M., & Lyapustin, A. (2017). Progress in remote sensing of photosynthetic activity over the Amazon Basin. *Remote Sensing, 9*(1), 48.

de Wijn, R., & van Gorkom, H. J. (2001). Kinetics of electron transfer Qa to Qb in photosystem II. *Biochemistry, 40*(39), 11912-11922.

Dietz, K.-J. (2015). Efficient high light acclimation involves rapid processes at multiple mechanistic levels. *Journal of Experimental Botany, 66*(9), 2401-2414.

Dodd, I. C., Puértolas, J., Huber, K., Pérez-Pérez, J., Wright, H. R., & Blackwell, M. S. (2015). The importance of soil drying and re-wetting in crop phytohormonal and nutritional responses to deficit irrigation. *Journal of Experimental Botany, 66*(8), 2239-2252.

Dong, T., Liu, J., Shang, J., Qian, B., Ma, B., Kovacs, J. M., . . . Shi, Y. (2019). Assessment of red-edge vegetation indices for crop leaf area index estimation. *Remote Sensing of Environment, 222*, 133-143.

Drusch, M., Moreno, J., Del Bello, U., Franco, R., Goulas, Y., Huth, A., . . . Verhoef, W. (2017). The FLuorescence EXplorer Mission Concept - ESA's Earth Explorer 8. *IEEE Transactions on Geoscience and Remote Sensing, 55*(3), 1273-1284.

Edmeades, G. O., McMaster, G. S., White, J. W., & Campos, H. (2004). Genomics and the physiologist: bridging the gap between genes and crop response. *Field Crops Research, 90*(1), 5-18.

Evans, J. R., & Santiago, L. S. (2014). PrometheusWiki Gold Leaf Protocol: gas exchange using LI-COR 6400. *Functional Plant Biology, 41*(3), 223-226.

Evans, N., Baierl, A., Semenov, M. A., Gladders, P., & Fitt, B. D. (2008). Range and severity of a plant disease increased by global warming. *Journal of the Royal Society Interface, 5*(22), 525-531.

Fang, Y., & Xiong, L. (2015). General mechanisms of drought response and their application in drought resistance improvement in plants. *Cellular and Molecular Life Sciences, 72*, 673-689.

Fang, Y., Du, Y., Wang, J., Wu, A., Qiao, S., Xu, B., . . . Chen, Y. (2017). Moderate drought stress affected root growth and grain yield in old, modern and newly released cultivars of winter wheat. *Frontiers in Plant Science, 8*, 672.

FAO. (2016). *The State of Food and Agriculture 2016. Climate change, agriculture and food security.* Rome: Food and Agriculture Organization of the United Nations.

Farooq, M., Hussain, M., & Siddique, K. H. (2014). Drought stress in wheat during flowering and grain-filling periods. *Critical Reviews in Plant Sciences, 33*(4), 331-349.

Farooq, M., Wahid, A., Kobayashi, N., Fujita, D., & Basra, S. M. (2009). Plant drought stress: effects, mechanisms and management. *Agronomy for Sustainable Development, 29*(1), 185-212.

Filella, I., & Peñuelas, J. (1994). The red edge position and shape as indicators of plant chlorophyll content, biomass and hydric status. *International Journal of Remote Sensing, 15*(7), 1459-1470.

Fiorani, F., & Schurr, U. (2013). Future scenarios for plant phenotyping. *Annual Review of Plant Biology, 64*(1), 267-291.

Flexas, J., & Medrano, H. (2002). Drought-inhibition of photosynthesis in C3 plants: stomatal and non-stomatal limitations revisited. *Annals of Botany, 89*(2), 183-189.

Flexas, J., Barón, M., Bota, J., Ducruet, J.-M., Gallé, A., Galmés, J., . . . Medrano, H. (2009). Photosynthesis limitations during water stress acclimation and recovery in the drought-adapted Vitis hybrid Richter-110 (V. berlandieri x V. rupestris). *Journal of Experimental Botany, 60*(8), 2361-2377.

Flexas, J., Escalona, J. M., & Medrano, H. (1998). Down-regulation of photosynthesis by drought under field conditions in grapevine leaves. *Australian Journal of Plant Physiology, 25*(8), 893-900.

Flood, P. J., Kruijer, W., Schnabel, S. K., van der Schoor, R., Jalink, H., Snel, J. F., . . . Aarts, M. G. (2016). Phenomics for photosynthesis, growth and reflectance in Arabidopsis thaliana reveals circadian and long-term fluctuations in heritability. *Plant Methods, 12*, 14.

Franks, P. J., Cowan, I. R., & Farquhar, G. D. (1997). The apparent feedforward response of stomata to air vapour pressure deficit: information revealed by different experimental procedures with two rainforest trees. *Plant, Cell and Environment, 20*(1), 142-145.

Fu, P., Meacham-Hensold, K., Siebers, M. H., & Bernacchi, C. J. (2020). The inverse relationship between solar-induced fluorescence yield and photosynthetic capacity: benefits for field phenotyping. *Journal of Experimental Botany*, eraa537. doi:https://doi.org/10.1093/jxb/eraa537

Furbank, R. T., & Tester, M. (2011). Phenomics - technologies to relieve the phenotyping bottleneck. *Trends in Plant Science, 16*(12), 635-644.

Galán, R. J., Bernal-Vasquez, A.-M., Jebsen, C., Piepho, H.-P., Thorwarth, P., Steffan, P., . . . Miedaner, T. (2020). Hyperspectral reflectance data and agronomic traits can predict biomass yield in winter rye hybrids. *BioEnergy Research, 13*, 168-182.

Galwey, N. W. (2014). *Introduction to Mixed Modelling: Beyond Regression and Analysis of Variance* (2nd ed.). Chichester, United Kingdom: John Wiley & Sons.

Garrett, K. A., Dendy, S. P., Frank, E. E., Rouse, M. N., & Travers, S. E. (2006). Climate change effects on plant disease: genomes to ecosystems. *Annual Review of Phytopathology, 44*(1), 489-509.

Gates, R. S., Zolnier, S., & Buxton, J. (1998). Vapor pressure deficit control strategies for plant production. *IFAC Proceedings Volumes, 31*(12), 271-276.

Genty, B., Briantais, J.-M., & Baker, N. R. (1989). The relationship between the quantum yield of photosynthetic electron transport and quenching of chlorophyll fluorescence. *Biochimica et Biophysica Acta (BBA) - General Subjects, 990*(1), 87-92.

Ghanem, M. E., Marrou, H., & Sinclair, T. R. (2015). Physiological phenotyping of plants for crop improvement. *Trends in Plant Science, 20*(3), 139-144.

Ghatak, A., Chaturvedi, P., & Weckwerth, W. (2017). Cereal crop proteomics: systemic analysis of crop drought stress responses towards marker-assisted selection breeding. *Frontiers in Plant Science, 8*, 757.

Gilmour, A. R., Cullis, B. R., & Verbyla, A. (1997). Accounting for natural and extraneous variation in the analysis of field experiments. *Journal of Agricultural, Biological, and Environmental Statistics, 2*(3), 269-293.

Gilmour, A. R., Thompson, R., & Cullis, B. R. (1995). Average information REML: an efficient algorithm for variance parameter estimation in linear mixed models. *Biometrics, 51*(4), 1440-1450.

Godfray, H. C., Beddington, J. R., Crute, I. R., Haddad, L., Lawrence, D., Muir, J. F., . . . Toulmin, C. (2010). Food security: the challenge of feeding 9 billion people. *Science, 327*(5967), 812-818.

Golding, A. J., & Johnson, G. N. (2003). Down-regulation of linear and activation of cyclic electron transport during drought. *Planta, 218*, 107-114.

Golding, A. J., Finazzi, G., & Johnson, G. N. (2004). Reduction of the thylakoid electron transport chain by stromal reductants - evidence for activation of cyclic electron transport upon dark adaptation or under drought. *Planta, 220*, 356-363.

Gosa, S. C., Lupo, Y., & Moshelion, M. (2019). Quantitative and comparative analysis of whole-plant performance for functional physiological traits phenotyping: new tools to support pre-breeding and plant stress physiology studies. *Plant Science, 282*, 49-59.

Govindjee. (2004). Chlorophyll a fluorescence: a bit of basics and history. In G. C. Papageorgiou, & Govindjee (Eds.), *Advances in Photosynthesis and Respiration. Chlorophyll a Fluorescence: A Signature of Photosynthesis* (Vol. 19, pp. 1-42). Dordrecht, The Netherlands: Springer.

Granier, C., & Vile, D. (2014). Phenotyping and beyond: modelling the relationships between traits. *Current Opinion in Plant Biology, 18*, 96-102.

Grieco, M., Roustan, V., Dermendjiev, G., Rantala, S., Jain, A., Leonardelli, M., . . . Teige, M. (2020). Adjustment of photosynthetic activity to drought and fluctuating light in wheat. *Plant, Cell and Environment, 43*(6), 1484-1500.

Gururani, M. A., Mohanta, T. K., & Bae, H. (2015). Current understanding of the interplay between phytohormones and photosynthesis under environmental stress. *International Journal of Molecular Sciences, 16*(8), 19055-19085.

Habash, D. Z., Baudo, M., Hindle, M., Powers, S. J., Defoin-Platel, M., Mitchell, R., . . . Nachit, M. M. (2014). Systems responses to progressive water stress in durum wheat. *PLOS ONE, 9*(9), e108431.

Habash, D. Z., Paul, M. J., Parry, M. A., Keys, A. J., & Lawlor, D. W. (1995). Increased capacity for photosynthesis in wheat grown at elevated CO2: the relationship between electron transport and carbon metabolism. *Planta, 197*, 482-489.

Halperin, O., Gebremedhin, A., Wallach, R., & Moshelion, M. (2017). High-throughput physiological phenotyping and screening system for the characterization of plant-environment interactions. *The Plant Journal, 89*(4), 839-850.

Hamdani, S., Wang, H., Zheng, G., Perveen, S., Qu, M., Khan, N., . . . Zhu, X.-G. (2019). Genome-wide association study identifies variation of glucosidase being linked to natural variation of the maximal quantum yield of photosystem II. *Physiologia Plantarum, 166*(1), 105-119.

Haupt-Herting, S., & Fock, H. P. (2002). Oxygen exchange in relation to carbon assimilation in water-stressed leaves during photosynthesis. *Annals of Botany, 89*(7), 851-859.

Havaux, M. (1992). Stress tolerance of photosystem II in vivo: antagonistic effects of water, heat, and photoinhibition stresses. *Plant Physiology, 100*(1), 424-432.

Havaux, M. (2020). Plastoquinone in and beyond photosynthesis. *Trends in Plant Science, 25*(12), 1252-1265.

Hayter, A. J. (1986). The maximum familywise error rate of Fisher's least significant difference test. *Journal of the American Statistical Association, 81*(396), 1000-1004.

Heim Jr., R. R. (2002). A review of twentieth-century drought indices used in the United States. *Bulletin of the American Meteorological Society, 83*(8), 1149-1166.

Hickey, L. T., Hafeez, A. N., Robinson, H., Jackson, S. A., Leal-Bertioli, S. C., Tester, M., . . . Wulff, B. B. (2019). Breeding crops to feed 10 billion. *Nature Biotechnology, 37*, 744-754.

Hincha, D. K., Höfner, R., Schwab, K. B., Heber, U., & Schmitt, J. M. (1987). Membrane rupture is the common cause of damage to chloroplast membranes in leaves injured by freezing or excessive wilting. *Plant Physiology, 83*(2), 251-253.

Horton, P. (2012). Optimization of light harvesting and photoprotection: molecular mechanisms and physiological consequences. *Philosophical Transactions of the Royal Society of London. Series B, Biological Sciences, 367*(1608), 3455-3465.

Hu, H., & Xiong, L. (2014). Genetic engineering and breeding of drought-resistant crops. *Annual Review of Plant Biology, 65*(1), 715-741.

Hubert, M., & Vandervieren, E. (2008). An adjusted boxplot for skewed distributions. *Computational Statistics and Data Analysis, 52*(12), 5186-5201.

Humplík, J. F., Lazár, D., Fürst, T., Husičková, A., Hýbl, M., & Spíchal, L. (2015). Automated integrative high-throughput phenotyping of plants shoots: a case study of the cold-tolerance of pea (Pisum sativum L.). *Plant Methods, 11*, 20.

IPCC. (2014). *Climate Change 2014: Synthesis Report. Contribution of Working Groups I, II and III to the Fifth Assessment Report of the Intergovernmental Panel on Climate Change.* (Core Writing Team, R. K. Pachauri, & L. Meyer, Eds.) Geneva, Switzerland: IPCC.

IPCC. (2019). *Climate Change and Land: an IPCC Special Report on climate change, desertification, land degradation, sustainable land management, food security, and greenhouse gas fluxes in terrestrial ecosystems.* Intergovernmental Panel on Climate Change. Retrieved November 11, 2020, from https://www.ipcc.ch/srccl/download/

Jansen, M., Gilmer, F., Biskup, B., Nagel, K. A., Rascher, U., Fischbach, A., . . . Walter, A. (2009). Simultaneous phenotyping of leaf growth and chlorophyll fluorescence via GROWSCREEN FLUORO allows detection of stress tolerance in Arabidopsis thaliana and other rosette plants. *Functional Plant Biology, 36*(11), 902-914.

Kaiser, W. M. (1987). Effects of water deficit on photosynthetic capacity. *Physiologia Plantarum, 71*(1), 142-149.

Kalaji, H. M., Schansker, G., Brestic, M., Bussotti, F., Calatayud, A., Ferroni, L., . . . Baba, W. (2017). Frenquently asked questions about chlorophyll fluorescence, the sequel. *Photosynthesis Research, 132*, 13-66.

Kanazawa, A., Ostendorf, E., Kohzuma, K., Hoh, D., Strand, D. D., Sato-Cruz, M., . . . Kramer, D. M. (2017). Chloroplast ATP synthase modulation of the thylakoid proton motive force: implications for photosystem I and photosystem II photoprotection. *Frontiers in Plant Science, 8*, 719.

Kao, W. Y., & Tsai, T. T. (1998). Tropic leaf movements, photosynthetic gas exchange, leaf δ13C and chlorophyll a fluorescence of three soybean species in response to water availability. *Plant, Cell and Environment, 21*(10), 1055-1062.

Kapoor, D., Bhardwaj, S., Landi, M., Sharma, A., Ramakrishnan, M., & Sharma, A. (2020). The impact of drought in plant metabolism: how to explot tolerance mechanisms to increase crop production. *Applied Sciences, 10*(16), 5692.

Karpisnka, B., Wingsle, G., & Karpinski, S. (2000). Antagonistic effects of hydrogen peroxide and glutathione on acclimation to excess excitation energy in Arabidopsis. *IUBMB Life, 50*(1), 21-26.

Katsoulas, N., Elvanidi, A., Ferentinos, k. P., Kacira, M., Bartzanas, T., & Kittas, C. (2016). Crop reflectance monitoring as a tool for water stress detection in greenhouses: a review. *Biosystems Engineering, 151*, 374-398.

Keller, B., Matsubara, S., Rascher, U., Pieruschka, R., Steier, A., Kraska, T., & Muller, O. (2019a). Genotype specific photosynthesis x environment interactions captured by automated fluorescence canopy scans over two fluctuating growing seasons. *Frontiers in Plant Science, 10*, 1482.

Keller, B., Vass, I., Matsubara, S., Paul, K., Jedmowski, C., Pieruschka, R., . . . Muller, O. (2019b). Maximum fluorescence and electron transport kinetics determined by light-induced fluorescence transients (LIFT) for photosynthesis phenotyping. *Photosynthesis Research, 140*, 221-233.

Kissoudis, C., van de Wiel, C., Visser, R. G., & van der Linden, G. (2016). Future-proof crops: challenges and strategies for climate resilience improvement. *Current Opinion in Plant Biology, 30*, 47-56.

Kohzuma, K., Cruz, J. A., Akashi, K., Hoshiyasu, S., Munekage, Y. N., Yokota, A., & Kramer, D. M. (2009). The long-term responses of the photosynthetic proton circuit to drought. *Plant, Cell and Environment, 32*(3), 209-219.

Kolber, Z. S., Prášil, O., & Falkowski, P. G. (1998). Measurements of variable chlorophyll fluorescence using fast repetition rate techniques: defining methodology and experimental protocols. *Biochimica et Biophysica Acta, 1367*(1-3), 88-106.

Kolber, Z., Klimov, D., Ananyev, G., Rascher, U., Berry, J., & Osmond, B. (2005). Measuring photosynthetic parameters at a distance: laser induced fluorescence transient (LIFT) method for remote measurements of photosynthesis in terrestrial vegetation. *Photosynthesis Research, 84*, 121-129.

Kono, M., & Terashima, I. (2014). Long-term and short-term responses of the photosynthetic electron transport to fluctuating light. *Journal of Photochemistry and Photobiology B: Biology, 137*, 89-99.

Kooyers, N. J. (2015). The evolution of drought escape and avoidance in natural herbaceous populations. *Plant Science, 234*, 155-162.

Krall, J. P., & Edwards, G. E. (1990). Quantum yields of photosystem II electron transport and carbon dioxide fixation in C4 plants. *Australian Journal of Plant Physiology, 17*(5), 579-588.

Krause, G. H., & Weis, E. (1984). Chlorophyll fluorescence as a tool in plant physiology. II. Interpretation of fluorescence signals. *Photosynthesis Research, 5*, 139-157.

Krause, G. H., & Weis, E. (1991). Chlorophyll fluorescence and photosynthesis: the basics. *Annual Review of Plant Physiology and Plant Molecular Biology, 42*(1), 313-349.

Krieger-Liszkay, A., & Feilke, K. (2016). The dual role of the plastid terminal oxidase PTOX: between a protective and a pro-oxidant function. *Frontiers in Plant Science, 6*, 1147.

Külheim, C., Ågren, J., & Jansson, S. (2002). Repid regulation of light harvesting and plant fitness in the field. *Science, 297*(5578), 91-93.

Lancashire, P. D., Bleiholder, H., van den Boom, T., Langelüddeke, P., Stauss, R., Weber, E., & Witzenberger, A. (1991). A uniform decimal code for growth stages of crops and weeds. *Annals of Applied Biology, 119*(3), 561-601.

Lawlor, D. W. (2002). Limitation to photosynthesis in water-stressed leaves: stomata vs. metabolism and the role of ATP. *Annals of Botany, 89*(7), 871-885.

Lazár, D. (2003). Chlorophyll a fluorescence rise induced by high light illumination of dark-adapted plant tissue studied by means of a model of photosystem II and considering photosystem II heterogeneity. *Journal of Theoretical Biology, 220*(4), 469-503.

Lazár, D., & Jablonský, J. (2009). On the approaches applied in formulation of a kinetic model of photosystem II: different approaches lead to different simulations of the chlorophyll a fluorescence transients. *Journal of Theoretical Biology, 257*(2), 260-269.

le Maire, G., François, C., & Dufrêne, E. (2004). Towards universal broad leaf chlorophyll indices using PROSPECT simulated database and hyperspectral reflectance measurements. *Remote Sensing of Environment, 89*(1), 1-28.

Lefebvre, V., Kiani, S. P., & Durand-Tardif, M. (2009). A focus on natural variation for abiotic constraints response in the model species Arabidopsis thaliana. *International Journal of Molecular Sciences, 10*(8), 3547-3582.

Levitt, J. (1980). *Responses of Plants to Environmental Stresses: Water, Radiation, Salt, and Other Stresses* (2nd ed., Vol. II). New York, NY, United States of America: Academic Press.

Liang, J., Zhang, J., & Wong, M. H. (1997). Can stomatal closure caused by xylem ABA explain the inhibition of leaf photosynthesis under soil drying? *Photosynthesis Research, 51*, 149-159.

Littell, R. C., Pendergast, J., & Natarajan, R. (2000). Modelling covariance structure in the analysis of repeated measures data. *Statistics in Medicine, 19*(13), 1793-1819.

Liu, J., Miller, J. R., Haboudane, D., & Pattey, E. (2004a). Exploring the relationship between red edge parameters and crop variables for precision agriculture. *2004 IEEE International Geoscience and Remote Sensing Symposium Proceedings. Science for Society: Exploring and Managing a Changing Planet. II*, pp. 1276-1279. Anchorage, AK: IEEE. doi:https://doi.org/10.1109/IGARSS.2004.1368649

Liu, L., Wang, J., Huang, W., Zhao, C., Zhang, B., & Tong, Q. (2004b). Estimating winter wheat plant water content using red edge parameters. *International Journal of Remote Sensing, 25*(17), 3331-3342.

Lobell, D. B., & Burke, M. B. (2008). Why are agricultural impacts of climate change so uncertain? The importance of temperature relative to precipitation. *Environmental Research Letters, 3*(3), 034007.

Lobell, D. B., Schlenker, W., & Costa-Roberts, J. (2011). Climate trends and global crop production since 1980. *Science, 333*(6042), 616-620.

Longenberger, P. S., Smith, C. W., Duke, S. E., & McMichael, B. L. (2009). Evaluation of chlorophyll fluorescence as a tool for the identification of drought tolerance in upland cotton. *Euphytica, 166*, 25-33.

Lu, C., & Zhang, J. (1999). Effects of water stress on photosystem II photochemistry and its thermostability in wheat plants. *Journal of Experimental Botany, 50*(336), 1199-1206.

Maccaferri, M., Sanguineti, M. C., Demontis, A., El-Ahmed, A., del Moral, L., Maalouf, F., . . . Tuberosa, R. (2011). Association mapping in durum wheat grown across a broad range of water regimes. *Journal of Experimental Botany, 62*(2), 409-438.

Maccaferri, M., Sanguineti, M. C., Natoli, V., Ortega, J. A., Salem, M. B., Bort, J., . . . Tuberosa, R. (2006). A panel of elite accessions of durum wheat (Triticum durum Desf.) suitable for association mapping studies. *Plant Genetic Resources, 4*(1), 79-85.

Maechler, M., Rousseeuw, P., Croux, C., Todorov, V., Ruckstuhl, A., Salibian-Barrera, M., . . . Anna di Palma, M. (2020). *robustbase: Basic Robust Statistics*. R package version 0.93-6. Retrieved from http://robustbase.r-forge.r-project.org/

Marcial, L., & Sarrafi, A. (1996). Genetic analysis of some chlorophyll fluorescence and productivity parameters in barley (Hordeum vulgare). *Plant Breeding, 115*(5), 339-342.

Marquet, P. A., Quiñones, R. A., Abades, S., Labra, F., Tognelli, M., Arim, M., & Rivadeneira, M. (2005). Scaling and power-laws in ecological systems. *The Journal of Experimental Biology, 208*, 1749-1769.

Martin-Vertedor, A., & Dodd, I. C. (2011). Root-to-shoot signalling when soil moisture is heterogeneous: increasing the proportion of root biomass in drying soil inhibits leaf growth and increases leaf abscisic acid concentration. *Plant, Cell and Environment, 34*(7), 1164-1175.

Massmann, A., Gentine, P., & Lin, C. (2019). When does vapor pressure deficit drive or reduce evapotranspiration? *Journal of Advances in Modeling Earth Systems, 11*(10), 3305-3320.

Mathobo, R., Marais, D., & Steyn, J. M. (2017). The effect of dorught stress on yield, leaf gaseous exchange and chlorophyll fluorescence of dry beans (Phaseolus vulgaris L.). *Agricultural Water Management, 180*(Part A), 118-125.

Matthews, J. S., Vialet-Chabrand, S., & Lawson, T. (2018). Acclimation to fluctuating light impacts the rapidity of response and diurnal rhythm of stomatal conductance. *Plant Physiology, 176*(3), 1939-1951.

Maxwell, K., & Johnson, G. N. (2000). Chlorophyll fluorescence - a practical guide. *Journal of Experimental Botany, 51*(345), 659-668.

McAusland, L., Atkinson, J. A., Lawson, T., & Murchie, E. H. (2019). High throughput procedure utilising chlorophyll fluorescence imaging to phenotype dynamic photosynthesis and photoprotection in leaves under controlled gaseous conditions. *Plant Methods, 15*, 109.

McAusland, L., Vialet-Chabrand, S., Davey, P., Baker, N. R., Brendel, O., & Lawson, T. (2016). Effects of kinetics of light-induced stomatal responses on photosynthesis and water-use efficiency. *New Phytologist, 211*(4), 1209-1220.

McDonald, A. E., Ivanov, A. G., Bode, R., Maxwell, D. P., Rodermel, S. R., & Hüner, N. P. (2011). Flexibility in photosynthetic electron transport: the physiological role of plastoquinol terminal oxidase (PTOX). *Biochimica et Biophysica Acta (BBA) - Bioenergetics, 1807*(8), 954-967.

Medrano, H., Escalona, J. M., Bota, J., Gulías, J., & Flexas, J. (2002). Regulation of photosynthesis of C3 plants in response to progressive drought: stomatal conductance as a reference parameter. *Annals of Botany, 89*(7), 895-905.

Messina, C. D., Podlich, D., Dong, Z., Samples, M., & Cooper, M. (2011). Yield-trait performance landscapes: from theory to application in breeding maize for drought tolerance. *Journal of Experimental Botany, 62*(3), 855-868.

Meyer, G. E., & Camargo Neto, J. (2008). Verification of color vegetation indices for automated crop imaging applications. *Computers and Electronics in Agriculture, 63*(2), 282-293.

Mishra, A. K., & Singh, V. P. (2010). A review of drought concepts. *Journal of Hydrology, 391*(1-2), 202-216.

Mohammadi, R. (2018). Breeding for increased drought tolerance in wheat: a review. *Crop and Pasture Science, 69*(3), 223-241.

Mohammed, G. H., Colombo, R., Middleton, E. M., Rascher, U., van der Tol, C., Nedbal, L., . . . Zarco-Tejada, P. J. (2019). Remote sensing of solar-induced chlorophyll fluorescence (SIF) in vegetation: 50 years of progress. *Remote Sensing of Environment, 231*, 111177.

Molero, G., & Lopes, M. (2012). Gas exchange and chlorophyll fluorescence. In A. Pask, J. Pietragalla, D. Mullan, & M. Reynolds (Eds.), *Physiological Breeding II: A Field Guide to Wheat Phenotyping* (pp. 63-70). Mexico, D.F.: CIMMYT.

Monneveux, P., Jing, R., & Misra, S. C. (2012). Phenotyping for drought adaptation in wheat using physiological traits. *Frontiers in Physiology, 3*, 429.

Mullan, D., & Pietragalla, J. (2012). Leaf relative water content. In A. Pask, J. Pietragalla, D. Mullan, & M. Reynolds (Eds.), *Physiological Breeding II: A Field Guide to Wheat Phenotyping* (pp. 25-27). Mexico, D.F.: CIMMYT.

Müller, M., & Munné-Bosch, S. (2021). Hormonal impact on photosynthesis and photoprotection in plants. *Plant Physiology*, kiaa119. doi:https://doi.org/10.1093/plphys/kiaa119

Müller-Linow, M., Wilhelm, J., Briese, C., Wojciechowski, T., Schurr, U., & Fiorani, F. (2019). Plant screen mobile: an open-source mobile device app for plant trait analysis. *Plant Methods, 15*, 2.

Munné-Bosch, S., & Alegre, L. (2004). Die and let live: leaf senescence contributes to plant survival under drought stress. *Functional Plant Biology, 31*(3), 203-216.

Murchie, E. H., & Lawson, T. (2013). Chlorophyll fluorescence analysis: a guide to good practice and understanding some new applications. *Journal of Experimental Botany, 64*(13), 3983-3998.

Mutanga, O., & Skidmore, A. K. (2007). Red edge shift and biochemical content in grass canopies. *ISPRS Journal of Photogrammetry and Remote Sensing, 62*(1), 34-42.

Nagarajan, R. (2009). *Drought Assessment.* Dordrecht, The Netherlands and New Delhi, India: Springer and Capital Publishing Company.

Nakhforoosh, A., Bodewein, T., Fiorani, F., & Bodner, G. (2016). Identification of water use strategies at early growth stages in durum wheat from shoot phenotyping and physiological measurements. *Frontiers in Plant Science, 7*, 1155.

Nawrocki, W. J., Tourasse, N. J., Taly, A., Rappaport, F., & Wollman, F.-A. (2015). The plastid terminal oxidase: its elusive function points to multiple contributions to plastid physiology. *Annual Review of Plant Biology, 66*(1), 49-74.

Negin, B., & Moshelion, M. (2017). The advantages of functional phenotyping in pre-field screening for drought-tolerant crops. *Functional Plant Biology, 44*(1), 107-118.

Neukam, D., Böttcher, U., & Kage, H. (2016). Modelling wheat stomatal resistance in hourly time steps from micrometeorological variables and soil water status. *Journal of Agronomy and Crop Science, 202*(3), 174-191.

Neumann, P. M. (2008). Coping mechanisms for crop plants in drought-prone environments. *Annals of Botany, 101*(7), 901-907.

Nezhadahmadi, A., Prodhan, Z. H., & Faruq, G. (2013). Drought tolerance in wheat. *The Scientific World Journal, 2013*, Article ID 610721.

NOAA. (2020). *Climate at a Glance: Divisional Rankings*. (National Centers for Environmental Information) Retrieved July 14, 2020, from https://www.ncdc.noaa.gov/cag/divisional/rankings/0206/zndx/201804

Nogués, S., & Alegre, L. (2002). An increase in water deficit has no impact on the photosynthetic capacity of field-grown Mediterranean plants. *Functional Plant Biology, 29*(5), 621-630.

Normanly, J. (Ed.). (2012). *High-Throughput Phenotyping in Plants: Methods and Protocols.* Totowa, NJ, United States of America: Humana Press.

O'Neill, P. M., Shanahan, J. F., & Schepers, J. S. (2006). Use of chlorophyll fluorescence assessments to differentiate corn hybrid response to variable water conditions. *Crop Science, 46*(2), 681-687.

Osmond, B., Chow, W. S., Pogson, B. J., & Robinson, S. A. (2019). Probing functional and optical cross-sections of PSII in leaves during state transitions using fast repetition rate light induced fluorescence transients. *Functional Plant Biology, 46*(6), 567-583.

Osmond, B., Chow, W. S., Wyber, R., Zavafer, A., Keller, B., Pogson, B. J., & Robinson, S. A. (2017). Relative functional and optical absorption cross-sections of PSII and other photosynthetic parameters monitored in situ, at a distance with a time resolution of a few seconds, using a prototype light induced fluorescence transient (LIFT) device. *Functional Plant Biology, 44*(10), 985-1006.

Oukarroum, A., Madidi, S., Schansker, G., & Strasser, R. J. (2007). Probing the responses of barley cultivars (Hordeum vulgare L.) by chlorophyll a fluorescence OLKJIP under drought stress and re-watering. *Environmental and Experimental Botany, 60*(3), 438-446.

Ouyang, W., Struik, P. C., Yin, X., & Yang, J. (2017). Stomatal conductance, mesophyll conductance, and transpiration efficiency in relation to leaf anatomy in rice and wheat genotypes under drought. *Journal of Experimental Botany, 68*(18), 5191-5205.

Palmer, W. C. (1965). *Meteorological drought. Research Paper No. 45.* Weather Bureau. Washington, D.C.: U.S. Department of Commerce.

Pask, A., Pietragalla, J., Mullan, D., & Reynolds, M. (Eds.). (2012). *Physiological Breeding II: A Field Guide to Wheat Phenotyping.* Mexico City, Mexico: CIMMYT.

Passioura, J. (2006). Increasing crop productivity when water is scarce - from breeding to field management. *Agricultural Water Management, 80*(1-3), 176-196.

Passioura, J. B. (1977). Grain yield, harvest index, and water use of wheat. *The Journal of the Australian Institute of Agricultural Science, 43*(3-4), 117-120.

Patterson, H. D., & Williams, E. R. (1976). A new class of resolvable incomplete block designs. *Biometrika, 63*(1), 83-92.

Payne, R., Welham, S., & Harding, S. (2019). A guide to REML in Genstat (20th Edition). Hemel Hempstead, Hertfordshire, United Kingdom: VSN International.

Pei, Z.-M., Murata, Y., Benning, G., Thomine, S., Klüsener, B., Allen, G. J., . . . Schroeder, J. I. (2000). Calcium channels activated by hydrogen peroxide mediate abscisic acid signalling in guard cells. *Nature, 406*, 731-734.

Pérez-Bueno, M., Pineda, M., & Barón, M. (2019). Phenotyping plant responses to biotic stress by chlorophyll fluorescence imaging. *Frontiers in Plant Science, 10*, 1135.

Piepho, H. P. (2018). Allowing for the structure of a designed experiment when estimating and testing trait correlations. *The Journal of Agricultural Science, 156*(1), 59-70.

Piepho, H. P. (2019). A coefficient of determination (R2) for generalized linear mixed models. *Biometrical Journal, 61*(4), 860-872.

Piepho, H. P., & Möhring, J. (2011). On estimation of genotypic correlations and their standard errors by multivariate REML using the MIXED procedure of the SAS system. *Crop Science, 51*(6), 2449-2454.

Piepho, H. P., Büchse, A., & Emrich, K. (2003). A Hitchhiker's guide to mixed models for randomized experiments. *Journal of Agronomy and Crop Science, 189*(5), 310-322.

Piepho, H. P., Büchse, A., & Richter, C. (2004). A mixed modelling approach for randomized experiments with repeated measures. *Journal of Agronomy and Crop Science, 190*(4), 230-247.

Piepho, H. P., Williams, E. R., & Michel, V. (2015). Beyond Latin squares: a brief tour of row-column designs. *Agronomy Journal, 107*(6), 2263-2270.

Pieruschka, R., Klimov, D., Kolber, Z. S., & Berry, J. A. (2010). Monitoring of cold and light stress impact on photosynthesis by using the lase induced fluorescence transient (LIFT) approach. *Functional Plant Biology, 37*(5), 395-402.

Podlich, D. W., Winkler, C. R., & Cooper, M. (2004). Mapping as you go: an effective approach for marker-assisted selection of complex traits. *Crop Science, 44*(5), 1560-1571.

Porter, J. R., Challinor, A. J., Cochrane, K., Howden, S., Iqbal, M. M., Lobell, D. B., & Travasso, M. (2014). Food security and food production systems. In C. B. Field, V. R. Barros, D. J. Dokken, K. J. Mach, M. D. Mastrandrea, T. E. Bilir, . . . L. L. White

(Eds.), *Climate Change 2014: Impacts, Adaptation, and Vulnerability. Part A: Global and Sectoral Aspects. Contribution of Working Group II to the Fifth Assessment Report of the Intergovernmental Panel on Climate Change* (pp. 485-533). Cambridge, United Kingdom and New York, United States of America: Cambridge University Press.

Qaseem, M. F., Qureshi, R., & Shaheen, H. (2019). Effects of pre-anthesis drought, heat and their combination on the growth, yield and physiology of diverse wheat (Triticum aestivum L.) genotypes varying in sensitivity to heat and drought stress. *Scientific Reports, 9*, 6955.

Qiao, C. G., Basford, K. E., DeLacy, I. H., & Cooper, M. (2000). Evaluation of experimental designs and spatial analyses in wheat breeding trials. *Theoretical and Applied Genetics, 100*, 9-16.

R Core Team. (2020). R a language and environment for statistical computing. Vienna, Austria: R Foundation for Statistical Computing. Retrieved from https://www.R-project.org/

Raesch, A. R., Muller, O., Pieruschka, R., & Rascher, U. (2014). Field observations with laser-induced fluorescence transient (LIFT) method in barley and sugar beet. *Agriculture, 4*(2), 159-169.

Ranalli, P., di Candilo, M., & Bagatta, M. (1997). Drought tolerance screening for potato improvement. *Plant Breeding, 116*(3), 290-292.

Rascher, U., & Pieruschka, R. (2008). Spatio-temporal variations of photosynthesis: the potential of optical remote sensing to better understand and scale light use efficiency and stresses of plant ecosystems. *Precision Agriculture, 9*, 355-366.

Ray, D. K., Mueller, N. D., West, P. C., & Foley, J. A. (2013). Yield trends are insufficient to double global crop production by 2050. *PLOS ONE, 8*(6), e66428.

Rehman, S. U., Bilal, M., Rana, R. M., Tahir, M. N., Shah, M. K., Ayalew, H., & Yan, G. (2016). Cell membrane stability and chlorophyll content variation in wheat (Triticum aestivum) genotypes under conditions of heat and drought. *Crop and Pasture Science, 67*(7), 712-718.

Resende, R. T., Piepho, H.-P., Rosa, G. J., Silva-Junior, O. B., Silva, F. F., de Resende, M. V., & Grattapaglia, D. (2021). Enviromics in breeding: applications and perspectives on envirotypic-assisted selection. *Theoretical and Applied Genetics, 134*, 95-112.

Reynolds, M., & Langridge, P. (2016). Physiological breeding. *Current Opinion in Plant Biology, 31*, 162-171.

Reynolds, M., Chapman, S., Crespo-Herrera, L., Molero, G., Mondal, S., Pequeno, D. N., . . . Sukumaran, S. (2020). Breeder friendly phenotyping. *Plant Science, 295*, 110396.

Richards, R. A. (2000). Selectable traits to increase crop photosynthesis and yield of grain crops. *Journal of Experimental Botany, 51*(Issue suppl_1), 447-458.

Robinson, G. K. (1991). That BLUP is a good thing: the estimation of random effects. *Statistical Science, 6*(1), 15-32.

Rochaix, J.-D. (2011). Regulation of photosynthetic electron transport. *Biochimica et Biophysica Acta (BBA) - Bioenergetics, 1807*(3), 375-383.

Rosenzweig, C., Iglesias, A., Yang, X. B., Epstein, P. R., & Chivian, E. (2001). Climate change and extreme weather events: implications for food production, plant diseases, and pests. *Global Change and Human Health, 2*(2), 90-104.

Royal Society. (2012). *People and the planet.* The Royal Society, Science Policy Centre. London: The Royal Society. Retrieved November 10, 2020, from https://royalsociety.org/topics-policy/projects/people-planet/report/

Rutkoski, J., Poland, J., Mondal, S., Autrique, E., Pérez, L. G., Crossa, J., . . . Singh, R. (2016). Canopy temperature and vegetation indices from high-throughput phenotyping improve accuracy of pedigree and genomic selection for grain yield in wheat. *G3: Genes, Genomes, Genetics, 6*(9), 2799-2808.

Sack, L., & Holbrook, N. M. (2006). Leaf hydraulics. *Annual Review of Plant Biology, 57*(1), 361-381.

Sadras, V. O., & Angus, J. F. (2006). Benchmarking water-use efficiency of rainfed wheat in dry environments. *Australian Journal of Agricultural Research, 57*(8), 847-856.

Sakoda, K., Yamori, W., Groszmann, M., & Evans, J. R. (2021). Stomatal, mesophyll conductance, and biochemical limitations to photosynthesis during induction. *Plant Physiology, 185*(1), 146-160.

Salekdeh, G. H., Reynolds, M., Bennett, J., & Boyer, J. (2009). Conceptual framework for drought phenotyping during molecular breeding. *Trends in Plant Science, 14*(9), 488-496.

Sallam, A., Alqudah, A. M., Dawood, M. F., Baenziger, P. S., & Börner, A. (2019). Drought stress tolerance in wheat and barley: advances in physiology, breeding and genetics research. *International Journal of Molecular Sciences, 20*(13), 3137.

Sanchez-Bragado, R., Newcomb, M., Chairi, F., Condorelli, G. E., Ward, R. W., White, J. W., . . . Molins, M. S. (2020). Carbon isotope composition and the NDVI as phenotyping

approaches for drought adaptation in durum wheat: beyond trait selection. *Agronomy, 10*(11), 1679.

Saradadevi, R., Palta, J. A., & Siddique, K. H. (2017). ABA-mediated stomatal response in regulating water use during the development of terminal drought in wheat. *Frontiers in Plant Science, 8*, 1251.

Sasidharan, R., Voesenek, L. A., & Pierik, R. (2011). Cell wall modifying proteins mediate plant acclimatization to biotic and abiotic stresses. *Critical Reviews in Plant Sciences, 30*(6), 548-562.

Schachtman, D. P., & Goodger, J. Q. (2008). Chemical root to shoot signaling under drought. *Trends in Plant Science, 13*(6), 281-287.

Schmidhuber, J., & Tubiello, F. N. (2007). Global food security under climate change. *Proceedings of the National Academy of Sciences of the United States of America, 104*(50), 19703-19708.

Schöttler, M. A., & Tóth, S. Z. (2014). Photosynthetic complex stoichiometry dynamics in higher plants: environmental acclimation and photosynthetic flux control. *Frontiers in Plant Science, 5*, 188.

Schreiber, U. (1986). Detection of rapid induction kinetics with a new type of high-frequency modulated chlorophyll fluorometer. *Photosynthesis Research, 9*, 261-272.

Seager, R., Naik, N., & Vecchi, G. A. (2010). Thermodynamic and dynamic mechanisms for large-scale changes in the hydrological cycle in response to global warming. *Journal of Climate, 23*(17), 4651-4668.

Sehgal, D., Singh, R., & Rajpal, V. R. (2016). Quantitative trait loci mapping in plants: concepts and approaches. In V. R. Rajpal, S. R. Rao, & S. N. Raina (Eds.), *Molecular Breeding for Sustainable Crop Improvement* (Vol. 2, pp. 31-59). Cham, Switzerland: Springer.

Seki, M., Umezawa, T., Urano, K., & Shinozaki, K. (2007). Regulatory metabolic networks in drought stress responses. *Current Opinion in Plant Biology, 10*(3), 296-302.

Shangguan, Z., Shao, M., & Dyckmans, J. (1999). Interaction of osmotic adjustment and photosynthesis in winter wheat under soil drought. *Journal of Plant Physiology, 154*(5-6), 753-758.

Shirao, M., Kuroki, S., Kaneko, K., Kinjo, Y., Tsuyama, M., Förster, B., . . . Badger, M. R. (2013). Gymnosperms have increased capacity for electron leakage to oxygen (Mehler and PTOX reactions) in photosynthesis compared with angiosperms. *Plant and Cell Physiology, 54*(7), 1152-1163.

Sim, C. H., Gan, F. F., & Chang, T. C. (2005). Outlier labeling with boxplot procedures. *Journal of the American Statistical Association, 100*(470), 642-652.

Sivakumar, M. V. (2005). World Meteorological Organization and agricultural droughts. In V. K. Boken, A. P. Cracknell, & R. L. Heathcote (Eds.), *Monitoring and Predicting Agricultural Drought: A Global Study* (pp. 401-410). New York, NY, United States of America: Oxford University Press.

Sivakumar, M. V. (2011). Agricultural Drought - WMO Perspectives. In M. V. Sivakumar, R. P. Motha, D. A. Wilhite, & D. A. Wood (Ed.), *Agricultural Drought Indices. Proceedings of the WMO/UNISDR Expert Group Meeting on Agricultural Drought Indices, 2-4 June 2010, Murcia, Spain* (pp. 22-34). Geneva, Switzerland: World Meteorological Organization.

Soares, G. F., Ribeiro Júnior, W. Q., Pereira, L. F., de Lima, C. A., Soares, D. d., Muller, O., . . . Ramos, M. G. (2021). Characterization of wheat genotypes for drought tolerance and water use efficiency. *Scientia Agricola, 78*(5), e20190304. doi:https://doi.org/10.1590/1678-992x-2019-0304

Stern, N. (2007). *The Economics of Climate Change: The Stern Review.* Cambridge, United Kingdom: Cambridge University Press.

Stirbet, A. D., & Strasser, R. J. (1995). Numerical simulation of the fluorescence induction in plants. *Archives des sciences et compte rendu des séances de la Société, 48*(1), 41-60.

Stirbet, A., & Govindjee. (2011). On the relation between the Kautsky effect (chlorophyll a fluorescence induction) and photosystem II: basics and applications of the OJIP fluorescence transient. *Journal of Photochemistry and Photobiology B: Biology, 104*(1-2), 236-257.

Stirbet, A., Lazár, D., Guo, Y., & Govindjee, G. (2020). Photosynthesis: basics, history and modelling. *Annals of Botany, 126*(4), 511-537.

Sun, J., Rutkoski, J. E., Poland, J. A., Crossa, J., Jannink, J.-L., & Sorrells, M. E. (2017). Multitrait, random regression, or simple repeatability model in high-throughput phenotyping data improve genomic prediction for wheat grain yield. *The Plant Genome, 10*(2), plantgenome2016.11.0111.

Taiz, L. (2013). Agriculture, plant physiology, and human population growth: past, present, and future. *Theoretical and Experimental Plant Physiology, 25*(3), 167-181.

Takahashi, F., Kuromori, T., Urano, K., Yamaguchi-Shinozaki, K., & Shinozaki, K. (2020). Drought stress responses and resistance in plants: from cellular responses to long-distance intercellular communication. *Frontiers in Plant Science, 11*, 556972.

Takahashi, S., Milward, S. E., Fan, D.-Y., Chow, W. S., & Badger, M. R. (2009). How does cyclic electron flow alleviate photoinhibition in Arabidopsis? *Plant Physiology, 149*(3), 1560-1567.

Tardieu, F., Cabrera-Bosquet, L., Pridmore, T., & Bennett, M. (2017). Plant phenomics, from sensors to knowledge. *Current Biology, 27*(15), R770-R783.

Tardieu, F., Parent, B., & Simonneau, T. (2010). Control of leaf growth by abscisic acid: hydraulic or non-hydraulic processes? *Plant, Cell and Environment, 33*(4), 636-647.

Tenhaken, R. (2015). Cell wall remodeling under abiotic stress. *Frontiers in Plant Science*(5), 771.

Tester, M., & Langridge, P. (2010). Breeding technologies to increase crop production in a changing world. *Science, 327*(5967), 818-822.

Tezara, W., Mitchell, V. J., Driscoll, S. D., & Lawlor, D. W. (1999). Water stress inhibits plant photosynthesis by decreasing coupling factor and ATP. *Nature, 401*, 914-917.

Tikhonov, A. N. (2013). pH-Dependet regulation of electron transport and ATP synthesis in chloroplasts. *Photosynthesis Research, 116*, 511-534.

Tikkanen, M., Grieco, M., Nurmi, M., Rantala, M., Suorsa, M., & Aro, E.-M. (2012). Regulation of the photosynthetic apparatus under fluctuating growth light. *Philosophical Transactions of the Royal Society of London. Series B, Biological Sciences, 367*(1608), 3486-3493.

Tilman, D., Balzer, C., Hill, J., & Befort, B. L. (2011). Global food demand and the sustainable intensification of agriculture. *Proceedings of the National Academy of Sciences of the United States of America, 108*(50), 20260-20264.

Trenberth, K. E., Dai, A., van der Schrier, G., Jones, P. D., Barichivich, J., Briffa, K. R., & Sheffield, J. (2014). Global warming and changes in drought. *Nature Climate Change, 4*, 17-22.

Tripathy, J. N., Zhang, J., Robin, S., Nguyen, T. T., & Nguyen, H. T. (2000). QTLs for cell-membrane stability mapped in rice (Oryza sativa L.) under drought stress. *Theoretical and Applied Genetics, 100*, 1197-1202.

Tschiersch, H., Junker, A., Meyer, R. C., & Altmann, T. (2017). Establishment of integrated protocols for automated high throughput kinetic chlorophyll fluorescence analyses. *Plant Methods, 13*, 54.

Tuberosa, R. (2012). Phenotyping for drought tolerance of crops in the genomics era. *Frontiers in Physiology, 3*, 347.

Turral, H., Burke, J., & Faurès, J.-M. (2011). *FAO Water Reports 36. Climate change, water and food security.* Rome: FAO.

UNEP. (2009). *Climate in Peril: A popular guide to the latest IPCC reports.* UNEP/GRID-Arendal. Birkeland, Norway: United Nations Environment Programme.

United Nations. (2019). *World Population Prospects 2019: Highlights (ST/ESA/SER.A/423).* Department of Economic and Social Affairs, Population Division. New York: United Nations.

van Eeuwijk, F. A., Bustos-Korts, D., Millet, E. J., Boer, M. P., Kruijer, W., Thompson, A., . . . Chapman, S. C. (2019). Modelling strategies for assessing and increasing the effectiveness of new phenotyping techniques in plant breeding. *Plant Science, 282*, 23-39.

van Genuchten, M. T. (1980). A closed-form equation for predicting the hydraulic conductivity of unsaturated soils. *Soil Science Society of America Journal, 44*(5), 892-898.

van Velthuizen, H., Huddleston, B., Fischer, G., Salvatore, M., Ataman, E., Nachtergaele, F. O., . . . Bloise, M. (2007). *Mapping biophysical factors that influence agricultural production and rural vulnerability.* Rome: FAO and IIASA.

Vercruyssen, L., Gonzalez, N., Werner, T., Schmülling, T., & Inzé, D. (2011). Combining enhanced root and shoot growth reveals cross talk between pathways that control plant organ size in Arabidopsis. *Plant Physiology, 155*(3), 1339-1352.

Verdeprado, H., Kretzschmar, T., Begum, H., Raghavan, C., Joyce, P., Lakshmanan, P., . . . Collard, B. C. (2018). Association mapping in rice: basic concepts and perspectives for molecular breeding. *Plant Production Science, 21*(3), 159-176.

Verslues, P. E., & Juenger, T. E. (2011). Drought, metabolites, and Arabidopsis natural variation: a promising combination for understanding adaptation to water-limited environments. *Current Opinion in Plant Biology, 14*(3), 240-245.

Verslues, P. E., Agarwal, M., Katiyar-Agarwal, S., Zhu, J., & Zhu, J.-K. (2006). Methods and concepts in quantifying resistance to drought, salt and freezing, abiotic stresses that affect plant water status. *The Plant Journal, 45*(4), 523-539.

Vile, D., Pervent, M., Belluau, M., Vasseur, F., Bresson, J., Muller, B., . . . Simonneau, T. (2012). Arabidopsis growth under prolonged high temperature and water deficit: independent or interactive effects? *Plant, Cell and Environment, 35*(4), 702-718.

Virlet, N., Sabermanesh, K., Sadeghi-Tehran, P., & Hawkesford, M. J. (2017). Field Scanalyzer: an automated robotic field phenotyping platform for detailed crop monitoring. *Functional Plant Biology, 44*(1), 143-153.

Visscher, P. M., Hill, W. G., & Wray, N. R. (2008). Heritability in the genomics era - concepts and misconceptions. *Nature Reviews Genetics, 9*, 255-266.

Vogelmann, J. E., Rock, B. N., & Moss, D. M. (1993). Red edge spectral measurements from sugar maple leaves. *International Journal of Remote Sensing, 14*(8), 1563-1575.

VSN International. (2019). Genstat for Windows 20th Edition. Hemel Hempstead, United Kingdom: VSN International. Retrieved from https://www.vsni.co.uk/

Wada, S., Takagi, D., Miyake, C., Makino, A., & Suzuki, Y. (2019). Responses of the photosynthetic electron transport reactions stimulate the oxidation of the reaction center chlorophyll of photosystem I, P700, under drought and high temperatures in rice. *International Journal of Molecular Sciences, 20*(9), 2068.

Walker, B. J., Kramer, D. M., Fisher, N., & Fu, X. (2020). Flexibility in the energy balancing network of photosynthesis enables safe operation under changing environmental conditions. *Plants, 9*(3), 301.

Walters, R. G. (2005). Towards an understanding of photosynthetic acclimation. *Journal of Experimental Botany, 56*(411), 435-447.

Wang, H., Qian, X., Zhang, L., Xu, S., Li, H., Xia, X., . . . Liu, X. (2018). A method of high throughput monitoring crop physiology using chlorophyll fluorescence and multispectral imaging. *Frontiers in Plant Science, 9*, 407.

Wang, W.-H., He, E.-M., Chen, J., Guo, Y., Chen, J., Liu, X., & Zheng, H.-L. (2016). The reduced state of the plastoquinone pool is required for chloroplast-mediated stomatal closure in response to calcium stimulation. *The Plant Journal, 86*(2), 132-144.

Wang, Z. X., Chen, L., Ai, J., Qin, H. Y., Liu, Y. X., Xu, P. L., . . . Zhang, Q. T. (2012). Photosynthesis and activity of photosystem II in response to drought stress in Amur Grape (Vitis amurensis Rupr.). *Photosynthetica, 50*(2), 189-196.

Watt, M., Fiorani, F., Usadel, B., Rascher, U., Muller, O., & Schurr, U. (2020). Phenotyping: new windows into the plant for breeders. *Annual Review of Plant Biology, 71*(1), 689-712.

White, J. W., & Conley, M. M. (2013). A flexible, low-cost cart for proximal sensing. *Crop Science, 53*(4), 1646-1649.

Wilhite, D. A. (2000). Drought as a natural hazard: concepts and definitions. In D. A. Wilhite (Ed.), *Drought: A Global Assessment* (Vol. I, pp. 3-18). London, United Kingdom: Routledge.

Wilhite, D. A., & Glantz, M. H. (1985). Understanding: the drought phenomenon: the role of definitions. *Water International, 10*(3), 111-120.

Wilkinson, S., & Davies, W. J. (2010). Drought, ozone, ABA and ethylene: new insights from cell to plant to community. *Plant, Cell and Environment, 33*(4), 510-525.

Wingler, A., & Roitsch, T. (2008). Metabolic regulation of leaf senescence: interactions of sugar signalling with biotic and abiotic stress responses. *Plant Biology, 10*(S1), 50-62.

Winterhalter, L., Mistele, B., Jampatong, S., & Schmidhalter, U. (2011). High throughput phenotyping of canopy water mass and canopy temperature in well-watered and drought stressed tropical maize hybrids in the vegetative stage. *Eurpean Journal of Agronomy, 35*(1), 22-32.

Wolfinger, R. (1993). Covariance structure selection in general mixed models. *Communications in Statistics - Simulation and Computation, 22*(4), 1079-1106.

Wyber, R., Osmond, B., Ashcroft, M. B., Malenovský, Z., & Robinson, S. A. (2018). Remote monitoring of dynamic canopy photosynthesis with high time resolution light-induced fluorescence transients. *Tree Physiology, 38*(9), 1302-1318.

Xin, C. P., Yang, J., & Zhu, X.-G. (2013). A model of chlorophyll a fluorescence induction kinetics with explicit description of structural constraints of individual photosystem II units. *Photosynthesis Research, 117*, 339-354.

Yadav, S., Sandhu, N., Majumder, R. R., Dixit, S., Kumar, S., Singh, S. P., . . . Kumar, A. (2019). Epistatic interactions of major effect drought QTLs with genetic background loci determine grain yield of rice under drought stress. *Scientific Reports, 9*, 2616.

Yan, H., Wu, L., Filardo, F., Yang, X., Zhao, X., & Fu, D. (2017). Chemical and hydraulic signals regulate stomatal behavior and photosynthetic activity in maize during progressive dorught. *Acta Physiologiae Plantarum, 39*, 125.

Yang, S., Vanderbeld, B., Wan, J., & Huang, Y. (2010). Narrowing down the targets: towards successful genetic engineering of drought-tolerant crops. *Molecular Plant, 3*(3), 469-490.

Yang, W., Feng, H., Zhang, X., Zhang, J., Doonan, J. H., Batchelor, W. D., . . . Yan, J. (2020). Crop phenomics and high-throughput phenotyping: past decades, current challenges, and future perspectives. *Molecular Plant, 13*(2), 187-214.

Yokoyama, R., & Nishitani, K. (2001). A comprehensive expression analysis of all members of a gene family encoding cell-wall enzymes allowed us to predict cis-regulatory regions involved in cell-wall construction in specific organs of Arabidopsis. *Plant Cell Physiology, 42*(10), 1025-1033.

Yordanov, I., Velikova, V., & Tsonev, T. (2003). Plant responses to drought and stress tolerance. *Bulgarian Journal of Plant Physiology, 29*(3-4), 187-206.

Yuan, W., Zheng, Y., Piao, S., Ciais, P., Lombardozzi, D., Wang, Y., . . . Yang, S. (2019). Increased atmospheric vapor pressure deficit reduces global vegetation growth. *Science Advances, 5*(8), eaax1396.

Zadoks, J. C., Chang, T. T., & Konzak, C. F. (1974). A decimal code for the growth stages of cereals. *Weed Research, 14*(6), 415-421.

Zhang, H., Zhao, Y., & Zhu, J.-K. (2020). Thriving under stress: how plants balance growth and the stress response. *Developmental Cell, 55*(5), 529-543.

Zhou, Y., He, R., Guo, Y., Liu, K., Huang, G., Peng, C., . . . Duan, L. (2019). A novel ABA functional analogue B2 enhances drought tolerance in wheat. *Scientific Reports, 9*, 2887.

Zhu, X.-G., Govindjee, Baker, N. R., deSturler, E., Ort, D. R., & Long, S. P. (2005). Chlorophyll a fluorescence induction kinectis in leaves predicted from a model describing each discrete step of excitation energy and electron transfer associated with photosystem II. *Planta, 223*, 114-133.

Zivcak, M., Kalaji, H. M., Shao, H.-B., Olsovska, K., & Brestic, M. (2014). Photosynthetic proton and electron transport in wheat leaves under prolonged moderate drought stress. *Journal of Photochemistry and Photobiology B: Biology, 137*, 107-115.

APPENDIX 1 – LIST OF GENETIC RESOURCES

Table A.1.1. List of elite durum wheat (*Triticum turgidum* L. ssp. *durum* Desf.) accessions, mainly cultivars and advanced lines, from the association mapping population 'UNIBO-Durum Panel' assembled at the University of Bologna, Italy, which were evaluated in the growing seasons 2017/2018 (Y1) and 2018/2019 (Y2) in Maricopa, AZ, USA. The subgroups were defined as reported by Condorelli et al. (2018).

Growing Season 2017/2018 (Y1)	Growing Season 2018/2019 (Y2)	UNIBO Panel Code	Subgroup	Origin	Accession Name
Yes	Yes	DP_001	S6	ITALY	BRADANO
Yes	Yes	DP_002	S6	ITALY	CANNIZZO
Yes	Yes	DP_004	Admixture	ITALY	LESINA
Yes	Yes	DP_005	S5	ITALY	MERIDIANO
Yes	Yes	DP_006	S6	ITALY	MONGIBELLO
Yes	Yes	DP_007	Admixture	ITALY	NORBA
Yes	Yes	DP_008	S6	ITALY	PIETRAFITTA
Yes	Yes	DP_009	S6	ITALY	QUADRATO
Yes	Yes	DP_010	S6	ITALY	TORREBIANCA
Yes	Yes	DP_011	S7	CIMMYT	CIMMYT23
Yes	Yes	DP_012	Admixture	CIMMYT	CIMMYT36
Yes	Yes	DP_013	Admixture	CIMMYT	CIMMYT41
Yes	Yes	DP_014	S7	CIMMYT	CIMMYT47
Yes	Yes	DP_015	S7	CIMMYT	CIMMYT52
Yes	Yes	DP_016	S7	CIMMYT	CIMMYT67
Yes	No	DP_017	S7	CIMMYT	CIMMYT73
Yes	No	DP_018	S7	CIMMYT	CIMMYT78
Yes	No	DP_019	S7	CIMMYT	CIMMYT104
Yes	Yes	DP_020	S7	CIMMYT	CIMMYT108
Yes	Yes	DP_021	S7	CIMMYT	CIMMYT136
Yes	Yes	DP_022	S7	CIMMYT	CIMMYT172
Yes	Yes	DP_023	S7	CIMMYT	CIMMYT198
Yes	Yes	DP_024	S7	CIMMYT	CIMMYT222
Yes	Yes	DP_025	S7	CIMMYT	CIMMYT247
Yes	Yes	DP_026	S7	CIMMYT	CIMMYT260
Yes	Yes	DP_027	Admixture	CIMMYT	CIMMYT266
Yes	Yes	DP_028	Admixture	IRTA	ALDEANO
Yes	Yes	DP_029	Admixture	IRTA	ARIESOL
Yes	No	DP_030	S3	IRTA	ARTENA
Yes	Yes	DP_031	S7	IRTA	ASTIGI
Yes	Yes	DP_032	Admixture	IRTA	BOABDIL
Yes	Yes	DP_033	Admixture	IRTA	BOLENGA
Yes	Yes	DP_034	S3	IRTA	BOLIDO
Yes	Yes	DP_035	Admixture	IRTA	BOLO
Yes	Yes	DP_036	S7	IRTA	BOMBASI
Yes	Yes	DP_037	S5	IRTA	BORLI
Yes	Yes	DP_038	Admixture	IRTA	CANYON
Yes	Yes	DP_039	S3	IRTA	DURCAL
Yes	Yes	DP_040	Admixture	IRTA	DUROI
Yes	Yes	DP_041	S7	IRTA	GALLARETA
Yes	Yes	DP_042	S7	IRTA	ILLORA
Yes	Yes	DP_043	S7	IRTA	JABATO
Yes	Yes	DP_045	S7	IRTA	SULA
Yes	Yes	DP_046	S3	INRAE	1804
Yes	Yes	DP_047	S5	INRAE	1805
Yes	Yes	DP_048	S3	INRAE	1807
Yes	Yes	DP_049	S3	INRAE	1808
Yes	Yes	DP_050	Admixture	INRAE	1809

(continue)

Growing Season 2017/2018 (Y1)	Growing Season 2018/2019 (Y2)	UNIBO Panel Code	Subgroup	Origin	Accession Name
Yes	Yes	DP_051	S5	INRAE	ANOUAR
Yes	Yes	DP_052	S3	INRAE	ISLY
Yes	Yes	DP_053	Admixture	INRAE	JAWHAR
Yes	Yes	DP_054	S7	INRAE	MARJANA
Yes	Yes	DP_055	S3	INRAE	MARZAK
Yes	Yes	DP_056	S5	INRAE	OURGH
Yes	Yes	DP_057	Admixture	INRAE	TAREK
Yes	Yes	DP_058	S2	INRAE	TOMOUH
Yes	Yes	DP_059	S5	INRAE	YASMINE
Yes	Yes	DP_060	S2	ICARDA	AW12/BIT
Yes	Yes	DP_061	S4	ICARDA	BIC/3/CHAM1//GRA//STK
Yes	Yes	DP_062	Admixture	ICARDA	CHABA/DERAA
Yes	Yes	DP_063	S4	ICARDA	CHACAN
Yes	Yes	DP_064	S5	ICARDA	KARIM
Yes	Yes	DP_065	Admixture	ICARDA	H.MOUL(MOR)/CHABA 88
Yes	Yes	DP_066	Admixture	ICARDA	KRS/HAUCAN
Yes	Yes	DP_067	Admixture	ICARDA	LAGOST 3
Yes	Yes	DP_068	S4	ICARDA	MOULSABIL 2
Yes	Yes	DP_069	Admixture	ICARDA	OMBAR
Yes	Yes	DP_070	S2	ICARDA	OMRABI 3
Yes	Yes	DP_071	S2	ICARDA	OMRABI 5
Yes	Yes	DP_072	Admixture	ICARDA	QUAD//ERP/MAL/3/UNKN
Yes	Yes	DP_073	S4	ICARDA	SEBAH
Yes	Yes	DP_074	S3	ICARDA	STOJOCRI-3
Yes	Yes	DP_075	S4	ICARDA	ZEINA 1
Yes	Yes	DP_076	S6	ICARDA	ANTON
Yes	Yes	DP_077	S3	ITALY	APPIO
Yes	Yes	DP_078	S1	ITALY	APPULO
Yes	Yes	DP_079	Admixture	ITALY	ARCANGELO
Yes	Yes	DP_080	S7	ITALY	ARCOBALENO
Yes	Yes	DP_081	Admixture	USA	BRAVADUR
Yes	Yes	DP_082	S5	ITALY	BRONTE
Yes	Yes	DP_083	S1	ITALY	CAPEITI 8
Yes	Yes	DP_084	S1	ITALY	CAPPELLI
Yes	Yes	DP_085	S1	ITALY	CICCIO
Yes	Yes	DP_086	S8	USA/ITALY	COLORADO
Yes	Yes	DP_087	S4	ITALY	COLOSSEO
Yes	Yes	DP_088	Admixture	USA	CORTEZ
Yes	Yes	DP_089	S4	ITALY	CRESO
Yes	Yes	DP_090	Admixture	ITALY	DON PEDRO
Yes	Yes	DP_100	Admixture	USA	KRONOS
Yes	Yes	DP_101	Admixture	ITALY	LIRA B 45
Yes	Yes	DP_102	S3	ITALY	MESSAPIA
Yes	Yes	DP_103	Admixture	ITALY	MEXICALI 75
Yes	Yes	DP_104	Admixture	ITALY	MOHAWK
Yes	Yes	DP_105	S6	ITALY	OFANTO
Yes	Yes	DP_106	Admixture	ITALY	PLATANI
Yes	Yes	DP_107	S6	ITALY	PLINIO
Yes	Yes	DP_108	S4	ITALY	PRODURA
Yes	Yes	DP_109	Admixture	ITALY	REVA
Yes	Yes	DP_110	S3	ITALY	ROQUENO
Yes	Yes	DP_111	S3	ITALY	SVEVO
Yes	Yes	DP_112	S1	ITALY	TRINAKRIA
Yes	Yes	DP_113	S1	ITALY	VALBELICE
Yes	Yes	DP_114	S6	ITALY	VALNOVA
Yes	Yes	DP_115	S6	ITALY	VARANO
Yes	Yes	DP_116	S8	USA	WEST BRED 881

(continue)

Growing Season 2017/2018 (Y1)	Growing Season 2018/2019 (Y2)	UNIBO Panel Code	Subgroup	Origin	Accession Name
Yes	Yes	DP_117	S5	USA	WEST BRED TURBO
Yes	Yes	DP_118	Admixture	ICARDA	AGHRASS-1
Yes	Yes	DP_119	S5	ICARDA	AINZEN-1
Yes	Yes	DP_120	Admixture	ICARDA	ANGRE
Yes	Yes	DP_121	Admixture	ICARDA	AMEDAKUL-1
Yes	Yes	DP_122	Admixture	ICARDA	AMMAR-1
Yes	Yes	DP_123	Admixture	ICARDA	ARISLAHN-5
Yes	Yes	DP_124	Admixture	ICARDA	ATLAST-1
Yes	Yes	DP_125	Admixture	ICARDA	AUS-1
Yes	Yes	DP_126	Admixture	ICARDA	AWALI-1
Yes	Yes	DP_127	S4	ITALY	RADIOSO
Yes	Yes	DP_128	Admixture	ICARDA	AZEGHAR-2
Yes	Yes	DP_129	S4	ICARDA	BCRCH-1
Yes	Yes	DP_130	S5	ICARDA	BICRE
Yes	Yes	DP_131	Admixture	ICARDA	BICREDERAA-1
Yes	Yes	DP_132	S5	ICARDA	BIGOST-1
Yes	Yes	DP_133	Admixture	ICARDA	BLK2
Yes	Yes	DP_134	Admixture	ICARDA	BRACHOUA
Yes	Yes	DP_135	S5	ICARDA	CHABHA 88
Yes	Yes	DP_136	Admixture	ICARDA	CHAM-1
Yes	Yes	DP_137	S4	ICARDA	DERAA
Yes	Yes	DP_138	Admixture	ICARDA	FURAT-1
Yes	Yes	DP_139	S4	ICARDA	GEROMTEL-1
Yes	Yes	DP_140	Admixture	ICARDA	GEZIRA 17
Yes	Yes	DP_142	Admixture	ICARDA	GUEROU-1
Yes	Yes	DP_143	S4	ICARDA	ADYT 02
Yes	Yes	DP_144	S1	ICARDA	HAURANI
Yes	Yes	DP_145	Admixture	ICARDA	HEIDER
Yes	Yes	DP_146	S4	ICARDA	ICARDA121
Yes	Yes	DP_147	S3	ICARDA	SEBOU
Yes	Yes	DP_148	S2	ICARDA	ICARDA125
Yes	Yes	DP_149	S3	ICARDA	ICARDA78
Yes	Yes	DP_150	Admixture	ICARDA	JORDAN
Yes	Yes	DP_151	Admixture	ICARDA	KABIR1
Yes	Yes	DP_152	S4	ICARDA	GR/BOY
Yes	Yes	DP_153	Admixture	ICARDA	KHABUR-1
Yes	Yes	DP_154	Admixture	ICARDA	KRF
Yes	Yes	DP_155	Admixture	ICARDA	LAGONIL-2
Yes	Yes	DP_156	S5	ICARDA	LAHN
Yes	Yes	DP_157	Admixture	ICARDA	LOUKOS-1
Yes	Yes	DP_158	Admixture	ICARDA	MAAMOURI-1
Yes	Yes	DP_159	Admixture	ICARDA	MARSYR-1
Yes	Yes	DP_160	S2	ICARDA	MASSARA-1
Yes	Yes	DP_161	Admixture	ICARDA	MIKI-1
Yes	Yes	DP_162	S2	ICARDA	MRB17
Yes	Yes	DP_163	S4	ICARDA	MURLAGOST-1
Yes	Yes	DP_164	Admixture	ICARDA	NILE
Yes	Yes	DP_165	S2	ICARDA	OMBIT-1
Yes	Yes	DP_166	S2	ICARDA	OMGENIL-3
Yes	Yes	DP_167	S2	ICARDA	OMLAHN-3
Yes	Yes	DP_168	Admixture	ICARDA	OMRUF-2
Yes	Yes	DP_169	Admixture	ICARDA	OMSNIMA-1
Yes	Yes	DP_170	Admixture	ICARDA	ORT-1
Yes	Yes	DP_171	S4	ICARDA	OTB-6
Yes	Yes	DP_172	S4	ICARDA	OUASERL-1
Yes	Yes	DP_173	S4	ICARDA	OUASLAHN-1
Yes	Yes	DP_174	Admixture	ICARDA	OUASLOUKOS-1

(continue)

Growing Season 2017/2018 (Y1)	Growing Season 2018/2019 (Y2)	UNIBO Panel Code	Subgroup	Origin	Accession Name
Yes	Yes	DP_175	S4	ICARDA	QUABRACH-1
Yes	Yes	DP_176	S3	ICARDA	QUADALETE
Yes	Yes	DP_177	S5	INRAE	RAZZAK
Yes	Yes	DP_178	Admixture	ICARDA	SAADA3/DDS//MTL1
Yes	Yes	DP_179	Admixture	ICARDA	SAJUR
Yes	Yes	DP_180	Admixture	ICARDA	SEBATEL-1
Yes	Yes	DP_181	S8	ICARDA	SHABHA
Yes	Yes	DP_182	Admixture	ICARDA	TELSET-5
Yes	Yes	DP_183	S5	ICARDA	TENSIFT-1
Yes	Yes	DP_184	Admixture	ICARDA	TERBOL97-3
Yes	Yes	DP_185	S4	ICARDA	TUNSYR-1
Yes	Yes	DP_186	S4	ICARDA	WADALMEZ-1
Yes	Yes	DP_187	S2	ICARDA	YOUNES-1
Yes	Yes	DP_188	Admixture	ICARDA	YOUSEF-1
Yes	Yes	DP_189	S8	USA	KOFA
Yes	No	DP_190	Admixture	FRANCE	ACALOU
Yes	Yes	DP_191	Admixture	FRANCE	AGRIDUR
Yes	Yes	DP_192	Unknown	FRANCE	ARAMON
Yes	Yes	DP_194	Admixture	FRANCE	ARDENTE
Yes	No	DP_195	S8	FRANCE	ARSTAR
Yes	Yes	DP_196	S8	FRANCE	BRINDUR
Yes	No	DP_197	S6	FRANCE	DURIAC
Yes	No	DP_199	Unknown	FRANCE	GALADUR
Yes	No	DP_200	S8	FRANCE	ORJAUNE
Yes	No	DP_201	S8	FRANCE	PRIMADUR
Yes	Yes	DP_202	S8	FRANCE	TETRADUR
Yes	Yes	DP_203	S8	FRANCE	AUROC
Yes	Yes	DP_204	S8	FRANCE	EXELDUR
Yes	No	DP_205	Admixture	FRANCE	NEFER
Yes	No	DP_206	S8	FRANCE	NEODUR
Yes	Yes	DP_207	S8	AUSTRALIA	ASTRODUR
Yes	No	DP_208	S8	AUSTRALIA	EXTRADUR
Yes	No	DP_209	Unknown	AUSTRALIA	GOLDUR
Yes	No	DP_210	Admixture	AUSTRALIA	GRANDUR
Yes	Yes	DP_212	S8	AUSTRALIA	HELIDUR
Yes	Yes	DP_213	S8	AUSTRALIA	SEMPERDUR
Yes	No	DP_215	S8	CANADA	AC_AVONLEA
Yes	Yes	DP_216	Unknown	CANADA	AC_MELITA
Yes	Yes	DP_217	S8	CANADA	AC_MORSE
Yes	Yes	DP_218	S8	CANADA	AC_NAVIGATOR
Yes	Yes	DP_219	S8	CANADA	AC_PATHFINDER
Yes	Yes	DP_220	S8	CANADA	HERCULES
Yes	No	DP_221	S8	CANADA	KYLE
Yes	No	DP_222	S8	CANADA	MEDORA
Yes	No	DP_223	S8	CANADA	PLENTY
Yes	No	DP_224	S8	CANADA	SCEPTRE
Yes	No	DP_225	Unknown	CANADA	WAKOOMA
Yes	Yes	DP_226	S8	USA	BEN
Yes	No	DP_227	S8	USA	BELZER
Yes	No	DP_228	S8	USA	PLAZA
Yes	No	DP_229	S8	USA	LLOYD
Yes	Yes	DP_230	Unknown	USA	MAIER
Yes	Yes	DP_231	Unknown	USA	MONROE
Yes	Yes	DP_232	S8	USA	MUNICH
Yes	No	DP_233	S8	USA	RENVILLE
Yes	Yes	DP_234	S8	USA	RUGBY
Yes	No	DP_235	S8	USA	LAKOTA

(continue)

(conclusion)

Growing Season 2017/2018 (Y1)	Growing Season 2018/2019 (Y2)	UNIBO Panel Code	Subgroup	Origin	Accession Name
Yes	No	DP_237	S8	USA	WASKANA
Yes	No	DP_238	S8	USA	EDMORE
Yes	Yes	DP_239	S8	USA	VIC
Yes	Yes	DP_240	S8	USA	MINDUM
Yes	Yes	DP_242	S8	USA	COLORADO
Yes	Yes	DP_243	Admixture	AUSTRALIA	YALLAROI
Yes	Yes	DP_244	S8	AUSTRALIA	KAMILAROI
Yes	Yes	DP_245	Admixture	AUSTRALIA	WOLLAROI
Yes	Yes	DP_246	Unknown	LANDRACE	RUSSELLO_SG7
Yes	No	DP_247	Unknown	LANDRACE	SARAGOLLA
Yes	Yes	DP_248	S1	ITALY	SIMETO
Yes	Yes	DP_249	Admixture	ITALY	LEVANTE
Yes	Yes	DP_250	Admixture	FRANCE	ARDENTE
Yes	Yes	DP_251	Admixture	CIMMYT	1A.1D 5+10-6/3*MOJO//RCOL
Yes	Yes	DP_252	Admixture	CIMMYT	SOOTY_9/RASCON_37 (ATIL C2000)
Yes	Yes	DP_253	S7	CIMMYT	STOT//ALTAR 84/ALD (JUPARE C2003)
Yes	Yes	DP_254	S5	CIMMYT	SOMAT_4/INTER_8 (SAMAYOA C2004)
Yes	Yes	DP_255	S7	CIMMYT	CHEN_1/TEZ/3/GUIL//CIT71/CII/4/SORA/PLATA_12/5/STOT //ALTAR 84/ALD
Yes	Yes	DP_256	Admixture	CIMMYT	MALMUK_1//LOTUS_5/F3LOCAL(SEL.ETHIO.135.85)
Yes	Yes	DP_257	S7	CIMMYT	1A.1D 5+10-6/2*WB881//1A.1D 5+10-6/3*MOJO/3/BISU_1/PATKA_3
Yes	Yes	DP_258	S7	CIMMYT	HESSIAN-F_2/3/STOT//ALTAR 84/ALD
Yes	Yes	DP_259	Admixture	CIMMYT	AJAIA_12/F3LOCAL(SEL.ETHIO.135.85)//PLATA_13/3/SOMAT_3/4/SOOTY_9/RASCON_37
Yes	Yes	DP_260	Admixture	CIMMYT	USDA595/3/D67.3/RABI//CRA/4/ALO/5/HUI/YAV_1/6/ARDENTE/7/HUI/YAV79/8/POD_9
Yes	Yes	DP_261	Admixture	CIMMYT	CNDO/PRIMADUR//HAI-OU_17/3/SN TURK MI83-84 375/NIGRIS_5//TANTLO_1
Yes	Yes	DP_262	S7	CIMMYT	GEDIZ/FGO//GTA/3/SRN_1/4/TOTUS/5/ENTE/MEXI_2//HUI/3/YAV_1/GEDIZ/6/SOMBRA_20/7/STOT//ALTAR 84/ALD
Yes	Yes	DP_263	Admixture	CIMMYT	VANRRIKSE_6.2//1A-1D 2+12-5/3*WB881
Yes	Yes	DP_264	Admixture	CIMMYT	RANCO//CIT71/CII/3/COMDK/4/TCHO//SHWA/MALD/3/CREX/5/SN TURK MI83-84 375/NIGRIS_5//TANTLO_1
Yes	Yes	DP_265	Admixture	CIMMYT	PLATA_10/6/MQUE/4/USDA573//QFN/AA_7/3/ALBA-D/5/AVO/HUI/7/PLATA_13/8/THKNEE_11/9/CHEN/ALTAR
Yes	Yes	DP_266	S5	CIMMYT	EUDO//CHEN_1/TEZ/3/TANTLO_1/4/PLATA_6/GREEN_17
Yes	Yes	DP_267	Admixture	CIMMYT	ROLA_5/3/AJAIA_12/F3LOCAL(SEL.ETHIO.135.85)//PLATA_13/4/MALMUK_1/SERRATOR_1
Yes	Yes	DP_268	Admixture	CIMMYT	ARMENT//SRN_3/NIGRIS_4/3/CANELO_9.1
Yes	Yes	DP_269	Admixture	CIMMYT	SOMAT_3/PHAX_1//TILO_1/LOTUS_4
Yes	Yes	DP_270	Unknown	CIMMYT	YAVAROS 79
No	Yes	n/a	Unknown	USA	TIBURON

APPENDIX 2 – FIELD MAPS

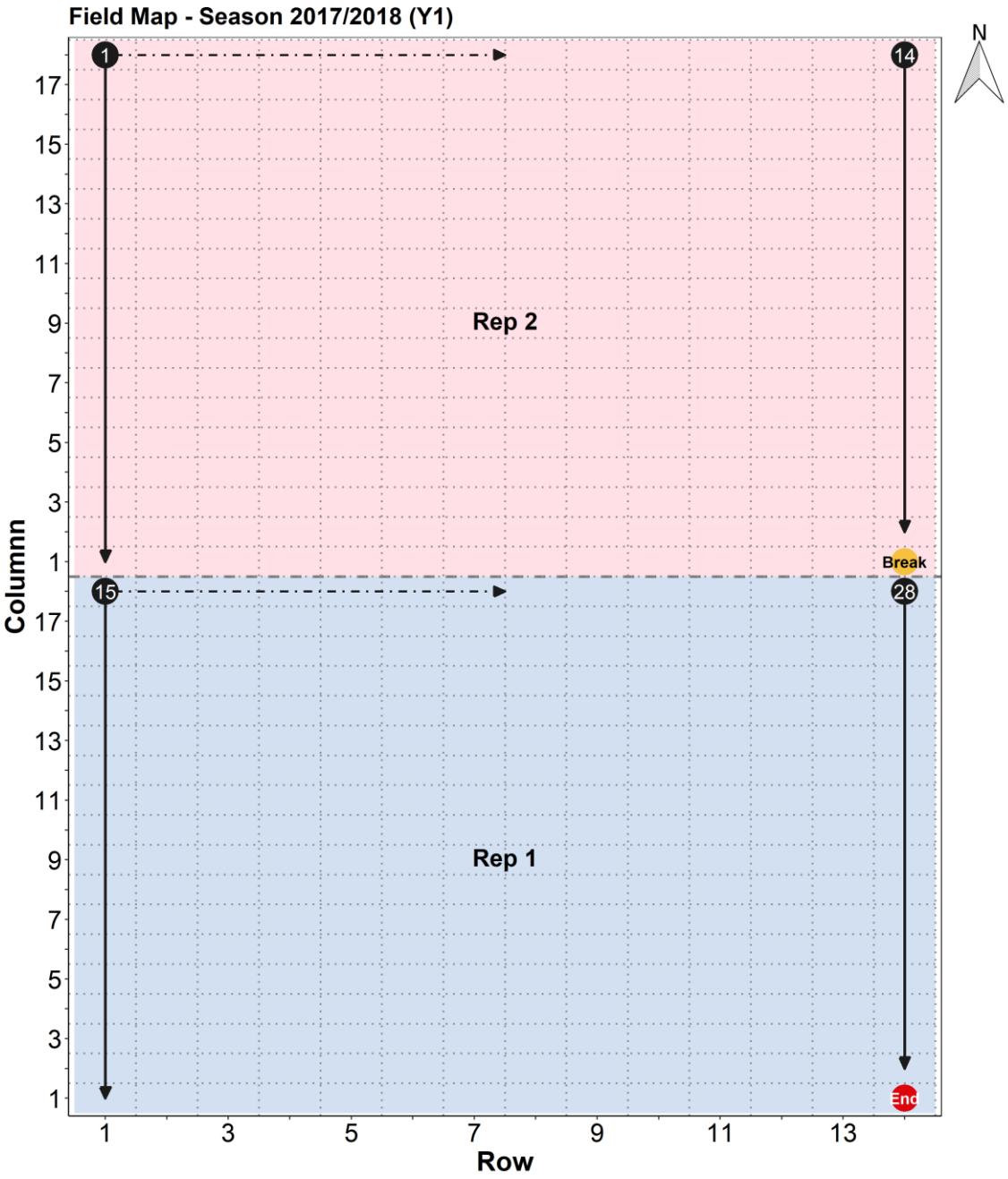

Figure A.2.1. Field map for the durum wheat panel grown under progressive drought in season 2017/2018. In Y1, all LIFT data were only taken in the western subplot row within the 2-row plots. The cart was manually pushed (starting in the black point 1) from north to south along the rows, one at a time, and from west to east within each replicate separately. Rep 2 was collected from early mornings up to midday, and Rep 1 from midday up to late afternoons with a ~30-min break (yellow point) between replicates. The red point indicates where a day of field phenotyping ended.

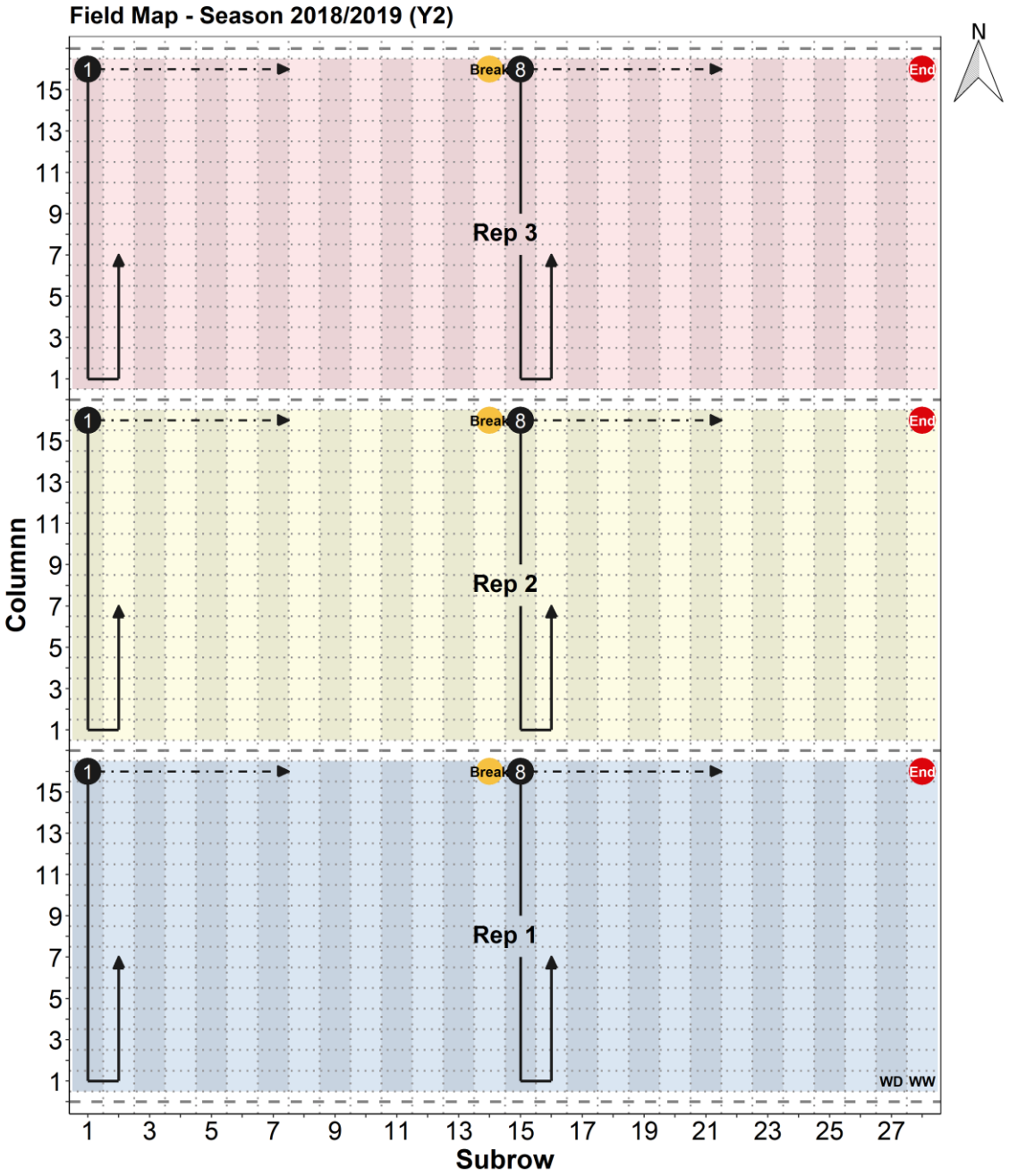

Figure A.2.2. Field map for the durum wheat panel grown under progressive drought in season 2018/2019. In Y2, LIFT data were taken in all the 1-row plots (i.e., all subrows) by following a zigzag path within each replicate. Manually pushing the cart forwards (starting in the black point 1), from north to south, a water-limited (WD; darker colour) subrow was measured and, immediately after, when pulling it backwards, from south to north, the neighbouring well-watered (WW; lighter colour) subrow was measured. This pattern moved from west (early mornings) to east (late afternoons) with a ~40-min break (yellow points) at around midday when half of a replicate was done. The red points indicate where a day of field phenotyping ended. In being a large experiment, only one replicate per day was operationally possible, and so three consecutive days were required to phenotype the entire experiment with three replicates.

APPENDIX 3 – STATISTICAL MODELS

Table A.3.1. All models fitted to analyse the operating efficiency of PSII (F_q'/F_m') in growing season 2017/2018 (Y1). $BL_{Cov+STM}$ is the final 'best' fit model that incorporates covariates and spatiotemporal modelling over the initial baseline model (BL), as explained in the text. The Kronecker product (i.e., the direct product) is denoted by ⊗, and *df* is the degrees of freedom for the model.

Model	Terms	AIC	Deviance	*df*
0	Intercept only model	-11272.63	-21449.69	5540
1	Baseline ($\boldsymbol{BL}$)	-19611.90	-29655.34	5510
2	1 + Covariates ($\boldsymbol{BL_{Cov}}$)	-20826.01	-30793.09	5503
Temporal covariance modelling over residuals ($\boldsymbol{R \cdot ROW \cdot COL \cdot T}$)				
3	$2 + I \otimes I \otimes I \otimes DIAG$	-21101.89	-31277.95	5493
4	$2 + I \otimes I \otimes I \otimes UN$	Failed to converge		
5	$2 + I \otimes I \otimes I \otimes ANTE1$	Failed to converge		
6	$2 + I \otimes I \otimes I \otimes POW$	-20655.20	-30813.26	5502
7	$2 + I \otimes I \otimes I \otimes POWH$	-21113.33	-31291.39	5492
8	$7 - R \cdot ROW \cdot COL$	-21016.90	-31192.95	5493
9	$2 + I \otimes I \otimes I \otimes BANDH1$	-21165.20	-31343.26	5492
10	$9 - R \cdot ROW \cdot COL$	-21089.93	-31265.98	5493
11	$2 + I \otimes I \otimes I \otimes BANDH2$	Failed to converge		
12	$11 - R \cdot ROW \cdot COL$	-21148.54	-31326.59	5492
13	$2 + I \otimes I \otimes I \otimes BANDH3$	Failed to converge		
14	$13 - R \cdot ROW \cdot COL$	-21200.47	-31380.53	5491
15	$2 + I \otimes I \otimes I \otimes BANDH4$	Failed to converge		
16	$15 - R \cdot ROW \cdot COL$	Failed to converge		
17	$2 + I \otimes I \otimes I \otimes CORH1$	-21221.89	-31417.94	5483
18	$17 - R \cdot ROW \cdot COL$	-21154.55	-31348.61	5484
19	$2 + I \otimes I \otimes I \otimes CORH2$	Failed to converge		
20	$19 - R \cdot ROW \cdot COL$	Failed to converge		
Spatial covariance modelling over residuals ($\boldsymbol{R \cdot ROW \cdot COL \cdot T}$)				
21	$2 + I \otimes LV \otimes I \otimes CORH1$	Failed to converge		
22	$2 + I \otimes I \otimes LV \otimes CORH1$	Failed to converge		
23	$2 + I \otimes LV \otimes LV \otimes CORH1$	Failed to converge		
24	$2 + I \otimes AR1 \otimes I \otimes CORH1$	-21221.29	-31429.35	5482
25	$2 + I \otimes I \otimes AR1 \otimes CORH1$	-21334.07	-31532.12	5482

Model	Terms	AIC	Deviance	*df*
26	$2 + I \otimes AR1 \otimes AR1 \otimes CORH1$	-21334.37	-31534.42	5481
27	$2 + I \otimes AR2 \otimes AR2 \otimes CORH1$	-21351.25	-31555.31	5479
28	$2 + I \otimes MA1 \otimes I \otimes CORH1$	-21221.21	-31419.27	5482
29	$2 + I \otimes I \otimes MA1 \otimes CORH1$	-21318.91	-31516.96	5482
30	$2 + I \otimes MA1 \otimes MA1 \otimes CORH1$	-21318.97	-31519.02	5481
31	$2 + I \otimes MA2 \otimes MA2 \otimes CORH1$	-21341.83	-31545.88	5479
32	$2 + I \otimes ARMA1 \otimes I \otimes CORH1$	-21225.82	-31425.87	5481
33	$2 + I \otimes I \otimes ARMA1 \otimes CORH1$	-21354.18	-31554.24	5481
34	$2 + I \otimes ARMA1 \otimes ARMA1 \otimes CORH1$	-21360.21	-31564.27	5479
Serial correlation modelling for genotype by time interaction ($G \cdot T$)				
35	$34 + I \otimes POW$	Failed to converge		
36	$34 + I \otimes POW - G$	-21405.75	-31609.80	5479
37	$34 + I \otimes LV - G$	-21413.51	-31617.56	5479
38	$34 + I \otimes LVH - G$	-21413.15	-31637.21	5469
PPFD and VPD were log-transformed				
39	$38 + \log PPFD \times \log VPD$	-21464.37	-31688.42	5469
Checking fixed effects (covariates were dropped if $p > .10$ for F-test)				
$\boldsymbol{BL_{Cov+STM}}$	39 and none fixed effect dropped	**-21464.37**	**-31688.42**	**5469**

Table A.3.2. All models fitted to analyse F'_{r1} (i.e., the kinetics of electron transfer from Q_A to *PQ* pool) in growing season 2017/2018 (Y1). $BL_{Cov+STM}$ is the final 'best' fit model that incorporates covariates and spatiotemporal modelling over the initial baseline model (BL), as explained in the text. The Kronecker product (i.e., the direct product) is denoted by ⊗, and *df* is the degrees of freedom for the model.

Model	Terms	AIC	Deviance	*df*
0	Intercept only model	-14287.25	-24464.31	5540
1	Baseline ($\boldsymbol{BL}$)	-22494.15	-32537.59	5510
2	1 + Covariates ($\boldsymbol{BL_{Cov}}$)	-23804.22	-33771.29	5503
Temporal covariance modelling over residuals ($\boldsymbol{R \cdot ROW \cdot COL \cdot T}$)				
3	$2 + I \otimes I \otimes I \otimes DIAG$	-24021.10	-34197.15	5493
4	$2 + I \otimes I \otimes I \otimes UN$	Failed to converge		
5	$2 + I \otimes I \otimes I \otimes ANTE1$	Failed to converge		
6	$2 + I \otimes I \otimes I \otimes POW$	-23684.66	-33842.71	5502
7	$2 + I \otimes I \otimes I \otimes POWH$	-24015.18	-34191.24	5493
8	$7 - R \cdot ROW \cdot COL$	-24018.69	-34194.74	5493
9	$2 + I \otimes I \otimes I \otimes BANDH1$	-24126.38	-34304.44	5492
10	$9 - R \cdot ROW \cdot COL$	-24099.89	-34275.94	5493
11	$2 + I \otimes I \otimes I \otimes BANDH2$	-24179.75	-34359.80	5491
12	$11 - R \cdot ROW \cdot COL$	-24172.35	-34350.40	5492
13	$2 + I \otimes I \otimes I \otimes BANDH3$	Failed to converge		
14	$13 - R \cdot ROW \cdot COL$	-24210.86	-34390.92	5491
15	$2 + I \otimes I \otimes I \otimes BANDH4$	Failed to converge		
16	$15 - R \cdot ROW \cdot COL$	Failed to converge		
17	$2 + I \otimes I \otimes I \otimes CORH1$	-24176.77	-34372.82	5483
18	$17 - R \cdot ROW \cdot COL$	-24147.98	-34342.04	5484
19	$2 + I \otimes I \otimes I \otimes CORH2$	-24229.92	-34443.98	5474
20	$19 - R \cdot ROW \cdot COL$	Failed to converge		
Spatial covariance modelling over residuals ($\boldsymbol{R \cdot ROW \cdot COL \cdot T}$)				
21	$2 + I \otimes LV \otimes I \otimes CORH2$	Failed to converge		
22	$2 + I \otimes I \otimes LV \otimes CORH2$	Failed to converge		
23	$2 + I \otimes LV \otimes LV \otimes CORH2$	Failed to converge		
24	$2 + I \otimes AR1 \otimes I \otimes CORH2$	-24231.62	-34447.67	5473
25	$2 + I \otimes I \otimes AR1 \otimes CORH2$	Failed to converge		
26	$2 + I \otimes AR1 \otimes AR1 \otimes CORH2$	Failed to converge		
27	$2 + I \otimes AR1 \otimes I \otimes CORH1$	-24178.01	-34376.06	5482
28	$2 + I \otimes I \otimes AR1 \otimes CORH1$	-24256.48	-34454.53	5482

Model	Terms	AIC	Deviance	*df*
29	$2 + I \otimes AR1 \otimes AR1 \otimes CORH1$	-24259.17	-34459.23	5481
30	$2 + I \otimes AR2 \otimes AR2 \otimes CORH1$	-24260.96	-34465.02	5479
31	$2 + I \otimes MA1 \otimes I \otimes CORH1$	-24177.88	-34375.94	5482
32	$2 + I \otimes I \otimes MA1 \otimes CORH1$	-24250.41	-34448.47	5482
33	$2 + I \otimes MA1 \otimes MA1 \otimes CORH1$	-24252.72	-34452.77	5481
34	$2 + I \otimes MA2 \otimes MA2 \otimes CORH1$	-24259.43	-34463.48	5479
35	$2 + I \otimes ARMA1 \otimes I \otimes CORH1$	-24182.91	-34382.97	5481
36	$2 + I \otimes I \otimes ARMA1 \otimes CORH1$	-24258.27	-34458.33	5481
37	$2 + I \otimes ARMA1 \otimes ARMA1 \otimes CORH1$	-24267.81	-34471.86	5479
Serial correlation modelling for genotype by time interaction ($G \cdot T$)				
38	$37 + I \otimes POW$	Failed to converge		
39	$37 + I \otimes POW - G$	-24309.50	-34513.55	5479
40	$37 + I \otimes LV - G$	-24316.22	-34520.28	5479
41	$37 + I \otimes LVH - G$	-24328.68	-34552.73	5469
PPFD and VPD were log-transformed				
42	$41 + \log PPFD \times \log VPD$	-24366.14	-34590.20	5469
Checking fixed effects (covariates were dropped if $p > .10$ for F-test)				
$\boldsymbol{BL_{Cov+STM}}$	42 and none fixed effect dropped	**-24366.14**	**-34590.20**	**5469**

Table A.3.3. All models fitted to analyse F'_{r2} (i.e., the kinetics of electron transfer from *PQ* pool to PSI) in growing season 2017/2018 (Y1). $BL_{Cov+STM}$ is the final 'best' fit model that incorporates covariates and spatiotemporal modelling over the initial baseline model (BL), as explained in the text. The Kronecker product (i.e., the direct product) is denoted by ⊗, and *df* is the degrees of freedom for the model.

Model	Terms	AIC	Deviance	*df*
0	Intercept only model	-17609.29	-27784.34	5540
1	Baseline ($\boldsymbol{BL}$)	-26443.66	-36487.10	5510
2	1 + Covariates ($\boldsymbol{BL_{Cov}}$)	-27433.87	-37400.94	5503
Temporal covariance modelling over residuals ($\boldsymbol{R \cdot ROW \cdot COL \cdot T}$)				
3	$2 + I \otimes I \otimes I \otimes DIAG$	-27609.31	-37785.36	5493
4	$2 + I \otimes I \otimes I \otimes UN$	Failed to converge		
5	$2 + I \otimes I \otimes I \otimes ANTE1$	Failed to converge		
6	$2 + I \otimes I \otimes I \otimes POW$	-27245.41	-37403.47	5502
7	$2 + I \otimes I \otimes I \otimes POWH$	-27579.11	-37755.17	5493
8	$7 - R \cdot ROW \cdot COL$	-27527.81	-37703.87	5493
9	$2 + I \otimes I \otimes I \otimes BANDH1$	-27665.54	-37843.60	5492
10	$9 - R \cdot ROW \cdot COL$	-27586.18	-37762.23	5493
11	$2 + I \otimes I \otimes I \otimes BANDH2$	Failed to converge		
12	$11 - R \cdot ROW \cdot COL$	-27639.69	-37817.74	5492
13	$2 + I \otimes I \otimes I \otimes BANDH3$	Failed to converge		
14	$13 - R \cdot ROW \cdot COL$	Failed to converge		
15	$2 + I \otimes I \otimes I \otimes BANDH4$	Failed to converge		
16	$15 - R \cdot ROW \cdot COL$	Failed to converge		
17	$2 + I \otimes I \otimes I \otimes CORH1$	-27698.81	-37894.87	5483
18	$17 - R \cdot ROW \cdot COL$	-27631.13	-37825.19	5484
19	$2 + I \otimes I \otimes I \otimes CORH2$	Failed to converge		
20	$19 - R \cdot ROW \cdot COL$	-27693.69	-37905.75	5475
Spatial covariance modelling over residuals ($\boldsymbol{R \cdot ROW \cdot COL \cdot T}$)				
21	$2 + I \otimes LV \otimes I \otimes CORH1$	-25393.38	-35591.43	5482
22	$2 + I \otimes I \otimes LV \otimes CORH1$	Failed to converge		
23	$2 + I \otimes LV \otimes LV \otimes CORH1$	Failed to converge		
24	$2 + I \otimes AR1 \otimes I \otimes CORH1$	-27697.25	-37895.30	5482
25	$2 + I \otimes I \otimes AR1 \otimes CORH1$	-27872.03	-38070.08	5482
26	$2 + I \otimes AR1 \otimes AR1 \otimes CORH1$	-27870.66	-38070.71	5481
27	$2 + I \otimes AR2 \otimes AR2 \otimes CORH1$	-27897.53	-38101.58	5479
28	$2 + I \otimes MA1 \otimes I \otimes CORH1$	-27697.23	-37895.29	5482

Model	Terms	AIC	Deviance	*df*
29	$2 + I \otimes I \otimes MA1 \otimes CORH1$	-27842.78	-38040.83	5482
30	$2 + I \otimes MA1 \otimes MA1 \otimes CORH1$	-27841.38	-38041.43	5481
31	$2 + I \otimes MA2 \otimes MA2 \otimes CORH1$	-27876.55	-38080.61	5479
32	$2 + I \otimes ARMA1 \otimes I \otimes CORH1$	-27699.18	-37899.23	5481
33	$2 + I \otimes I \otimes ARMA1 \otimes CORH1$	-27910.68	-38110.73	5481
34	$2 + I \otimes ARMA1 \otimes ARMA1 \otimes CORH1$	-27912.24	-38116.29	5479
Serial correlation modelling for genotype by time interaction ($G \cdot T$)				
35	$34 + I \otimes POW$	Failed to converge		
36	$34 + I \otimes POW - G$	-27980.26	-38184.31	5479
37	$34 + I \otimes LV - G$	-27990.10	-38194.16	5479
38	$34 + I \otimes LVH - G$	-27986.57	-38210.62	5469
PPFD and VPD were log-transformed				
39	$38 + \log PPFD \times \log VPD$	-28048.35	-38272.41	5469
Checking fixed effects (covariates were dropped if $p > .10$ for F-test)				
$\boldsymbol{BL_{Cov+STM}}$	39 and none fixed effect dropped	**-28048.35**	**-38272.41**	**5469**

Table A.3.4. All models fitted to analyse the operating efficiency of PSII (F_q'/F_m') in growing season 2018/2019 (Y2). $BL_{Cov+STM}$ is the final 'best' fit model that incorporates covariates and spatiotemporal modelling over the initial baseline model (BL), as explained in the text. The Kronecker product (i.e., the direct product) is denoted by ⊗, and *df* is the degrees of freedom for the model.

Model	Terms	AIC	Deviance	*df*
0	Intercept only model	-13079.01	-20481.20	4030
1	Baseline ($\boldsymbol{BL}$)	-16257.14	-23609.01	4002
2	1 + Covariates ($\boldsymbol{BL_{Cov}}$)	-17134.54	-24309.81	3984
Temporal covariance modelling over residuals ($\boldsymbol{R \cdot COL \cdot ROW \cdot SUB \cdot T}$)				
3	$2 + I \otimes I \otimes I \otimes DIAG$	-16942.29	-24337.47	3982
4	$2 + I \otimes I \otimes I \otimes UN$	Failed to converge		
5	$2 + I \otimes I \otimes I \otimes ANTE1$	-16566.18	-23963.36	3981
6	$5 - R \cdot COL \cdot ROW \cdot SUB$	-16942.61	-24339.79	3981
7	$2 + I \otimes I \otimes I \otimes POW$	-16916.63	-24309.81	3984
8	$7 - R \cdot COL \cdot ROW \cdot SUB$	-16917.56	-24308.74	3985
9	$2 + I \otimes I \otimes I \otimes POWH$	-16940.58	-24337.76	3981
10	$9 - R \cdot COL \cdot ROW \cdot SUB$	-16941.29	-24336.47	3983
11	$2 + I \otimes I \otimes I \otimes CORH1$	-16940.62	-24339.81	3980
12	$11 - R \cdot COL \cdot ROW \cdot SUB$	-16942.62	-24339.81	3981
13	$2 + I \otimes I \otimes I \otimes CORH2$	Failed to converge		
14	$13 - R \cdot COL \cdot ROW \cdot SUB$	-16940.64	-24339.82	3980
15	$2 + I \otimes I \otimes I \otimes BANDH1$	-16942.13	-24339.31	3981
16	$15 - R \cdot COL \cdot ROW \cdot SUB$	-16944.13	-24339.31	3982
17	$2 + I \otimes I \otimes I \otimes BANDH2$	Failed to converge		
18	$17 - R \cdot COL \cdot ROW \cdot SUB$	-16942.14	-24339.32	3981
Spatial covariance modelling over residuals ($\boldsymbol{R \cdot COL \cdot ROW \cdot SUB \cdot T}$)				
19	$16 + I \otimes I \otimes I \otimes UN \otimes BANDH1$	Failed to converge		
20	$16 + I \otimes I \otimes I \otimes DIAG \otimes BANDH1$	-16942.17	-24339.35	3981
21	$16 + I \otimes I \otimes I \otimes COR1 \otimes BANDH1$	-16942.57	-24339.76	3981
22	$16 + I \otimes I \otimes AR1 \otimes I \otimes BANDH1$	-16943.73	-24340.91	3981
23	$16 + I \otimes AR1 \otimes I \otimes I \otimes BANDH1$	-16956.43	-24353.61	3981
24	$16 + I \otimes AR1 \otimes AR1 \otimes I \otimes BANDH1$	-16956.00	-24355.18	3980
25	$16 + I \otimes I \otimes MA1 \otimes I \otimes BANDH1$	-16943.79	-24340.98	3981
26	$16 + I \otimes MA1 \otimes I \otimes I \otimes BANDH1$	-16954.96	-24352.15	3981
27	$16 + I \otimes MA1 \otimes MA1 \otimes I \otimes BANDH1$	-16954.61	-24353.79	3980
28	$16 + I \otimes I \otimes ARMA1 \otimes I \otimes BANDH1$	-16941.82	-24340.92	3980
29	$16 + I \otimes ARMA1 \otimes I \otimes I \otimes BANDH1$	-16961.82	-24361.00	3980

Model	Terms	AIC	Deviance	*df*
30	$16 + I \otimes AR2 \otimes I \otimes I \otimes BANDH1$	-16963.16	-24362.34	3980
31	$16 + I \otimes MA2 \otimes I \otimes I \otimes BANDH1$	-16962.65	-24361.83	3980
32	$16 + I \otimes ARH2 \otimes I \otimes I \otimes BANDH1$	-16961.85	-24391.03	3965
33	$16 + I \otimes ARH2 \otimes DIAG \otimes I \otimes BANDH1$	-16951.42	-24406.60	3952
PPFD and VPD were log-transformed				
34	$32 + \log PPFD \times \log VPD$	-17014.74	-24443.92	3965
Checking fixed effects (covariates were dropped if *p* > .10 for *F*-test)				
$\boldsymbol{BL_{Cov+STM}}$	$34 - (\log PPFD \cdot \log VPD)/TRT - \log PPFD \cdot TRT - \log VPD \cdot TRT - ZDS \cdot TRT - VOGREI \cdot TRT - ZDS \cdot T - VOGREI \cdot T$	**-17217.07**	**-24554.40**	**3975**

Table A.3.5. All models fitted to analyse F'_{r1} (i.e., the kinetics of electron transfer from Q_A to PQ pool) in growing season 2018/2019 (Y2). $BL_{Cov+STM}$ is the final 'best' fit model that incorporates covariates and spatiotemporal modelling over the initial baseline model (BL), as explained in the text. The Kronecker product (i.e., the direct product) is denoted by ⊗, and *df* is the degrees of freedom for the model.

Model	Terms	AIC	Deviance	*df*
0	Intercept only model	-13167.87	-20570.05	4030
1	Baseline ($\boldsymbol{BL}$)	-17545.75	-24897.62	4002
2	1 + Covariates ($\boldsymbol{BL_{Cov}}$)	-18292.44	-25467.71	3984
Temporal covariance modelling over residuals ($\boldsymbol{R \cdot COL \cdot ROW \cdot SUB \cdot T}$)				
3	$2 + I \otimes I \otimes I \otimes DIAG$	-18077.75	-25472.93	3982
4	$3 - R \cdot COL \cdot ROW \cdot SUB$	-18074.20	-25467.38	3983
5	$2 + I \otimes I \otimes I \otimes UN$	Failed to converge		
6	$2 + I \otimes I \otimes I \otimes ANTE1$	-18075.84	-25475.02	3980
7	$6 - R \cdot COL \cdot ROW \cdot SUB$	-18075.99	-25473.17	3981
8	$2 + I \otimes I \otimes I \otimes POW$	-18075.56	-25468.74	3983
9	$8 - R \cdot COL \cdot ROW \cdot SUB$	-18076.38	-25467.56	3984
10	$2 + I \otimes I \otimes I \otimes POWH$	-18075.75	-25472.93	3982
11	$10 - R \cdot COL \cdot ROW \cdot SUB$	-18077.50	-25472.69	3982
12	$2 + I \otimes I \otimes I \otimes CORH1$	-18075.84	-25475.03	3980
13	$12 - R \cdot COL \cdot ROW \cdot SUB$	-18075.84	-25473.02	3981
14	$2 + I \otimes I \otimes I \otimes CORH2$	Failed to converge		
15	$14 - R \cdot COL \cdot ROW \cdot SUB$	-18075.84	-25475.03	3980
16	$2 + I \otimes I \otimes I \otimes BANDH1$	-18075.94	-25473.13	3981
17	$16 - R \cdot COL \cdot ROW \cdot SUB$	-18075.95	-25471.13	3982
18	$2 + I \otimes I \otimes I \otimes BANDH2$	Failed to converge		
19	$18 - R \cdot COL \cdot ROW \cdot SUB$	-18075.76	-25472.94	3981
Spatial covariance modelling over residuals ($\boldsymbol{R \cdot COL \cdot ROW \cdot SUB \cdot T}$)				
20	$3 + I \otimes I \otimes I \otimes UN \otimes DIAG$	Failed to converge		
21	$3 + I \otimes I \otimes I \otimes DIAG \otimes DIAG$	-18075.54	-25472.72	3981
22	$3 + I \otimes I \otimes I \otimes COR1 \otimes DIAG$	Failed to converge		
23	$3 + I \otimes I \otimes AR1 \otimes I \otimes DIAG$	-18076.41	-25473.59	3981
24	$3 + I \otimes AR1 \otimes I \otimes I \otimes DIAG$	-18098.08	-25495.27	3981
25	$3 + I \otimes AR1 \otimes AR1 \otimes I \otimes DIAG$	-18096.74	-25495.93	3980
26	$3 + I \otimes I \otimes MA1 \otimes I \otimes DIAG$	-18076.46	-25473.65	3981
27	$3 + I \otimes MA1 \otimes I \otimes I \otimes DIAG$	-18095.17	-25492.36	3981
28	$3 + I \otimes MA1 \otimes MA1 \otimes I \otimes DIAG$	-18093.90	-25493.08	3980

Model	Terms	AIC	Deviance	*df*
29	$3 + I \otimes I \otimes ARMA1 \otimes I \otimes DIAG$	Failed to converge		
30	$3 + I \otimes ARMA1 \otimes I \otimes I \otimes DIAG$	-18105.79	-25504.98	3980
31	$3 + I \otimes AR2 \otimes I \otimes I \otimes DIAG$	-18107.43	-25506.62	3980
32	$3 + I \otimes MA2 \otimes I \otimes I \otimes DIAG$	-18107.65	-25506.83	3980
33	$3 + I \otimes ARH2 \otimes I \otimes I \otimes DIAG$	-18101.68	-25530.87	3965
34	$3 + I \otimes ARH2 \otimes DIAG \otimes I \otimes DIAG$	-18135.74	-25590.93	3952
35	$3 + I \otimes MAH2 \otimes I \otimes I \otimes DIAG$	-18108.38	-25537.57	3965
36	$3 + I \otimes MAH2 \otimes DIAG \otimes I \otimes DIAG$	-18133.85	-25589.03	3952
PPFD and VPD were log-transformed				
37	$34 + \log PPFD \times \log VPD$	-18204.38	-25659.56	3952
Checking fixed effects (covariates were dropped if p > .10 for F-test)				
$\boldsymbol{BL_{Cov+STM}}$	$37 - (\log PPFD \cdot \log VPD)/TRT - \log PPFD \cdot TRT - ZDS \cdot TRT - VOGREI \cdot TRT - VOGREI \cdot T$	-18392.80	-25727.25	3959

Table A.3.6. All models fitted to analyse F'_{r2} (i.e., the kinetics of electron transfer from *PQ* pool to PSI) in growing season 2018/2019 (Y2). $BL_{Cov+STM}$ is the final 'best' fit model that incorporates covariates and spatiotemporal modelling over the initial baseline model (BL), as explained in the text. The Kronecker product (i.e., the direct product) is denoted by ⊗, and *df* is the degrees of freedom for the model.

Model	Terms	AIC	Deviance	*df*
0	Intercept only model	-15792.65	-23194.83	4030
1	Baseline ($\boldsymbol{BL}$)	-19421.38	-26773.25	4002
2	1 + Covariates ($\boldsymbol{BL_{Cov}}$)	-20377.64	-27552.92	3984
Temporal covariance modelling over residuals ($\boldsymbol{R \cdot COL \cdot ROW \cdot SUB \cdot T}$)				
3	$2 + I \otimes I \otimes I \otimes I \otimes DIAG$	-20169.24	-27564.43	3982
4	$2 + I \otimes I \otimes I \otimes I \otimes UN$	Failed to converge		
5	$2 + I \otimes I \otimes I \otimes I \otimes ANTE1$	-20163.80	-27562.99	3980
6	$5 - R \cdot COL \cdot ROW \cdot SUB$	-20164.89	-27562.07	3981
7	$2 + I \otimes I \otimes I \otimes I \otimes POW$	Failed to converge		
8	$7 - R \cdot COL \cdot ROW \cdot SUB$	Failed to converge		
9	$2 + I \otimes I \otimes I \otimes I \otimes POWH$	-20167.60	-27564.78	3981
10	$9 - R \cdot COL \cdot ROW \cdot SUB$	Failed to converge		
11	$2 + I \otimes I \otimes I \otimes I \otimes CORH1$	-20167.74	-27566.92	3980
12	$11 - R \cdot COL \cdot ROW \cdot SUB$	-20169.74	-27566.92	3981
13	$2 + I \otimes I \otimes I \otimes I \otimes CORH2$	Failed to converge		
14	$13 - R \cdot COL \cdot ROW \cdot SUB$	-20167.82	-27567.00	3980
15	$2 + I \otimes I \otimes I \otimes I \otimes BANDH1$	-20168.77	-27565.95	3981
16	$15 - R \cdot COL \cdot ROW \cdot SUB$	-20170.78	-27565.96	3982
17	$2 + I \otimes I \otimes I \otimes I \otimes BANDH2$	Failed to converge		
18	$17 - R \cdot COL \cdot ROW \cdot SUB$	-20168.83	-27566.02	3981
Spatial covariance modelling over residuals ($\boldsymbol{R \cdot COL \cdot ROW \cdot SUB \cdot T}$)				
19	$16 + I \otimes I \otimes I \otimes UN \otimes BANDH1$	Failed to converge		
20	$16 + I \otimes I \otimes I \otimes DIAG \otimes BANDH1$	-20168.96	-27566.15	3981
21	$16 + I \otimes I \otimes I \otimes COR1 \otimes BANDH1$	-20166.57	-27563.74	3981
22	$16 + I \otimes I \otimes AR1 \otimes I \otimes BANDH1$	-20169.83	-27567.02	3981
23	$16 + I \otimes AR1 \otimes I \otimes I \otimes BANDH1$	-20185.67	-27582.85	3981
24	$16 + I \otimes AR1 \otimes AR1 \otimes I \otimes BANDH1$	-20184.69	-27583.88	3980
25	$16 + I \otimes I \otimes MA1 \otimes I \otimes BANDH1$	-20169.86	-27567.05	3981
26	$16 + I \otimes MA1 \otimes I \otimes I \otimes BANDH1$	-20184.04	-27581.22	3981
27	$16 + I \otimes MA1 \otimes MA1 \otimes I \otimes BANDH1$	-20183.10	-27582.29	3980
28	$16 + I \otimes I \otimes ARMA1 \otimes I \otimes BANDH1$	Failed to converge		

Model	Terms	AIC	Deviance	*df*
29	$16 + I \otimes ARMA1 \otimes I \otimes I \otimes BANDH1$	Failed to converge		
30	$16 + I \otimes AR2 \otimes I \otimes I \otimes BANDH1$	-20191.59	-27590.78	3980
31	$16 + I \otimes MA2 \otimes I \otimes I \otimes BANDH1$	-20190.51	-27589.69	3980
32	$16 + I \otimes ARH2 \otimes I \otimes I \otimes BANDH1$	-20184.47	-27613.66	3965
33	$16 + I \otimes ARH2 \otimes DIAG \otimes I \otimes BANDH1$	-20171.75	-27626.93	3952
PPFD and VPD were log-transformed				
34	$32 + \log PPFD \times \log VPD$	-20228.87	-27658.06	3965
Checking fixed effects (covariates were dropped if *p* > .10 for *F*-test)				
$\boldsymbol{BL_{Cov+STM}}$	$34 - (\log PPFD \cdot \log VPD)/TRT - \log PPFD \cdot TRT - \log VPD \cdot TRT - ZDS \cdot TRT - VOGREI \cdot TRT - ZDS \cdot T - VOGREI \cdot T$	**-20432.77**	**-27770.10**	**3975**

APPENDIX 4 – CONDITIONAL *F*-TEST STATISTIC FOR FIXED EFFECTS

Table A.4.1. Conditional *F*-test statistic for the fixed effects based on the 'best' fit models ($BL_{Cov+STM}$) for each chlorophyll fluorescence trait (F'_q/F'_m, F'_{r1} and F'_{r2}) measured in light-adapted durum wheat plants under progressive drought stress for both growing seasons, 2017/2018 (Y1) and 2018/2019 (Y2).

Year	Trait	Covariate[†]	Effect	*SE*	*F*-statistic (*ndf*, *ddf*)	*p*-value
Y1	$\boldsymbol{F'_q/F'_m}$					
		$RelF$	-0.059	0.007	74.8 (1, 400)	< .001
		$iZDS$	0.001	0.0002	29.4 (1, 353)	< .001
		$VOGREI$	0.10	0.011	79.6 (1, 10.4)	< .001
		$\log PPFD$	-0.017	0.002	143 (1, 1376)	< .001
		$\log VPD$	-0.054	0.016	49.9 (1, 251)	< .001
		$\log\ PPFD \cdot \log\ VPD$	-0.029	0.007	16.0 (1, 894)	< .001
	$\boldsymbol{F'_{r1}}$					
		$RelF$	0.026	0.004	35.6 (1, 421)	< .001
		$iZDS$	-0.0007	0.0001	34.9 (1, 370)	< .001
		$VOGREI$	-0.084	0.009	85.2 (1, 10.2)	< .001
		$\log PPFD$	0.007	0.002	38.3 (1, 1447)	< .001
		$\log VPD$	-0.013	0.012	114 (1, 262)	< .001
		$\log\ PPFD \cdot \log\ VPD$	0.015	0.005	7.48 (1, 846)	.006
	$\boldsymbol{F'_{r2}}$					
		$RelF$	0.038	0.004	101 (1, 388)	< .001
		$iZDS$	-0.0002	0.0001	3.09 (1, 357)	.080
		$VOGREI$	-0.051	0.005	111 (1, 10.9)	< .001
		$\log PPFD$	0.011	0.001	210 (1, 1421)	< .001
		$\log VPD$	0.047	0.010	224 (1, 235)	< .001
		$\log\ PPFD \cdot \log\ VPD$	0.018	0.004	17.1 (1, 925)	< .001
Y2	$\boldsymbol{F'_q/F'_m}$					
		$RelF$	-0.018	0.012	64.1 (1, 1035)	< .001
		$RelF \cdot T$			25.7 (2, 682)	< .001
		$RelF \cdot TRT$			15.7 (1, 456)	< .001
		ZDS	0.0005	0.0001	15.1 (1, 1071)	< .001
		$VOGREI$	0.091	0.003	1041 (1, 3532)	< .001
		$\log PPFD$	-0.055	0.008	48.5 (1, 278)	< .001

Year	Trait	Covariate†	Effect	*SE*	*F*-statistic (*ndf*, *ddf*)	*p*-value
		$\log VPD$	-0.022	0.008	7.30 (1, 85.0)	.008
	F'_{r1}					
		$RelF$	0.024	0.011	72.9 (1, 1267)	< .001
		$RelF \cdot T$			5.16 (2, 717)	.006
		$RelF \cdot TRT$			14.7 (1, 485)	< .001
		ZDS	-0.0004	0.0003	0.040 (1, 1189)	.843
		$ZDS \cdot T$			4.96 (2, 717)	.007
		$VOGREI$	-0.072	0.002	889 (1, 3588)	< .001
		$\log PPFD$	0.021	0.007	9.38 (1, 291)	.002
		$\log VPD$	-0.066	0.007	77.3 (1, 80.0)	< .001
		$\log VPD \cdot TRT$			7.80 (1, 28.8)	.009
	F'_{r2}					
		$RelF$	0.013	0.008	68.0 (1, 1022)	< .001
		$RelF \cdot T$			26.7 (2, 676)	< .001
		$RelF \cdot TRT$			26.4 (1, 457)	< .001
		ZDS	-0.0002	0.00008	8.02 (1, 1061)	.005
		$VOGREI$	-0.063	0.002	1113 (1, 3571)	< .001
		$\log PPFD$	0.035	0.006	39.6 (1, 299)	< .001
		$\log VPD$	0.037	0.006	42.8 (1, 82.0)	< .001

†Covariates: $\log PPFD$ is the log-transformed photosynthetic photon flux density; $\log VPD$ is the log-transformed vapour pressure deficit; $VOGREI$ is the Vogelmann red edge index; $iZDS$ is the initial growth stage in the Zadoks scale measured two days before withholding water (in Y1); ZDS is the growth stage in the Zadoks scale (in Y2); T is the time points after imposing water treatment (i.e., the levels of drought severity); TRT is the water treatment; $RelF$ is the relative deviation of the target area from the focal point of the LIFT light beam set at 0.60 m, calculated as $\left[\frac{LIFT_{height}-PH}{60}\right]$, where $LIFT_{height}$ is the distance from the soil surface to the LIFT lens [cm] and PH is the plant height [cm].